Photofragmentation of molecular adsorbats : Theoretical study of photoionization, photodesorption and related processes.

Matthias Büchner

ORSAY

N° D'ORDRE : 3659

UNIVERSITE DE PARIS-SUD
U.F.R. SCIENTIFIQUE D'ORSAY

THESE

présentée

Pour obtenir

Le Grade de DOCTEUR EN SCIENCES
DE l'UNIVERSITE PARIS XI Orsay

par
Matthias Büchner

SUJET :

Photofragmentation des adsorbats moléculaires: étude théorique de la photoionisation, de la photodésorption et des processus connexes.

Soutenue le 19 avril 1995 devant la Commission d'examen

Mme.	Irene	Nenner	(présidente)
M.	Claude	Girardet	(rapporteur)
M.	Hans–Joachim	Freund	(rapporteur)
M.	Osman	Atabek	
M.	Marc	Chatelet	
M	Gheorghe	Raşeev	
M.	Daniel	Spaanjard	

”Die Gedanken sind frei, wer kann sie erraten,
sie fliehen vorbei wie nächtliche Schatten.
Kein Mensch kann sie wissen, kein Kerker einschliessen.
Es bleibet dabei: die Gedanken sind frei.”

Deutsche Weise [1]

Remerciements

Quand j'ai pris la décision de commencer une thèse en France dans le Laboratoire de Photophysique Moléculaire à Orsay, j'ai eu peur: habiter dans un pays que je ne connaissais qu'à travers de courts séjours de vacances, parler une langue étrangère et se plonger dans une culture qui, malgré le voisinage et l'histoire commune entre la France et l'Allemagne, diffère en de nombreux points. Pendant les premières semaines du séjour je me suis posé la question, si je n'avais pas fait la plus grande erreur de ma vie.

Trois ans après, je peux confirmer que la réponse est définitivement 'non'. L'atmosphère de bienvenue dans ce laboratoire autant que le comportement chaleureux de toutes les personnes, des chercheurs et non–chercheurs, des jeunes et personnes plus âgées, des professeurs et des étudiants, a créé un milieu agréable à vivre et des conditions optimales pour une bonne réussite du travail. Il me semble difficile d'établir une liste complète des personnes à remercier, et en conséquence je remercie l'ensemble des personnes du Laboratoire et de l'Association des Etudiants d'Ici et d'Ailleurs pour des discussions nombreuses sur tous les aspects imaginables de la culture française y compris la richesse des régions et de la cuisine française.

L'atmosphère de travail était également déterminée par les nombreuses discussions et les suggestions scientifiques. Comme exemple, je voudrais remercier le directeur Michel Gaillard pour avoir suggéré la prise en considération de la rotation empêchée, qui apparait comme le fil directeur de toute ma thèse. Comme représentant de l'ensemble des chercheurs, je tiens à remercier tout particulièrement Pascal Parneix, Pavel Budău, Doina Bejan, Nadine Halberstadt pour toutes les discussions scientifiques.

Ce travail était fait dans un groupe et en conséquence la richesse des différents aspects du sujet nécessitait l'aide de tous les membres du groupe. En particulier, j'exprime ma reconnaissance à Pavel Budău et Pascal Parneix pour toute l'aide sur les aspects de la rétrodiffusion des photoélectrons et l'influence de la couverture d'adsorbats sur une surface, ainsi qu'à Pascal Parneix et Doina Bejan pour une lecture critique de ma thèse et Hélène Lefebvre–Brion pour l'aide sur les finesses de la langue française.

Je suis conscient de tout le support de Gheorghe Raşeev. J'ai apprécié ses qualités humaines autant que son comportement comme directeur de ma thèse. Nous avons eu de nombreuses discussions, parfois vives, mais toujours guidées par le but de l'avancement de la physique et de la clarification des idées scientifiques. Il était toujours prêt à accepter les objections et les idées non conventionnelles. Grâce à son raisonnement scientifique, il y a eu un vrai échange d'idées, qui était essentiel pour la réussite des travaux scientifiques. Je souhaite aussi remercier Osman Atabek, le co–directeur de ma thèse, pour ses remarques critiques et son apport sur les aspects des mouvements des noyaux. Son point de vue complémentaire a bien aidé à une meilleure compréhension des phénomènes physiques.

Je tiens enfin à exprimer ma gratitude à Messieurs C. Girardet et H.–J. Freund pour avoir accepté d'être les rapporteurs de ce travail ainsi qu'à Madame I. Nenner et à Messieurs D. Spaanjard et M. Chatelet pour leur présence en tant que membres de mon jury de thèse.

Mes remerciements sont aussi destinés à l'Institut du Développement et des Ressources en Informatique Scientifique (IDRIS) et Centre des Ressources en Informatique (CRI) pour l'aide technique et la possibilité d'utiliser du matériel informatique.

Cette thèse a été réalisée avec l'aide d'une bourse européenne dans le cadre du projet 'SCIENCE'. *J'encourage toute personne à profiter des possibilités de mobilité que cette époque, ou plus précisément que l'esprit ouvert des peuples accompagné d'une politique européenne nous offre. En effet, ce n'est pas toujours la voie la plus facile, mais pour en montrer l'importance je voudrais terminer par une question: en supposant une bonne volonté, oh combien on apprend sur les points de vue, les problèmes et les espoirs des autres si on est entouré par des nationalités, des cultures et des religions différentes comme celles de la France, d'Israël, de l'Allemagne, de la Russie, des Pays–Bas, de l'Angleterre, du Canada, de la Grèce, des Etats–Unis, du Venézuela, du Brésil, de la Roumanie et de la Turquie ?*

Contents

Part I

Introduction

Introduction

Les gaz, les liquides, les solides et plasmas forment des phases homogènes séparées par des interfaces. Une surface est une interface solide–gaz (ou solide–liquide) ayant des propriétés reliées à l'ordre et à la périodicité du solide. Elle permet l'adsorption des objets microscopiques de la phase gazeuse possédant leur propre symétrie. A l'adsorption, les propriétés électroniques de l'adsorbat changent, une liaison entre avec la surface se forme et les mouvements translationnels et rotationnels deviennent empêchés. Sur la surface, des réactions très spécifiques ont lieu entre adsorbats de nature différente ou entre adsorbats et molécules provenant de la phase gazeuse. En pratique ces types de réactions chimiques ont lieu en catalyse hétérogène à l'interface solide–gaz ou solide–liquide. Elles sont aussi responsables de la corrosion des métaux, apparaissent sur les grains interstellaires et atmosphériques autant que sur les glaciers et les rochers. Les surfaces renforcent ou affaiblissent les liaisons internes de l'adsorbat et créent des nouvelles liaisons adsorbat–surface. C'est la raison pour laquelle les réactions chimiques sur les surfaces sont accélérées, ralenties ou même empêchées. Les surfaces jouent aussi un rôle important pour la dissipation d'énergie qui est libérée pendant une réaction chimique à l'interface ou encore peuvent favoriser des collisions à plusieurs corps.

Un processus utile pour l'étude des interactions surface–adsorbat est la photofragmentation: l'impact photonique produit des photoélectrons ou des fragments nucléaires qui, en quittant la surface, sont analysés en énergie cinétique et angle d'éjection. Les distributions résultantes sont des sondes fines des interactions adsorbat–surface et des mécanismes de photodésorption ou de photoréaction. Dans cette thèse, je traite du point de vue théorique l'influence des mouvements des noyaux sur la photofragmentation des adsorbats moléculaires. Trois domaines sont abordés: la photoionisation, utilisée pour caractériser le complexe adsorbat–surface, le comportement angulaire de l'adsorbat moléculaire en fonction de la couverture (i.e. la quantité d'adsorbats présents sur la surface) ainsi que la photodésorption des adsorbats moléculaires prototype des réactions chimiques en catalyse hétérogène. En photoionisation, le rayon lumineux excite les électrons des couches internes ou de valence dans le continuum électronique leur permettant de quitter la surface et être analysés pour obtenir une image directe de la structure électronique de l'adsorbat. Habituellement, on mesure en fonction de l'énergie du photon la distribution angulaire des photoélectrons et leurs énergies cinétiques. Les mouvements nucléaires de l'adsorbat et de la surface élargissent les raies du spectre de photoélectrons. Si la résolution de l'analyseur le permet, dans des cas proches de la physisorption les mouvements nucléaires de rotation empêchée apparaissent dans les spectres sous forme de satellites. La rotation empêchée présente une particularité étant le seul mode qui change l'orientation de l'axe intramoléculaire modifiant directement la distribution angulaire de photoélectrons.

Dans la littérature, l'interprétation des spectres de photoélectrons est basée sur le modèle de la photoionisation d'une molécule orientée par la surface. Cette orientation change les règles de sélections de transition entre états électroniques et modifie la probabilité d'éjection de l'électron dans une direction donnée. A partir de ce modèle, dit orienté dans l'espace ('oriented–in–space'), on estime l'angle d'inclinaison de l'adsorbat moléculaire par rapport à la normale à la surface [2–10]. Les mouvements nucléaires, en particulier la rotation empêchée qui modifie constamment cet angle, sont complètement négligés. L'énergie du point zéro de ces mouvements nucléaires [11] implique qu'ils sont toujours présents et détruisent le modèle de la molécule orientée et les règles de sélection associées. Par conséquent, ces mouvements doivent être pris en considération dans un modèle de la photoionisation de l'adsorbat moléculaire. Un autre effet de la surface sur le spectre de photoionisation est la rétrodiffusion des photoélectrons [12, 13]. Les électrons, éjectés directement et ceux réfléchis par la surface, interfèrent

modifiant la probabilité d'éjection de l'électron.

Dans la première partie de cette thèse, je dérive un modèle introduisant la rotation empêchée et je discute séparément l'influence de ce mouvement et de la rétrodiffusion des photoélectrons sur les spectres de photoionisation. J'applique le modèle de la rotation empêchée dans le cas de la molécule CO chimisorbée sur Ni(111) ainsi que pour CO faiblement physisorbée sur une surface d'argon [11]. Comparé au modèle de la molécule orientée dans l'espace pour laquelle l'axe intermoléculaire est figé, le modèle que je développe permet l'introduction d'une population de niveaux des états initiaux en fonction de la température. Cette population influence l'angle moyen d'orientation de l'axe intermoléculaire de l'adsorbat et change la distribution angulaire des électrons éjectés. Pour de l'excitation en couche interne du carbone 1s de la molécule CO chimisorbée sur Ni(110), Wesner et ses collaborateurs [14] ont observé expérimentalement un changement de la distribution angulaire relié à la température. Le modèle de rétrodiffusion basé sur un potentiel marche est appliqué à l'étude de la photoionisation de la molécule CO chimisorbée sur Ni en négligeant la rotation empêchée.

Je compare qualitativement les deux modèles évoqués plus haut au modèle de la molécule orientée. Particulièrement, dans le cas de la rotation empêchée, je présente une règle simple, qui permet de prédire d'angle d'inclinaison de l'adsorbat moléculaire en prenant explicitement en considération la rotation empêchée. Je discute aussi la brisure de la symétrie, due à la rétrodiffusion, des spectres de molécules adsorbées en position inclinée par rapport à la normale à la surface.

A ma connaissance, l'influence de la couverture sur les adsorbats moléculaires incluant le comportement angulaire a été négligée jusqu'à présent dans les modèles théoriques microscopiques. Expérimentalement l'adsorption d'un gaz sur une surface est contrôlée par le temps d'ouverture de la valve d'admission et si la pression du gaz n'est pas suffisamment basse, une couverture faible est difficile à atteindre. Même si cette situation est réalisée, le courant de photoélectrons ou des fragments photodésorbés est faible et difficile à mesurer. Par conséquent dans le voisinage d'une molécule adsorbée d'autres molécules sont présentes et leurs interactions mutuelles doivent être prises en considération dans un modèle théorique. En augmentant la couverture, la modification de la forme d'une raie induite par l'adsorbat est observée expérimentalement en photoémission [15, 16]. De plus, la présence des molécules voisines influence les sites d'adsorption et les mouvements nucléaires des adsorbats [17] notamment l'orientation moyenne de l'axe intramoléculaire. Les énergies de la vibration interne changent avec la couverture. Cet effet a été observé par les techniques de spectroscopie infrarouge (IRS: InfraRed Spectroscopy) et de diffraction d'électrons lents (LEED: Low Energy Electron Diffraction) [18]. En utilisant la technique de la désorption intruite par impact d'électron résolue angulairement (ESDIAD: Electron Stimulated Desorption in Angular Distribution) for CO/Ni(110) dans le régime d'une couverture dense, Alvey et ses collaborateurs [19] et Riedl et Menzel [20] ont observé une inclination de l'axe intramoléculaire de 19° par rapport à la normale de la surface dans la direction [100], tandis que à des couvertures faibles la molécule CO est normale à la surface [19, 20]. L'influence de l'orientation de cet axe sur la distribution angulaire des photoélectrons a été expérimentalement observée par Wesner et ses collaborateurs [14] pour CO/Ni(100) en couches internes.

Les résultats expérimentaux évoqués ci–dessus montrent que la couverture influence fortement les mouvements des noyaux de l'adsorbat et donc la distribution angulaire des photofragments. La seconde partie de cette thèse contient les résultats d'une étude utilisant la dynamique classique et d'une analyse par la mécanique quantique de l'influence de la couverture pour CO physisorbé sur Ar(100). Le modèle comporte une surface réaliste construite de trois couches d'atomes d'argon, sur laquelle on dépose jusqu'à

une monocouche de molécules de CO en interaction incluant un terme angulaire d'interaction CO- CO. En comparant le calcul correspondant à une molécule unique à celui d'une monocouche complète, on constate que les positions d'équilibre de l'agrégat de CO et la dynamique de son mouvement sont très différentes [21]. L'analyse quantique de ce modèle classique me permet de mettre en valeur les changements du mouvement de la rotation empêchée dus à la couverture.

La troisième et dernière partie de ma thèse contient un modèle de photodésorption en régime nonthermique valable dans le cas des énergies d'excitations photoniques autour de quelques électron–volts (2–6 eV). La difficulté du développement d'un tel modèle réside dans la découverte du mécanisme qui permet la concentration d'énergie disponible dans le mode de photodésorption, c'est–à–dire la vibration entre adsorbat et surface, et ce dans un temps très court. Entre l'étape d'excitation et l'étape de désorption il y a des processus mal compris que les expérimentateurs et les théoriciens essaient d'éclaircir. Le transfert d'énergie entre les électrons excités par le photon et les noyaux transite par un ensemble d'étapes intermédiaires. Le mécanisme n'est pas indépendant du mode d'excitation de l'adsorbat. Dans le cas de la désorption à température controlée (TPS: Temperature Programmed Desorption), le substrat est chauffé et ces sont les phonons du solide qui transfèrent d'une manière nonrésonante leurs énergies au mode de désorption. Pour la technique de la désorption intruite par impact d'électrons (ESD: Electron Stimulated Desorption) ou photointruite (PSD: Photon Stimulated Desorption) un mode de vibration est initialement excité, suivi par un transfert vers le mode de désorption qui permet la fragmentation. Un mécanisme plus probable que celui évoqué ci– dessus implique l'excitation directe des électrons du substrat ou de l'adsorbat suivie du transfert de l'énergie accumulée, soit directement, soit via un autre mode de vibration, au mode de désorption permettant la fragmentation. Pour certaines énergies d'excitation, ce mécanisme est résonant et on parle de photodesorption en régime nonthermique. Expérimentalement, la désorption nonthermique est mise en évidence par des techniques comme ionisation multiphotonique résonante (REMPI: Resonant Enhanced Multi Photon Ionization) ou fluorescence induite pas laser (LIF: Laser Induced Fluorence) permettant l'analyse des distributions rotationelles, translationelles et vibrationelles des fragments. La photodésorption stimulée par laser permet l'étude des systèmes comme les molécules CO et NO adsorbées sur les surfaces métalliques [22–29] ou leurs oxydes [30–36] dans le regime nonthermique en utilisant les techniques d'analyse des fragments précédemment citées. On observe une désorption nonthermique caractérisée par des fragments ayant des températures de rotation et de vibration élevées bien supérieures à la température thermodynamique de la surface [32]. Si le régime de désorption était thermique l'équipartition de l'énergie engendrerait des fragments ayant une température proche de celle de la surface.

En général, tous les modes électroniques et nucléaires sont couplés et le transfert d'énergie d'un mode à l'autre peut se produire d'une manière indirecte. Une multitude de modèles théoriques de la désorption nonthermique ont vu le jour, mais ces modèles sont généralement limités à un ou deux dégrés de liberté. Dans la dernière partie de ma thèse, je présenterai un modèle introduisant les dégrées de liberté importants pour la photodésorption en régime non thermique. Ce modèle est utilisé pour l'étude de la photodésorption CO/Cu(111) en régime nonthermique ou je calcule et discute les distributions rotationelles translationelles et vibrationelles de la molécule de CO neutre. Expérimentalement, une distribution bimodale de la translation a été observée attribuée d'une part à un canal nonthermique, provenant d'une désorption rapide et résonante et d'autre part à un canal thermique, provenant d'une désorption lente et nonrésonante. Mes résultats, permettent de supposer que les deux composantes de la distribution bimodale ont une origine non thermique la composante lente se superposant au mode thermique.

En résumé, les questions auxquelles cette thèse tente de répondre, sont les suivantes:

- Photoionisation:

  – Comment la rotation empêchée influence les spectres de photoélectrons ?
  Jusqu'à quel point le modèle de la molécule orientée est valable et quelle est l'importance de modification qui entraine sa mise en question ?
  La théorie peut–elle expliquer la dépendance en fonction de la température des spectres de photoélectrons observés expérimentalement ?

  – Quelle est l'influence de la rétrodiffusion des électrons par la surface sur la section efficace de photoionisation ? Existe–t'il des différences entre les spectres des adsorbats moléculaires inclinés ou perpendiculaires à la surface ?

- Influence de la couverture

  – Comment le site d'adsorption change avec le taux de couverture et quels sont les sites préférés dans le cas d'une couverture faible (moins qu'une monocouche) ou dense (une monocouche)?

  – Quel est l'influence de la couverture sur les mouvements nucléaires, en particulier sur la libration et la précession associées à la rotation empêchée ?

- Photodésorption

  – Quelle est l'influence de la multidimensionalité d'un modèle de photodésorption sur le couplage des mouvements nucléaires et les distributions en énergie interne et cinétique des photofragments ?

  – Peut-on imaginer qu'un seul mécanisme de désorption nonthermique soit suffisant pour expliquer les deux composantes de la distribution bimodale de l'énergie translationnelle des photofragments observée expérimentalement?

Introduction

Gases, liquids, solids and plasmas form homogeneous phases separated by interfaces. Usually a solid–gas (or solid –liquid) interface is called surface. It has particular properties related to the ordering and periodicity of the solids but it allows adsorption of microscopic objects from the gas phase having their own symmetry properties. At adsorption the electronic properties of the adsorbate change, a bond between adsorbate and the surface is formed and the free translational and rotational motions of the gas phase become hindered. Adsorbates can react with other types of adsorbed molecules present on surface or with molecules from gas phase giving rise to very specific reaction products. These chemical reactions at solid–gas or solid–liquid interface take place in heterogeneous catalysis. They also cause corrosion of metals and alloys. Similar processes take place also on interstellar, atmospheric grains, on mountain rocks and on glaciers. Surfaces are strengthening or weakening internal bonds of the adsorbate creating new surface–adsorbate bonds. This is the reason why in heterogeneous catalysis chemical reactions are fastened or hindered by the presence of surfaces. The surfaces play also an important role in dissipating energies which can be liberated during a chemical reaction at interface or in favouring many body collision.

A powerful tool to investigate the surface–adsorbate interactions is the photo-fragmentation: after a photon impact one detects the photoelectrons or photodesorbed nuclear fragments with their internal degrees of freedom distributions. These are fingerprints of the characteristic adsorbate–surface interactions and of photo-desorption or photo-reaction mechanisms. The aim of this thesis is to study, the influence of the nuclear motions on photofragmention, using theoretical models. It contains three parts: the photoionization used to characterise the adsorbate–surface complex, the relation between the angular behaviour of the adsorbate and its coverage and the photodesorption of molecular adsorbates as a simulation of an essential step in chemical reactions in heterogeneous catalysis. In photoionization, radiation projects valence or inner shell electrons into the continuum allowing a direct insight in the electronic structure of the adsorbate. One usually measures the photoelectron angular distribution depending on the electron emission angle, the kinetic energy of the photoelectron and the photon energy. The nuclear motions of the adsorbate broaden the spectra and, if the resolution is sufficient, give rise to satellite structures. An exception is the hindered rotation because it is the only nuclear mode that changes also the orientation of the intra-molecular axis of the adsorbate having a strong and direct influence on the photoelectron angular distribution.

For interpretations of photoelectron spectra in literature, the molecule is supposed to be frozen (oriented) in space, selection rules based only on electronic states are derived [37–39] and with them the symmetry of electronic orbitals and the inclination angle of the molecular adsorbate about the surface estimated [2–10]. The corresponding model is known as 'oriented–in–space' model. Strictly speaking this model is not correct. Nuclear motions and particularly hindered rotation are quantum mechanical phenomena and are always present due to their zero–point energy [11]. They break the 'oriented–in- space' model and the corresponding selection rules. Another effect of the surface is backscattering of the photoelectrons by the surface [12, 13]. Interference between direct and scattered waves take place and modify the calculated photoelectron spectrum.

In the first part of my thesis, I will derive a model for hindered rotation of adsorbates and discuss backscattering of photoelectrons. The hindered rotation was studied for strongly chemisorbed CO/Ni(111) and weakly physisorbed CO/Ar systems. Compared to the 'oriented–in–space' model where the intermolecular axis is frozen, in the present model the initial hindered rotational states of the adsorbate are populated

due to temperature. For photoionization, this population influences the mean orientation of the molecular axis and the angular distribution of ejected electrons. Experimentally, a thermal dependent change in angular distribution attributed to hindered rotation has been observed by Wesner *et al* [14]) for inner shell core level excitation of carbon 1s electrons of CO chemisorbed on Ni(110). The backscattering model was studied for CO/Ni neglecting hindered rotation.

In both models, special attention was attached to a qualitative discussion based on a simple model of the breaking of 'oriented-in-space' symmetries due to backscattering and hindered rotation. I will present a simple rule to predict the inclination angle of the adsorbed molecule, taking into account hindered rotation. The influence of tilt angle on backscattering which also breaks the symmetry will also be discussed in this part.

To my knowledge, the influence of the coverage including angular behaviour of the adsorbate, has so far been neglected in the microscopic theoretical models. Because the adsorption of a gas on a surface is monitored by the time the entrance valve is open and the gas pressure not low enough, very low coverage can hardly be obtained experimentally. Even if such an experimental situation is realized, the photoelectron current or photodesorbed fragments yield become very low and difficult to measure. Consequently in the immediate neighbourhood of a molecule several other molecules are present and their mutual interaction have to be considered in a theoretical model. When rising coverage, one observes experimentally a shift of the adsorbate induced peak in photoemission [15, 16]. The presence of near neighbours also influences the adsorbate sites and the nuclear degrees of freedom [17]. The energies of the internal vibration of the adsorbate change with coverage, as observed in InfraRed Spectroscopy (IRS) and Low Energy Electron Diffraction (LEED) [18]. The mean orientation of the intra-molecular axis is also sensitive to coverage effects. In Electron Stimulated Desorption in Angular Distribution (ESDIAD) for CO/Ni(110) at high coverage, Alvey *et al.* and Riedl and Menzel observed an inclination of the intra-molecular axis by 19° from the surface normal in the [100] direction, while at low coverage CO is adsorbed in upright position [19, 20]. I already mentioned, that in photoemission, the orientation of this axis influences the photoelectron angular distribution. So it is not a surprise, that experimentally a dependence of this distribution on coverage was observed by Wesner *et al.* [14] in the case of CO/Ni(100) in core level excitation.

From these experimental results it is evident, that the coverage influences strongly all nuclear motions of the adsorbate and therefore photofragmention distributions. The second part of this thesis contains results of classical dynamical studies and a quantum mechanical analysis for CO/Ar(100) physisorbed system. The model includes a realistic three layers surface, up to one full monolayer adsorbate coverage and an angular term in the adsorbate–adsorbate potential. From a single molecule on surface to one monolayer the position and dynamics of the adsorbate changes strongly [21]. The quantum mechanical approach helps me to detail the changes in the hindered rotation motion due to coverage.

The third and last part of this thesis contains a model for photodesorption in the non-thermal regime valid for photon excitation energies of few electron-volts (2–6 eV). Such theoretical models have to give a mechanism of energy concentration in photodesorption mode, i.e. adsorbate–surface stretch. Usually an electron is excited and finally it transfers some energy to the photodesorption mode. Between these two known stages there is a black box the experimentalists and theoreticians try to study. The electron–nuclei energy transfer can happen by a manifold of mechanisms, that depends also on the excitation technique. In Temperature Programmed Desorption (TPD) the substrate is heated and the phonons of the solid transfer their energies to the desorption mode in a nonresonant way. In Electron Stimulated

Desorption (ESD) or Photon Stimulated Desorption (PSD) one primarily excites a nuclear vibrational mode of the adsorbate, then, due to coupling of nuclear modes, a transfer to the desorption mode occurs giving rise to fragmentation. A more probable mechanism is the excitation of electrons of the substrate or adsorbate, the electronic energy is transfered either directly or via another nuclear mode to desorption and fragmentation occurs. For particular excitation energies, the latter mechanism can be resonant and then one speaks about non- thermal desorption. Experimentally, evidence for this non-thermal desorption is found by analysing the photodesorbed fragments with respect to their translational, rotational and vibrational energies. Examples of such techniques are Resonant Enhanced Multi Photon Ionization (REMPI) and Laser Induced Fluorence (LIF). They allow the measurement of these energy distributions. Many systems, mainly CO and NO adsorbed on metallic [22–29] and oxide surfaces [30–36], were studied by photodesorption stimulated by lasers followed by fragment analysis using such techniques. The main result is that of a non-thermal desorption process can be well characterised by high translational and rotational temperatures of the desorbed molecules, well above the thermodynamic temperature of the surface [32]. In thermal regime the over–all partition of energy does not allow such a situation.

In general, all electronic and nuclear degrees of freedom are coupled and an energy transfer from one mode to another can also process indirectly. There is a manifold of theoretical models for non-thermal photodesorption but none includes the full multidimensionality of the problem. In the last part of my thesis, I present a model, that includes the degrees of freedom essential to describe the photodesorption in non-thermal regime. The application concerns CO photodesorbed from Cu(111) and I calculate and discuss the rotational, vibrational and translation distributions of neutral CO. Experimentally, one observes a bimodal distribution of translational motion, which is attributed to a non-thermal, fast resonant desorption channel and a thermal, slow and nonresonant desorption channel. But, is this the only possible explication or can a non-thermal resonant desorption mechanism explain both components of the bimodal distribution too ?

Summarising , the main questions this thesis tries to answer, are:

- Photoionization:
  - How hindered rotation influences photoelectron spectra ?
    Does breaking of 'oriented–in–space' model occurs and how important is it ?
    Can the theory explain the experimentally found role of temperature on photoelectron spectrum ?
  - What is the influence on the photoionization cross section of backscattering of photoelectrons by the surface? Are there differences between molecules adsorbed upright and species adsorbed in a bent position ?
- Influence of coverage
  - How the site occupation changes with coverage and what are the favoured adsorption sites at low (sub-monolayer) and high (monolayer) coverage?
  - What is the influence of coverage on nuclear motions, especially angular like libration and precession associated to hindered rotation ?
- Photodesorption

- What is the influence of the multidimensionality of a photodesorption model on the coupling of nuclear motions and on photo-fragment energy distributions?
- Can a non-thermal resonant desorption mechanism alone explain an experimentally observed bimodal distribution of translational motion ?

Part II

Photoionization of molecular adsorbates

Résumé

Les spectres des photoélectrons ou de photoionisation ont été utilisés, dès l'avènement des ces techniques, pour caractériser les adsorbats moléculaires. Cette caractérisation consiste en une comparaison entre les spectres en phase gazeuse avec ceux des adsorbats moléculaires. Dans les modèles théorique développés jusqu'à présent, la molécule était considérée comme figée ou orientée dans l'espace avec des règles de symétrie permettant la sélection des transitions dans les spectres des photoélectrons.

Cette première partie de ma thèse discute des phénomènes spécifiques aux adsorbats moléculaires sur les surfaces, négligés jusqu'à présent, comme la rotation empêchée et la rétrodiffusion des photoélectrons. Parmi les divers mouvements nucléaires de l'adsorbat moléculaire, la rotation empêchée joue un rôle essentiel étant le seul mouvement nucléaire, qui change l'orientation de l'axe intramoléculaire et modifie directement la distribution angulaire des photoélectrons. De plus, la rotation empêchée brise la symétrie de la molécule orientée par l'apparition d'un angle d'inclinaison de l'axe intramoléculaire par rapport à la normale à la surface et la précession moléculaire autour de cette normale. L'énergie du point–zéro de ce mouvement et la distribution Bolzmanienne dans l'état initial font que ce mouvement est toujours présent. La rétrodiffusion des photoélectrons modifie l'amplitude et l'angle d'éjection des photoélectrons par l'interférence constructive ou destructive entre les ondes associées aux électrons, directes et celles réfléchies par la surface.

J'ai développé un modèle théorique introduisant la rotation empêchée et étudié la photoionisation de l'électron (4σ) de CO dans la région de la résonance de forme pour deux exemples typiques: la physisorption de CO sur Ar et la chimisorption de CO sur Ni(111). Dans le cas de la physisorption j'ai montré que l'effet de la rotation empêchée est important et place l'adsorbat dans une situation entre celle de la phase gazeuse et celle d'une molécule orientée dans l'espace. Pour la chimisorption dans un arrangement expérimental appelé permis, la modélisation de l'adsorbat orienté dans espace est une bonne approximation, mais l'effet de la population thermique des états rotationnels initiaux se manifeste par un élargissement des structures dans le spectre de photoélectrons. Cet effet a été observé expérimentalement pour l'excitation des couches internes de CO et je montre qu'il provient de la rotation empêchée.

Pour des arrangements expérimentaux appelés interdits qui sont très défavorables à l'émission des électrons, l'intensité dans le spectre est due uniquement à des effets de rotation empêchée ou rétrodiffusion et je présente une méthode simple pour estimer l'angle d'inclinaison en incluant explicitement la rotation empêchée. Cette méthode remplace celle très approximative basée sur les règles de sélection de transition d'une molécule orientée dans espace et permet une estimation de l'importance de la rotation empêchée.

En utilisant un modèle théorique développé dans notre groupe, j'ai discuté la rétrodiffusion des électrons suite à l'impact d'un photon. Cette rétrodiffusion a été introduite en considérant la surface comme un potentiel marche permettant une réflexion partielle des électrons émis. La molécule CO chimisorbée sur nickel a été étudiée dans deux configurations géométriques figées dans l'espace: perpendiculaire et inclinée par rapport à la normale de la surface. Pour une molécule parallèle à la normale les spectres de photoélectrons sont modifiés tandis que pour une molécule inclinée l'interférence des ondes directes et réfléchies, mélange

les symétries moléculaires. Pour minimiser l'effet de la rotation empêchée négligée dans ce modèle, l'arrangement expérimental permi a été choisi. L'étude de la résonance de forme (4σ) montre que l'émission vers la surface est négligeable et par conséquent l'effet de la rétrodiffusion est mineur. Pour la résonance (5σ), il y a une forte émission d'électrons vers la surface et la rétrodiffusion modifie considérablement la distribution angulaire des photoéléctrons.

En résumé, les effets dus à la rotation empêchée et à la rétrodiffusion des photoélectrons ont été négligés dans les modèles développes jusqu'à présent, bien qu'ils modifient d'une manière significative les spectres des photoélectrons. Pour certains arrangements expérimentaux et systèmes adsorbats–surface ces effets sont essentiels tandis que dans d'autres cas ils sont moins importants. Dans tous les cas ils doivent être pris en considération.

Chapter 1

Photoionization of adsorbates: experimental data and theoretical models

The investigation of adsorbate structures are essential to understand processes taking place at surfaces and interfaces particularly heterogeneous catalytical reactions [40]. If a molecule adsorbs on a surface, its electronic structure is changed, bonds are created or their strength modified and consequently the efficiency of chemical reaction is enhanced or inhibited. Photoionization is one of the powerful tools allowing to understand the structure of adsorbates. In PhotoElectron Spectra (PES) the photon energy is fixed and the photoelectron intensity is recorded as function of the electron kinetic energy. In PhotoIonization Spectra (PIS) one varies the photon energy and records only electrons, which leave the ion in a specific final state. The presence of the surface and the bulk introduces a manifold of processes, which complicates the interpretation of the PES and PIS spectra. Normally, one studies different adsorbate–surface systems and compares the PES and PIS to the gas phase spectra. For the detailed understanding of the difference between adsorbate and gas phase spectra a theoretical modelling is essential. This theoretical modelling has the advantage to introduce successively the different phenomena and therefore can highlight their relative importance.

In the following I want to take the widely studied example of CO molecules adsorbed on different substrates and compare its photoelectron spectra to that in gas phase. By appropriately changing the surfaces, one can study their influence on PES, ranging from CO spectrum in gas phase to a strongly chemisorbed CO molecule on palladium metal. In Fig.1.1 Freund and Neumann [41] display photoelectron spectra of different adsorbate–surface systems. The photon energy corresponds to the valence region where excitations of the 4σ,1π or 5σ orbitals of the ground state $^1\Sigma_0^+$ $((1\sigma)^2(2\sigma)^2(3\sigma)^2(4\sigma)^2(1\pi)^4(5\sigma)^2)$ into the electronic continuum are accessible. The kinetic energy distribution of the photoelectrons is measured and plotted against the binding energy $\mathrm{E}_{bin} = h\nu - E_{kin}$.

The binding strength between the molecular adsorbate and the surface can be measured as the condensation (E_{cond}) or adsorption (E_{ad}) energy, shown on the right hand side in Fig.1.1. On the bottom of the Figure, one can see the photoelectron spectrum of CO in gas phase with vibrationally resolved structures corresponding to 4σ,1π and 5σ excitations. Due to adsorption the structures are shifted and broadened as a consequence of many different processes. Among them are the electronic and nuclear motion and interactions, which will be briefly described in this introduction.

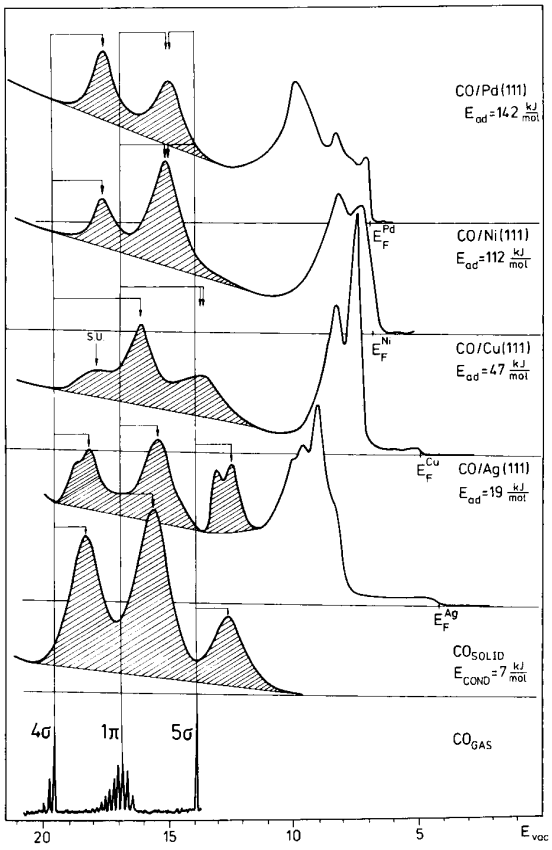

Figure 1.1: *Different adsorbate systems in normal emission, the binding energy $E_B = h\nu - E_{kinetic}$ is given with respect to the vacuum level E_{vac} (from [41]). One can see a shifting of ionization potentials and a broadening depending on the substrates.*

In the following I discuss the interactions between the adsorbate and the different types of surfaces. These interactions act on the electronic and nuclear motions in absence or presence of the incident photon. First, in absence of light the molecule is adsorbed which means that the interactions with the surface are established. For physisorption the electronic interaction is weak and no exchange or significant electronic cloud deformation takes place. For chemisorption the adsorbate–surface interaction may cause electron exchange between the surface or the bulk and the molecular adsorbate. This leads to a modification of the ionization potential.

Now, if ionizing radiation falls on the adsorbate–surface system, the electronic excitation takes place either in the adsorbate or in the bulk. If the energy allows an ionization of the adsorbate, the process of backscattering of photoelectrons emitted from the molecular adsorbate by the surface is the first indirect process that can change the differential cross section [13]. The photon can not only excite or ionize the adsorbate electrons, but also generate such electrons from the bulk or the surface. This is the well known photoeffect and it contributes to the photoionization intensity as a large, nonresonant background. The excited electrons, emitted by either the surface or the adsorbate, can escape directly into the continuum, or they can be scattered by the adsorbate or the surface, giving rise to elastic and inelastic collisions, called backscattering [12, 13]. Because of the high collision probability, the electron–adsorbate collision process is important for high adsorbate coverage.

During the process of photoionization the photon creates a hole in the adsorbate, that is neutralised by electrons from the solid after some time. Two situations can be distinguished. First the energy level of the hole, the unoccupied state, may be degenerate with an electronic solid state. This situation is common for metallic systems, as the electrons in the band structures occupy a wide range of energies. If the interaction between adsorbate and solid is strong (chemisorption), an electron from the solid fills the hole in the adsorbate state. But, owning to the electron–hole interaction, such a process does not depend on the photon energy. It is a competitive, but a nonresonant process and therefore can be considered as a background process. Secondly some electron from a non-degenerate energy level can occupy the hole, which is a common situation for non-metallic systems. The difference in energy may be transferred to other electrons or to nuclear motions. For photoionization of valence state, the electron–hole or neutralisation processes are slow and are part of post–collision processes, not influencing the photoionization cross section.

I want to mention briefly some other electronic processes. In the bulk, there are competitive electronic motions. Electron–hole pairs can be created by photon excitation, that can carry some energy out of the local (photoionization) region. Especially for high photon energy (core level excitation), two electron processes (e.g.Auger) may also take place. The processes mentioned above are not directly related to adsorbates, excited by ultraviolet light in the valence region, and are neglected in this thesis.

Not mentioned up to now are all nuclear motions. Specifically the nuclear motions are associated to phonons of the surface and the bulk, internal vibration of the adsorbed molecule, the adsorbate–surface vibration, hindered translation and rotation of the molecular adsorbate. In photoionization they give rise essentially to broadening (see Fig.1.1), as I detail later in this section. The hindered rotation motion occupies a particular place in photoionization, as it is the only nuclear motion, that modifies the orientation of the molecular axis and therefore influences the photoelectron angular distribution.

Specifically for the CO molecule, chemisorbed on metallic surfaces, a realistic pictural representation of the electronic clouds and interactions is the model of Blyholder [42, 43], represented in Fig.1.2. One can

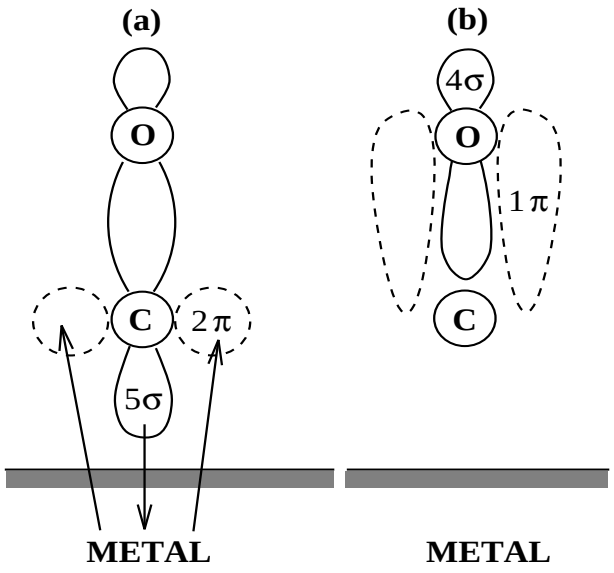

Figure 1.2: *Blyholder model ([42, 43] Fig.from Brodén [44]) On the left part of the Figure (a) the electron orbitals of CO are shown for the occupied 5σ and the unoccupied 2π states as full and dashed lines, respectively. The occupied 4σ and 1π orbitals are shown in the right part (b). There is a electron donation from the molecular orbital 5σ to unoccupied electronic states of the metal and a back-donation from occupied metallic states to the unoccupied 2π orbital.*

see the CO–molecule in upright position on the metal. In this thesis, I am interested in PES/PIS spectra in the energy region of valence shape resonances. For these resonances, the electronic clouds associated with occupied 4σ, 1π and 5σ valence orbitals are essential for the understanding of the photoionization process. One part of the 5σ orbital (full drawn lines in Fig.1.2 (a)) is located at the C end of the molecule and points towards the surface. The electrons from this orbital are donated to the metal and contributes to the formation of the CO metal bond. The metal back-donates electrons that partly fill the unoccupied 2π orbitals of CO (dashed lines in Fig.1.2 (b)), with its lobes parallel to the surface, receive electrons from the bulk. Due to the anti-bonding character of the 2π bonds, the C–O bond is weakened, while the non bonding contribution of the 5σ orbital does not affect the internal C–O bond . The 4σ orbital (full line in Fig.1.2 (b)) is located at the O end, while the 1π orbitals are lying parallel to the internuclear axis. Both 4σ and 1π orbitals are located toward the vacuum and therefore are only weakly influenced by the surface.

While adsorbed the molecule is at least partly frozen in space. In gas phase, there is a free rotation with random orientation of the molecular axis. If one neglects hindered rotation, a strongly chemisorbed molecule may be considered as oriented with respect to the surface and supplementary selection rules can be derived. In the following I describe the model of Davenport, Dill and Dehmer [37, 38], known as 'oriented–in–space' model. In this model the adsorption consists essentially in the orientation of the internuclear axis and all other surface–molecule effects are neglected. The 'oriented–in–space' model has been widely used to derive either molecular orientations or electronic symmetries of PES peaks for chemisorbed [2–8] as well as for physisorbed species [9, 10].

One can derive selection rules for such 'oriented–in–space' molecules, ruling the photoelectron emission

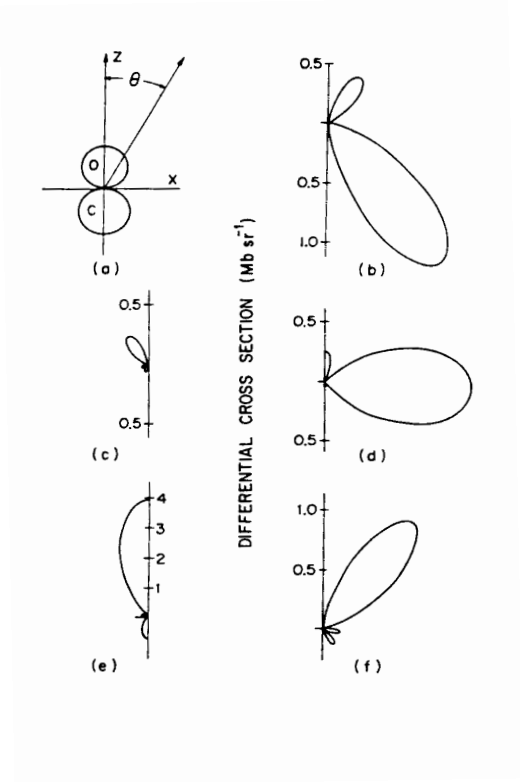

Figure 1.3: *Photoelectron emission of 'oriented–in–space' molecules in the Davenport, Dill and Dehmer model, using linear polarized light. (from Davenport [37]). The intensities are given in polar plot representation, (see (a), where θ is the ejection angle of the photoelectron) for two experimental geometries: (c),(e) polarization vector parallel, (b),(d),(f) perpendicular to z–axis. Curve (b) shows excitations from a 5σ, (c),(d) from 1π and (e),(f) from 4σ orbitals.*

pattern (see [39]). The photoemission intensity is proportional to the square of transition moments. The integrand appearing in this transition moment integral is a product of initial and final total wave functions multiplied by the matter–field interaction. For photonic excitations this interaction can be simply written as $\vec{A} \cdot \vec{p}$, where $\vec{A}$ is the vector potential for the incoming radiation and $\vec{p}$ the electronic momentum operator. In the following, I restrict this matter–field interaction to the one photon absorption in weak photon fields. One can further restrict the interaction to its simplest form, corresponding to the dipole approximation, called dipole transition operator. The selection rules can now be derived by using symmetries under mirror transformations (σ_v) with the mirror plane containing the molecular axis (z-axis in Fig.1.3). In the 'oriented–in–space' model, the initial and final wave functions keep their gas phase symmetries and they are either symmetric (σ, δ ... type) or antisymmetric (π,...) under σ_v transformation. The transition operator can be symmetric or antisymmetric, depending on the experimental geometry: symmetric (or of σ type), if the polarization vector is parallel to the molecular axis ((c) and (e) in Fig.1.3) and antisymmetric (or of π type), if it is perpendicular to this axis ((b),(d) and (e)). In the first set–up only initial and final states are coupled, which have the same symmetry, e.g. $\sigma \leftarrow \sigma$ and $\pi \leftarrow \pi$. In the second experimental geometry the transition operator couples states of different symmetry, e.g. $\pi \leftarrow \sigma$ and $\sigma \leftarrow \pi$. The resulting angular distribution patterns, calculated by using Xα method [45], are shown in Fig.1.3, where a polar plot representation is used, with θ the ejection angle of the photoelectron (see

1.3(a)).

The photon has an energy of 41 eV (He II lamp) and a 5σ ((b) in Fig.1.3), 1π ((c), (d)) and 4σ ((e)), (f)) electrons are excited into continuum. One can see that for 5σ (Fig.1.3(b)) and 4σ (Fig.1.3(f)) excitations, the electron emission normal to the molecular axis (assimilated to the surface normal) vanishes. The angular behaviour of the 1π (Fig.1.3(c)) excitation final state forbids emission in a direction parallel to the internuclear axis. The experimental geometry of the first column is known as 'allowed' (p–polarization of light), whereas that of the second column as 'forbidden' (s–polarization) geometry. They permit to distinguish between σ and π transitions.

Figure 1.4 shows experimental photoelectron spectra of CO/Ni(100) for 'allowed' p– (a) and 'forbidden' s–polarized (b) light at $h\nu = 28$ eV. For the 'allowed' geometry, two peaks appear at 11 eV and 8 eV below the Fermi level E_F. The first peak is attributed to 4σ excitation, whereas the second seems to be a superposition of 5σ, and 1π excitations. In the 'forbidden' geometry, only the $5\sigma/1\pi$ peak survives, but its maxima and form changes. It appears that this peak is due to π excitation and corresponds to $\sigma \leftarrow \pi$ or $\delta \leftarrow \pi$ transitions allowed by the selection rules. Recently a different explanation was presented by Budau and Raşeev [46], which is based on the presence of an allowed $\pi \leftarrow \sigma$ transition for 5σ excitation and a $d\pi$ shape resonance. The explanation was given for the photoionization spectrum but should also apply for photoelectron spectra.

In fact, the 'oriented–in–space' model neglects the surface completely. The surface imposes its local symmetry on the molecular orbitals and the gas phase axial symmetry about the molecular axis is lifted.

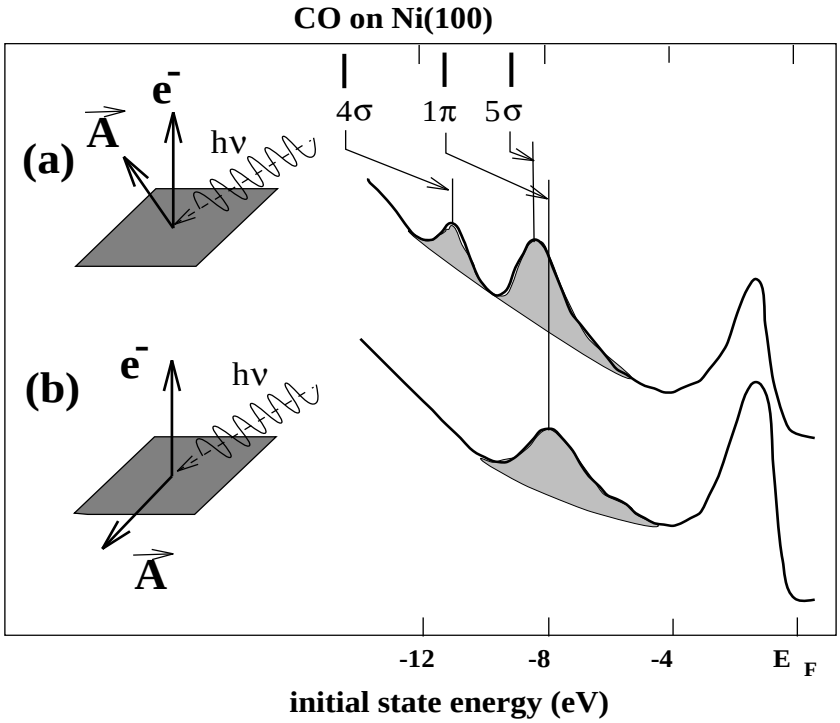

Figure 1.4: *Photoelectron emission at 28 eV for p–polarization ('allowed') (a) and s–polarization ('forbidden' geometry) (b) (from Smith et al. [2]).*

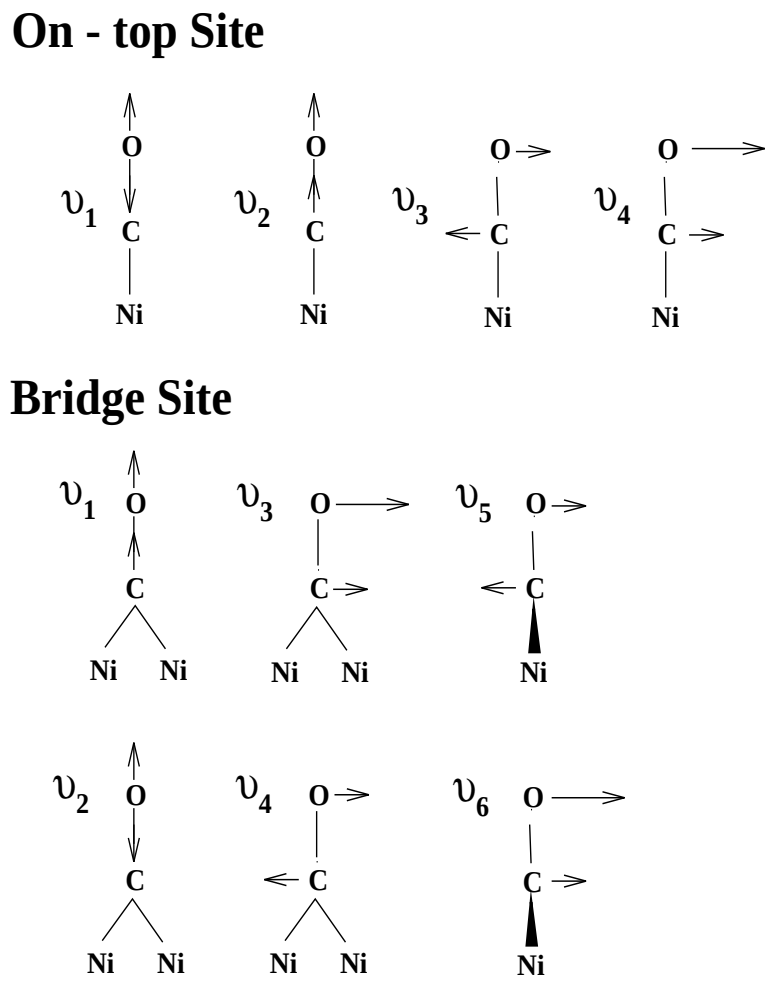

Figure 1.5: *Normal modes of on–top and bridge–bonded CO (from Richardson and Bradshaw [47]).*

In addition, backscattering of photoelectrons from the surface takes place. This effect is known to be important for upright adsorbed molecules [13]. Its influence on tilted molecules is not known up to now and I will discuss the breaking of 'oriented–in–space' symmetries for tilted molecules due to backscattering in this thesis.

In the following, I discuss in detail the nuclear motions and its influence on photoionization spectra. In gas phase the only vibrational model is internal vibration. At adsorption the free translation and rotation of the molecule become hindered due to the surface and new vibrational modes appear.

Figure 1.5 shows the representation of the normal vibrational modes for molecules adsorbed on top and on bridge positions, where the surface is represented as one nickel atom with infinite mass. For on top sites, there are the antisymmetric and symmetric stretches (ν_1, ν_2) of the linear Ni–CO. They correspond to internal CO and to the molecule–surface stretch and are weakly coupled. One can easily distinguish them by their vibrational quantum of energy. Two other vibrations can be identified as the hindered rotation (ν_3) and, in some extend, the hindered translation (ν_4). The (ν_4) motion corresponds to right displacement direction, but no jumping to another adsorption site is allowed. It is worth to mention, that

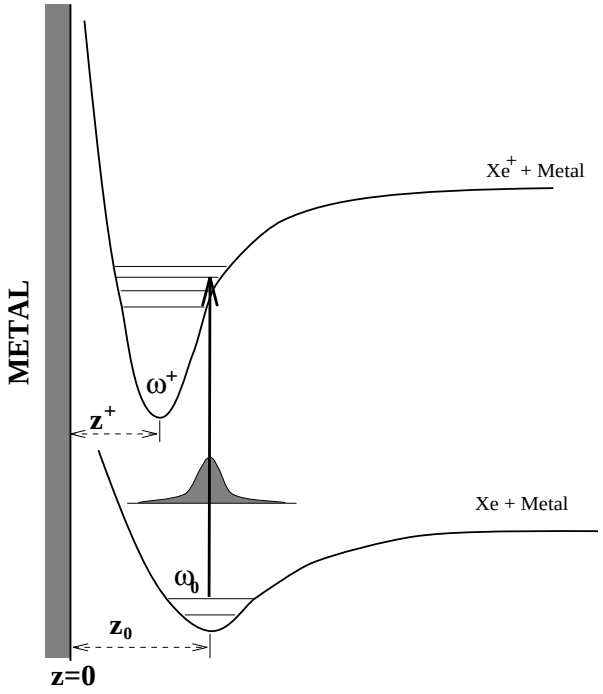

Figure 1.6: *Model of Gadzuk for vibrational excitation after photoionization. Due to the attractive ion – image ion interaction, the potential of the final ionic state is deeper and shifted towards the surface, causing Franck–Condon type excitation of the final xenon–surface vibrational state (from Gadzuk [52]).*

for some systems (CO/Cu) the energy associated to hindered rotation is at the order of the one for the molecule–surface stretch mode and they may consequently be coupled. On bridge adsorption sites, the situation is similar. But, there are additional vibrations, due to vibrations in the plane perpendicular to the surface plane and containing two nickel atoms (ν_1,ν_2,ν_3,ν_4) and out of plane vibrations (ν_5, ν_6).

The nuclear motions discussed above can directly be excited in Electron Energy Loss Spectroscopy (EELS), InfraRed Spectroscopy (IRS) and Helium Atom Scattering (HAS) experiments. They can be seen as resonance structures (IRS) and resonant energy losses (EELS, HAS) in the experimental spectra. As an example, the hindered rotation has been observed in IRS [48, 49], as well as in EELS [50] and HAS [51].

In photoionization, these nuclear modes are not directly excited. The photon excites the molecular adsorbate or the surface electronically. The accumulated electronic energy is then transferred to the nuclear motions. In gas phase, one can observe satellite structure with an energy difference which is typical to nuclear motions. For adsorbates, several surface induced processes may hide these satellite structures associated to this excitation and one observes a broadening, caused by an average over all nuclear motions.

A model to treat molecule–surface vibrations was proposed by J.W. Gadzuk [52] for photoionization of physisorbed xenon atom on platinum surfaces. The potential energy curves as function of Xe–Metal distance z is displayed on Figure 1.6. There is one potential energy curve for the neutral initial and another for the ionic final electronic state after photoionization. The minimum of the initial state potential

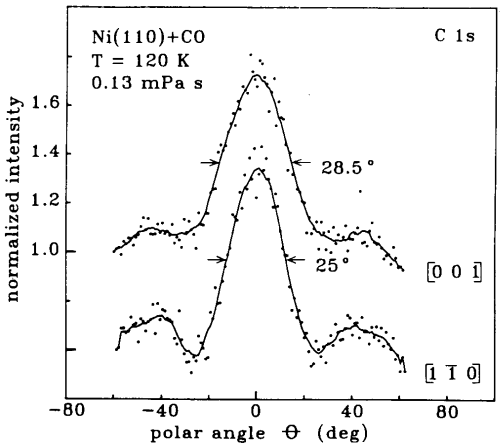

Figure 1.7: *1253.6 eV photoelectrons ionize CO/Ni(110). The polar dependence of the photoelectrons coming from the carbon 1s shell are plotted for electron emission in* [001] *and* [1$\bar{1}$0] *directions and for a sample temperature 120 K, (from Wesner et al. [14]).*

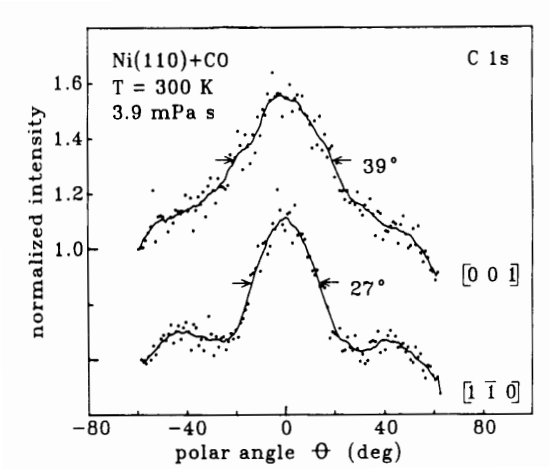

Figure 1.8: *Same set–up as in Fig.1.7, sample temperature of 300 K. (from Wesner et al. [14]).*

is at z_0 and the first vibrational states have a frequency ω_0. The potential of the ionic state is shifted towards the surface and the first vibrational states have a vibrational frequency $\omega^+ > \omega_0$. The reason for this shift is, that the metals behaves as a perfect mirror and the ion creates an image charge. Consequently the attractive Coulomb interaction shifts the potential minimum and deepens the xenon–metal potential.

The photon excites the physisorbed xenon atom and an electron escapes, leaving the xenon ion in some excited vibrational state. In the Franck–Condon picture this vibrational excitation is proportional to the overlap of the vibrational wave functions (Herzberg, p.199 [53]). As the two potential curves are different in shape and their minima are at different positions, the vibrational excitation is expected to be important. Because of the shifting of peaks related to energy conservation and the finite resolution in the experiment, a broadening of the line due to the atom–surface vibration appears and reproduces the experimentally observed broadening. If the sample temperature rises, a larger number of vibrational states of this vibrational mode are Boltzmann populated, giving rise to a larger number of excited final states. Due to the lack of resolution this large number of transitions are not resolved and one sees a temperature dependent broadening of the spectra. This model was developed for a stretching adsorbate–surface, but it can be generalized for all other surface induced modes.

In photoionization experiments, the influence of the nuclear modes described above has been observed as temperature dependent broadening of resonance structures. H. Antonsson *et al.* [54] observed such a broadening in core level photoelectron spectroscopy. Monochromatized Al K_α radiation ionizes the inner shell electrons. The photoelectron spectra show an important broadening of the oxygen 1s and carbon 1s core line profiles for the system CO/Ni(100) c(2$\times$2). The FWHM (Full Width at Half Maximum) is 0.71 eV for C1s and 1.2 eV for O1s excitations at 80 K and increases to 0.96 eV and 1.47 eV at 340 K. Following the argumentation detailed above, the authors explain this broadening by the large number of non-resolved transitions.

One can think that the broadening due to vibration should include the different vibrational modes in an indistinct way. But the broadening originating from hindered rotation can directly be seen in the photoelectron angular distribution (see experiment of Wesner *et al* [14]). In that experiment the inner shell core level carbon 1s electrons of CO chemisorbed on Ni(110) are ionized by 1253.6 eV photons. Due to main contributing $\sigma \leftarrow \sigma$ transition and the high kinetic energy of the electrons ($\approx$ 1000 eV) the photoelectrons are emitted in a small cone around the molecular axis direction. Figures 1.7 and 1.8 show the angular distribution of photoelectrons in two surface directions, [001] and [1$\bar{1}$0] at two temperatures, 120 (Fig.1.7) and 300 K (Fig.1.8). One can see, that in [1$\bar{1}$0] direction the FWHM is 25° at 120 K, where for 300 K the angular distribution is broadened to 27° . Following the authors, the different coverage in the two graphs (0.13 mPa s, 3.9 mPa s) does not explain this broadening. This hypothesis of the hindered rotation influence on the angular distribution is supported by a theoretical model of Thompson and Fadley [55], who introduced in a statistical way the effects of hindered rotation for energetic photoelectrons (0.5–10 keV).

In fact, this experimental study shows clearly that hindered rotation is present for chemisorbed systems. For physisorbed systems, the surface potential governing this motion is weaker and the effects are larger. The experimental facts presented above have determined me to study hindered rotation in photoionization. Beside the effect of broadening the study of hindered rotation presented in this thesis shows other effects, e.g. the breaking down of 'oriented–in–space' selection rules explained in this introduction.

Dispersion occurs, if quantum mechanical properties depend on linear momentum in reciprocal space. In Angular Resolved Ultraviolet Photoelectrons Spectroscopy (ARUPS) one can cite the dependence of ionization potentials of a single adsorbate, which may vary with respect to the ejection direction of the electron and therefore to the momentum in reciprocal space.

Finally there is an effect of coverage on adsorbate and photoionization spectrum. This effect influences the nuclear motions like hindered rotation and will be presented in part III of this thesis [21]. The coverage can also change the electronic properties of the adsorbate. At high coverage these adsorbed molecules can be close to each other and form by orbital overlapping two–dimensional Bloch states [41]. This kind of dispersion can by measured by ARUPS. In the PES, the maxima energetic position of the different ionizations again depends on the electron emission angle and therefore on the linear momentum wave vector parallel to the surface. Dispersion appears if the energy position of a maximum varies with this linear momentum wave vector. Rieger [56] measured the dispersion of the $(4\sigma)^{-1}$ and $(5\sigma)^{-1}$, $(1\pi)^{-1}$ ionization for CO/Ni(100) c(2$\times$2) and found a variation of 0.21 (0.24) eV and 0.19 (0.27) eV along the [100] $\overline{\Gamma} - \overline{X}$ ([110] $\overline{\Gamma} - \overline{M}$) direction for $(4\sigma)^{-1}$ and $(5\sigma)^{-1}$ excitations, respectively.

Summarising, there are different open questions for photoionization experiments, which I will try to answer in the photoionization part of this thesis.

- What is the role of backscattering of photoelectrons by the surface ? Are there differences between molecules adsorbed upright and species adsorbed in a bent position ?
- How hindered rotation influences photoelectron spectra ?
  Does breaking of 'oriented–in–space' model occur and how important it is ?
  Can the theory explain experimentally found role of temperature on photoelectron spectra ?

Chapter 2

Theoretical model

In this chapter I present a recently published model [11] for photoionization of diatomic molecules adsorbed on surfaces including hindered rotation. It includes the electronic motion necessary to explain photoionization in the hν=11 - 50 eV region as well as one of the nuclear motions of the adsorbate: the rotation of the diatomic adsorbate hindered due to the surface. This nuclear motion is the only nuclear mode, which changes the orientation of the molecular axis of the adsorbate and therefore influences significantly the photoelectron angular distribution. The present chapter is divided in three parts:

First, a general overview is given in 2.1. In order to classify the relative importance of phenomena taking place for adsorbed species, I present in section 2.1.1 the energies and characteristic times. This helps me to justify the approximations used in the theoretical model (2.1.2). The next section 2.2 starts by defining the different coordinate systems attached to the preferential directions (incoming photon, surface, molecular axis of the adsorbate and the escaping electron). Experimentally, all observables like differential cross sections are measured in laboratory frame. Theoretically, the results of the theoretical calculation should be presented in this frame. But, some calculations become less difficult in the molecular frame, which is attached to the molecular axis. To connect the directions mentioned above and transform the results of calculation to the laboratory frame, one performs frame transformations presented in section 2.2.

Secondly, the present model is based on the Born–Oppenheimer approximation, separating the calculation of the electronic motion from the nuclear ones. The section 2.1.2 discusses this approximation, defines the laboratory coordinate system and frame transformations and gives the expression of the total photoionization cross section. The electronic part of the theoretical model is presented in section 2.3. In subsection 2.3.1, I describe briefly the ab–initio method used to calculate the electronic wave functions and photoionization transition moment. This moment can be used in different expressions of the cross section. The simplest one is based on the 'oriented–in–space' molecule, that neglects all nuclear motions (2.3.2) and is not valid for tilted molecular adsorbates. The same electronic transition moment can be used as a starting point for models introducing tilted molecules (2.3.2,2.3.4) and backscattering of photoelectrons by the surface (2.3.3). In the following section 2.3.4, I discuss qualitatively the effects of inclination of adsorbed molecules on the photoionization cross section, highlighting the difference between the 'oriented–in–space' (normal to the surface) model and a model, taking explicitly into account the inclination.

Thirdly, the hindered rotational motion is introduced in section 2.4. The starting point is the calculation of the corresponding nuclear wave function for the initial neutral and the final ionic state (subsection 2.4.1). New formulae for the photoionization differential cross section, including now the hindered rotation, are derived in subsection 2.4.2.

2.1 Overview

2.1.1 Energies and time scales

In the following I discuss the energies of the processes, which are taking place at surfaces, and the associated characteristic time scales. The characteristic energies depend strongly on the surface, bulk characteristics and the adsorbate coverage.

First I discuss the nuclear motions of the adsorbate, shown in Table 2.1. Some nuclear motions are strongly influenced by the surface. The translation of a molecule in space is free and becomes hindered due to the surface, giving rise to CO–surface stretch and hindered translation in the plane of the surface. For this hindered translation the associated energies are discretized, the adsorbate is either trapped by the surface well, or it becomes nearly free and may be allowed to move across the surface. The energy associated to the molecule–surface stretch is strong and causes deep potential well and high discrete energies. The rotation of the molecule is also strongly influenced by the surface. Depending on the type of the surface, one sees a considerable change in rotational energies. For CO in gas phase, the difference in rotational energies levels is about few cm^{-1}. This difference is increased by a factor of 100 for strongly chemisorbed species. The internal vibration of the CO–molecule (C–O stretch) is only slightly influenced ($\leq$10%) by adsorption.

It is interesting to look at 'characteristic' times associated to each motion. Below, the characteristic energies and times in photoionization are discussed. The hindered rotation can be taken as a 'clock' of the system and one can compare the other motions to it. This clock determines, if photoionization is a fast or a slow process.

From the quantum mechanical point of view one distinguishes stationary and decaying states. In photoionization, all nuclear motions, as hindered rotation, correspond to stationary states, which are eigensolutions of the Schrödinger equation with a well defined energy. If photodissociation processes do not contribute, these states can be considered to be stable and the distributions of their positions and momenta are time independent (see Messiah, p.137 [65]). Consequently the associated lifetimes are infinite. But, a classical oscillation time can be calculated and be taken as a characteristic time.

The escaping electron is described by a propagating dispersing wave packet, for which the distribution of positions and momenta is time dependent. Therefore one can write the uncertainty relation $\Delta E \Delta t \geq \hbar$, which connects the energy of the particle and a characteristic time ([65], p.136), which is an escape time from some spatial region. The process of photoionization in the presence of shape resonances is connected at least to two states (initial/final), which are coupled by the photon. In such a case, one can speak of a decay time of the initial into the final state. If one supposes, that one mechanism dominates the process, the characteristic time Δt associated to this decay mechanism is directly related to the experimental width of a resonance by the uncertainty relation given above.

	Chemisorption	Physisorption	gas phase
internal vibration C–O	2088 cm^{-1}	2145 cm^{-1}	2143 cm^{-1}
CO–surface stretch	437 cm^{-1}	37cm^{-1}	————
hindered rotation	411 cm^{-1}	20 cm^{-1}	5 cm^{-1}
hindered translation	82 cm^{-1}	26cm^{-1}	continuous
phonons	32–180 cm^{-1}	80 cm^{-1}	————
shape resonance (4σ) (FWHM)	$\approx$ 80000 cm^{-1}	not known	$\approx$ 80000 cm^{-1}
electronic autoionization (FWHM) in C1s excitation	10500 cm^{-1}	not known	6400 cm^{-1}

Table 2.1: *Typical energies for the photoionization process and the nuclear motions for chemisorbed, physisorbed and molecules in gas phase, respectively. As chemisorbed species CO/Ni(100) was chosen and the values for internal vibration C–O, CO–surface stretch, hindered rotation and translation have been obtained by Richardson and Bradshaw from a cluster calculation CO/Ni(100) [47]. The widths of shape resonance electronic autoionization of C1s excitation are taken from Allyn et al. [57] and Björneholm [58], respectively. Those for gas phase are taken from Leyh [59] and W.Eberhardt et al. [60]. As physisorbed system I chose CO/Ar and the values are obtained from classical trajectory calculation by Parneix [61] or from quantum mechanical methods (hindered rotation: Table.3.1 in this work). The value for internal vibration for CO/Al obtained by Bertolo [62] is taken as prototype of a physisorbed system. The phonon frequencies for nickel and argon solid are taken from Berndt et al [63] and Gupta and Gupta [64], resp.*

The energies given in Table 2.1 imply some characteristic times, which are shown in Table 2.2. The classical oscillation times were calculated by taking the experimentally known energies, assuming the potential to be harmonic and finally calculating the oscillation period in the classical limit. The hindered rotation has to be treated in a different way due to its twodimensionality, but the same guideline, mentioned above, was used (see Appendix B for more details). In fact, one can distinguish two motions, precession, the molecule is spinning around the surface normal at some inclination angle, and libration, the molecule is moving in a plane perpendicular to the surface. The associated times are found to be comparable for chemisorbed systems. For chemisorbed CO, the hindered rotation characteristic time is quite short (10^{-13} s), much shorter than the one of CO in gas phase (10^{-12} s). This fact can be explained as follows. For CO adsorbed on top of Ni, CO is oriented nearly normal to the surface and the hindered rotation potential is strong. Therefore a fast libration with small amplitudes takes place. The corresponding momentum of inertia is small, giving rise to a fast precession around the surface normal.

Compared to the characteristic time of rotation, slow and fast excitation processes can be distinguished. The full collision of a slow electron with an adsorbate in an usual EELS experiment takes place slowly in 10^{-12} – 10^{-14} seconds. During this time an efficient exchange of energy between the approaching/escaping electron and vibrational excitation (e.g. hindered rotation) takes place. Enhanced peaks in the electron spectra are observed, indicating the efficient excitation of vibrational modes. PS/PIS techniques are related to half collision process, the range of photon energies is wide and the escaping photoelectron may be slow or fast. As an realistic example, the direct photoionization for an electron, escaping with 12 eV kinetic energy (see Table 2.2) is fast and from the width of the resonances (Table 2.1), their decay times can be estimated to 10^{-15} and 10^{-16} seconds for electronic autoionization and

	Chemisorption	Physisorption	gas phase
internal vibration C–O	10^{-14}	10^{-14}	10^{-14}
CO–surface stretch	10^{-13}	10^{-12}	———
hindered rotation	10^{-13}	10^{-12}	10^{-12}
hindered translation	10^{-11}	10^{-11}	———
phonons	10^{-13}	10^{-13}	———
relaxation	10^{-16}	10^{-14}–10^{-15}	———
direct photoionization (electron of 12 eV)		10^{-15}	
shape resonance (lifetime)	10^{-16}	10^{-16}	10^{-16}
electronic autoionization in C1s excitation	10^{-15}	—	10^{-15}
reneutralization	10^{-16}	10^{-14}–10^{-15}	———

Table 2.2: *Typical times scales in seconds for the photoionization process and the nuclear motions for chemisorbed, physisorbed and molecules in gas phase, respectively.*

shape resonances, respectively. Therefore the photoionization process in the 30–50 eV energy region of shape resonances (E_{kin}=12-55 eV) is faster than the characteristic time for hindered rotation ($\approx 10^{-13}$ s).

An additional electronic process can happen: the neutralisation of a electron hole in the bulk, created by the incoming photon. The associated times are short for chemisorption systems, (see Table 2.2) (10^{-16} s), but in general quite longer for physisorbed systems (10^{-14}–10^{-15}). As already explained before, neutralisation of chemisorbed adsorbates is a competitive, but nonresonant process, it may change quantitatively but not qualitatively the photoionization cross section. For non–metallic systems it can be considered as a post–collision process, which does not in influence the photoionization cross section.

Finally, the surface and bulk electrons behave as a bath and receive the energy directly from the photon or through an intermediate process, created by it. For example, if by photoionization of an adsorbate an ion is formed, the electrons in the solid reorganise themselves and create a charge image. The time of this reorganisation is determined by the bandwidth of electron band of the surface or the bulk. For metallic systems, the width of the conduction band is large and the time of relaxation is short (10^{-16} s). In section 3.2.2, I take advantage of the fast relaxation to build a surface potential for the final ionic state of CO/Ni(100).

2.1.2 Framework of the model

In this subsection I describe briefly the approximations, that are used in the present theoretical model for photoionization. Recall, that experimentally one is interested in resonance phenomena like shape resonances and autoionization taking place in photoionization of molecules in the energy region of valence and core levels excitations. For the photoexcitation process, generated by weak light intensities ($\leq 10^{10}$ W/cm^2), the initial neutral and final wave functions (ion + continuum electron) are coupled through the dipole transition operator. This is a good approximation for the experimentally used light

sources, mainly synchrotron radiation and rare gas lamps.

In photoionization of adsorbates one measures the photoelectron intensities of electrons in laboratory frame, defined by the surface normal and a preferential direction on the surface. The ejection probability of the electron depends also on the position of the molecular axis and on the direction of the incoming photon. Therefore there are four different preferential directions in space: the incoming photon, the surface normal, the molecular axis and the escaping electron. These directions create four different coordinate frames, in which quantum mechanical quantities of the related particles are expressed in their simplest way. A realistic model introducing electronic and nuclear motion in a dynamical process like photoionization should express the calculated cross section in laboratory frame. It further should apply the appropriate coordinate systems for the electronic and nuclear motions. In the models published up to now, the direction of internuclear axis was always identified with the direction of the laboratory z–axis. This can generate misleading conclusions in the analysis of the experimental data.

The ionization is an electronic process, which is weakly coupled to nuclear motions of the adsorbate. In the presence of resonances, this coupling can be enhanced. If one compares the time scales given in the previous subsection, one can see, that for photoionization in the presence of shape resonances, the characteristic decay times are shorter than the nuclear motions. Consequently, the molecular adsorbate can be considered as frozen during the photoionization process and the Born–Oppenheimer approximation can be applied for the initial and final states. If further the parametric dependence of the electronic wave function on nuclear motions is neglected, the Franck–Condon approximation (see Herzberg, p.199 [53]) is applied. The electronic part of the total wave function can be calculated at some mean values of the nuclear coordinates and the dependence on the nuclear degrees of freedom appears in the nuclear wave functions only. The transition moment is then a product of an electronic and a nuclear parts.

In this work on photoionization, one of the nuclear modes is taken into consideration: the rotation of the adsorbate hindered by the surface. It is the only mode, that changes the orientation of the molecular axis and therefore influences strongly the angular distribution in photoelectron emission. The other nuclear motions, like internal vibration, hindered translation and adsorbate–surface stretch and surface or bulk phonons, are neglected here. The surface potential that governs the hindered rotation is taken to be axial symmetric. The author verified, that this approximation is justified for on–top adsorption sites (CO/Ni(100), CO/Ar) in a low coverage limit. Evidently this is not true for bridge sites and/or for high coverage environment. The potential is different for the initial and final electronic state, essentially because of the presence of the ion and image charges in the final state.

The present model uses the energy and angular momentum conservation laws. For the energy, bulk effects, like excitons, are considered as a post–collision process. The angular momentum is also conserved in the final state. The electron escapes with its momentum and the ion is first found in a state that conserves the total angular momentum of the system. Therefore any momentum transfer from the adsorbed ion is considered as a post collision process.

On the level of electronic surface effects, the excitation of electron–hole pairs are neglected (excitons). In contrast to the photoionization, which is a local phenomena, this kind of excitation is non local, but does not qualitatively influence the numerical calculation. It may broaden the resonances or it may carry some energy out of the local adsorbate region, but does not significantly change the angular distribution. As I want to study the influence of the hindered rotation on valence shell excitation, all neutralisation effects are also neglected for the photoionization itself and they are taken to be post–collision processes.

Up to now, I have briefly presented the framework of the present model, independent of the specific approximations related to actual applications. The electronic transition moments were calculated numerically reducing the initial and final state to a bound initial and continuum final molecular orbital belonging to the same molecular basis set. The final continuum orbital was calculated in the Frozen Core Static Exchange (FCSE) approximation with exchange ([66]). Further, these molecular orbitals were not perturbed by the surface. The backscattering was introduced for CO/Ni(111) as a step potential. For the hindered rotation the surface was simulated by only one atom for CO/Ni and CO/Ar. No simultaneous introduction of backscattering and hindered rotation was considered in this thesis.

Summary of the Framework of the model:

- weak photon intensities (dipole approximation)
- Born–Oppenheimer, Franck–Condon approximation allowing a two step model:
  - electronic motion
  - nuclear motion
- realistic (experimental) coordinate system allowing tilted molecules and nuclear motions
- conservation of total energy and angular momentum
- initial and final electronic states calculated by ab–initio models
  - one electronic configuration for initial and final states
  - continuum electron wave function calculated numerically in the FCSE approximation
  - backscattering of electrons using a step potential (without hindered rotation) from an isotropic surface
- all nuclear motions are neglected, but the hindered rotation using axial symmetric surface potential
- no post–collision processes as neutralisation or energy relaxation during photoionization
- hindered rotor wave function, calculated as a linear combination of free rotor functions calculated in realistic surface potential
- different surface potential for the hindered rotation motion of the adsorbate in the initial and final states

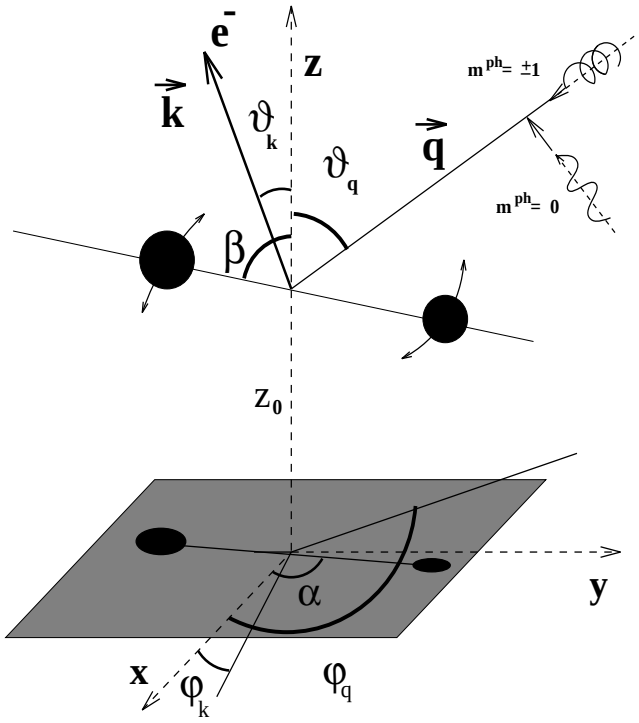

Figure 2.1: *Laboratory coordinate system. The z–axis is oriented normal to the surface. The centre of mass of the molecule is situated at a distance of z_0 from surface, while the molecule makes an angle β with z and the other two Euler angles are α and γ (not represented). The electron is ejected along $\vec{k}$ (ϑ_k, φ_k) and the photon is incident in the direction $\vec{q}$ (ϑ_q, φ_q) (see text).*

2.2 Coordinate systems, frame transformations and cross section

Fig.2.1 represents an image of the photoionization of an adsorbed molecule. At the bottom of this figure the surface is represented as a structureless plane and the laboratory z–axis is defined normal to it. Four preferential directions are present for photoionization processes: the incoming photon, the surface normal, the internuclear axis and the direction of the electron. In a theoretical formulation, all observables, measured in experiment, are expressed in the laboratory coordinate frame, which can be identified with the surface one with the z–axis parallel to the surface normal.

The position of the diatomic molecule (Fig.2.1) with respect to the surface (laboratory) coordinate system is given by six coordinates: Three spatial coordinates of the centre of mass (CM), called x_0,y_0 (not indicated on Fig.2.1) and z_0, two angles (α, β) indicating the orientation of the molecular axis with regard to the surface and the internuclear distance R. The angle α encloses the projection of the internuclear axis onto the surface and the x–axis, while β is defined as the inclination angle between the internuclear axis and the surface normal (z–axis). Throughout this thesis, I use these three Euler angles α, β and γ, although only two angles are independent for a diatomic molecule. The first two angles are already defined above, while γ (not shown here) connects the two coordinate systems, one attached to the surface and the other to the molecule, in a more complicated way (see e.g. Zare, p.78 [67]).

Now a photon hits the adsorbate and a photoelectron escapes. There are two additional preferential

directions, one given by $\vec{q}$ (photon), the other by $\vec{k}$ (photoelectron) (see Fig.2.1). According to the literature ([68]), for circular polarized light ($m_{ph}=\pm 1$), the photon incident direction $\vec{q}$ is defined by the photon momentum and its quantisation axis. For linear polarized light ($m_{ph}=0$) the polarization vector $\vec{\varepsilon}$ of the incoming light defines $\vec{q}$. The linear momentum $\vec{k}$ of the escaping photoelectron gives the second preferential direction. Each of the two directions in space is described by two angles relative to the surface system: ϑ_q, φ_q (photon) and ϑ_k, φ_k (electron).

The coordinate system shown in Fig.2.1 allows the introduction of all adsorbed molecule nuclear degrees of freedom: the adsorbate–surface vibration (z), the internal vibration (R), the hindered translation (x , y) and the hindered rotation (α, β, γ), but also the backscattering of the photoelectrons from a tilted molecule. The 'oriented–in–space' model, introduced in section 1, eliminates the angular motion of the molecular axis and can be used without approximation only for molecules adsorbed normal to the surface.

For an isotropic surface, the two spatial variables x and y of CM or the angle α, indicating the molecular orientation, can be chosen arbitrary. If an observable changes with the angle α, the surface must be considered as anisotropic and one can measure this variation as the dispersion in α of the observable. As already cited in section 1, we may find such a case for molecules in an environment, which owns a low symmetry, e.g. 2–fold bridge sites. The low symmetry can be induced by corrugation of the surface or by the presence of near neighbours (dense coverage) [21].

For clarity, I represented in Fig.2.2, the different directions discussed above. Each operator or wave function has its simplest representation in its natural coordinate system. Experimentally, the surface coordinate system ((s) on Fig.2.2) is the reference systems for all observed quantities like the linear momentum of the escaping photoelectron and its spin polarization in molecular frame. But, the simplest expression and the most straightforward calculation of the electronic part of the cross section is in molecular frame (indicated by a subindex mol, and as (m) in Fig. 2.2). For the hindered rotation of the adsorbate the natural coordinate system is the laboratory frame. For the photon and the electron (photon: (p) in Fig.2.2, electron: not shown), the natural coordinate systems are obvious. In the following, I present the wave functions (electronic, hindered rotation), the transition operator, the integral giving the transition moment and the transformations in detail.

The starting point for both the initial and final state is the Born–Oppenheimer approximation, expressing the total wave function as a product of an electronic ($\psi_{\Omega,\vec{k}}$) and the nuclear part.

$$\Psi^{tot}_{M,\Omega,n,\mu,\vec{k}}(\{\vec{r}\}_N, \vec{R}) = \quad \psi_{\Omega,\mu,\vec{k}}(\{\vec{r}\}_N; R) \quad \Theta^n_{M\Omega}(\hat{R}) \tag{2.1}$$

In 2.1, the spatial positions of all electrons are represented by $\{\vec{r}\}_N$=($\vec{r}_1$, ..., $\vec{r}_N$), $\vec{R} = (\hat{R}, R)$ describes the orientation ($\hat{R}$) of the internuclear axis and the distance of the two nuclei (R) both in laboratory frame. The linear momentum of the escaping photoelectron in the final state is $\vec{k}$=(ϑ, φ, k) and has to be omitted for the initial state wave function. The projection of the spin of the photoelectron onto the surface normal is$\hbar\mu$ and has also to be omitted for initial state wave function.

Throughout this thesis, I neglect all nuclear motions, but the hindered rotation. Therefore the nuclear wave function ($\Theta^n_{M\Omega}$) in equation 2.1 simplifies to the one for hindered rotation. M and Ω are the quantum numbers, that represent the projections of the total angular momentum onto the surface normal

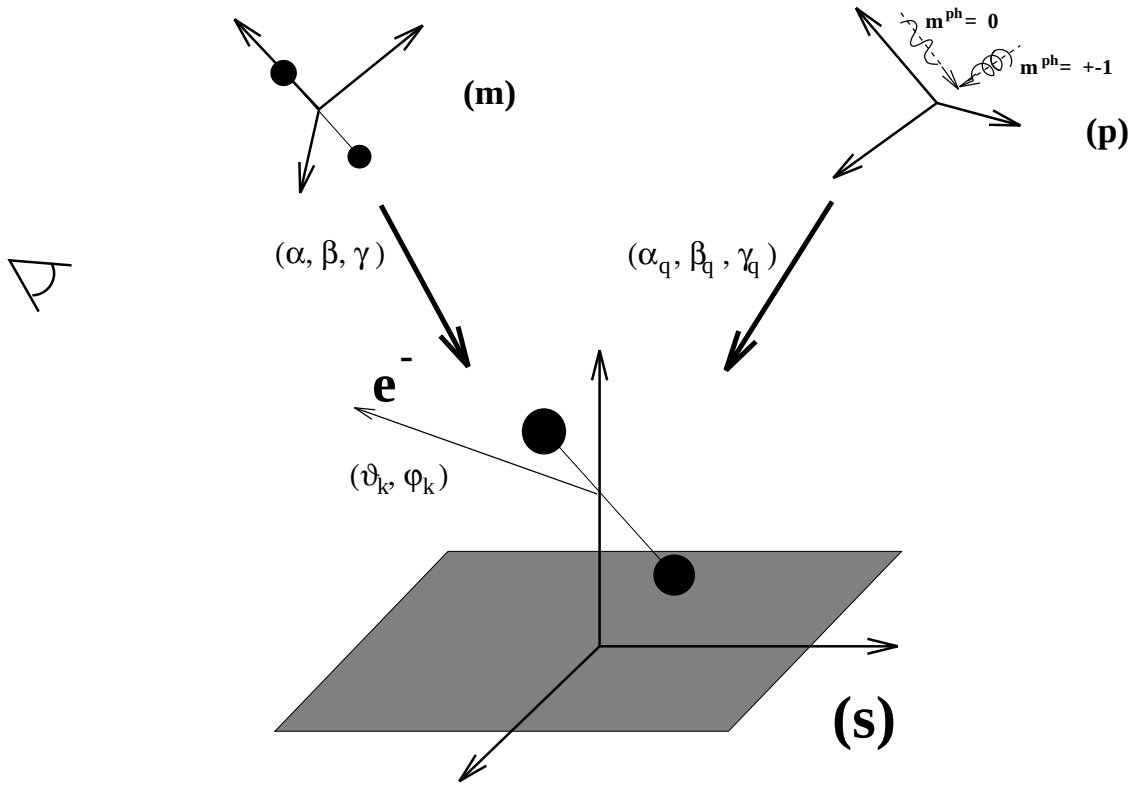

Figure 2.2: *Frame transformations for molecular adsorbates. Each of the wave functions/operators associated to the different particles is defined in its own coordinate system and has to be transformed in one common frame (see arrows and transformation angles). The dependences of the used qualities on observables must be expressed in the surface frame (s), while those on position in space have to given with respect to the molecule frame (m).*

and the molecular axis, respectively. n ($n \geq |(M,\Omega)|$, integer) is a label for the energy levels of the hindered rotor. In the present approximation M, and Ω, are assumed to be good quantum numbers (see section 2.4.1). This is the axial symmetry approximation which means that the adsorbate–surface system is invariant under the rotation about the surface normal. In the model detailed in 2.4.1 I suppose Franck–Condon approximation, i.e. the radial electronic wave function does not depend parametrically on $\hat{R}$. The hindered rotation wave function is obtained by solving exactly the Schrödinger equation in axial symmetry approximation. No average operator for rotation is introduced like when considering the coupling between stretching and rotation, in the infinite order sudden approximation [69].

For photoionization experiments, which do not resolve the spin polarization of the photoelectron [70,71], the following formula for the differential cross section for photoionization (${}^{m^{ph}}\mathrm{I}(\vec{k},\vec{q})$) depending on the incident photon angles $\hat{q} = (\vartheta_q, \varphi_q)$, the absolute value of the linear momentum (k) and the direction of the escaping electron ($\hat{k}$=ϑ_k, φ_k)) holds:

$$ {}^{m^{ph}}\mathrm{I}\,{}^{\Omega^+}_{\Omega^{"}}(\vec{k},\vec{q}) = N_E \sum_{\mu} \left| \left\langle \psi_{\,\Omega^+,\mu,\vec{k}}(\{\vec{r}\};R) \quad \Theta^{\,n^+}_{\mathrm{M}^+\,\Omega^+}(\hat{R}) \right| {}^{m^{ph}}\tilde{\mathcal{T}} \left| \psi_{\,\Omega^{"}}(\{\vec{r}\};R_0) \quad \Theta^{\,n^{"}}_{\mathrm{M}^{"}\,\Omega^{"}}(\hat{R}) \right\rangle \right|^2_{\{\vec{r}\},\vec{R}} \tag{2.2} $$

Here N_E is the normalisation constant, given explicitly in section 2.3.2 below. As one can see from equation 2.2, the dipole operator ${}^{m^{ph}}\tilde{\mathcal{T}}$ couples the initial ($\Omega^{"}$, $\mathrm{M}^{"}$, $n^{"}$) and the final ($\Omega^+, \mu, n^+, \mathrm{M}^+$) state. This operator for dipole transitions reads ([72], p.170):

$$ {}^{m^{ph}}\tilde{\mathcal{T}} = \sqrt{\frac{4\pi}{3}} r_{photon} \mathrm{Y}_{1\,m^{ph}}(\hat{r}_{photon}) \tag{2.3} $$

Here, $\vec{r}_{photon}$ is the electron position vector in the photon frame ((p) in Fig. 2.2) with its absolute value r_{photon} and orientation $\hat{r}_{photon}$=(ϑ_q, φ_q). $\mathrm{Y}_{1\,m^{ph}}$ is the spherical harmonics with m^{ph} as the projection of the photon spin onto the surface normal.

I summarise below the transformations and calculations needed to obtain the photoionization cross section:

For the electronic transition moment:

- The transition operator is initially given in photon frame (eq.(2.3), see (p) in Fig.2.2). The transformation from the photon frame to the molecular frame is performed in two steps, shown in Figure 2.2:
  - First, one passes from the photon (p) to the surface frame (s). This transformation is a rotation, described by three Euler angles $\alpha_q, \beta_q, \gamma_q$=$\hat{q}$.
  - Secondly, one has to transform the dipole operator from surface (s) to the molecular frame (m), given by second rotation with the angles $-\alpha, -\beta, -\gamma$=$-\hat{R}$ ($\hat{R}$: orientation of the molecular adsorbate).
- The calculation of the electronic transition moment is most simply performed in the molecular frame. To obtain the transition moment, one performs an integration over all spatial positions $\{\vec{r}_{mol}\}_N$. However, the transition moment depends on $\vec{k}$ and this moment must be converted to laboratory frame:
  - A rotational transformation (α, β, γ) transforms the final wave function depending on the linear momentum $\vec{k}$ from molecular (m) to the surface (s) frame. The spatial dependence of the photoelectron spin wave function is also given in this frame and must be transformed in the same manner.

For the rotational motion:

This motion is defined in laboratory frame and no transformation is required.

After these frame transformations and integrations, one obtains the photoionization cross section (2.2) for the ejection of an electron in direction $\vec{k}$ defined in laboratory frame.

2.3 The electronic motion

In the last section, I explained, that the calculation of the electronic transition moment is performed in molecular frame and then transformed to laboratory frame of the experiment. In this section, I detail the method used in the calculation of this electronic transition moment: ab–initio methods in section 2.3.1, transformation to laboratory frame and the expression of the cross section for the general case of tilted molecules in section 2.3.2. I show, that the present formulation has a limiting simple case, the commonly used 'oriented–in–space' model. The surface is present not only by its interaction with the bound initial state, but it also modifies the electron flux of the escaping electron through backscattering (section 2.3.3). Using the 'oriented–in–space' model, one can derive selection rules and I show in 2.3.4 that the explicit presence of the surface causes a breaking of these selection rules. This section 2.3 is discarding the nuclear motion which is presented in section 2.4.

2.3.1 Ab–initio method for discrete–continuum transitions

In the following I want to summarise the ab–initio method, used to calculate the electronic wave function of the initial and final states in the molecular coordinate frame. The method is well established in literature [73–75, 46, 66], and for a more detailed discussion the reader is referenced to [74, 46]. The electronic wave function for the initial (final) state can be written as an antisymmetric linear combination of a bound (continuum) electron and ionic core wave function for one electronic configuration [74, 46]:

$$\psi_{\Omega,\vec{k}_{mol}}(\{\vec{r}_{mol}\}_N;R) = |\Phi^{core}_{\Omega^+}(\{\vec{r}_{mol}\}_{N-1};R)\phi(\vec{r}_{mol};R)| \tag{2.4}$$

In 2.4, $\{\vec{r}_{mol}\}_N$ is the ensemble of electron position coordinates in space $\{\vec{r}_{mol}\}$=($\vec{r}^{(1)}_{mol}$, ..., $\vec{r}^{(N)}_{mol}$), while $\vec{r}_{mol}$ are those for the Nth electron. For the initial state, $\phi(\vec{r}_{mol};R) \equiv \phi^{discrete}_{\lambda,\kappa}(\vec{r}_{mol};R)$ is the wave function of the Nth electron, that is excited by the photon, having the symmetry λ and the quantum number κ. After the photoionization took place, there is a photoelectron in the continuum state, described by $\phi \equiv \phi^{contiuum}_{\vec{k}_{mol},\lambda,\sigma}(\vec{r}_{mol};R)$. Here, $\vec{k}_{mol}$ is the linear momentum and σ the spin projection of the escaping electron in molecular frame.

For the ground initial state, the LCAO–SCF (Linear Combination of Atomic type Orbitals– Self Consistant Field) method is used. The atomic basis set is of Slater type and the molecular orbital expansion coefficients are obtained by a variational principle. This molecular basis set of electronic wave functions for both the initial and final states is chosen to be orthogonal to the continuum electron wave function.

The continuum electron wave function $\phi^{continuum}_{\vec{k}_{mol},\lambda,\sigma}(\vec{r}_{mol};R)$ is calculated in the FCSE (Frozen Core Static Exchange) approximation [66]. In this model, the wave function of the ionic core is supposed not to be modified by the continuum electron, i.e. no relaxation effects for the molecule are taken into account. The ionic core wave function is derived from the ground state one by omitting the excited electron in the electronic configuration. Using the orthogonality of the molecular basis set, the transition moment simplifies to a one–electron integral between a bound and a continuum electron. In order to analyse the dependence of this integral on the emission angle of the electron, one expands it in spherical

harmonics:

$$\phi^{continuum}_{\vec{k}_{mol},\lambda,\sigma}(\vec{r}_{mol};R) = \sum_{\ell\geq\lambda} \mathrm{Y}^{*}_{\ell\lambda}(\hat{k}_{mol})\varphi_{k,\ell\lambda\sigma}(\vec{r}_{mol}) \tag{2.5}$$

In (2.5)$\hbar\sqrt{\ell(\ell+1)}$ can be identified with the length of the orbital momentum vector ($\vec{\ell}$ of the escaping photoelectron, while$\hbar\lambda$ is its projection onto the molecular axis. $\hbar\sigma$ is the projection of the photoelectron spin onto the molecular axis.

For the detailed calculation, one further expands the electronic motion potential and the continuum wave function in spherical harmonics around the centre of mass (*one centre expansion*) of the molecular cluster used in the calculation. Exchange interactions are taken into account by solving numerically the resulting close coupling set of integrodifferential equations [66].

2.3.2 Tilted molecular adsorbates

In this section, I give the differential cross section for tilted, non–rotating molecular adsorbates, neglecting the effect of photoelectron backscattering. Due to the inclination of the molecular axis with respect to the surface normal, all transformations, cited in section 2.2, will be considered. One limiting case, a molecule adsorbed normal to the surface, was derived in literature [73, 13, 70, 46, 71] and is known as the 'oriented–in–space' model. But, due to interactions between the surface or neighbouring molecules, the molecule can be inclined with respect to the surface.

In section 2.2, I already gave a general form of the differential cross section (${}^{m^{ph}}\mathrm{I}(\vec{k},\vec{q})$) for experiments discarding spin. One can write ${}^{m^{ph}}\mathrm{I}(\vec{k},\vec{q})$ in a slightly different form [70, 71]:

$${}^{m^{ph}}\mathrm{I}\,{}^{\Omega^{+}}_{\Omega^{"}}(\vec{k},\vec{q}) \quad = \quad N_E \sum_{\mu} \left| {}^{m^{ph}}\mathcal{T}\,{}^{\Omega^{+},\mu}_{\Omega^{"}}(\vec{k},\hat{q}) \right|^2 \tag{2.6}$$

The differential cross section for photoionization (${}^{m^{ph}}\mathrm{I}(\vec{k},\vec{q})$) depends on the incident photon angles $\hat{q} = (\vartheta_q,\varphi_q)$ and the direction of the escaping electron. In (2.6) N_E=$4\pi^2\alpha E_{ph}$ is a normalisation coefficient related to the Einstein coefficient A for spontaneous emission ([72], p.169) with α the fine structure constant and E_{ph} the photon energy. ${}^{m^{ph}}\mathrm{T}\,{}^{\Omega^{+}}_{\Omega^{"}}(\vec{k},\hat{q})$ is the complex transition moment for dipole transition from the initial ($\Omega^{"}$) to the final state, consisting of ionic (Ω^{+}) and continuum electron ($\vec{k}$) states. Introducing the wave functions of (2.4), (2.5) and the dipole operator (2.3) and taking into account all the transformations, explained in section 2.2, one obtains the following equation for the transition moment ${}^{m^{ph}}\mathcal{T}\,{}^{\Omega^{+},\mu}_{\Omega^{"}}(\vec{k},\hat{q})$ in (2.6):

$${}^{m^{ph}}\mathcal{T}\,{}^{\Omega^{+},\mu}_{\Omega^{"}} = \tag{2.7a}$$

$$\sum_{\ell=0}^{\infty}\sum_{\substack{m=-\ell\\ \lambda=-\ell}}^{\ell} \mathrm{Y}_{\ell m}(\hat{k})\ {}^{\lambda^\gamma}\mathrm{t}^{\Omega^+\,\ell\lambda\sigma}_{\Omega''}(k,R)\,\mathcal{D}^{(\ell)}_{m\lambda}(\hat{R})\,\mathcal{D}^{(1/2)}_{\mu\sigma}(\hat{R})\,\mathcal{D}^{(1)}_{m^\gamma\ \lambda^\gamma}(\hat{R})\left(\ \mathcal{D}^{(1)}_{m^{ph}\ m^\gamma}(\hat{q})\right)^*$$

with

$${}^{\lambda^\gamma}\mathrm{t}^{\Omega^+\,\ell\lambda\sigma}_{\Omega''}(k,R) = \left\langle \varphi_k^{\Omega^+,\ell\lambda\sigma}(\vec{r}_{mol};R)\left|r_{mol}\mathrm{Y}_{1\ \lambda^\gamma}(\hat{r}_{mol})\right|\phi_{\ \Omega''}(\vec{r}_{mol},R)\right\rangle_{\vec{r}_{mol},R} \tag{2.7b}$$

Equation (2.7) contains two parts: an angular transformation between different coordinate frames and an electronic dipole transition moment. The dipole transition moment ${}^{\lambda^\gamma}\mathrm{t}^{\Omega^+\,\ell\lambda\sigma}_{\Omega''}(k,R)$ in (2.7), expressed in molecular frame as one–electron integrals, is calculated by the ab–initio method, described in 2.3.1. The angular part in (2.7) is valid for linear $m^{ph}=0$ or circularly polarized light $m^{ph}=\pm1$. In Equation (2.7) λ^γ and λ are the projection of the photon polarization vector, and electron angular momentum on the molecular axis. The corresponding projection of the photoelectron spin is called σ and $\mathcal{D}$ are the Wigner functions. In the following, I want to give the analytic form of the transformations, presented in section 2.2. For the photon, one passes from photon (projection m^{ph}) to laboratory frame (m^γ) and finally to molecular frame (λ^γ). The dipole operator (2.3) transforms as:

$$\mathrm{Y}_{1\ m^{ph}}(\hat{r}_{photon}) = \sum_{m^\gamma,\ \lambda^\gamma} \mathcal{D}^{(1)}_{m^\gamma\ \lambda^\gamma}(\hat{R})\left(\ \mathcal{D}^{((1))}_{m^\gamma\ \lambda^\gamma}(\hat{q})\right)^* \mathrm{Y}_{1\ \lambda^\gamma}(\hat{r}_{mol}) \tag{2.8}$$

The final electron wave function is calculated in molecular frame, but the observable $\vec{k}_{mol}$ (photoelectron linear momentum) must be expressed in laboratory frame. The corresponding transformation 2.5 reads:

$$\mathrm{Y}^*_{\ell\lambda}(\hat{k}_{mol}) = \sum_m \left(\ \mathcal{D}^{(\ell)}_{m\lambda}(\hat{R})\right)^* \mathrm{Y}^*_{\ell m}(\hat{k}) \tag{2.9}$$

The photoelectron spin function $\chi^{1/2}_\mu$ transforms as:

$$\chi^{1/2}_\mu = \sum_\sigma\ \mathcal{D}^{(1/2)}_{\mu\sigma}(\hat{R})\chi^{1/2}_\sigma \tag{2.10}$$

Introducing (2.7) in (2.6), one obtains the following equation for the differential cross section for a molecule, adsorbed in a tilted position $\hat{R}=(\alpha,\beta,\gamma)$ relative to the surface coordinate system:

$${}^{m^{ph}}\mathrm{I}^{\Omega^+}_{\Omega''}(\vec{k},\vec{q}) = \tag{2.11}$$

$$N_E \sum_{\substack{K=0\\ M_K=-K}}^{\substack{K\\ \infty}} \sum_{\substack{L=0\\ M_L=-L}}^{\substack{L\\ \infty}} [L,K]^{1/2}\quad \mathrm{Y}_{KM_K}(\hat{q})\quad \mathrm{Y}_{LM_L}(\hat{k})\times$$

$$\times \sum_{\ell_1=0}^{\infty}\sum_{\ell_2=0}^{\infty}[\ell_1,\ell_2]^{1/2}\sum_{\substack{m_1=-\ell_1\\ \lambda_1=-\ell_1}}^{\ell_1}\sum_{\substack{m_2=-\ell_2\\ \lambda_2=-\ell_2}}^{\ell_2}(-1)^{\lambda_1-\lambda_1^\gamma+m^{ph}}\ {}^{\lambda_1^\gamma}\mathrm{t}^{\Omega^+}_{\Omega''}{}^{\ell_1\lambda_1\sigma_1}(k,R)\left({}^{\lambda_2^\gamma}\mathrm{t}^{\Omega^+}_{\Omega''}{}^{\ell_2\lambda_2\sigma_2}(k,R)\right)^*$$

$$\mathcal{D}^{(\ell_1)}_{m_1\lambda_1}(\hat{R})\,\mathcal{D}^{(1/2)}_{\mu_1\sigma_1}(\hat{R})\,\mathcal{D}^{(1)}_{m_1^\gamma\ \lambda_1^\gamma}(\hat{R})\left(\mathcal{D}^{(\ell_2)}_{m_2\lambda_2}(\hat{R})\,\mathcal{D}^{(1/2)}_{\mu_2\sigma_2}(\hat{R})\,\mathcal{D}^{(1)}_{m_2^\gamma\ \lambda_2^\gamma}(\hat{R})\right)^*$$

$$\begin{pmatrix}\ell_1 & \ell_2 & L\\ -m_1 & m_2 & M\end{pmatrix}\begin{pmatrix}\ell_1 & \ell_2 & L\\ 0 & 0 & 0\end{pmatrix}\begin{pmatrix}1 & 1 & K\\ -m_1^\gamma & m_2^\gamma & M_K\end{pmatrix}\begin{pmatrix}1 & 1 & K\\ -m^{ph} & m^{ph} & 0\end{pmatrix}$$

In 2.11, $[L]$ is defined as $[L]=2L+1$ and the 2×3 matrices are Wigner coefficients. The transformations cited above manifest themselves by the presence of the 3j–coefficients, the Wigner rotational functions and the summation over all projections in molecular frame (λ^γ,λ). The dependence of the photon incident direction and the angular distribution is governed by two spherical harmonics $\mathrm{Y}_{KM_K}(\hat{q})$ and $\mathrm{Y}_{LM_L}(\hat{k})$.

Before discussing qualitatively the effects of tilt position on the surface, I present a model for photoelectron backscattering.

2.3.3 The backscattering of photoelectrons by the surface

As mentioned in the section 1, the photoelectrons can be either reflected (backscattered) by the surface or penetrate in the solid and are lost for the photoelectron detection. This process can be taken partly into account using a simple model [12, 13], following mainly the ideas of Budău *et al.* [13, 46]. The model is extended to molecular adsorbates in a position, that is not normal to the surface (tilted molecules).

The photoelectron is reflected by the surface potential, that, in the limit of low coverage, can be realized by a smooth step potential defined in z–direction, parallel to the surface normal [76]. The surface is taken to be isotropic in x, y direction. In the case of high coverage or for other kinds of surfaces the potential has a more complicated form. For electrons of high kinetic energies (> 20 eV) the structure of the surface has explicitly to be taken into account [77–79]. In the following, I consider low coverage and photoelectrons of low kinetic energies, i.e. the surface potential is modeled by a step potential.

There are two steps in the model. First, the transition moments of an adsorbed molecule are calculated. The hindered rotation is frozen and therefore the formula 2.7 holds. Secondly the photoelectron is reflected on the step potential. Within the solid ($z \leq 0$), the potential is taken to be constant at $-V_0$, outside ($z > 0$) it is vanishing. The centre of mass of the molecule is fixed at z_0 above the surface. The geometry of the model is visualised in Fig. 2.3. Except for backscattering the Figure 2.3 is similar to Figure 2.1.

There are now two waves interfering in the electron detector. One electron wave is emitted directly from the adsorbate at an angle ϑ_k (d), the other (b) is first emitted in $\pi-\vartheta_k$ direction towards the surface, then reflected with a probability ($R(k,\vartheta_k)$) by the surface and finally interfere with (d) at the detector. Standard quantum mechanics derivations for the reflection on a finite step potential (e.g. Messiah, p.80 [65]) leads to formula 2.12:

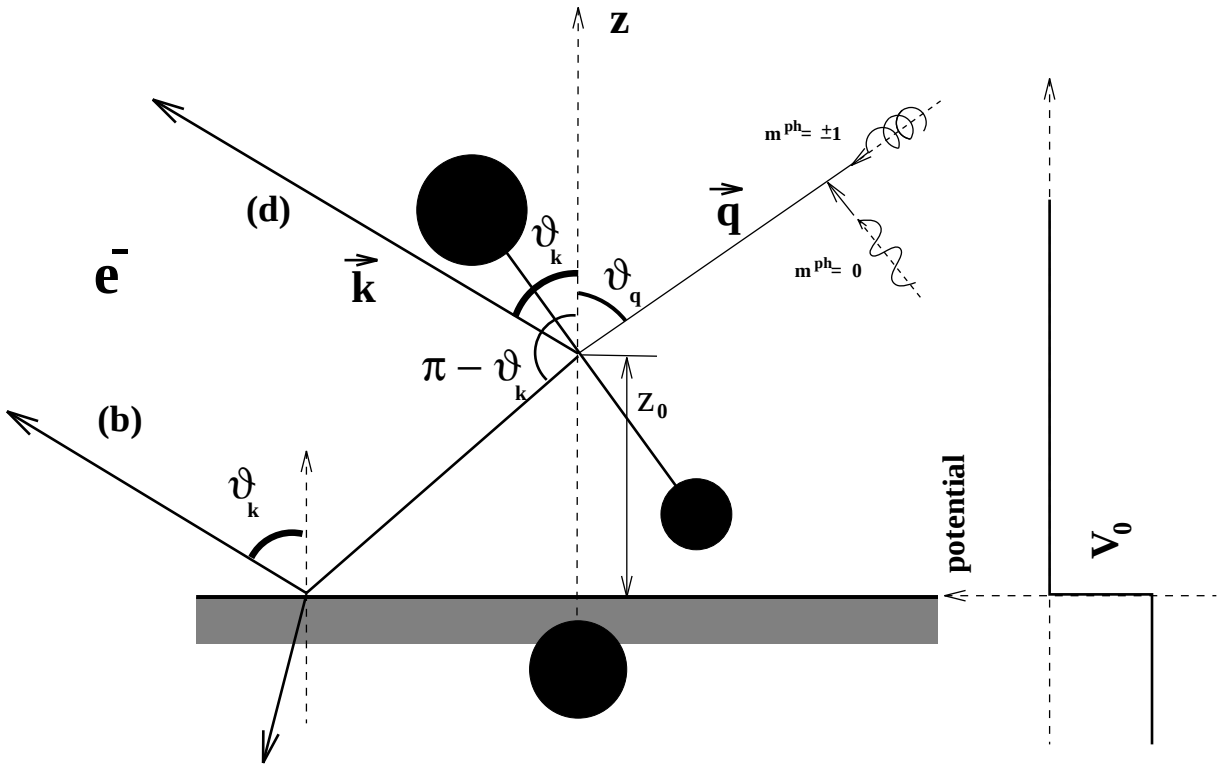

Figure 2.3: *Model of photoelectron backscattering. Two possible electron paths, direct (d) and backscattered wave (b) interfere with each other.*

$$\mathcal{R}(k,\vartheta_k) = \frac{|k_z| - k_z^{'}}{|k_z| + k_z^{'}} \exp(-2ik_z z_0) \tag{2.12}$$

Here $\vec{k}$ is the linear momentum in the vacuum with its projection $k_z = k\cos\vartheta_k$, while $\vec{k'}$ is the corresponding one in the bulk, with the projection $k_z^{'} = \sqrt{k_z^2 - 2m_e V_0/\hbar^2}$ onto the surface normal. m_e is the electron mass, V_0 the finite potential step.

In order to take into account the effect of backscattering for photoionization, one has to distinguish between two half spaces, each containing direct emitted and reflected electrons, respectively (see Fig.2.3). In the model without backscattering, these subspaces are identical to the $0 \leq \vartheta_k \leq \pi/2$ and $\pi/2 \leq \vartheta_k \leq \pi$ half spaces. But, experimentally, only electrons in the first subspace are detected. Consequently, one has to restrict the detection angle ϑ_k to $0 \leq \vartheta_k \leq \pi/2$ and to take into account the backscattered electrons. When including backscattering, the transition moment ${}^{m^{ph}}\mathrm{T}_{\Omega"}^{\Omega^+}((k,\vartheta_k,\varphi_k),\hat{q})$ in Equation (2.6) and (2.7) is modified in the following way:

$${}^{m^{ph}}\mathcal{T}_{\Omega"}^{\Omega^+}((k,\vartheta_k,\varphi_k),\hat{q}) \rightarrow {}^{m^{ph}}\mathcal{T}_{\Omega"}^{\Omega^+}((k,\vartheta_k,\varphi_k),\hat{q}) + {}^{m^{ph}}\mathcal{T}_{\Omega"}^{\Omega^+}((k,\pi-\vartheta_k,\varphi_k),\hat{q}) \tag{2.13}$$

For the differential cross section for photoionization including backscattering, the right part of formula

(2.13) must replace the transition moments in Equation (2.6). Following the ideas presented in 2.3.2, one can derive easily the corresponding formula for the differential cross section (2.11), now containing backscattering from an isotropic surface:

$$
{}^{m^{ph}}\mathrm{I}\,{}^{\Omega^+}_{\Omega^"}(\vec{k},\vec{q}) = \tag{2.14a}
$$

$$
N_E \sum_{\substack{K=0 \\ M_K=-K}}^{\substack{K \\ \infty}} \sum_{\substack{L=0 \\ M_L=-L}}^{\substack{L \\ \infty}} [L,K]^{1/2} \quad \mathrm{Y}_{KM_K}(\hat{q}) \quad \mathrm{Y}_{LM_L}(\hat{k})
$$

$$
\sum_{\ell_1=0}^{\infty}\sum_{\ell_2=0}^{\infty}[\ell_1,\ell_2]^{1/2} \sum_{\substack{m_1=-\ell_1 \\ \lambda_1=-\ell_1}}^{\ell_1} \sum_{\substack{m_2=-\ell_2 \\ \lambda_2=-\ell_2}}^{\ell_2} (-1)^{\lambda_1 - \lambda_1^\gamma + m^{ph}}
$$

$$
\left[1+(-1)^{\ell_1+\lambda_1}\mathcal{R}^*(k,\vartheta_k)\right]\left[1+(-1)^{\ell_2+\lambda_2}\mathcal{R}(k,\vartheta_k)\right] \quad {}^{\lambda_1^\gamma}\mathrm{t}\,{}^{\Omega^+\,\ell_1\lambda_1\sigma_1}_{\Omega^"}(k,R)\left({}^{\lambda_2^\gamma}\mathrm{t}\,{}^{\Omega^+\,\ell_2\lambda_2\sigma_2}_{\Omega^"}(k,R)\right)^*
$$

$$
\mathcal{D}^{(\ell_1)}_{m_1\lambda_1}(\hat{R})\,\mathcal{D}^{(1/2)}_{\mu_1\sigma_1}(\hat{R})\,\mathcal{D}^{(1)}_{m_1^\gamma\ \lambda_1^\gamma}(\hat{R})\left(\mathcal{D}^{(\ell_2)}_{m_2\lambda_2}(\hat{R})\,\mathcal{D}^{(1/2)}_{\mu_2\sigma_2}(\hat{R})\,\mathcal{D}^{(1)}_{m_2^\gamma\ \lambda_2^\gamma}(\hat{R})\right) * 2 \tag{2.14b}
$$

$$
\begin{pmatrix} \ell_1 & \ell_2 & L \\ -m_1 & m_2 & M \end{pmatrix}\begin{pmatrix} \ell_1 & \ell_2 & L \\ 0 & 0 & 0 \end{pmatrix}\begin{pmatrix} 1 & 1 & K \\ -m_1^\gamma & m_2^\gamma & M_K \end{pmatrix}\begin{pmatrix} 1 & 1 & K \\ -m^{ph} & m^{ph} & 0 \end{pmatrix}
$$

The expression (2.14) differs from (2.6) because one restricts the emission angle of the electron ϑ_k to $0 \leq \vartheta_k \leq \pi/2$ (accessible half-space for observation) and includes two additional factors $\left[1+(-1)^{l_1+\lambda_1}R^*(k,\vartheta_k)\right]$ and $\left[1+(-1)^{l_2+\lambda_2}R(k,\vartheta_k)\right]$ in Equation (2.14). These factors are related to backscattering, where $R(k,\vartheta_k)$ is the complex reflection function, given in Equation 2.12. For $R=0$, the formula 2.6 for tilted molecules is recovered. Some consequences of backscattering for such molecules is discussed in the next section.

2.3.4 An example: tilted molecules including backscattering of the electron

I will present in this section a comparison between species adsorbed upright or tilted for a particular experimental set–up. I will highlight the qualitative changes in the photoemission spectrum due to the presence of the surface.

For molecules adsorbed upright the molecular axis is identified with the surface normal. In the literature the corresponding model is known as 'oriented–in–space' model. This model was sometimes abusively used by experimentalists and theoreticians [80, 6] to obtain the tilt angle of the molecule on the surface. In fact the angle between the molecular axis and the incident direction of the photon was identified with the angle between molecular axis and the surface normal. This identification is relatively correct for the following assumptions. The incident light fall in normal to the surface. The surface is explicitly neglected and the 'oriented–in–space' model is applied. Then the angle between the internuclear axis

and the incoming photon corresponds to the tilt angle of the molecular adsorbate with regard to the surface. In the framework of 'oriented–in–space' model the formula 2.11 simplifies, because α, β, γ=0, $m^{\gamma} = \lambda^{\gamma}, m = \lambda$, and $\mu = \sigma$ and only incoherent sums over these projections are kept. The selection rules becomes more rigid and one can find experimental geometries ('forbidden geometry'), where particular resonances are forbidden [39].

For an excitation from a σ orbital in the σ electronic continuum ($\sigma \rightarrow \sigma$ transition) the electrons can be emitted only along the internuclear axis. For a linearly polarized photon (m^{ph}=0) with the polarization vector perpendicular to the internuclear axis (ϑ=90° , λ^{γ}=$\pm$1) no $\sigma \rightarrow \sigma$ transition is allowed and only π electrons emitted perpendicularly to the surface ($\sigma \rightarrow \pi$) will be observed.

With such a experimental geometry, a particular resonance can be studied, e.g. the 4σ shape resonance of CO at $h\nu$=36 eV. For such a resonance, the initial state is $^1\Sigma_0^+$, and the final ionic core one is $^2\Sigma$. The total final state (ionic core + continuum electron) is either a Σ or Π state (dipole excitation), giving rise to a continuum electron with a σ or π–symmetry. For a light molecule as CO, the angular coupling of the adsorbate (neutral/ion) is described in Hund's case (a) and the following selection rule holds:

$$\Lambda^{''} + \lambda^{\gamma} = \lambda + \Lambda^{+} \tag{2.15}$$

$\Lambda^{''}$ and Λ^{+} are the projections of the orbital momentum on the internuclear axis of the initial and final ionic core state, respectively. Remembering, that $\Lambda^{''}$=Λ^{+}=0 and λ^{γ}=$\pm$1, one sees, that only electron partial waves with π–symmetry ($\lambda \pm 1$) are allowed in forbidden geometry set–up. But, in ϑ_k=0° direction, the spherical harmonics $Y_{l\pm1}(0°, 0°)$ in zero and the electron emission for π–waves is vanishing.

The actual situation is more complicated than the simple 'oriented–in–space' model. One can consider, that a molecule is absorbed in some bent position ($\hat{R} = (\alpha, \beta, \gamma)$) with respect to the surface normal. There are now several effects due to the surface and I want to discuss two among them. First, if the interaction is strong, the electronic clouds are influenced by the surface. In such a case, all quantum numbers attached to projections onto the molecular axis (e.g. $\Lambda^{''}, \Lambda^{+}$) are no longer good quantum numbers. The selection rules discussed above do not apply strictly and 'forbidden' electron emission may be allowed. As previously the backscattering takes place but the surface is no longer perpendicular to the internuclear axis. I want to discuss this effect for 'forbidden geometry' experimental set–up.

Suppose, that the linearly polarized light comes along the molecular axis ($\lambda^{\gamma} \pm 1$) and only electrons emitted along this axis are detected. In Fig. 2.4 the experimental set–up and the mechanism of backscattering is shown. Two electron waves, emitted from the inclined molecule, interfere with each other, one directly emitted (d) in the direction of the molecular axis (ϑ=β, φ=α), the other emitted in direction (ϑ=π-β, φ=α) and then backscattered by the surface. In this Figure 2.4, I also show π–symmetry photoelectrons density distribution as two lobes perpendicular to the molecular axis and centred at the centre of mass of the molecular adsorbate. For the direct emitted wave (d), the discussion for the 'oriented–in–space' molecule holds and the emission along the molecular axis vanishes (see also Fig.2.4). But, for the backscattered wave (b), the transition moment may be non–vanishing and a non–vanishing photoelectron intensity may be measured. The photoelectron intensity depends on the inclination angle β and of the efficacy of $\epsilon\pi + {}^2\Sigma_{1/2} \leftarrow {}^1\Sigma_0 + h\nu$ transitions. This is the fundamental difference between the 'oriented–in–space' model and tilted molecules model. In fact, not only the

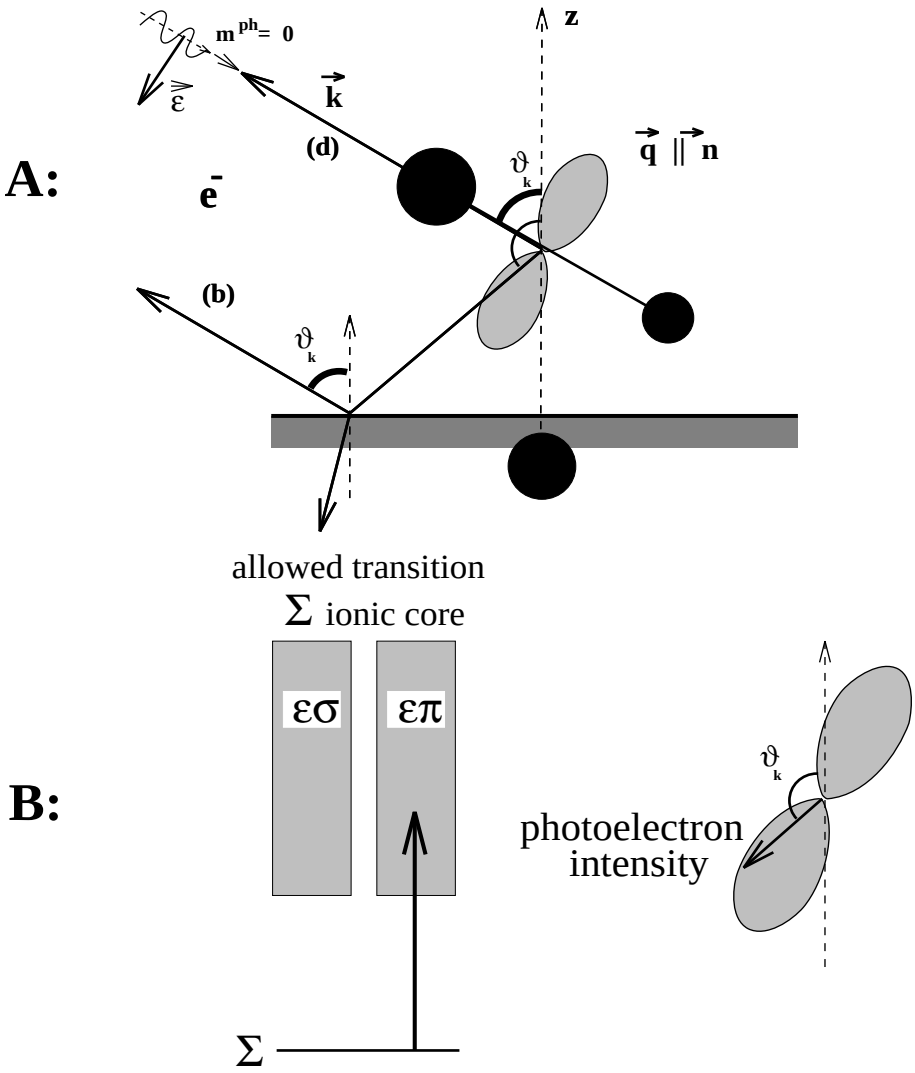

Figure 2.4: *Effects of inclination on photoelectron emission of tilted molecular adsorbates.*
A) The adsorbate is tilted with respect to the surface, described by the three Euler angles α, β, γ. The incident direction of the linear polarized photon is supposed to be parallel to the molecular axis with its perpendicular polarization vector $\vec{\epsilon}$ (ϑ_q=90° +β). The electron emission angle are along the molecular axis ϑ_k=β,φ=α. The simplified angular distribution of photoelectrons is represented in a polar plot as two lobes perpendicular to the molecular axis (see also B))
B) Left hand side: Only partial wave electrons with a π symmetry can be observed for the specified set–up. Right hand side: Simplified angular distribution for π symmetry continuum states.

selection rules are less rigid but also the explicit presence of the surface, as demonstrated by the example of backscattering, which shows the weakness of the ’oriented–in–space’ model.

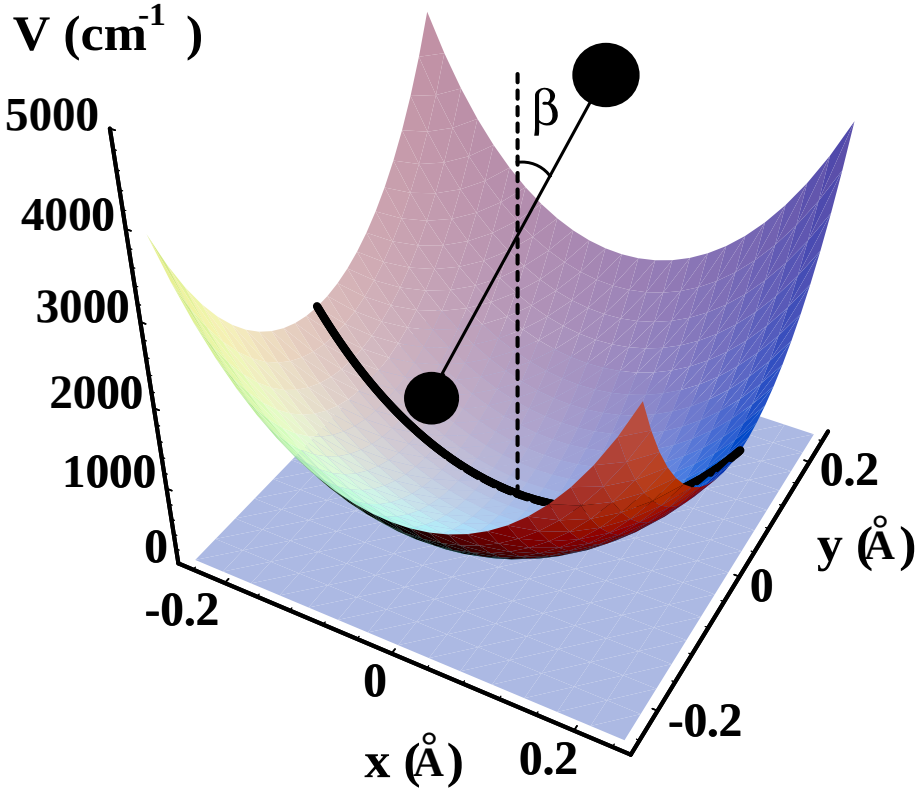

Figure 2.5: *Hindered rotation of molecular adsorbates*

2.4 Introducing a nuclear motion: The rotation of the adsorbate hindered by the surface

In the section 2.3.3 and 2.3.4, I have shown how the bent position of the internuclear axis of an adsorbate with regard to the surface normal changes the photoionization spectrum. I have neglected all the motions of the nuclei: internal vibration, molecule–stretch, hindered translation and hindered rotation. In this section, I show how one can introduce the hindered rotation, the only nuclear motion that changes the orientation of molecular adsorbate axis. Its influence on photoionization spectrum goes beyond a simple consideration of a mean tilt angle. In the present model I used the Born–Oppenheimer and Franck–Condon approximation without further approximation like infinite–order sudden approximation (see section 2.1.2).

First chemisorbed species are considered. Experimentally one finds that the stable position of CO molecules adsorbed on nickel surfaces at low coverage is normal to the surface with error bar of 15° [57]. But, if hindered rotation is introduced, the libration and precession around the surface normal are allowed (see Figure 2.5). Therefore the normal position of the adsorbate is forbidden because the precession moment of inertia is zero and the energy of the spherical oscillator is infinite. Consequently the adsorbate

avoids this position.

In fact, quantum mechanical probability to find the molecule perpendicular to the surface is vanishing (CO/Ni: see 2.4.1). If the adsorption site has a high symmetry (e.g C_{6v}), the surface is nearly axial symmetric and the molecule is moving freely around the surface normal, but enclosing a tilt angle between the surface normal and the molecular axis. This tilt angle can be small (6°) for the strong chemisorbed systems (CO/Pt) and relatively large for weakly chemisorbed species (14° for CO/Cu).

For physisorbed systems the surface potential is not strong enough to orient the molecule 'completely'. The effects of a dense coverage may restrict the rotational motion, but even in this case, rotational effects are still present due to zero–point vibrations. This argumentation holds also for chemisorbed molecules adsorbed at a low symmetry site or a dense coverage environment, but the picture of a completely oriented (but perhaps tilted) molecule may then be considered as a good approximation.

In the following, I restrict myself to chemisorbed and physisorbed CO molecules in a low coverage limit, for which the picture of an oriented molecule does not hold. In part III of this thesis, I will introduce the influence of the coverage on the angular motion of the adsorbate using a classical approach. In section 2.4.1, I present the framework of the model giving the formulae for a numerically based model, calculating the hindered rotation wave functions for the initial (neutral) and the final (ionic) state, respectively. New formulae for the differential cross section for photoionization are derived (section 2.4.2), including now the effects of hindered rotation. The application of the present model for a physical system is discussed in the next chapter 3.

2.4.1 The hindered rotation wave function

The surface potential for hindered rotation is assumed to have axial symmetry. Furthermore, all properties of the adsorbed molecule are considered to be invariant under an arbitrary rotation around the molecular axis, i.e. the electron clouds keep their axial symmetry. Therefore the dependence of the surface potential V on β can be expanded in Legendre polynomials:

$$V(R_0, z_0, \beta) = \sum_{L=0}^{\infty} V_L(R_0, z_0) P_L(\cos\beta) \tag{2.16}$$

In (2.16), no other vibrational modes are taken into consideration, and coordinates, R and z are frozen to the values R_0 and z_0, respectively. For an axial symmetric potential the dependence of V on the three Euler angles (α, β, γ) restricts to the tilt angle β only.

The axial symmetry of the systems imposes the wave function of the hindered rotor to be of the form:

$$\Theta^n_{M\Omega}(\hat{R}) = \quad e^{iM\alpha} \quad f^n_{M\Omega}(\beta) \quad e^{i\Omega\gamma} \tag{2.17}$$

As already defined Eq.(2.1) (p.42) n labels the different energy levels of the hindered rotor with $n \geq \|(M, \Omega)\|$, with M and Ω are the projections of the total momentum $\vec{J}$ onto the surface normal and the

molecular axis, respectively. Here, the system is supposed to be invariant under two arbitrary rotations, one around the surface normal, the other around the molecular axis. An isotropic surface implies an axial symmetry around the surface normal and consequently M is a good quantum number. Similarly, if the electronic clouds are supposed not to be influenced by the surface, the system is invariant under any rotation around the molecular axis and Ω is a good quantum number, dependent parametrically only on R, the internuclear distance. The angles α, β and γ are the three Euler angles, defined in section 2.2 and shown in Figure 2.1. The invariance under two rotations mentioned above imposes an exponential dependence of the wave function on the associated rotational angles α and γ. $f^n_{M\Omega}(\beta)$ contains the dependence on the tilt angle β. The function is strongly dependent on the form of the surface potential. It can be calculated either analytically in the case of a particular potential (see Appendix A) or numerically in the case of an arbitrary potential fulfilling the symmetry constraints discussed above. This numerical method is detailed in the present paragraph.

The hindered rotor wave function $\Theta^n_{M\Omega}(\hat{R})$ can be expanded using the Wigner functions $\mathcal{D}^{(J)*}_{M\Omega}(\hat{R})$ of the free rotor in active rotation notation (active rotation conversion in this thesis, see e.g. Zare [67], p.78):

$$\Theta^n_{M\Omega}(\hat{R}) = \sum_{J \geq |M|,|\Omega|}^{\infty} c^{J,n}_{M,\Omega} \quad \mathcal{D}^{(J)*}_{M\Omega}(\hat{R}) \tag{2.18}$$

In (2.18) $\hbar J(J+1)$ is the length of the total angular momentum. The symmetry constraints discussed above allow the sum over J but no sum over the projections M and Ω. Consequently the system is not invariant under rotations around any arbitrary axis in space.

In order to obtain the hindered rotor wave function, the starting point is the time independent Schrödinger equation:

$$\left(B\vec{R}^2 + V(\vec{R})\right)\Theta^n_{M\Omega}(\hat{R}) = E_n(R)\Theta^n_{M\Omega}(\hat{R}) \tag{2.19}$$

Here $B\vec{R}^2$ is the kinetic energy operator for a rotor [81], where B is the rotational constant in gas phase (B_{CO}=1.93 cm^{-1}). Note, that the internuclear distance R is fixed to R_0.

If I insert formulae (2.16) and (2.18) in the Schrödinger equation (2.19), multiply (2.19) by $\sqrt{\frac{2J+1}{8\pi^2}}\mathcal{D}^{(J)}_{M\Omega}(\hat{R})$ and finally integrate over the three Euler angles α, β and γ I obtain a set of linear equations. Written in matrix form for Ω=0 and M=1 this set of linear equations reads:

$$(\mathcal{V} - \mathcal{D})\mathcal{C} = \mathcal{E}\mathcal{C} \tag{2.20a}$$

with

$$\mathcal{V} = \sum_{L=0}^{\infty} V_L$$

$$\begin{pmatrix} \left[1,1\right]^{1/2}\begin{pmatrix} 1 & L & 1 \\ 1 & 0 & -1 \end{pmatrix}\begin{pmatrix} 1 & L & 1 \\ 0 & 0 & 0 \end{pmatrix} & \cdots & \left[1,J'\right]^{1/2}\begin{pmatrix} 1 & L & J' \\ 1 & 0 & -1 \end{pmatrix}\begin{pmatrix} 1 & L & J' \\ 0 & 0 & 0 \end{pmatrix} & \cdots \\ \vdots & \ddots & \vdots & \ddots \\ \left[J,1\right]^{1/2}\begin{pmatrix} J & L & 1 \\ 1 & 0 & -1 \end{pmatrix}\begin{pmatrix} J & L & 1 \\ 0 & 0 & 0 \end{pmatrix} & \cdots & \left[J,J'\right]^{1/2}\begin{pmatrix} J & L & J' \\ 1 & 0 & -1 \end{pmatrix}\begin{pmatrix} J & L & J' \\ 0 & 0 & 0 \end{pmatrix} & \cdots \\ \vdots & \ddots & \vdots & \ddots \end{pmatrix} \tag{2.20b}$$

$$\mathcal{D} = \begin{pmatrix} 2B & 0 & \cdots\cdots\cdots\cdots \\ 0 & \ddots & \\ \vdots & & BJ(J+1) \\ \vdots & & & \ddots \end{pmatrix}, \qquad \mathcal{E} = \begin{pmatrix} E_1 & 0 & \cdots\cdots \\ 0 & \ddots & \\ \vdots & & E_n \\ \vdots & & & \ddots \end{pmatrix} \tag{2.20c}$$

$$\mathcal{C} = \begin{pmatrix} c_{1,0}^{0,0} & c_{1,0}^{1,1} & \cdots & c_{1,0}^{1,n}\cdots & \\ c_{1,0}^{1,0} & c_{1,0}^{2,1} & \cdots & c_{1,0}^{2,n}\cdots & \\ \vdots & \vdots & \ddots & \vdots & \ddots \\ c_{1,0}^{J,0} & c_{1,0}^{J,1} & \cdots & c_{1,0}^{J,n}\cdots & \\ \vdots & \vdots & \ddots & \vdots & \ddots \end{pmatrix} \tag{2.20d}$$

Here, $[J, J']^{1/2}$ stands for $\sqrt{(2*J+1)*(2*J'+1)}$. In (2.20) V is the interaction matrix, where the square brackets define one of its matrix elements, taking the basis set wave function defined in (2.18). To obtain one elements one starts from (2.16) and carries out analytically the integration over the three Euler angles. D and E are diagonal matrices, containing the rotational energies of the gas phase (unperturbed energy levels) and the energies for the hindered rotor, respectively. The matrix C contains the coefficient of the hindered rotor wave function expansion (2.18).

The calculation of the hindered rotor wave function is now a eigenvalue problem, which can be solved by standard computational techniques (ESSL subroutines [82]). The eigenvectors are the coefficients in the wave function expansion, the eigenvalues are the energies for the hindered rotor, labelled by the quantum number n.

2.4.2 Photoionization cross section including hindered rotation

In this section, I present formulae for the photoionization differential cross section, including hindered rotation. As for the tilted molecules (section 2.3.2), one needs the electronic transition moments (section 2.3). Here, I rederive the photoionization cross section including the hindered rotation in Born–Oppenheimer and Franck–Condon approximation.

The photon of the energy $h\nu$ excites the molecular adsorbate from a initial neutral electronic ($\Omega^{"}$) and

rotational ($n^{"}$, $\mathrm{M}^{"}$, $\Omega^{"}$) to a final ionic core one, that has an Ω^{+} electronic and (n^{+}, M^{+}, Ω^{+}) rotational state. A photoelectron escapes with a direction $\vec{k}$ and a kinetic energy $E_k in$. The energy conservation law reads:

$$E_{elec}(\ \Omega^{"}) + h\nu + E_{rot}(\ n^{"},\ \mathrm{M}^{"},\ \Omega^{"}) = E_{elec}(\ \Omega^{+}) + \frac{1}{2} m_e k^2 + E_{rot}(\ n^{+},\ \mathrm{M}^{+},\ \Omega^{+}) \qquad (2.21)$$

Here $E_{elec}(\ \Omega^{"})$ is the electronic and $E_{rot}(\ n^{"},\ \mathrm{M}^{"},\ \Omega^{"})$ the rotational energy of the initial neutral state. The electronic and rotational energies of the ion are $E_{elec}(\ \Omega^{"})$ and $E_{rot}(\ n^{"},\ \mathrm{M}^{"},\ \Omega^{"})$, respectively. The photon ($h\nu$) ionizes the adsorbate. The electron escapes with a kinetic energy of $\frac{1}{2} m_e k^2$, where m_e is the electron mass.

If the molecular adsorbate is undergoing a hindered rotation and one has to introduce probability to find the adsorbate in a definite position in space. The corresponding probability is the square of the overlap integral between the hindered rotor wave functions (eq.(2.17)) of the initial and final states. In the Franck–Condon approximation the probability appears as weighting functions in the expression for differential cross section. For a transition from a given initial rotational ($n^{"}$, $\mathrm{M}^{"}$, $\Omega^{"}$) to a final one (n^{+}, M^{+}, Ω^{+}), i.e. state–to–state cross section, the transition moment reads:

$$ {}^{m^{ph}}_{\mu}\mathrm{T}^{\ \Omega^{+}\ \mathrm{M}^{+}\ n^{+}}_{\Omega^{"}\ \mathrm{M}^{"}\ n^{"}}(\vec{k},\hat{q}) = \qquad (2.22)$$

$$\int_0^{2\pi} d\alpha \int_0^{2\pi} d\gamma \int_0^{\pi} d\beta \sin\beta \times \times \quad \Theta^{\ n^{+}*}_{\mathrm{M}^{+}\ \Omega^{+}}(\alpha,\beta,\gamma) \quad \Theta^{\ n^{"}}_{\mathrm{M}^{"}\ \Omega^{"}}(\alpha,\beta,\gamma)\, {}^{m^{ph}}_{\mu}\mathcal{T}^{\ \Omega^{+}}_{\Omega^{"}}(\vec{k},\hat{q},\hat{R})$$

Here, $\Theta^{\ n^{"}}_{\mathrm{M}^{"}\ \Omega^{"}}(\alpha,\beta,\gamma)$ and $\Theta^{\ n^{+}*}_{\mathrm{M}^{+}\ \Omega^{+}}(\alpha,\beta,\gamma)$ are the wave functions of the initial and final rotational state, having the general form (2.18). The transition moment ${}^{m^{ph}}_{\mu}\mathcal{T}^{\ \Omega^{+}}_{\Omega^{"}}(\vec{k},\hat{q},\hat{R})$ contains exactly the same coefficients as ${}^{m^{ph}}\mathcal{T}^{\ \Omega^{+},\mu}_{\ \Omega^{"}}$ in equation (2.7). In the present approach the electron transition moment depends not on $\hat{R}$ and is identified to a transition moment ${}^{m^{ph}}_{\mu}\mathcal{D}^{\ \Omega^{+}\ \mathrm{M}^{+}\ n^{+}}_{\Omega^{"}\ \mathrm{M}^{"}\ n^{"}}(\vec{k},\hat{q})$ by taking into account the energy conservation including hindered rotation (2.21). Taking into account this conservation law means that the continuum electron function appearing in the electronic transition moment (2.7) should be shifted by the rotational energy of the hindered rotor.

Inserting the expansion of the hindered rotation wave function (2.18) and integrating (2.22) over all Euler angles (α,β,γ), the differential cross section for photoionization of rotating adsorbates is found to be:

$$ {}^{m^{ph}}\mathrm{I}^{\ \Omega^{+}\ \mathrm{M}^{+}\ n^{+}}_{\Omega^{"}\ \mathrm{M}^{"}\ n^{"}}(\vec{k},\hat{q}) = \qquad (2.23a)$$

$$N_E \sum_{\substack{K=0 \\ M_K=-K}}^{\infty}{}^{K} \sum_{\substack{L=0 \\ M_L=-L}}^{\infty}{}^{L} [L,K]^{1/2} \quad \mathrm{Y}_{KM_K}(\hat{q}) \quad \mathrm{Y}_{LM_L}(\hat{k}) \times$$

$$\times \sum_{\substack{\ell_1=0 \\ m_1=-\ell_1}}^{\infty} \sum_{\substack{\ell_2=0 \\ m_2=-\ell_2}}^{\infty} \sum_{\substack{m_1^\gamma=-1,\cdots,1 \\ m_2^\gamma=-1,\cdots,1}} [\ell_1,\ell_2]^{1/2}(-1)^{m_1-\ m_1^\gamma+\ m^{ph}}$$

$$\begin{pmatrix} \ell_1 & \ell_2 & L \\ -m_1 & m_2 & M \end{pmatrix} \begin{pmatrix} \ell_1 & \ell_2 & L \\ 0 & 0 & 0 \end{pmatrix} \begin{pmatrix} 1 & 1 & K \\ -\ m_1^\gamma & m_2^\gamma & M_K \end{pmatrix} \begin{pmatrix} 1 & 1 & K \\ -\ m^{ph} & m^{ph} & 0 \end{pmatrix} B^{\ell_1 m_1\ m_1^\gamma}_{\ell_2 m_2\ m_2^\gamma}$$

$$B^{\ell_1 m_1\ m_1^\gamma}_{\ell_2 m_2\ m_2^\gamma} = \tag{2.23b}$$

$$\sum_{\substack{\mathrm{J}_1'',\mathrm{J}_2'' \geq |M'',\ \Omega"| \\ \mathrm{J}_1^+,\mathrm{J}_2^+ \geq |M+,\ \Omega+|}} [\mathrm{J}_1'',\mathrm{J}_2'',\mathrm{J}_1^+,\mathrm{J}_2^+]^{1/2} \quad c^{\mathrm{J}_1''}_{\mathrm{M"}\ \Omega"} c^{\mathrm{J}_2''}_{\mathrm{M"}\ \Omega"} c^{\mathrm{J}_1^+}_{M+\ \Omega+} c^{\mathrm{J}_2^+}_{M+\ \Omega+}$$

$$\sum_{\substack{J_1 M_1 \Omega_1 \\ J_2 M_2 \Omega_2}} \sum_{\substack{\lambda_1^\gamma=-1,\cdots,1 \\ \lambda_2^\gamma=-1,\cdots,1}} \sum_{\substack{j_1 m_1^j \omega_1 \\ j_2 m_2^j \omega_2}} [J_1,J_2] \sum_{\sigma_1\sigma_2} \tilde{T}^{\ \Omega^+ l_1\lambda_1 m_1\sigma_1 j_1 m_1^j}_{\Omega"\ \lambda_1^\gamma}(\vec{k}) \quad \left(\tilde{T}^{\ \Omega^+ l_2\lambda_2 m_2\sigma_2 j_2 m_2^j}_{\Omega"\ \lambda_2^\gamma}(\vec{k})\right)^*$$

$$\begin{pmatrix} \mathrm{J}_1'' & 1 & J_1 \\ \mathbf{M"} & m_1^\gamma & -M_1 \end{pmatrix} \begin{pmatrix} \mathrm{J}_1'' & 1 & J_1 \\ \mathbf{\Omega"} & \lambda_1^\gamma & -\mathbf{\Omega}_1 \end{pmatrix} \begin{pmatrix} \mathrm{J}_1^+ & j_1 & J_1 \\ \mathbf{M}+ & m_1^j & -M_1 \end{pmatrix} \begin{pmatrix} \mathrm{J}_1^+ & j_1 & J_1 \\ \mathbf{\Omega}+ & \omega_1 & -\mathbf{\Omega}_1 \end{pmatrix}$$

$$\begin{pmatrix} \mathrm{J}_2'' & 1 & J_2 \\ \mathbf{M"} & m_2^\gamma & -M_2 \end{pmatrix} \begin{pmatrix} \mathrm{J}_2'' & 1 & J_2 \\ \mathbf{\Omega"} & \lambda_2^\gamma & -\mathbf{\Omega}_2 \end{pmatrix} \begin{pmatrix} \mathrm{J}_2^+ & j_2 & J_2 \\ \mathbf{M}+ & m_2^j & -M_2 \end{pmatrix} \begin{pmatrix} \mathrm{J}_2^+ & j_2 & J_2 \\ \mathbf{\Omega}+ & \omega_2 & -\mathbf{\Omega}_2 \end{pmatrix}$$

$$\tilde{T}^{\ \Omega^+\ell\lambda m\sigma j m^j}_{\Omega"\ \lambda^\gamma}(\vec{k}) = (-1)^{\omega-m_j}[j] \begin{pmatrix} \ell & 1/2 & j \\ m & \mu & -m_j \end{pmatrix} \begin{pmatrix} \ell & 1/2 & j \\ \lambda & \sigma & -\omega \end{pmatrix} {}^{\lambda^\gamma}\mathrm{t}^{\Omega^+\ell\lambda\sigma}_{\Omega"}(k,R)$$

The main differences between the differential cross section for tilted adsorbates (eq.(2.11)) and rotating molecular adsorbates (eq.(2.23)) are related to the presence of a geometrical coefficient $B^{\ell_1 m_1\ m_1^\gamma}_{\ell_2 m_2\ m_2^\gamma}$, the modified energy and angular momentum conservation law. The coefficient $B^{\ell_1 m_1\ m_1^\gamma}_{\ell_2 m_2\ m_2^\gamma}$ mixes different ℓm–continuum states of the escaping electron and depends in an implicit manner strongly on the type of adsorbate–surface system. This geometrical coefficient contains the expansion coefficients ($c^{\mathrm{J}''}_{\mathrm{M"}\ \Omega"}, c^{\mathrm{J}^+}_{M+\ \Omega+}$) of the hindered rotor wave function (eq.(2.18)) and integrals corresponding to the coupling of angular momenta. During the photoionization process transfer of angular momenta towards the surface is not considered, and together with the use of the basis set of gas phase wave functions the use of known angular coupling techniques ([68]) can be applied. This technique generates eight 3j–Wigner coefficients and a sum over all intermediate total angular momenta J_1, J_2 and their projections. In the next chapter, results for CO adsorbed on Ni(100) and Ar are presented.

Chapter 3

Application to physisorbed and chemisorbed CO: CO/Ar and CO/Ni(100)

In this chapter, I will present and discuss the influence of backscattering and hindered rotation of adsorbates on photoionization. The model for backscattering and Franck–Condon type argument for hindered rotation were detailed in the previous chapter. For backscattering the chemisorbed system CO/Ni(100) was taken. For the influence of the hindered rotation two examples were chosen, one for the chemisorbed molecular adsorbate CO/Ni(100), the other for the physisorbed system CO/Ar, both at on top adsorbation sites for a low coverage. For photoionization spectra, I chose the 4σ–shape resonance of CO, which was intensively studied in literature [41–43, 37, 2, 38, 3–10].

In section 3.2, I discuss the potentials and hindered rotor wave functions for CO absorbed on argon (3.2.1) and on Ni(100) (3.2.2). For both systems, realistic surface potentials have been chosen for the initial and final states. The angular distribution of photoelectrons at the maximum of the 4σ–shape resonance ($h\nu$=36 eV) is presented in section 3.3 for these two examples. As the emphasis in this work is the influence of hindered rotation on photoionization I used the electronic transition moments of CO–molecules, that neglect the electronic interaction between the molecule and surface in the initial state. The influence of the hindered rotation is highlighted by comparing the present sophisticated approach to simple models, as the 'oriented–in–space' model. But, the hindered rotation breaks symmetries, based on such an 'oriented–in–space' model. In the last section 3.4, a new recipe is presented, which allows the determination of the mean inclination of molecular axis. This recipe is compared to the tilted molecule approach, presented in section 2.3.2.

3.1 CO/Ni(100): Influence of backscattering

In this section I want to highlight the main results of a model for photoionization including backscattering for upright adsorbed CO molecules on nickel surface. The theoretical model, recently published by P. Budău *et al* [13], was presented in section 2.3.3. This work includes the model and the results for $(5\sigma)^{-1}$, $(1\pi)^{-1}$ (not presented here) and $(4\sigma)^{-1}$ ionization of CO. In this model, backscattering of photoelectrons is introduced by a constant step potential. The step constant of step potential is set to

V_0=-12.5 eV [6], located at z_0=2.31 Å from the centre of mass of CO, taken from LEED and EELS experiments [83,84].The distance z_0 represents in fact the position of an effective potential located near the surface. The internuclear distance R=1.128 Å is taken from gas phase [85]. The electronic transition moments are those of an 'oriented–in–space' CO molecule without interaction with the metallic surface atoms.

In Figure 3.1 I present the angular distribution for $(5\sigma)^{-1}$ ionization at the maximum of the shape resonance. The linear polarized light ($h\nu$=28.5 eV, ϑ_q=45° incident angle of the photon) ionizes the upright adsorbed molecule. The surface is located in the lower half of the plane of the figure. The angular distribution is shown in polar plot representation (see inset of Fig.3.1). More precisely, the photoelectron intensity is given by the length of the vector pointing from the origin to one point of the curve, where the electron emission angle θ is given by the angle between the y–axis and this vector (φ=0°). In (a) the angular distribution neglecting backscattering displays a large photoelectron emission towards the surface. In reality, these electrons are partially backscattered or partially adsorbed by the surface.

The backscattered electrons interfere with the direct ones giving rise to a modification of the emission pattern (Fig.3.1(b)) where the emission towards the surface disappears and a lobe appears at around θ=70° . Because of the chosen distance z_0 between the molecule and the surface the interference between the direct and the backscattered electrons is not really constructive and the emission pattern towards the vacuum is modified.

In Figure 3.2 I present the angular distribution of $(4\sigma)^{-1}$ ionization channel at the maximum ($h\nu$=32.8 eV) of the corresponding shape resonance. Because the 4σ electrons are located as a lone pair at the oxygen end the influence of the backscattering is minor. From Figs.3.1 and 3.2 one can conclude that the 'oriented–in–space' model of Davenport, Dill and Dehmer [37,38] neglecting backscattering can be used to explain the angular distribution the angular distribution results for the $(4\sigma)^{-1}$ but backscattering can not be neglected for the $(5\sigma)^{-1}$ ionization channel.

Allyn *et al.* [4] measured the angular distribution of the $(4\sigma)^{-1}$ ionization at the photon energy of $h\nu$=35 eV. Their relative intensities (dots) and the theoretical results (full line) are plotted on Fig.3.3 as function of the emission angle θ (φ=0°) of the electron. If one compares the theoretical with the normalised experimental results, one sees, that the experimental points are in general reproduced by theory. But, theory predicts a vanishing intensity around θ=48° , contrary to experiment. I will show in section 3.3.2, that in a model, including the nuclear motion of hindered rotation explains this non vanishing electron intensity.

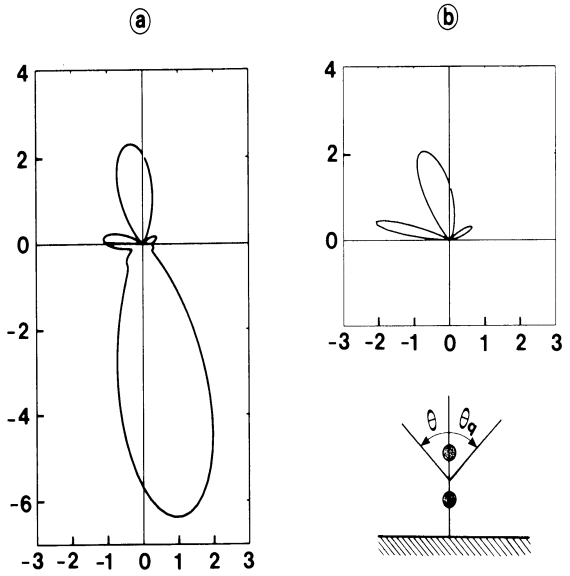

Figure 3.1: *Angular distribution of photoelectrons in polar plot representation at the maximum of the* 5σ *shape resonance. The CO molecule is adsorbed perpendicular to the surface. The linear polarized light (28.5 eV) makes an angle of 45° (*θ_q*) with the surface normal and an electron is ejected at* θ *in the photon–surface normal plane. Here, the differential cross section is defined as a vector from the origin to a point of the curve, where the length is photoelectron intensity in Mb/sr and* θ *defines the angle between the vector and the* y*–axis. a) without backscattering, b) backscattering included (from Budău et al. [13]).*

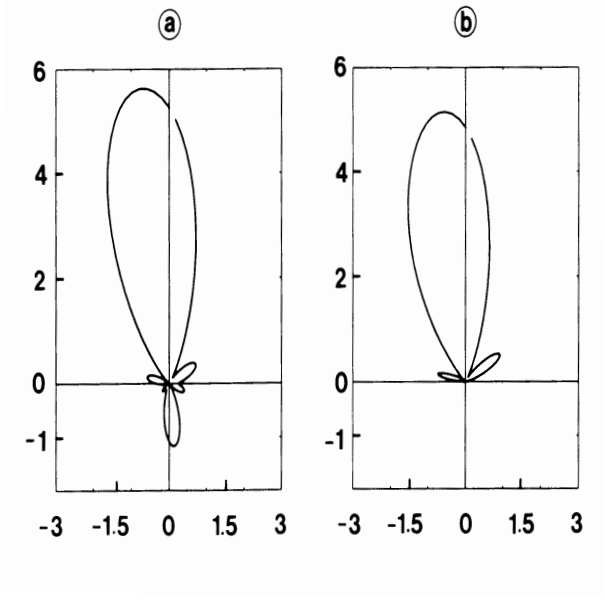

Figure 3.2: $(4\sigma)^{-1}$ *ionization. The photon has the energy of 32.8 eV. Same set–up as in Fig.3.1.*

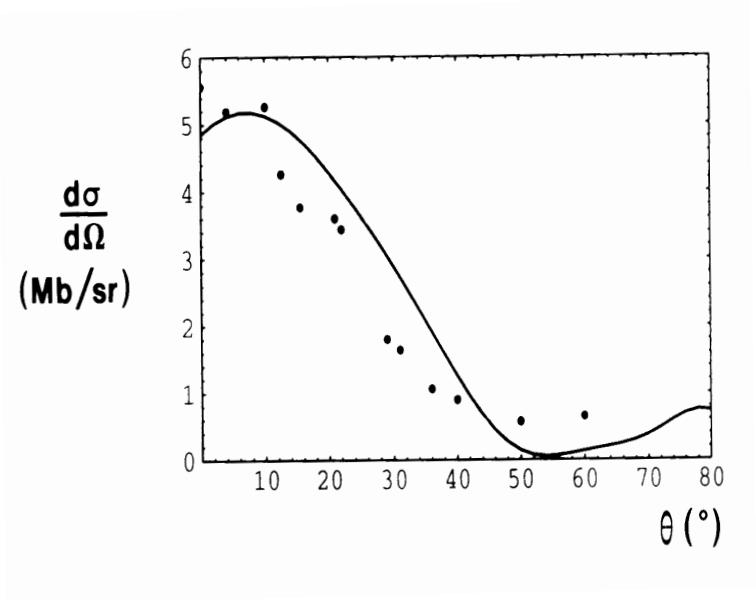

Figure 3.3: *Angular photoelectron distribution of the* $(4\sigma)^{-1}$ *ionization. The light (35 eV) is linear polarized, while* Θ *is the photoelectron ejection angle in the photon – surface normal plane (*φ*=0°). The full line is the theoretical calculation. The dots are experimental results from Allyn et al. [4], normalised to the theoretical curve (from Budău et al. [13]).*

	$V_1(z_0)$	$V_2(z_0)$	$V_3(z_0)$	$V_4(z_0)$
initial state	104.0	136.5	40.5	21.0
final state	-220.9	388.4	/	/

Table 3.1: *Coefficients of the expansion of the hindered rotor potential in* cm^{-1} *for CO/Ar*

a) initial state	M"	n"	$E^{(initial)}(cm^{-1})$	$\bar{\beta}$	Boltzmann factor T_{rot}=40 K
Ω"=0	0	0	0.0	102.5	0.14
	1	1	2.3	105.9	0.13
	2	2	9.1	107.4	0.10
	3	3	20.1	107.4	0.10
	0	1	26.7	108.3	0.05
	1	2	29.4	107.5	0.05

b) final state	M^+	n^+	$E^{(final)}$ (cm^{-1})	$\bar{\beta}$
Ω^+=1/2	1/2	0	0.0	89.2
	-1/2	0	0.4	69.4
	3/2	1	3.8	86.9
	-3/2	1	5.1	66.9
	5/2	2	11.9	84.0
	-5/2	2	14.0	65.5
	7/2	3	24.2	81.4
	-7/2	3	27.1	64.8
	...	..	...	...
	1/2	1	64.2	79.2
	-1/2	1	64.8	69.4

Table 3.2: *Rotational energies, Boltzmann factors and mean values of* β *for CO on top of Ar: a) initial state, b) final state.*

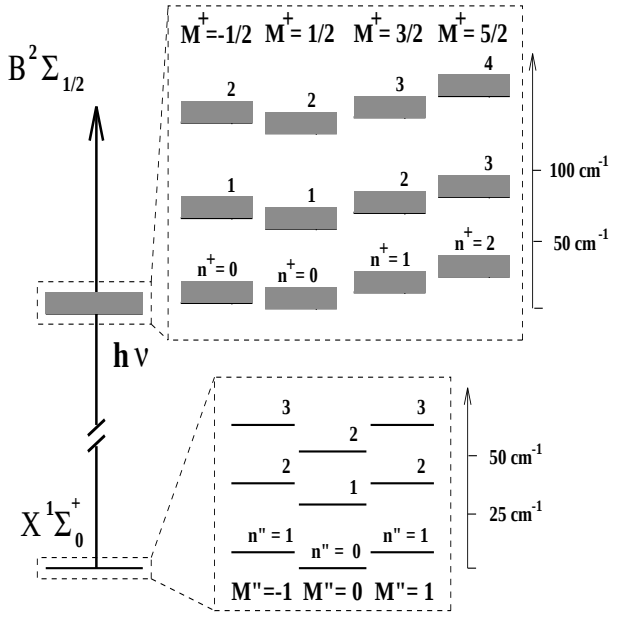

Figure 3.4: *Rotational energy levels of CO/Ar for the initial ($X\ ^1\Sigma_0^+$) and the final ($B\ ^2\Sigma_{1/2}$) electronic states. Note, that the energy scales for the initial and final states are different (from Büchner and Raşeev [11]).*

3.2 Hindered rotation: surface potential and wave functions

3.2.1 CO/Ar

To represent the hindered rotation, I use a crude surface potential, where the internal, the surface–molecule vibrations and all hindered translations are frozen. For physisorbed CO/Ar, the interaction between adsorbate and surface is restricted to a CO–(one argon atom) interaction, using the potential of Mirsky [86]. The CO–Ar potential has its minimum at $z_0^{''}$=3.63 Å and $\beta \approx 100°$. For the final state, the associated potential is different to the initial one due to the presence of the ion. I used a potential (CO^+–Ar), proposed by Parlant and Gislason [87] for the $B^2\Sigma$ state of CO^+ (minimum at z_0^+=3.56 Å). Following the Equation (2.16), the potentials of the initial $V(z = z_0^{''}, \beta)$ and final $V(z = z_0^+, \beta)$ was expanded in terms of Legendre polynomials up to the fourth order. The resulting coefficients of the expansion are shown in Table 3.1. Using these coefficients, the systems of linear equations (2.20) can be solved numerically ($J_{max} = 30$). The resulting rotational energies, the Boltzmann factors for a temperature of 40 K and the means values of β are shown in Table 3.2.

To understand the qualitative changes which take place when rotation becomes hindered let us briefly describe CO in gas phase situation. The wave function of a free rotor is simply represented by one Wigner function $\mathcal{D}^{(J)*}_{M\Omega}(\hat{R})$ and the total angular momentum J is a good quantum number. The energy levels are degenerate with respect to M and the sign of Ω. The spacing between energy levels are small and the time scale for a rotation is long. When, due to the surface, the rotation becomes hindered, the M and Ω degeneracies are lifted and J is no longer a good quantum number. There remains a degeneracy with respect to the simultaneous change of signs of all the projections M and Ω. I represent in the Figures

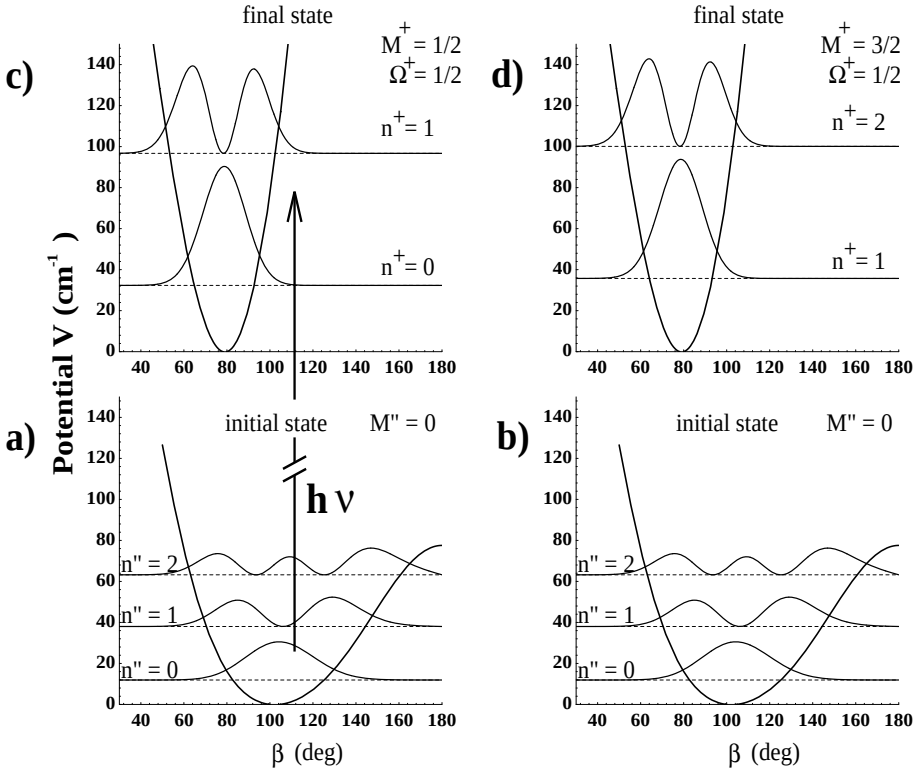

Figure 3.5: *CO/Ar: Hindered rotation potential, for one initial state M"=0 Ω"=0 (fig.a) and b)) and two final states with M+ = 1/2, Ω+ =1/2 (fig.c)), M+ = 3/2, Ω+ =1/2 (fig.d)). For each potential I represent rotational energy levels and the corresponding density functions (square of the wave function multiplied by* sin β*) (from Büchner and Raşeev [11]).*

3.4 and 3.5, the positions of the energy levels, labelled by M, Ω and n, where the label " is used for the initial neutral and the label + for the final ionic states. If one compares the rotational energies of the hindered molecule (Table 3.2) with those of the gas phase ($BJ(J+1)$, B_{CO}=1.93 cm^{-1}), one sees that the difference between the ground and the first excited one for M=0 is considerable: 5.8 cm^{-1} in the gas phase and 26.7 cm^{-1} for the CO–Ar system. In the gas phase, the energy levels are degenerated with respect to the quantum number M. For the adsorbate, this degeneracy is slightly lifted (2.3 cm^{-1}).

In Figure 3.5, the wave function density (square of the wave function multiplied by sin β) of one initial neutral (M"=0 Ω"=0) and two ionic final rotational states (M^+= 1/2, Ω+=1/2 (fig.c)), M+= 3/2, Ω+=1/2 (fig.d)) in the hindered rotation potential well is plotted. Before ionization, the surface potential for hindered rotation is not very strong, the molecular adsorbate is not just oriented parallel to the surface, but can undergo wide rotations ($\Delta\beta \approx 20°$) around the minimum $102° \leq \beta \leq 108°$ (see Table 3.2). After photoionization, the surface potential is much deeper and the minimum is shifted to lower values. Consequently, the rotations are restricted ($\Delta\beta \approx 10°$) around $65° \leq \beta \leq 89°$ (Table 3.2). This difference is reflected in the rotational energy levels, given in Table 3.4 and also in Figure 3.5. spacing between the energy levels for the final state is larger separated (64.2 cm^{-1}, Δn^+=1, M+=1/2) given M+ (M+=1/2) than for the initial state (26.7 cm^{-1}; M"=0).

Summarising, one can say, that the normal picture of a physisorbed CO–molecule adsorbed in a lying

position on the surface (β=90°) is not correct for both the initial and final states. The present results are for on-top species, but for bridge adsorption sites this difference should be much larger. The surface potential for the initial state differ from the final one, as I will detail in section 3.3. The difference in hindered rotation motion causes rotational excitation in the final ionic state, even in the Franck–Condon approximation.

3.2.2 CO/Ni(100)

In the case of chemisorbed CO/Ni(100) there are no detailed hindered rotation potentials published for both the initial and the final states. To find these potentials as function of β for a frozen value of z and R, I used experimental data for CO/Ni(100) in an iterative procedure and derive the coefficients of the potential expansion in terms of Legendre polynomials (Eq. 2.18) for the initial neutral state. For the ionic state potential I first convert the neutral state potential to an atom–atom (C–surface, O–surface) expansion, add the ion-induced interactions and expand the resulting potential back in Legendre polynomials.

More precisely, for the neutral ground state of CO molecule on top of Ni(100) one has R_0=1.15 Å, $z_0^{"}$=2.33 Å and $\beta \approx 0°$ [47]. The molecule–surface vibration (z) is taken harmonic and the force constant is directly related to the energy difference between the ground and first excited vibrational level (437 cm^{-1}, [47]). For the hindered rotation (β variable) I use an iterative procedure, which consists in solving the Schrödinger equation for hindered rotation with some guess coefficients in the Legendre polynomial potential expansion (2.16). The obtained rotational energy differences are then compared to the published ones (411 cm^{-1} for CO/Ni(100) [47]), which were obtained by a cluster calculation, and the coefficients of the Legendre polynomial potential expansion modified accordingly. The procedure is repeated until the difference between the calculated and the published [47] energies is smaller than a given threshold. The starting guess of the above iteration is taken from an analytical model, developed essentially by von Meyenn [88] and given in detail in Appendix A. This model relates energy and potential for a hindered rotor undergoing small oscillations in β.

For the B $^2\Sigma_{1/2}$ state of CO^+ ion I started from the neutral molecule potential, according to (2.18):

$$V^{\text{neutral}}(z,\beta) = k(z - z_0^{"})^2 + V_1(z_0^{"})P_1(\cos\beta) + V_2(z_0^{"})P_2(\cos\beta) + const. \tag{3.1}$$

Here, I have discarded the distance between the two nuclei R_0 and allowed the variation of z in a harmonic way (k is taken from [47]). Note, that the coefficients of the Legendre expansion in (3.1) are calculated for the neutral molecule at z=$z_0^{"}$ and they will be modified by the procedure described below to obtain those of the ion. First, I convert (3.1) to an atom–atom potential of the following form:

$$\begin{aligned} V^{\text{neutral}}(z,\beta) \;=\; & c^{(1)}_{O,\mathcal{S}}(r_{O,\mathcal{S}} - z_0^{"}) + c^{(2)}_{O,\mathcal{S}}(r_{O,\mathcal{S}} - z_0^{"})^2 + \\ & c^{(1)}_{C,\mathcal{S}}(r_{C,\mathcal{S}} - z_0^{"}) + c^{(2)}_{C,\mathcal{S}}(r_{C,\mathcal{S}} - z_0^{"})^2 + const \end{aligned} \tag{3.2}$$

	$V_1(z_0)$	$V_2(z_0)$
initial state CO/Ni(100)	-29764.5	6405.7
final state	-29971.7	6450.1

Table 3.3: *Coefficients of the expansion of the hindered rotor potential in* cm^{-1} *for CO/Ni(100)*

In (3.2) $\mathcal{S}$ is a point on the surface corresponding to $x-y$ position of the centre of mass of CO. Obviously $r_{O,\mathcal{S}}$ and $r_{C,\mathcal{S}}$ depend on z and β and the coefficients of (3.2) have been obtained by comparison to (3.1). Secondly, I add to the potential (3.2) the terms corresponding to the electrostatic interaction of the adsorbate. The metallic surface is considered as a perfect mirror, i.e. immediately after ionization (10^{-16}s) the electrons of the solid form an image charge of the adsorbed ion, situated at -z_0 below the surface. The ion–surface interactions I considered are the ion charge—image charge, the ion—image dipole and the dipole—image charge. The complete ionic potential now reads:

$$V^{\text{ionic}}(z,\beta) = V^{\text{neutral}}(z,\beta) + C_{a.u.\rightarrow cm^{-1}}\left\{-\frac{e_0^2}{(2z)^2} + \frac{e_0 d}{(2z)^3}\right\} \tag{3.3}$$

Here, $V^{\text{neutral}}(z,\beta)$ is given by Eq.(3.2), e_0 is the electron charge and d is the dipole moment for the ionic state, obtained from the asymptotic expansion potential of the gas phase molecular ion (d= 0.8373 a.u., [66, 59]). In (3.3) $C_{a.u.\rightarrow cm^{-1}}$ is the conversion constant between the atomic units and cm^{-1}.

One now search for the minimum of (3.3) as function of z for an upright orientation of the adsorbate. This minimum is found at z_0^+ = 2.26 Å and the ionic potential is expanded back in Legendre polynomials up to the second order. The coefficients of the expansion for both the initial and the final state potentials are summarised in Table 3.3. With this potential, I numerically calculate the rotational energies and wave functions of the ion, by solving the hindered rotor Schrödinger equation (Eq.(2.19) with J_{max}=400). The energies together with the Boltzmann factors and mean values of β are presented in Table 3.4.

One finds, that the degeneracy in M of the gas phase is considerably lifted (205 cm^{-1}), in contrast to the physisorbed system CO/Ar (2.3 cm^{-1}). The rotation energy levels spacing is of orders of magnitude higher than the physisorbed or the gas phase case ((CO/Ni) (CO/Ar:CO) (gas phase) = 411.7, 26.7, 5.8 cm^{-1}). Due to the large energy spacing, only the first two energy levels are Boltzmann–populated (T_{rot}=300 K). Note, that the energy spacings in the initial and final states are comparable. The molecular ion is attracted towards the surface due to the ion–image ion interaction and the hindered rotation motion is restricted. But, the repulsive dipole–image ion and ion–image dipole interactions compensate the restriction. This behaviour might be changed by a surface potential, including explicitly neighboured atoms of the surface.

In Figures 3.6 and 3.7 I display the energy levels of the initial and the final states for CO/Ni(100) in two different representations: one corresponding to positions of levels, the other to the potential wells and density of the wave function for each level. Note that in Figure 3.7, I establish an one–to–one correspondence between $\beta \leq 0°$ φ=0° and $\beta \geq 0°$, φ=180° . This is because in an usual tridimensional coordinate system β can not be negative.

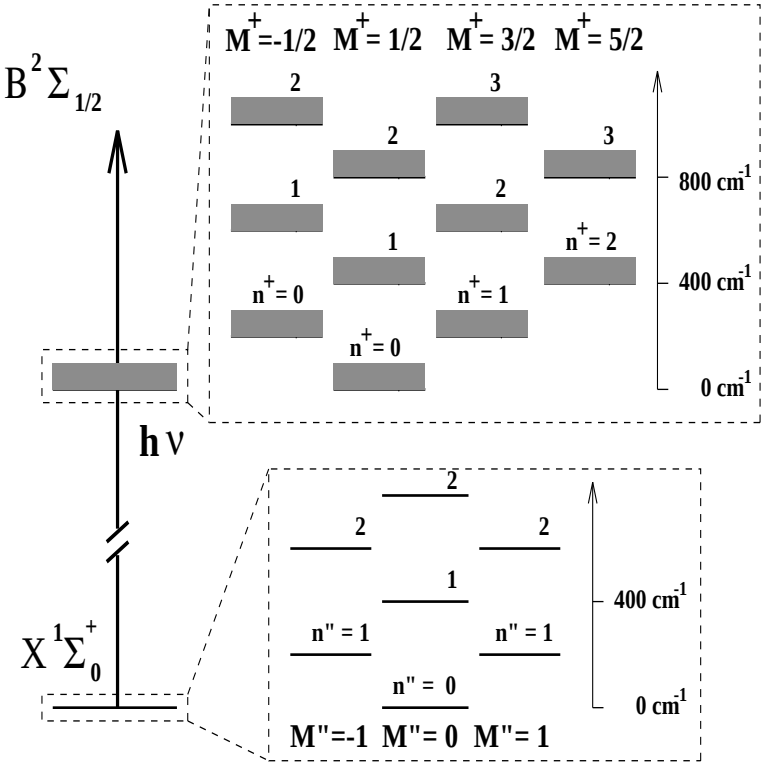

Figure 3.6: *Rotational energy levels of CO/Ni(100) for the initial ($X\ ^1\Sigma_0^+$) and the final ($B\ ^2\Sigma_{1/2}$) electronic states (from Büchner and Raşeev [11]).*

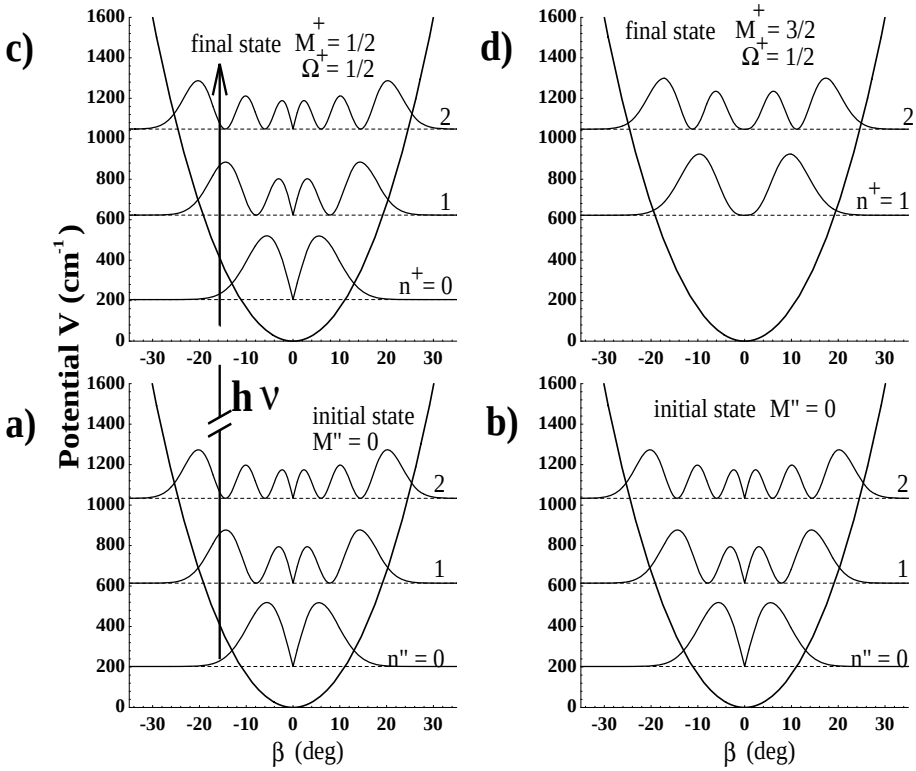

Figure 3.7: *CO/Ni(100): Hindered rotation potentials, for the initial state with M"=0 $\Omega^{"}$=0 (fig.a), b)) and two final states with M^{+} = 1/2, Ω^{+}=1/2 (fig.c)) and M^{+} = 3/2, Ω^{+}=1/2 (fig.d)). For each potential the rotational energy levels and the corresponding density functions (square of the wave function multiplied by* $\sin\beta$*) are represented (from Büchner and Raşeev [11]).*

a) initial state	M"	n"	E(initial)(cm^{-1})	$\bar{\beta}$	Boltzmann factor T_{rot}=120 K	Boltzmann factor T_{rot}=300 K
Ω"=0	0	0	0.0	11.6	0.85	0.50
	1	0	205.2	8.9	0.07	0.18
	0	1	411.7	15.4	0.01	0.07

b) final state	M+	n+	E(final)(cm^{-1})	$\bar{\beta}$
Ω+=1/2	1/2	0	0.0	13.3
	-1/2	0	207.1	8.8
	3/2	1	209.0	9.2
	-3/2	1	416.8	8.4
	1/2	1	417.5	16.7
	5/2	2	420.8	8.5
	-1/2	1	628.4	14.1

Table 3.4: *Rotational energies, Boltzmann factors and mean values of β. CO on top of Ni(100): a) initial state, b) final state.*

One can see, that the hindered rotation is restricted and only librations within a small region are allowed ($\Delta\beta$=10°). Note, that the wave function density is vanishing at β=0° . This is the effect of spherical oscillator, discussed previously in section 2.4. Briefly, for molecules adsorbed perpendicular to the surface, the precession momentum of inertia is zero and rotational energies are infinite. The molecule tries to avoid this position and consequently the probability to find the molecular adsorbate at β=0 ° is vanishing and the mean angle $\bar{\beta}$ is nonzero. From Table 3.4 one finds, that the higher the rotational quantum number n, the higher the mean angle. Specifically for the first three rotational levels of the initial state of CO/Ni(100), $\bar{\beta}$ is 11.6° , 8.9° and 15.4° , respectively. For the final state, the mean values are of the same order of magnitude.

The conclusion of the analysis of the potential and wave function is, that the well accepted picture of a molecule absorbed upright is not correct. The tilt angle between the internuclear axis and the surface normal is never zero and its value is depending on the type of adsorbate–surface system. For a given hindered rotational level, the stronger the chemisorption is, the smaller is the tilt angle. The temperature is another important factor. But the temperature of the surface–adsorbate system can play a role, because the population of hight hindered rotation level become significant. These levels have a larger mean tilt angle and a model based in an upright position of the adsorbate will be a less correct approximation.

3.3 The photoionization cross section in the energy region of the 4σ shape resonance: Results and Discussion

In this section, I present the results for the photoionization angular distribution of CO–molecules physisorbed on argon (3.3.1) and chemisorbed on Ni(100) (3.3.2) in the region of the 4σ shape resonance ($h\nu$=36 eV). These two systems can be considered as prototypes for physisorption and chemisorption. The system CO/Ni(100) has been extensively studied in literature, in experiment [2–4, 6, 54, 89, 90, 15, 91–94] as well as in theory [95, 54]. Following the Blyholder model (see Fig.1.2 on page 28) the electrons of the 4σ orbital are localised at the oxygen end. For physisorption the molecule is usually lying down on the surface but is far from it. Therefore the surface molecule interaction is week. For chemisorption CO is standing up on the surface with the oxygen atom oriented towards the vacuum. Consequently the 4σ orbital is only slightly influenced by the surface–molecule interaction. As a result of the above discussion it is obvious that one can use as a first approximation the ab–initio electronic transition moments of free CO molecules. Note, that the influence of the surface can be considered through the backscattering of the electrons. Its influence for the considered examples seems to be secondary [13]. The hindered rotation is fully introduced here, using the model presented in the preceeding section (2.4.2).

3.3.1 CO/Ar

For CO physisorbed on argon, I compare the results of the present elaborated approach for photoionization including hindered rotation to three simple models. This comparison helps me to show the role of hindered rotation for physisorbed species. The experimental geometry is chosen as follows. Linear polarized light with an energy of 36 eV is incident to the normal to the surface, i.e. the polarization vector is parallel to the surface (s–polarization, ϑ_q=90°). The electron is detected at ϑ_k in the plane, spanned by the polarization vector of the incident light and the surface normal ($\varphi_q = \varphi_k$=0°).

The four models mentioned above are visualised in Figure 3.8: the free molecule in gas phase (a), the 'oriented–in–space' model of Dill [38] and Davenport [37] (b), a 'helicopter motion' model (c) and the present approach, taking into account a realistic surface potential (d). In the 'oriented–in–space' model the molecule is frozen in a definite position in space, in our case parallel to the surface (β=90°) and directed along the x–axis (α=0°). In the 'helicopter motion' model, β is frozen at 90° and the molecule is allowed to undergo a free precession around the surface normal. In the gas phase model the CO–molecule is allowed to rotate freely in space. In our realistic hindered rotation model there is a free precession in α and a hindered rotation in β governed by the potential introduced in section 3.2.1.

Figure 3.9 shows the results of the photoelectron angular distribution at the maximum of the 4σ shape resonance ($h\nu$=36 eV). The full curve corresponds to the present hindered rotation model where the

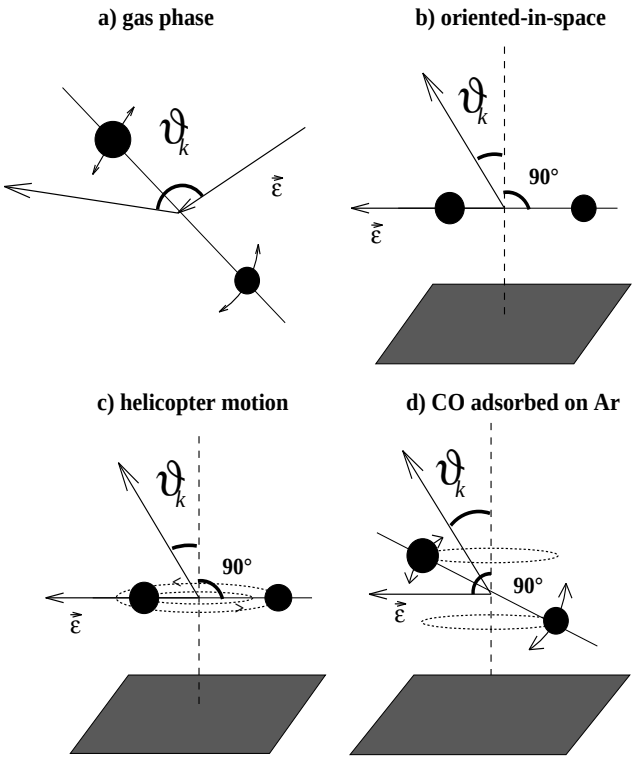

Figure 3.8: *Pictural representation of models which simulate the physisorbed CO molecule: a) gas phase, b) 'oriented–in–space', c) "helicopter motion', d) hindered rotation model (from Büchner and Raşeev [11]).*

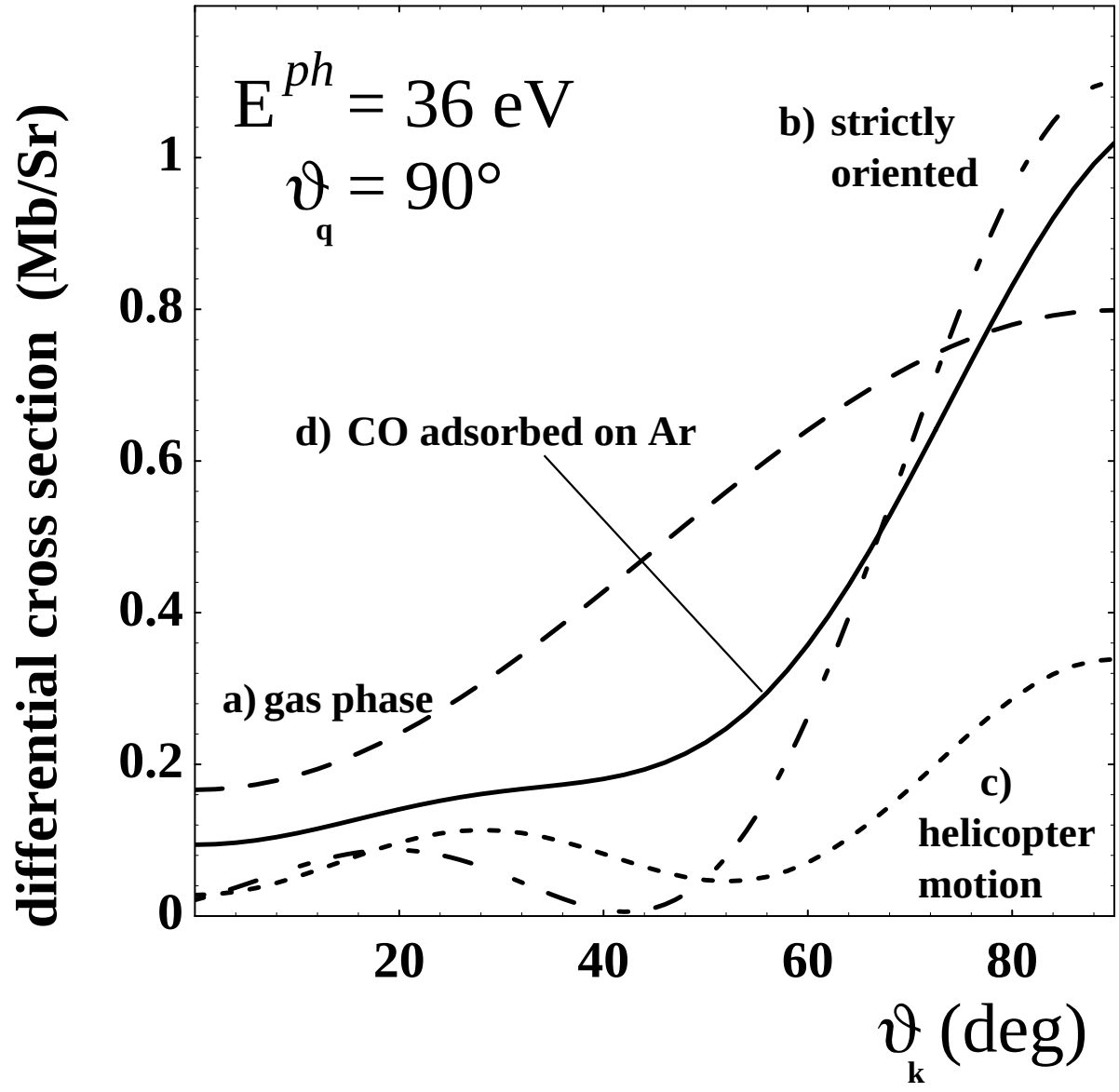

Figure 3.9: *Angular distribution of photoelectrons emitted from CO/Ar in the case of* $B^2\Sigma_{1/2} \leftarrow X^1\Sigma_0^+$ *excitation. The photon is linearly polarized with* ϑ_q*=90°,* φ_q*= 0° and its energy is 36 eV. The electrons are emitted in the plane defined by the polarization vector of the light and the surface normal (*φ_k*= 0°). Four models were considered: a) gas phase, b) 'oriented–in–space' (intensity scaled by a factor of 1/10), c) 'helicopter motion', d) hindered rotation model (from Büchner and Raşeev [11]).*

differential cross section was obtained using equations (2.23). To obtain this curve I took into account all initial hindered rotational states populated at T_{rot}=40 K with M"=-2,-1,0,1,2 and n"=0,1,2 and summed up over all allowed hindered rotation transitions. In Table 3.2 I show among possible initial states six, the corresponding Boltzmann factors and the final states reached by the dipole transition excitation together with the mean value of β ($\bar{\beta}$). From this table, one sees that there is no unique predominant state and that $\bar{\beta}$ is similar for different initial or final rotational states, being around 105° for the initial and between 65° and 89° for the final states.

At the maximum of the 4σ shape resonance, the largest contribution to the cross section comes from the energy–degenerate continua $\epsilon f\sigma$, but $\epsilon s\sigma$, $\epsilon p\sigma$ and $\epsilon d\sigma$ continua contribute also. The angular behaviour of the cross section plotted in Figure 3.9 can mainly be understood in terms of the square of the ℓ=3 ($\epsilon f\sigma$) continuum. The analytic expression of the corresponding Legendre polynomial is $P_3(\cos\vartheta'_k) = \frac{1}{2}(5\cos^3\vartheta'_k - 3\cos\vartheta'_k)$, where the angle ($\vartheta_k$) in the Figs.3.9 and 2.1 is related to the polynomial angle by $\vartheta'_k = 90° - \vartheta_k$. In terms of ϑ_k, P_3 has two maxima at ϑ_k=90° and 27° and a minimum at 51° . If the tilt angle β is restricted to a small region around β=90° , the addition of the other terms to the cross section, mainly $\epsilon p\sigma$ and $\epsilon d\sigma$, will mainly preserve the angular behaviour corresponding to $\epsilon f\sigma$ continuum.

Now if one considers the cross section of each model separately, the maximum at ϑ_k=90° in the gas phase photoionization cross section (see Figure 3.9a) and the pictural representation (3.8a) is an average over the random orientations of the molecule. This average preserves the strong maximum in the direction of light polarization (σ–σ transitions), but washes out completely the $\epsilon f\sigma$ minimum at 51° mentioned above. In fact, the curve obeys the well–known angular dependency $[1 + \beta/4(1 + 3\cos(2\vartheta))]$ for photoionization of unpolarized targed with linear polarized light [96]. In the 'oriented–in–space' model (Figure 3.9b) and the model representation (3.8b) the intensity is about 10 times larger than in other models, and one sees an enhancement of the $\epsilon f\sigma$ partial wave because the internuclear axis and the polarization vector of the light are collinear and no average over nuclear motions is performed. The cross section minimum is at about 41° compared to 51° for a pure $\epsilon f\sigma$ wave. Following the 'oriented–in–space' model selection rule, for all electron emission angles ϑ_k, $\epsilon\pi$ waves are strictly forbidden. This selection rule is lifted in the case of "helicopter motion" model (Fig.3.9 c), in which the molecule is allowed to undergo precession in a plane parallel to the surface (see the pictural representation in Figure 3.8c).

But, in the case of electrons ejected at ϑ_k=0° , a supplementary non physical selection rule holds in the 'helicopter motion' model. At ϑ_k=0° , this rule forbids the main contributions to the shape resonance 4σ, namely the odd partial waves $\epsilon p\sigma$, $\epsilon f\sigma$ but also $\epsilon d\pi$. This non physical selection rule is derived below. For electron emission normal to the surface the spherical harmonic $Y_{\ell m}(\hat{k})$ in Eq.2.7 imposes the projection m of the photoelectron angular momentum $\vec{\ell}$ to be zero for non vanishing photoemission intensities. In the 'helicopter motion' approximation the surface potential fixes the molecular axis at β=90° . The transformation function $\mathcal{D}^{(\ell)}_{m=0\lambda}(\alpha, \beta = 90°, \gamma)$ is zero for odd $\ell + \lambda$ and in the differential cross section these terms do not contribute. The spherical harmonic in (2.9), which governs the angular distribution of photoelectron, is vanishing at ϑ_k=0° for $\ell + m$ odd (p.158 in [97]). The orientation of the molecule is given by three Euler angles. For the helicopter motion one of them is fixed (β=90°), while the two other can have any value. This and the preceding considerations explain the low cross section of the 'helicopter' model at 90° . At different ejection angles the cross section of 'helicopter motion' model is closer to the other models. Particularly the difference between the cross section minima in the "oriented–in–space" and "helicopter motion" models can be explained by the mixing of $\epsilon f\sigma$ with $\epsilon d\pi$

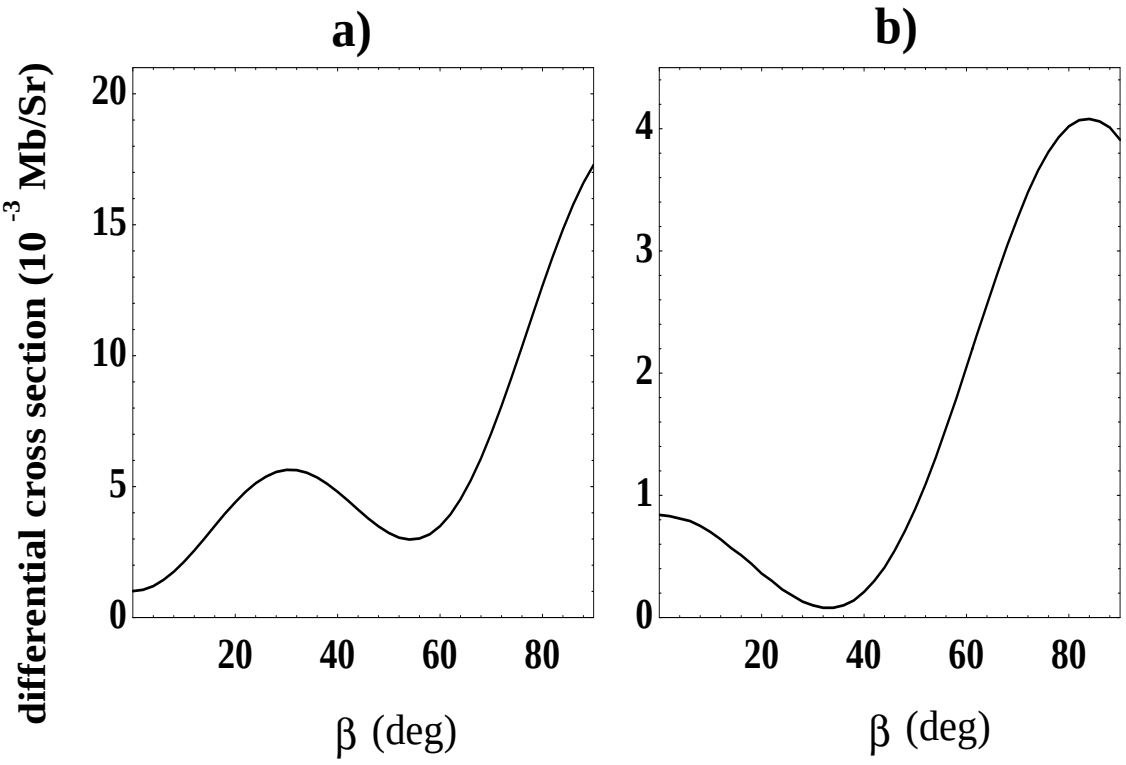

Figure 3.10: *Angular distribution of electrons emitted from CO/Ar. Same set–up as in figure 3.9. Two rotational state–to–state transitions are shown: a)* M^+*=1/2,* Ω^+*=1/2,* n^+*=0* $\leftarrow$ $M^{"}$*=0,* $\Omega^{"}$*=0,* $n^{"}$*=0; b)* M^+*=3/2,* Ω^+*=1/2,* n^+*=2* $\leftarrow$ $M^{"}$*=0,* $\Omega^{"}$*=0,* $n^{"}$*=2 (from Büchner and Raşeev [11]).*

(minimum at 45°) and $\epsilon p\pi$ (minimum at 90°) continua, which are forbidden in the 'oriented–in–space' model.

The elaborate hindered rotation model (Fig.3.9d) and (3.8d), displays an intermediate situation between the models presented above. In this model the rotation is constrained and, as already explained, one introduces a Boltzmann distribution of initial states and sums over the final degenerate states. Inspection of the hindered rotation model curve shows that the maximum around ϑ_k=90° is conserved, but the minimum is partly washed out by the average.

Out of a large manifold of state–to–state cross sections which contribute to the averaged cross section in Figure 3.9, I present in Figure 3.10 two typical examples of state–to–state excitations. As one can see, each state–to–state cross section minimum corresponds to a different ejection angle ϑ_k, explaining the shallow inflection in the average curve (Figure 3.9d). Using the Franck–Condon approximation, as I did in the present model, one can analyse these cross sections by discarding the dependence on β in the transition moment (see section 3.4). The state–to–state cross sections can now be interpreted in terms of hindered rotation wave function overlaps. In the state–to–state cross section presented in Fig.3.10a), the maximum density in the rotational functions corresponds roughly to $\beta \approx 90^\circ$ (see Fig.3.5 on page 67), and one obtains a picture close to the 'helicopter motion' model. In the second example (Fig.3.10b)) both rotational states (initial/final) are excited, and the maximum of the density can be estimated to be around $\beta \approx 75°$ (see Fig.3.5). From Figure 3.10 one sees that the extrema in the cross section appear in

the two cases presented, but compared to the average curve in Fig.3.9, their position is shifted and their relative maxima appear at different angles.

One can summarise the discussion about the physisorbed system CO/Ar, by saying that the hindered rotation allows a large variation of the angular motion of the internuclear axis. The divergence between the realistic approach and the simple models as gas phase, 'helicopter motion' or 'oriented–in–space' models is remarkable. One can explain this divergence by the difference of surface potentials for the final ionic and the initial neutral states. One observes a manifold of rotational state–to–state transitions contributing to the averaged photoelectron angular distribution. This fact stresses the usefulness of a model including hindered rotation.

3.3.2 CO/Ni(100)

In the following, I want to present the results of the photoelectron angular distribution of CO/Ni in the same energy region as for CO/Ar. For a given experimental geometry, I want to compare the results of the present model including hindered rotation with the 'oriented–in–space' model, where the molecular adsorbate is considered to be in upright adsorption position without rotation.

The incident light is linearly polarized with the polarization vector $\vec{\epsilon}$ oriented at 45° (usual experimental set–up) with respect to the surface normal and parallel to the x–axis (φ_q=0°). The electrons are emitted in the direction ϑ_k with φ_k= 0° , 180° in a plane defined by the surface normal and the polarization vector of the light. For convenience in Figure 3.11 I make a correspondence (as already done in the case of position of the internuclear axis, Figure 3.7) between a cut $\vartheta_k \geq 0°$, φ_k= 180° and $\vartheta_k \leq 0°$, φ_k= 0° . The hindered rotation model calculation presented in Figure 3.11 was obtained using the hindered rotation potential explained in section 3.2.2 and displayed in Figure 3.7 on page 71.

In the case of an adsorbed molecule on top of a nickel atom, the mean tilt angle β is small (around 10° , see table 3.4 on page 72). Using the hindered rotation model I have calculated the cross sections at two temperatures: 120 K and 300 K. Because the spacing between the rotational levels is larger than in physisorption, the number of Boltzmann populated states is restricted to two and three for 120 K and 300 K, respectively. Remember, that in the particular case of the hindered rotation potential I used for CO/Ni(100) (see Figure 3.7, p.71 and tables 3.3, 3.4 on page 69 and 72, resp.), the initial and the final states are very similar. To obtain the hindered rotation unresolved cross section displayed in Figure 3.11, I used the same procedure as for physisorption. Namely I summed up over state–to–state cross sections, taking into account the Boltzmann factors for the initial rotational states.

In Fig.3.11, I compare the calculations using hindered rotation and 'oriented–in–space' models. In this latter model the molecular axis was frozen normal to the surface. As in the case of physisorption, the results displayed in Figure 3.11 for the maximum of the 4σ shape resonance at 36 eV show the signature of a dominant $\epsilon f\sigma$ continuum. The maximum in the cross section is at about 10° and the two minima at about 40° and 60° . In the case of the $P_3(\cos\vartheta_k)=\frac{1}{2}(5\cos\vartheta_k^3 - 3\cos\vartheta_k)$ Legendre polynomial, corresponding to $\epsilon f\sigma$ continuum, the maximum is at 0° and the minimum at 39° . The displacement is mainly due to the geometry of the calculation where the incident photon angle is 45° . In the hindered rotation model, there is a small shift in the maximum and the minima of the angular distribution due to the tilted molecular axis (β=10°).

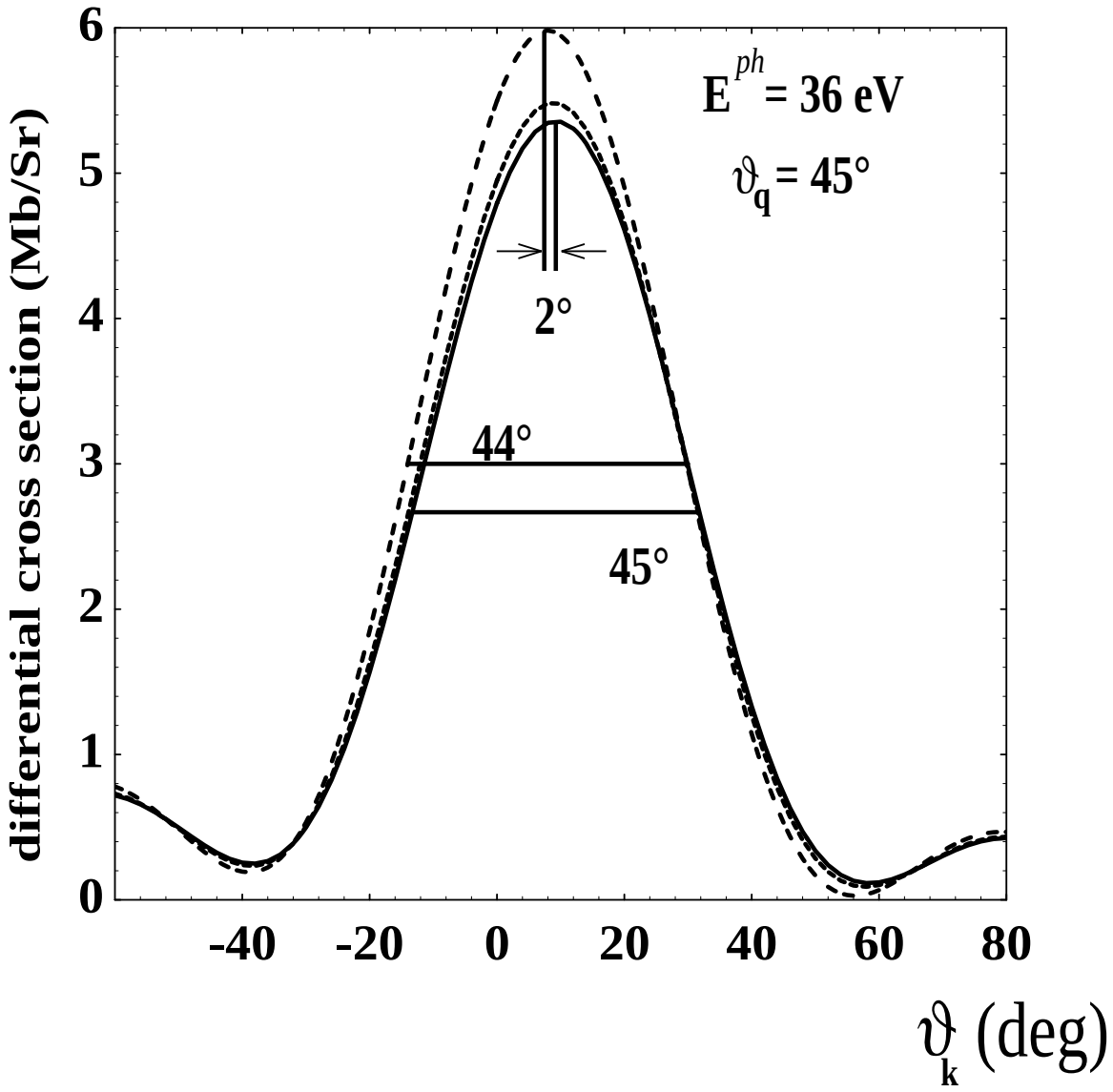

Figure 3.11: *Angular distribution of electrons emitted from CO/Ni(100) in the case of* $B^2\Sigma_{1/2} \leftarrow X^1\Sigma_0^+$ *excitation. The polarization vector of the linearly polarized light makes an angle of* ϑ_q*=45° with the surface normal. The other quantities are the same as in Figure 3.9. Calculation of two models is presented: a) 'oriented–in–space' (long–dashed line) and hindered rotation for two temperatures: b)* T_{rot}*= 120 K (short–dashed line), c)* T_{rot}*= 300 K (full line) (from Büchner and Raşeev [11]).*

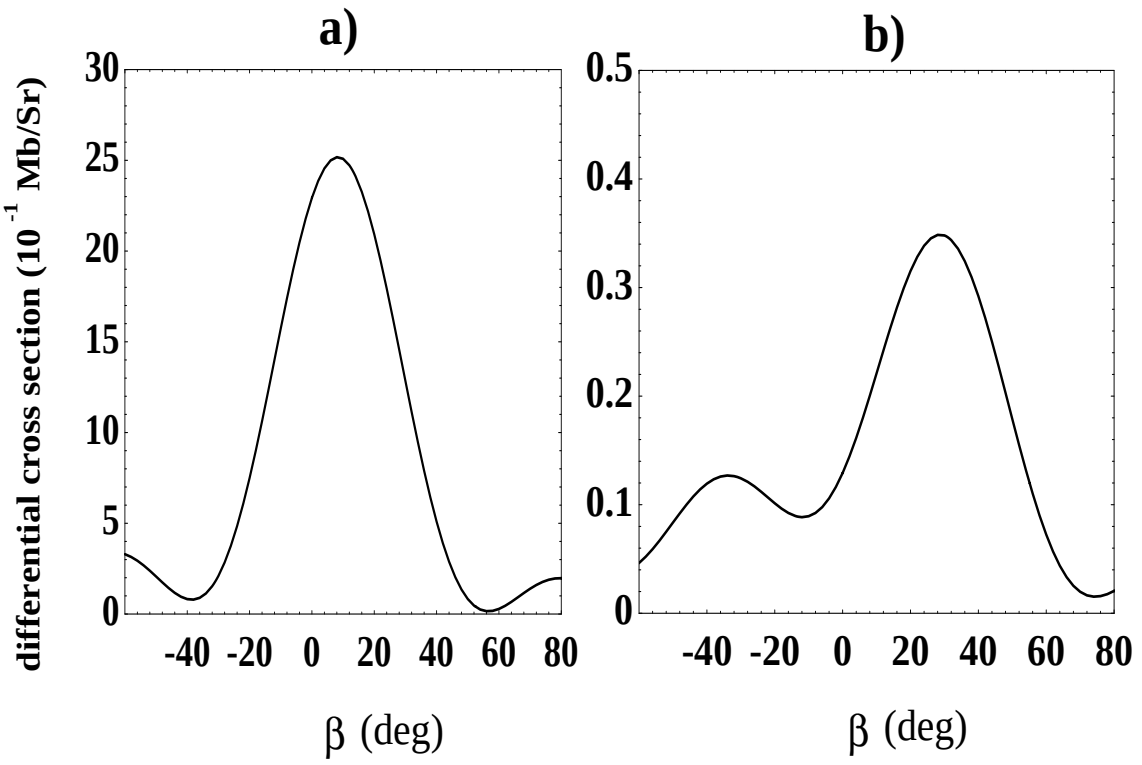

Figure 3.12: *Angular distribution of electrons emitted from CO/Ni(100). Same set–up as in Fig.3.11. a)* M^+*=1/2,* Ω^+*=1/2,* n^+*=0,* $\leftarrow$ $M^{"}$*=0,* $\Omega^{"}$*=0,* $n^{"}$*=0 b)* M^+*=3/2,* Ω^+*=1/2,* n^+*=2* $\leftarrow$ $M^{"}$*=0,* $\Omega^{"}$*=0,* $n^{"}$*=2 (from Büchner and Raşeev [11]).*

Inspection of Fig.3.11 shows also that, when introducing hindered rotation in the calculations, there is a drop in the maximum of the cross section which can be explained by the hindered rotation averaging over the angle β. Concerning the minimum at positive ϑ_k, one sees that in the "oriented–in–space" model the cross section approaches zero at around 60° . For the hindered rotation model this minimum is slightly displaced and the cross section at the minimum is larger. Due to temperature, one also sees a broadening of the resonance feature in the hindered rotation model calculation (45° compared to 44° in the "oriented–in–space model"). The broadening and the nonzero cross section at the minimum have been already observed in the experimental PS particularly in the case of inner shell ionization [14]. This ionization is a more favourable case than the shape resonance I have studied here because of a strong well known focussing effect of the ejected photoelectrons along the molecular axis.

A deeper interpretation of the results presented in figure 3.11 can be reached if one analyses the state–to–state cross sections. Figure 3.12 presents the dominant state–to–state cross section (Ω^+=1/2, M^+=1/2, n^+=0 $\leftarrow$ $\Omega^{"}$=0, $M^{"}$=0, $n^{"}$=0) and also the next strongest one (Ω^+=1/2, M^+=3/2, n^+=2 $\leftarrow$ $\Omega^{"}$=0, $M^{"}$=0, $n^{"}$=2). The intensity of this latter excited state–to–state transition is about fifty times smaller than the strongest one and therefore it will only weakly contribute to the averaged cross section. But one can see its very different angular behaviour, with the two maxima at about -40° and 20° and the two minima at about 10° and 70° . As the main state–to–state transition has a behaviour close to the "oriented–in–space" model, particularly with the minimum going down to zero cross section at around 60° , the temperature effects one sees on the average cross section are all due to the weak excited state–

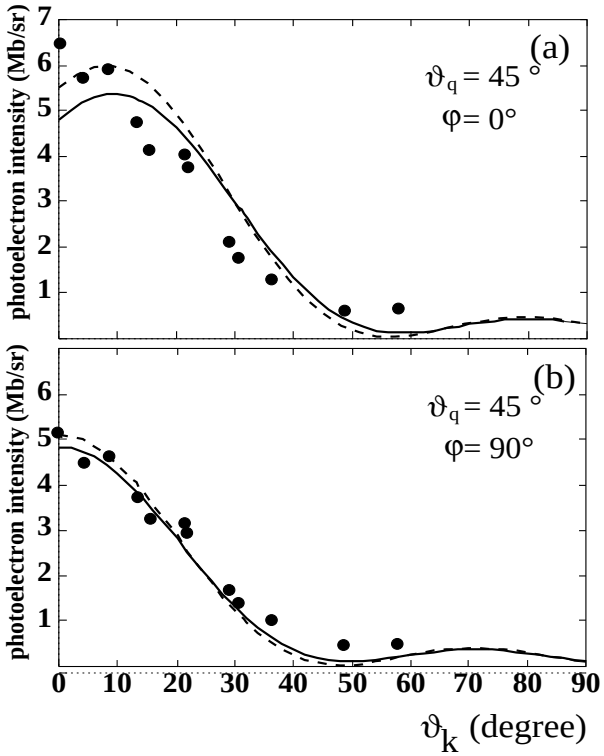

Figure 3.13: *Photoelectron angular distribution for CO/Ni(100) for* $(4\sigma)^{-1}$ *ionization. The photon is linearly polarized with* ϑ_q*=45° . The full line corresponds to the theoretical results* $h\nu$*=36 eV including hindered rotation at* T_{rot}*=300 K, while the dashed line to an 'oriented–in–space' model with CO adsorbed upright on the surface. The points are experimental results from Allyn et al. [4] (*$h\nu$*=35 eV), normalised to the theoretical ones. (a)* φ*=0° (b)* φ*=90° . Note, that the scaling in (a) and (b) is not the same (from Büchner and Raşeev [11]).*

to–state cross sections. One can say that the weak effect of the temperature on CO/Ni(100) calculations is mainly due to the particular potential I have used for this system, which I believe corresponds to reality. The spacing and the mean values of β for the initial neutral and ionic final states are so close that no significant intensity is allowed for excited states of the hindered rotation. Consequently the 'oriented–in–space' and hindered rotation models gives similar results.

This will not be necessarily the case for a different (more accurate) hindered rotation potential of CO/Ni(100) or for other chemisorbed systems. For these systems, even if the hindered rotation potentials are of the same strength and curvature, the initial and final potentials can be shifted against each other due to stronger charge image effects in the ion. Then the excited hindered rotation transitions will have larger intensities and will modify the angular behaviour of the cross section with respect to the "oriented–in–space" model.

For the $(4\sigma)^{-1}$ ionization of CO/Ni(100) experimental results have been obtained from Allyn *et al.* [4] and Rieger *et al.* [6]. In the following I compare the relative electron intensities of Allyn *et al.* to the ones obtained with the present theoretical model, as the other experimental data are not sufficient to disentangle the influence of hindered rotation on the spectra.

In Figure 3.13 I compare the theoretical results, already been presented in Fig.3.11 to experimental ones, obtained by Allyn *et al.* [4] for the $(4\sigma)^{-1}$ ionization. The used experimental geometry in [4] is ambiguous, the description indicates that the photoelectrons are measured in the polarization vector–surface normal plane (φ=0°), while for a comparison with the results of the 'oriented–in–space' model [37] the distribution of photoelectrons emitted perpendicular to this plane (φ=90 °) are shown. There I show the experimental results together with calculated results in both experimental geometries ((a): φ=0° , (b): φ=90°). The full line corresponds to the angular distribution obtained by the present model including hindered rotation at a temperature of 300 K, whereas the dashed line to the 'oriented–in–space' model. In Fig.3.13(a) the experimental relative intensities have been scaled to obtain a better agreement with theory. One can see, that either the 'oriented–in–space' or the present model can approach the experimental data on the angular distribution. For the other geometry the overall agreement is better and the model including hindered rotation are slightly closer to the experimental reality. Mainly at ϑ_k=48° the 'oriented–in–space' model predicts a vanishing angular distribution, which is not confirmed by experiment. In this region, the experiment shows a considerable intensity (18 % of maximal intensity). The present model predicts also a non vanishing intensity, but its value is too small.

I have presented above the photoionization of CO molecules adsorbed on top on Ni(100). The difference between the present approach, including hindered rotation and the 'oriented–in–space' model is small, but measurable, especially by changing the temperature of the sample. A comparison of the present model with experiment at 300 K shows a slightly better agreement than the results predicted by the 'oriented–in–space' model, but there are still discrepancies between experiment and theory. For the photoionization transition moments the present model has used the free CO molecule and the hindered rotation potential was derived using a single nickel atom. This can be changed by using transition moments for a NiCO cluster and including other surface atoms in the hindered rotation potential.

On bridge adsorption sites, one has observed experimentally [98] a large tilted angle that is a signature of a stronger influence of hindered rotation. Features due to hindered rotation may be enhanced by coverage of the surface (see part III of this thesis).

3.4 Recipe to determine a "mean" tilt angle for the adsorbate: The β–centroid approximation

The simplest way to take into account the nuclear motion in gas phase calculations is the Franck–Condon approximation and the related use of a frozen mean internuclear distance in the calculation of the electronic transition moment (Herzberg, p.194f [53]). The electronic and nuclear calculations become decoupled and a simple qualitative picture emerges. In this section, I introduce the same approximation for the hindered rotation angle β.

We first integrate the transition moment (2.7) over α and γ of $\hat{R} = \{\alpha, \beta, \gamma\}$ Euler angles. This integration gives rise simply to Kronecker symbols $\delta_{\mathrm{M}"+\ m\gamma,\ \mathrm{M}^+ + m+\mu}$ and $\delta_{\Omega"+\ \lambda\gamma,\ \Omega^+ + \lambda+\sigma}$ and consequently to selection rules with respect to the projections on laboratory or molecular frames of the angular momenta. The result in terms of Kronecker symbols originates from axial symmetry of the hindered rotation potential, i.e. from the simple form of rotational and Wigner functions assumed in (2.18) and (2.23), respectively. The electronic transition moment, independent of α and γ but transformed from molecular to laboratory frame, is now expanded in Taylor series around a mean value $\bar{\beta}$ (or $\cos\bar{\beta}$):

$$
\begin{aligned}
{}^{m^{ph}}_{\mu}\mathcal{T}^{\Omega^+\ \mathrm{M}^+\ n^+}_{\Omega"\ \mathrm{M}"\ n"}(\vec{k},\hat{q},\beta) = {}& {}^{m^{ph}}_{\mu}\mathcal{T}^{\Omega^+\ \mathrm{M}^+\ n^+}_{\Omega"\ \mathrm{M}"\ n"}(\vec{k},\hat{q},\bar{\beta}) \quad + \\
& + \frac{d}{d(\cos\frac{\beta}{2})}\ {}^{m^{ph}}_{\mu}\mathcal{T}^{\Omega^+\ \mathrm{M}^+\ n^+}_{\Omega"\ \mathrm{M}"\ n"}(\vec{k},\hat{q},\beta)\Big|_{\beta=\bar{\beta}}\left(\cos\frac{\beta}{2}-\cos\frac{\bar{\beta}}{2}\right) + \\
& + \mathcal{O}\left(\left(\cos\frac{\beta}{2}-\cos\frac{\bar{\beta}}{2}\right)^2\right)
\end{aligned}
\tag{3.4}
$$

The total transition moment, including integration over hindered rotation, analogue to (2.23) now reads:

$$
\begin{aligned}
{}^{m^{ph}}_{\mu}\mathrm{T}^{\Omega^+\ \mathrm{M}^+\ n^+}_{\Omega"\ \mathrm{M}"\ n"}(\vec{k},\hat{q}) = {}& \\
& W^{\mathrm{M}^+\ \Omega^+\ n^+}_{\mathrm{M}"\ \Omega"\ n"}\quad {}^{m^{ph}}_{\mu}\mathcal{T}^{\Omega^+\ \mathrm{M}^+\ n^+}_{\Omega"\ \mathrm{M}"\ n"}(\vec{k},\hat{q},\bar{\beta}) \quad + \\
& P^{\Omega^+\ \mathrm{M}^+ lm\lambda\mu\sigma}_{\Omega"\ \mathrm{M}",\ m^\gamma\ \lambda^\gamma}(\bar{\beta})\left(\frac{d}{d(\cos\frac{\beta}{2})}\ {}^{m^{ph}}_{\mu}\mathcal{T}^{\Omega^+\ \mathrm{M}^+\ n^+}_{\Omega"\ \mathrm{M}"\ n"}(\vec{k},\hat{q},\beta)\right)\Big|_{\beta=\bar{\beta}}
\end{aligned}
\tag{3.5}
$$

where

$$
W^{\mathrm{M}^+\ \Omega^+\ n^+}_{\mathrm{M}"\ \Omega"\ n"} = \int_0^{\pi} d\beta \sin\beta \quad f^{(\mathrm{final})\ n^+}_{\mathrm{M}^+\ \Omega^+}(\beta) \quad f^{(\mathrm{initial})\ n"}_{\mathrm{M}"\ \Omega"}(\beta)
\tag{3.6}
$$

and

$$P^{\Omega^+\ M^+ lm\lambda\mu\sigma}_{\Omega^{"}\ M^{"},\ m^\gamma\ \lambda^\gamma}(\bar{\beta}) = \tag{3.7}$$

$$-W^{M^+\ \Omega^+\ n^+}_{M^{"}\ \Omega^{"}\ n^{"}}\cos\frac{\bar{\beta}}{2} + \int_0^\pi d\beta \sin\beta \quad f^{(\text{final})\ n^+}_{M^+\ \Omega^+}(\beta) \quad \cos\frac{\beta}{2} \quad f^{(\text{initial})\ n^{"}}_{M^{"}\ \Omega^{"}}(\beta)$$

In the usual centroid approximation, one starts from a known potential for the nuclear coordinate and then calculates the overlap $W^{M^+\ \Omega^+\ n^+}_{M^{"}\ \Omega^{"}\ n^{"}}$ and the integral corresponding to the second term in $P^{\Omega^+\ M^+ lm\lambda\mu\sigma}_{\Omega^{"}\ M^{"},\ m^\gamma\ \lambda^\gamma}(\bar{\beta})$ (3.7). Then one obtains the centroid value by solving (3.7) for P = 0 which cancels the second term in expansions (3.4) and (3.5). In a similar way using the hindered rotation potentials of CO/Ar or CO/Ni(100) one can calculate for these systems $\bar{\beta}$ for a definite hindered rotational state. The values of $\bar{\beta}$ displayed in Tables 3.2 and 3.4 are calculated in this way.

Moreover the exact expression (2.23) can be replaced by the approximate expression (3.5), calculated for $\bar{\beta}$, and then used in the photoionization cross section (2.23). The discussion concerning the state–to–state cross section for CO/Ar or CO/Ni(100) in section 3.2 was led by using this β–centroid approximation.

One can also use the β–centroid approximation to predict, in a more precise way than by the use of the "oriented–in–space" model of Dill [38] and Davenport [37], the tilt angle of molecules adsorbed on surfaces. Let us take the example of a chemisorbed molecule oriented normal to the surface at a temperature low enough that mainly a single initial hindered rotational state contributes to the cross section. Supposed, that one uses linearly polarized light (m^{ph}=0) with $\vec{\epsilon}$ parallel to the surface (ϑ_q= 90°) and the x–axis (φ_q= 0°). For the case of the maximum of the shape resonance 4σ, or in the case of inner shell excitation, this corresponds to an experimental set–up or a calculation where the $\epsilon\sigma$, resonant or nonresonant, continua are forbidden in the "oriented–in–space"model, i.e. the cross section is zero for ϑ_k=0° . Now let us define a new quantity, namely the ratio between two differential cross sections corresponding to two ejection angles (ϑ'_k and ϑ''_k) or linear momenta ($\vec{k}'$ and $\vec{k}''$) calculated using (3.5) and (2.23). If, as in the β–centroid approximation, the second term of (3.5) is set zero, the ratio is proportional to the square of the transition moments:

$$\left(\frac{d\sigma}{d\vartheta_k}\right)_{\vartheta'_k} \Bigg/ \left(\frac{d\sigma}{d\vartheta_k}\right)_{\vartheta''_k} \propto \frac{\left|\mathrm{T}\left(\vec{k}', \hat{q}, \bar{\beta}\right)\right|^2}{\left|\mathrm{T}\left(\vec{k}'', \hat{q}, \bar{\beta}\right)\right|^2} \tag{3.8}$$

I chose ϑ'_k= 0° for the numerator cross section of (3.8), which corresponds to forbidden geometry. Because of hindered rotation included in the present model this numerator cross section will have small but measurable value. The denominator cross section is calculated at ejection angles ϑ''_k= 20° , 30° and 50° , φ''_k= 0° .

In Figure 3.14, I display the ratio (3.8) as function of $\bar{\beta}$ for different ϑ''_k given above. The curves of Figure 3.14 can be used to obtain the $\bar{\beta}$–centroid angle from the experimental cross section. Namely,

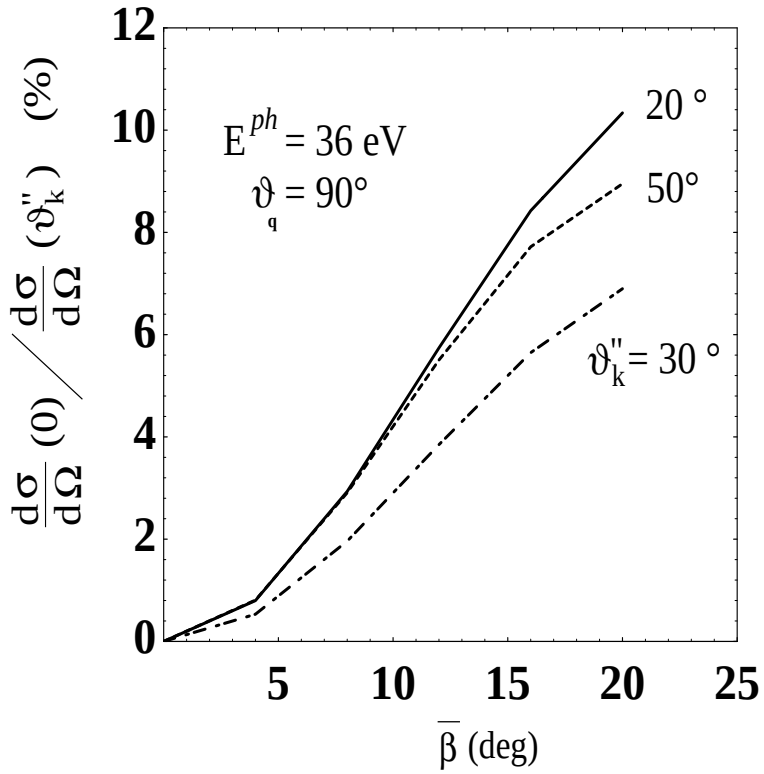

Figure 3.14: *Ratio of differential cross sections in % calculated in the β–centroid approximation as function of β–centroid angle. The photon of 36 eV is linearly polarized (ϑ_q=90° , φ_q=0°), while the electron emission in the plane defined by the surface normal and the light polarization vector is calculated for the angles: ϑ''_k= 20° , 30° , 50° , φ''_k= 0° .*

given experimental photoelectron intensities obtained for adsorbed CO at the 4σ resonance maximum, one first calculates from them the intensity ratio (3.8) for ϑ'_k= 0° and ϑ''_k corresponding to 20° , 30° or 50° . Then, knowing ϑ''_k, this ratio corresponds to a particular value of the ordinate, particular curve and value of $\bar{\beta}$ on abscissa on Fig.3.14. It follows that the present β–centroid model, where the hindered rotation appears explicitly, can be used to obtain a β–centroid angle from experiment. In the case of a different excitation of CO or another molecule, one simply needs the calculation of the corresponding electronic transition moments and of the ratio of squares (3.8) which will be displayed on a new plot equivalent to the Fig.3.14. The search of the average angle $\bar{\beta}$ by the present approach is limited to cases where a single hindered rotation initial state is predominant, which in practice means low temperature.

The β–centroid model used to obtain the tilt angle of the molecule adsorbed on a surface does not use explicitly the hindered rotation overlaps, but it takes properly into account the hindered rotation, i.e. the tilt angle and the molecular precession. A procedure like the one described above can not be based on the "oriented–in–space" model mainly because, in that model, the molecule does not undergo libration and precession. To understand this statement, let us consider a molecule tilted (β–centroid $\neq 0°$) with respect to the surface normal. We now try to find this tilt angle using the "oriented–in–space" model. First of all $\bar{\beta}$ is not defined in the "oriented–in–space" model. Usually one relates $\bar{\beta}$ to $\tilde{\vartheta}_q$, the angle between the molecular axis and the incident direction of the photon. Using the "oriented–in–space" model, one first calculates the photoionization cross section for several angles $\tilde{\vartheta}_q$. Then one compares these theoretical

curves with the experimental ones and search for the best fit between theory and experiment, obtaining an optimal value for $\tilde{\vartheta}_q$. The resulting $\tilde{\vartheta}_q$ can be approximatively related back to β. Unfortunately the above procedure implies a completely frozen position (α and β fixed on Fig.2.1) of the molecule with respect to the nuclear motion on surface. In reality, and of course in the present model, the molecule undergoes precession (α is changing) and it is only accidentally that $\bar{\beta}$ derived from "oriented–in–space" model will correspond to $\bar{\beta}$ of the β–centroid model. Given the coordinate system introduced in this paper with the z–axis parallel to the surface normal, one can imagine an intermediate approach between the present and the "oriented–in–space" models. Namely one performs calculations at fixed angle α (see Fig.2.1), takes into account precession around the laboratory z–axis and averages the result. This approach discards rotations and will be valid if the rotational spacing is small and the temperature is high.

These models were derived for axial symmetry where hindered rotation can be defined. When vibration in zx and/or zy perpendicular plane are nonequivalent the standard 'oriented–in–space' model also breaks down and does not allow the derivation of the mean tilt angle. This is because it is impossible to reduce even low amplitude nuclear motion to a fixed position in space and derive a mean position of an axis associated with this motion.

Chapter 4

Conclusion and perspectives for photoionization

In this first part of my thesis, I discussed specific phenomena that are related to photoionization of molecular adsorbates. I treated two phenomena, backscattering and hindered rotation, which were nearly ignored up to now in literature. Both processes are important as backscattering causes a constructive or destructive interference of photoelectron waves and hindered rotation is the only nuclear mode, that changes the orientation of the molecular axis and therefore the photoelectron angular distribution.

I developed a theoretical model for hindered rotation and applied it to two adsorbate systems, CO physisorbed on an argon and CO chemisorbed on a nickel surface, both at on top sites and low coverage limit. New formulae for the differential cross section, including the hindered rotation, were derived. The model is based on the dipole, the Born–Oppenheimer and the Franck–Condon approximations. A realistic coordinate system allows the modelisation of vibrating molecular adsorbates in a tilted configuration about the surface normal. The photoionization electronic transition moments are calculated by ab–initio methods, including the continuum wave function of the escaping photoelectron calculated in the field of the adsorbate. For the nuclear motion, the hindered rotation was considered, by using an axial symmetric surface potential adapted from literature. The hindered rotor wave function was developed in free rotor functions and the resulting Schrödinger equation was solved numerically, separately for the initial neutral and final ionic states.

For the chemisorbed system CO/Ni(100) the effects of hindered rotation are small, but measurable. I show that for $(4\sigma)^{-1}$ ionization of the ground state of CO in given experimental arrangements ('allowed' geometry), the model of Davenport, Dill and Dehmer [37, 38] can model the experimental data. In this model, called 'oriented–in–space' model, the influence of the surface reduces to an orientation of the molecule in space. But experimentally in the case of CO/Ni core level excitation, hindered rotation has been observed by a temperature broadening in the angular distribution [14]. In this thesis, I showed that this broadening is caused by additional transitions from thermally occupied hindered rotational levels in the ground state.

For the physisorbed system CO/Ar, I again calculated the photoelectron angular distribution at the maximum of the 4σ shape resonance. In this case my sophisticated model gives results, which are very

different from the 'oriented–in–space' model. To analyse this difference I compared the two models mentioned above with the one where angular motion of the adsorbate corresponds to gas phase or to a 'helicopter motion' parallel to the surface. None of the limiting models is able to reproduce the present model, including hindered rotation motion in a realistic surface potential.

This hindered rotation also breaks 'oriented–in–space' selection rules. These selection rules have been used in literature to derive tilt angle of the molecular adsorbate or symmetries of the contributing transitions. For chemisorbed molecules, I presented a recipe to derive a mean tilt angle, now including the effect of hindered rotation. With this method, one can also judge the importance of this breaking of symmetry and therefore the influence of hindered rotation on photoionization spectra.

The effect of backscattering was taken into account using a simple model, developped in our group mainly by Pavel Budău [13], where the surface is introduced as a step potential. This potential allows a partial reflection of photoelectron waves, which interfere together with the direct emitted waves. In this first application of the model I neglected the hindered rotation and CO was assumed to be adsorbed in upright position. To minimise the influence of hindered rotation a given experimental arrangement was chosen, called 'allowed' geometry. For the 4σ shape resonance of CO (photon energy 36 eV) the contribution of electron emission towards the surface is small, and the effect of electrons backscattered by the surface is minor. For the 5σ shape resonance (28.5 eV) there is important contribution from backscattered electrons that changes significantly the angular distribution. I showed in this part of my thesis, that for tilted molecules, backscattering is also important for the breaking of 'oriented–in–space' selection rules.

The first and straightforward extension of the present model is a combined method including hindered rotation and backscattering. This work is now in process. The chemisorbed adsorbates should be modelled by a cluster including at least one surface atom. Such calculations were already published [46] and in our group calculations, including hindered rotation, are in process [99].

Another extension of the model is the introduction of the adsorbate coverage of the surface in photoionization. In the next part of my thesis, I will show how coverage restricts the hindered rotation. From this work, one can extract a local effective potential for hindered rotation, replacing the one–adsorbate–surface potential used up to now. This potential is asymmetric with respect to precession of the adsorbate and therefore one should extend the photoionization model of hindered rotation to include such potentials.

In the future the present model should be applied to systems where the adsorbate–surface interaction is intermediate between physisorption and chemisorption. Particularly one can think at systems including a spacer or interlayer. The analysis of hindered rotation has to be done over a whole energy region of a resonance and may include autoionization and cooper minimum.

The present model including hindered rotation in relation with electronic processes can be used in closely related fields. One can cite electron–molecule collisions for physisorbed molecular adsorbates, where the role of hindered rotation is a hot topic and is intensely discussed [100–102].

Summarising, the technique of photoionization allows a snapshot of the adsorbate–surface system. In photoionization electronic and nuclear excitations are simultaneously present and the corresponding spectra hide additional informations that can be obtained by other experimental techniques like Electron Energy Loss Spectroscopy , InfraRed Spectroscopy , and photodesorption. This work can be regarded as

a challenge to experimentalists to search for the role of hindered rotation by studying different adsorbate–surface systems, varying the coverage. Its role is essential in dynamical processes related to the motion of electrons or nuclei as hindered rotation influences the angular distribution of fragments.

Part III

Coverage and nuclear motion of adsorbates

Résumé

Les modèles théoriques de la première et dernière parties de ma thèse, s'appliquent strictement uniquement pour une seule molécule adsorbée sur la surface ou pour un taux de couverture de celle-ci très faible. Dans une expérience de photofragmentation d'adsorbats, le taux de couverture de la surface est contrôlé par la pression du gaz de l'enceinte et le temps d'ouverture de la valve d'admission. Un taux de couverture faible est difficile à réaliser expérimentalement et même si on l'obtient il ne permet pas d'avoir un flux des photofragments suffisant pour une détection avec une statistique acceptable. Le cas d'une couverture dense est le plus souvent rencontré dans l'expérience et par conséquent un modèle théorique réaliste doit inclure les interactions entre les adsorbats voisins.

Dans cette deuxième partie de ma thèse, l'influence de la couverture des adsorbats moléculaires sur la géométrie des sites d'adsorption et la dynamique vibrationnelle en tenant compte du mouvement angulaire de la molécule sont étudiées avec des modèles théoriques issues de la mécanique classique et quantique.

Le cas de la molécule de CO physisorbée sur une surface (100) d'argon a été étudié par une technique de trajectoire classique. On a déterminé les sites préférentiels d'adsorption en tenant compte du changement de mouvement angulaire des adsorbats moléculaires en fonction du taux de couverture. Pour une couverture faible, une seule molécule CO adsorbée simule parfaitement cette situation. Par contre, pour une couverture dense, la simulation doit inclure plusieurs adsorbats et le nombre de dégré de liberté devient important. Pour minimiser les interactions CO–CO, les molécules CO ont tendance à se grouper pour former des agrégats. Dans le cas d'un agrégat de neuf molécules CO tous les sites accessibles sont occupés, la molécule centrale est complètement entourée des molécules voisines et on modélise localement une monocouche complète. En variant le nombre des molécules de l'agrégat, un changement de couverture est simulé pour la molécule centrale. Le résultat le plus marquant de l'étude par dynamique classique est la rigidification du mouvement azimutal de la molécule centrale (précession) en augmentant le taux de couverture.

J'ai fait une analyse basée sur la mécanique quantique du mouvement angulaire d'une seule molécule CO et de la molécule centrale dans un agrégat de sept molécules CO adsorbées sur Ar(100). Les résultats vérifient la rigidification trouvée par la dynamique classique, qui se manifeste par une augmentation d'espacement entre les niveaux d'énergie rotationelles et par une localisation de la densité de la fonction d'onde. L'approche quantique montre des aspects qui ne peuvent pas être obtenus par des modèles de dynamique classique. Si l'on analyse l'énergie de point–zéro en termes de température rotationnelle classique, on obtient 117 K bien au dessus de la température de l'étude classique de 10.5 K. Ce fait permet au système traité quantiquement une accessibilité à d'autres minima que le minumum absolu. Cette accessibilité fait qu'on obtient quatre configurations géométriques qui sont presque dégénérés en énergie. Pour certaines de ces configurations, les densités des fonctions d'ondes indiquent qu'il y a des effets tunnel entre elles provoquant des changements d'orientation de l'adsorbat moléculaire par rapport à la surface. Ces densités montrent aussi que le mouvement angulaire est dominé par un compromis entre plusieurs géometries équivalentes (ou leurs minima de potentiel) et des effets tunnel à travers des barrières du potentiel. Il faut souligner que l'existence de plusieurs configurations presque dégénérées et des effets tunnel entre elles montre que sur

la surface il y a plusieurs orientations des adsorbats presque equivalentes et qu'une rotation libre de l'adsorbat n'est pas permise. Cette analyse par la mécanique quantique montre bien la complémentarité entre les deux approches classique et quantique utilisées dans cette étude.

En résumé, la couverture modifie le mouvement angulaire de la molécule CO physisorbée sur Ar(100) et plus généralement toute sa dynamique nucléaire. Ces résultats sur le comportement des adsorbats moléculaires en fonction de la couverture ont une portée générale et les modèles étudiant les spectres de photoionisation et de photodésorption doivent inclure les effets correspondants. Pour cette raison les résultats obtenus dans cette partie seront utilisés prochainement pour améliorer les modèles développes dans la première et troisième partie de cette thèse.

Chapter 1

Introductory remarks in adsorbate coverage

Experimentally, the adsorption of a molecular gas on a surface is monitored by the dose of the gas, i.e. by the time the entrance valve is opened, its dimensions and the gas pressure during this time. One can not adsorb a single molecule on a surface. Low coverage of the adsorbate is realizable, but in a photoionization experiment the flux of photoelectrons is low and the data analysis becomes difficult. The usual theoretical models consider either a single molecule on a surface or a full mono-layer of adsorbed molecules. In this part of the thesis I will present a work that shows how the adsorbate–surface system changes from a single molecular adsorbate to a full mono-layer. This work is intended to fill the gap between the two approaches mentioned above.

When the coverage is high, the distance between neighboured molecules becomes small and their electronic clouds overlap, resulting in a shift of the adsorbate induced peak in photoionization [15, 16]. In photodesorption mechanism the hindered rotation (and also translation) is strongly coupled with the desorption mode. Therefore the analysis of the kinetic energy of the fragments and their angular distribution also changes with coverage.

More specifically in the photoionization part of this thesis (part II), I discussed the influence of hindered rotation on the orientation of the molecular axis of the adsorbate and on the ejection of the electrons. There, I used the approximation of low coverage, i.e. a single molecule on a surface. But, adsorbate–adsorbate interactions, mainly dipole–dipole interactions, modify nuclear motions [17] and change the orientation of the internuclear axis of the adsorbate about the surface. It has been observed in InfraRed Spectroscopy (IRS) and in Low Energy Electron Diffraction (LEED), that the separation of energy levels of the internal vibrational mode of chemisorbed CO changes with coverage [18]. In Electron Stimulated Desorption in Angular Distribution (ESDIAD) for CO/Ni(110) at high coverage, Alvey *et al.* and Riedl and Menzel observed an inclination of the intra-molecular axis by 19° from the surface normal in the [100] direction, while at low coverage CO is adsorbed in upright position [19, 20]. For CO/Ni(100) in the case of core level excitation in photoionization, Wesner *et al.* observed that the photoelectron angular distribution depends strongly on the adsorbate coverage [14].

Considering all these experimental results, it is evident, that the coverage influences the photoionization

spectrum indirectly through modification of nuclear motions and particularly changes of orientation of internuclear axis. This orientation influences strongly the angular distribution of the ejected photoelectrons. There are several theoretical approaches studying the coverage dependence of nuclear motions. Batra *et al.* and Persson *et al.* used Monte–Carlo simulations to model LEED and infrared spectra of CO/Pt(111) [103, 104], but they do not take into account the angular motion of the molecular adsorbate. Evens *et al.* [105] and Lynden–Bell et al. [106] considered temperature dependent phase transitions in N_2 films on graphite but coverage dependence was not studied explicitly even if the temperature change modifies the coverage.

None of the models mentioned above introduce explicitly the angular motion of the internuclear axis. To simulate the coverage, one can develop a quantum mechanical model including several neighbours. But the number of degrees of freedom is high. The adsorbate – adsorbate interaction is essentially dipole – dipole and therefore relatively weak but long range. Consequently a full quantum mechanical approach is not tractable for this problem.

In this part of the thesis, I present a different approach based on classical trajectory calculations which can give the stable configuration and the corresponding dynamical evolution of the system. One can use these stable configurations to calculate an effective local potential, seen by the central molecule. This effective potential includes now the interactions of the neighbouring adsorbates and can be introduced back in the quantum mechanical photofragmentation methods (photoionization and photodesorption), giving observables influenced by the coverage.

The influence of the coverage on the position of the internuclear axis (angular behaviour) in the case of the physisorbed system CO/Ar(100) was calculated, using the classical approach. The argon surface is represented by three layers, with the first consisting by 10×10 argon atoms. To simulate the transition from low to high coverage (full mono-layer), one up to nine CO molecules are adsorbed on the argon surface. As the CO molecules tend to form a cluster, the central molecule is surrounded by eight adsorbates occupying all the available sites. The effective potential felt by the central molecule corresponds to a full mono-layer.

In section 2.1.1, I briefly present the results based on the classical dynamical approach. The stable adsorption geometries and the dynamical motion of the adsorbate is presented in sections 2.1.2 and 2.1.3, respectively. The coverage dependent effective local potential is derived and discussed in section 2.2, detailing its use in a quantum–mechanical model. To study the influence of adsorbate coverage, the surface potential is non-axial symmetric about the surface normal and consequently the precession around this axis may perform a complicated motion. No free rotation, as assumed in part II of the thesis, can be supposed. Consequently, I generalize the model of the photoionization part of this thesis (p.56) to include a non–axial symmetry (part III, section 2.2.1). In section 2.2.2, I present results for the hindered rotation wave function. This part of the thesis ends with a conclusion (3.1) and an outlook (3.2), emphasising the aspects of photoionization and photodesorption.

Chapter 2

CO/Ar(100): A model including several CO molecules

To study the influence of coverage a model system, CO physisorbed on the (100) surface of a fcc argon crystal was chosen [21]. The influence of coverage is simulated by varying the number of CO molecules from one (low coverage) to nine (high coverage). For CO/Ar the interaction between neighbouring adsorbates is higher than the CO–Ar one and adsorbate clustering is favoured. Consequently the latter configuration can simulate a full monolayer (called hereafter high coverage), as one CO molecule is surrounded by eight other CO molecules, occupying all the available sites. The surface coordinate system has its z–axis parallel to the surface normal, while the x and the y axis are defined by the [010]

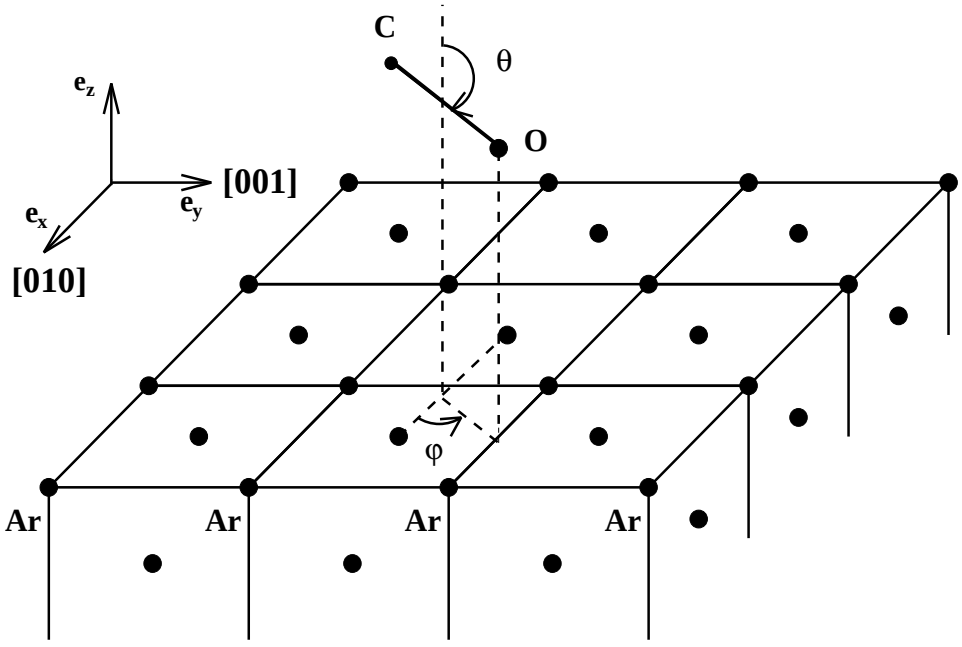

Figure 2.1: *CO physisorbed one Ar(100) (from Parneix et al. [21].*

and [001] directions, respectively. The surface coordinate system is represented as an inset on Figure 2.1. The position of adsorbed molecule is defined by its centre of mass and the orientation of molecular axis relative to the surface normal is (z–axis) given by the polar angle θ and the azimuthal angle φ. In the present model no internal vibration and no phonons were considered, the adsorbate internuclear distance is fixed to 1.1283 Å and the surface atoms are in the Ar(100) fcc configuration. The surface consists of 321 argon atoms in two layers separated by the lattice constant of l_0=5.31 Å.

2.1 Configurations and nuclear motions: Classical approach

2.1.1 Theoretical model: Potential and classical trajectories

In this subsection I give the total potential for the CO–CO and CO–Ar interaction and describe briefly the molecular dynamics simulation model, which uses the technique of classical trajectories and an algorithm developped by F. Amar and P. Parneix [107].

The potential energy function of the problem consists of the CO–Ar and the CO–CO interactions, taken from literature. The form of the CO–Ar potential was proposed by K.Mirsky [86] and was already used for the CO/Ar photoionization in this thesis (part II, section 3.2.1). It has the form:

$$V_{Surface-CO} = \sum_{i=1}^{2} \sum_{j=1}^{321} B_i \, e^{-\beta_i r_{ij}} - \frac{A_i}{{r_{ij}}^6} \tag{2.1}$$

In Equation (2.1) r_{ij} is the distance of the j^{th} surface atom to the oxygen (i=1) and the carbon (i=2) atom. The values B_i, β_i and A_i are summarised in Table 2.1.

The CO–CO (lateral) interaction is close to the one given by Picaud *et al.* [108]. It was slightly modified and is given here by the pairwise interaction developed in local charge and dipole interactions, each situated at the oxygen, the carbon atom and the centre of mass. The equation for an interaction between two molecules A and B contains Lennard–Jones and multipole interaction terms:

$$V_{(CO)_A-(CO)_B} = \sum_{i=1}^{2}\sum_{j=1}^{2}\left(\frac{C_{12}^{ij}}{{r_{ij}}^{12}} - \frac{C_6^{ij}}{{r_{ij}}^6}\right) + \frac{1}{4\pi\epsilon_0}\sum_{k=1}^{3}\sum_{l=1}^{3}\left(\frac{q_k q_l}{r_{kl}} - \frac{q_k \mu_l}{{r_{kl}}^3}\vec{e}_B.\vec{r}_{kl} - \frac{q_l \mu_k}{{r_{kl}}^3}\vec{e}_A.\vec{r}_{kl}\right) \tag{2.2}$$

	A (cm^{-1} Å^6)	B (10^{-5} cm^{-1})	β (Å^{-1})
carbon atom	282462	260.812	3.493
oxygen atom	228795	274.187	3.706

Table 2.1: *Potential coefficients for CO–Ar (from K.Mirsky [86]).*

	q (a.u.)	μ (a.u.)
C atom	0.5655	1.0573
O atom	0.2994	-0.4142
CM of CO	-0.8649	-0.2866

Table 2.2: *Modelisation of CO–CO interaction: charges (q) and dipoles (μ) located at the C, O atom and the centre of mass (CM) of CO (from Picaud et al. [108]).*

		C	O
C	C_6	16301	14332
	C_{12}	17833914	12354606
O	C_6	14332	12476
	C_{12}	12354606	8391594

Table 2.3: *Modelisation of CO–CO interaction: values for the parameters C_6 and C_{12} of Eq.(2.2) in meV/Å^6 and meV/Å^{12}, resp. (from Picaud et al. [108]).*

In the first parenthesis of (2.2) i and j labels the C and O atoms. ϵ_0 is the permittivity of free space and in the second parenthesis the indices k and l label the location of the three charges q_k and dipoles μ_k on C, the O atom or CO centre of mass. $\vec{e}_A$ and $\vec{e}_B$ are the unit vectors along the intra-molecular axis of molecule A and B, respectively. Picaud *et al.* [108] use also three quadrupoles to model the CO–CO interaction. From the three charges, dipoles and quadrupoles (not shown in Eq.2.2) one can calculate the dipole and quadrupole of isolated CO. One finds that if these quadrupoles are neglected, the dipole of CO does not change, but the quadrupole is slightly closer to experiment. Therefore here the quadrupole interaction is neglected and the lateral interaction is assumed to have the form of Eq.(2.2) using the coefficients of Tables 2.2 and 2.3.

Secondly, the technique of classical trajectories is used to obtain stable configurations for $(CO)_n$/Ar(100) (n=1,...,9), a technique which is well known and also intensively used in surface science [109–111]. Below I briefly summarise the used algorithm. For a detailed description, the reader is referred to the PhD thesis of P. Parneix [107] or M. P. Allen and D. J. Tildesley [112].

The equations of motion consist of a classical Hamiltonian for generalized coordinates, i.e. time dependent spatial coordinates and generalized velocities building the phase space. One obtains differential equations, that connect the potential to these generalized coordinates. Starting from initial values, the equations are solved by propagation techniques in time space. The 'Adams–Moulton Predictor–Corrector' propagation method [113, 114] of order 4 (rotation) and 5 (translation) is used in the present algorithm. It has three steps: the initialisation of all coordinates at time t=0 s, a prediction of the generalized coordinates at time $t + \Delta t$ and finally their correction. Taking as example the translation, the spatial coordinates and their derivatives in time up to the 5^{th} order are considered in the propagation [107]. First, for the initialisation at t=0 s the coordinate and the velocity are arbitrarily chosen. These initial values and the acceleration due to the potential define the zero, first and second order derivatives, while the higher ones are taken to be zero. Secondly, for the prediction, these initial values and a Taylor expansion are used to estimate all coordinates and their derivatives at time $t + \Delta t$. Thirdly, the predicted values are corrected by a weighted difference between the predicted second derivative and the force acting on the system at the predicted coordinate position at time $t + \Delta t$. The latter correction can be iteratively repeated until convergence. Using the corrected values of all derivatives, the full procedure, prediction and correction, is repeated for the next time step $t + 2\Delta t$. For the present application, this method was used with a time step Δt of 5 fs and one correction iteration [61, 21]. The used propagation technique with this time step determines an excellent energy conservation of the order of 10^{-5} after trajectories of 5 ns duration [21].

The structures of minimal energy are calculated in the following way. At the beginning of the calculation,

the total energy of the molecules is high and their motions at constant total energy allow a large occupation of phase space. In order to prevent the CO molecules to desorb, a repulsive potential located outside a sphere with its origin on the surface and a radius varying from 2.5 to 7.5 Å for $(CO)_1$ and $(CO)_9$ molecules, respectively, was added to Eq.(2.2) The potential is dependent on the distance of the CO–centre of mass from the origin and has a harmonic form with the harmonic constant of 600 $cm^{-1}/Å$. It forces the molecules to be repelled towards the inner sphere. Each 5 ps friction forces are added and the energy of the molecules decreases [61]. With this procedure local minima of the potential hyper-surface are found. The global minimum defines the most stable configuration of the molecular adsorbates. To search for a global minimum several initial values were chosen randomly. As the system does not contain a large number of moving particles, the number of local minima is restricted and the global minimum is easy to identify. Knowledge of the stable configurations from gas phase, considerations about the structure of the surface potential and previous calculation for a lower number of CO molecules can also help to test if a minimum is global.

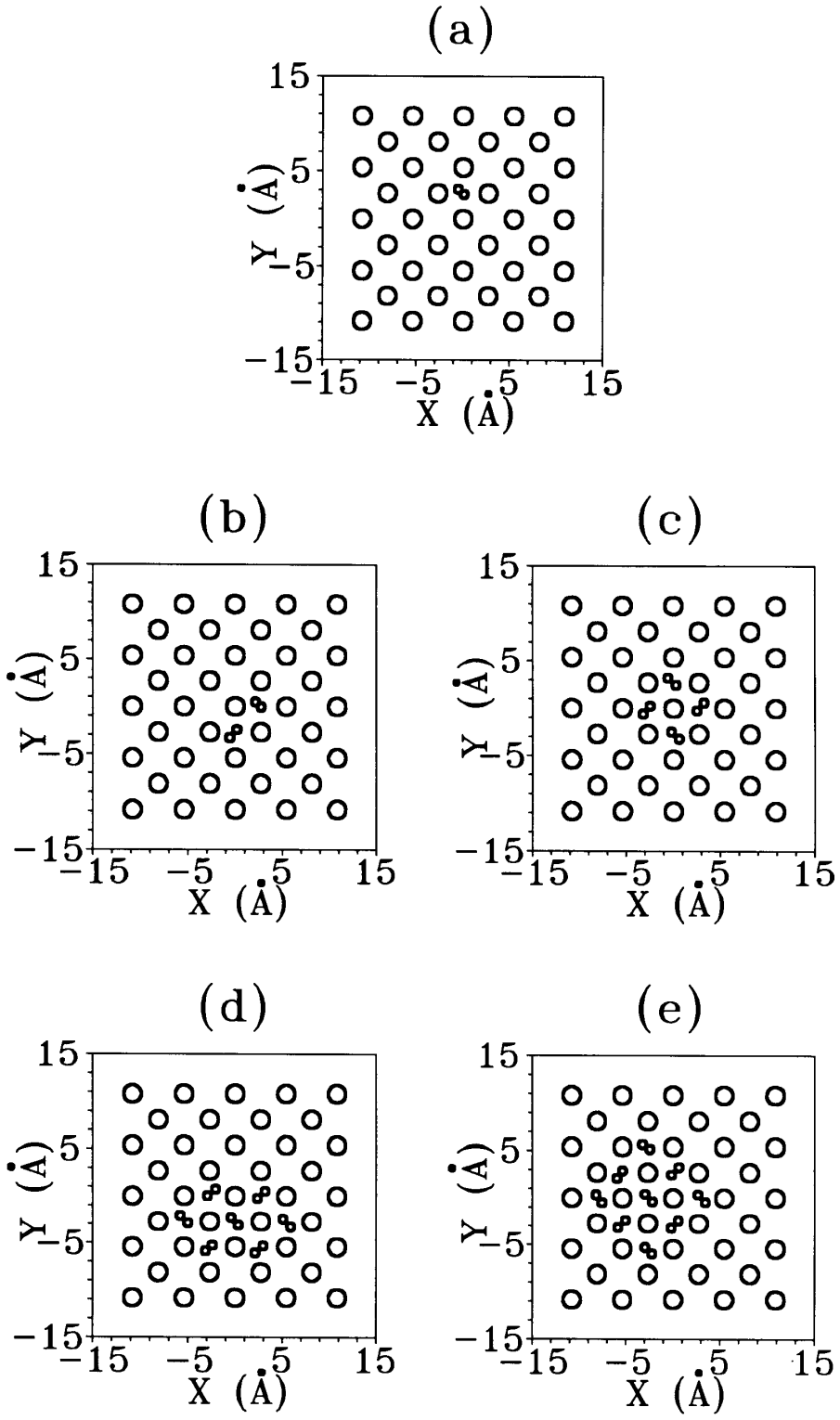

Figure 2.2: *Stable adsorption geometries for $(CO)_n$, n=1 (a), n=2 (b) n=4 (c), n=7 (d) and n=9 (e) (from Parneix et al. [21]).*

2.1.2 Adsorption geometries and effective potentials of $(CO)_n$ /Ar(100)

In this section I present the results of a classical dynamical calculation for the physisorbed system CO/Ar(100) at low temperature performed in collaboration with P. Parneix, G. Raşeev and N. Halberstadt [21]. The influence of adsorbate coverage on angular motion is simulated by varying the number of CO molecules from one to seven.

Figure 2.2 shows the stable configurations of CO/Ar(100) for one (a), two (b), four (c), seven (d) and nine (e) adsorbed CO molecules. A single CO molecule adsorbs with a binding energy of -545.3 cm^{-1} preferentially parallel to the surface (θ=134° , φ=-44°) with a slightly displaced two–fold bridge adsorption site (x=-0.19 Å, y= -2.83 Å) and a distance centre of mass of CO — surface of 2.59 Å. In Fig.2.2(b) the most stable adsorption geometry for two CO molecules is shown (see also the next paragraph). The binding energy of the present adsorbed dimer configuration is -1276.3 cm^{-1}, while for an isolated molecule the energy is higher (-1090.6 cm^{-1}). The formation of dimers is energetically favoured and so is the formation of CO clusters with higher number of molecules (see Fig.2.2(c),(d) and (e)).

In fact, I present the most stable adsorbate geometries. But, other geometries are possible and may play an important role in adsorption. In Fig.2.3 I show the first three configurations and their binding energies for $(CO)_2$/Ar(100). Fig.2.3(a) is identical to Fig.2.2(b), it displays the most stable configuration at -1276 cm^{-1}. Both molecules are adsorbed on slightly displaced two–fold bridge sites with the inclination angles of $\theta_1 \approx 130°$ and a flat lying second molecule $\theta_2 \approx 90°$. One molecule is in a perpendicular adsorbate position with respect to the second one (φ_1=135° , φ_2=45°). In the next stable adsorbate geometry the two molecules still keep their adsorption sites but they are nearly parallel to each other. Note, the binding energy is close to the one of the most stable configuration (-1251 cm^{-1}). In the third configuration (Fig.2.2(c)) the two CO molecules are adsorbed near two–fold bridge sites, but contrary to the first two configurations one argon atom separates the two molecular adsorbates. The binding energy is -1164 cm^{-1} and therefore 87 cm^{-1} higher than the energy of the second adsorption geometry (b).

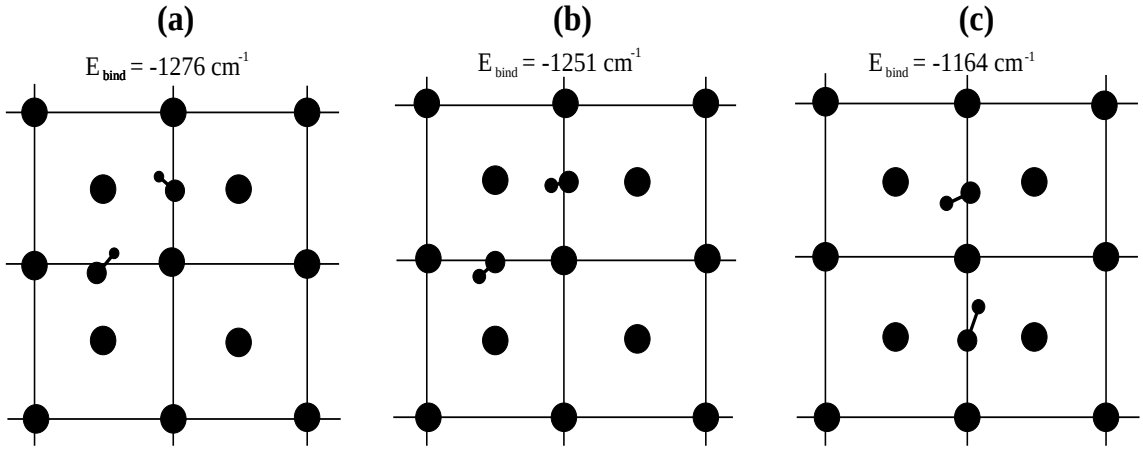

Figure 2.3: *The energetically lowest adsorption geometries of two CO molecules adsorbed on Ar(100) (fcc). The adsorption energy E_{bind} is -1276, -1251 and -1164 cm^{-1}, respectively (from Parneix [61]).*

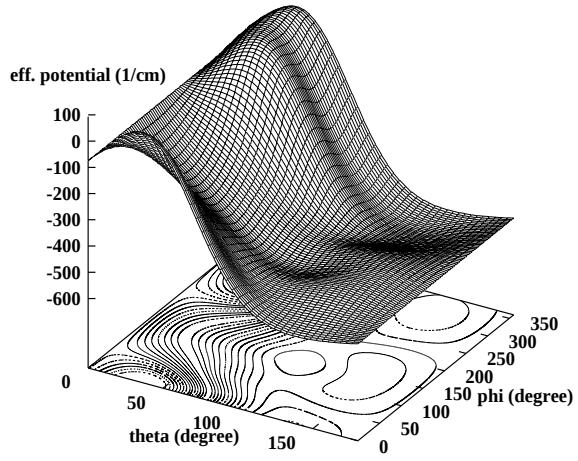

Figure 2.4: *Potential for single CO adsorbed on Ar(100). The dependence of the potential on the molecular orientation angles θ and φ is plotted (data from Parneix [61]).*

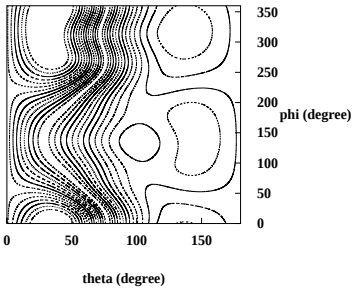

Figure 2.5: *Contour plot representation of Fig.2.4. The minimum is at θ=135° , φ=316° and V = -545.3 cm^{-1}. Each line indicates a difference of 20 cm^{-1} starting at -550 cm^{-1}.*

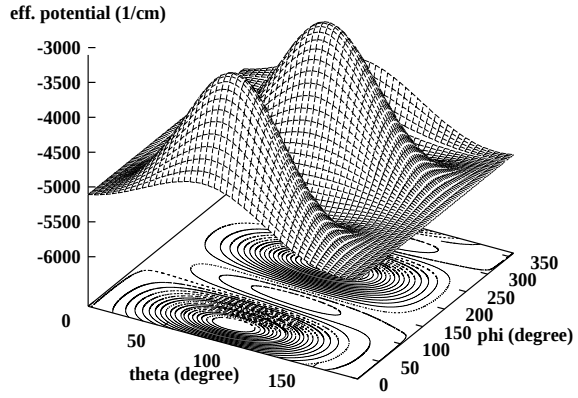

Figure 2.6: *Effective potential for the central CO of the $(CO)_7$ cluster absorbed on Ar(100) (data from Parneix [61]). Same representation as in Fig.2.4.*

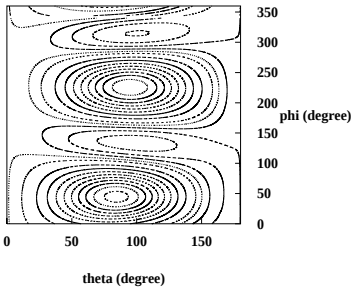

Figure 2.7: *Contour plot representation of Fig.2.6. The minimum is at θ=100° , φ=314° and V = -5509.6 cm^{-1}. Each line indicates a difference of 100 cm^{-1} starting at -5600 cm^{-1}.*

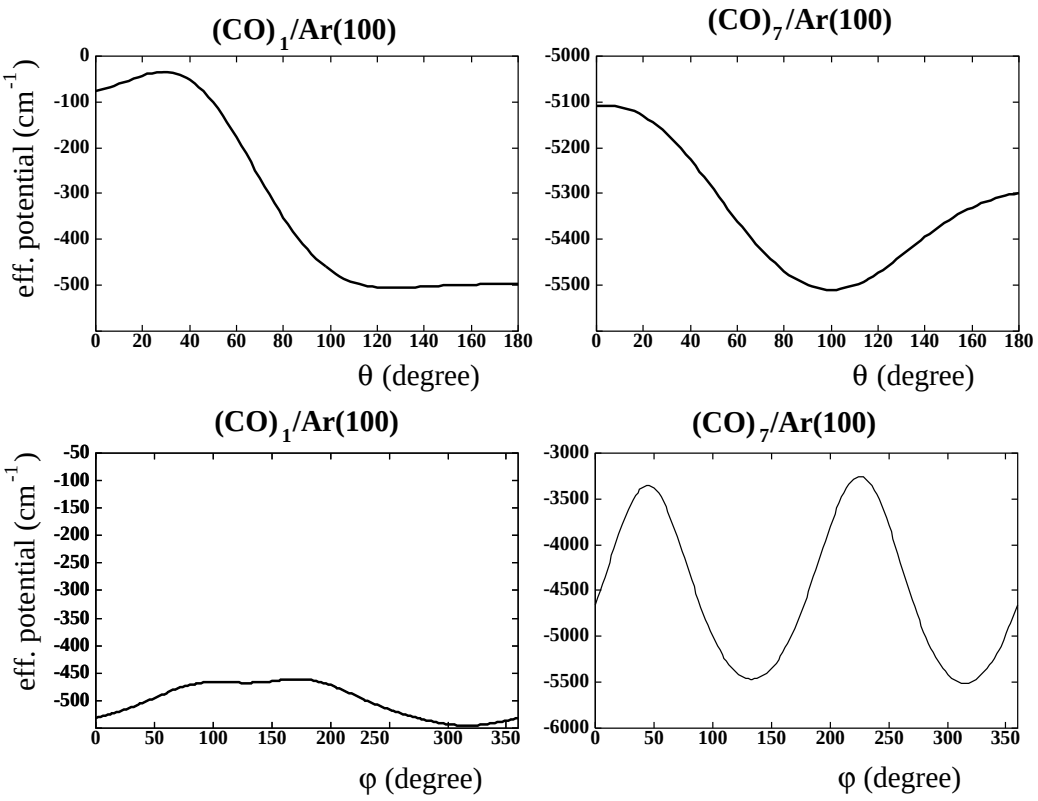

Figure 2.8: *Cut of the two-dimensional potential surface (see Fig.2.4– 2.7) at the global minimum. $(CO)_1$ in the left column and the central CO in the $(CO)_7$ cluster in the right column adsorbed on Ar(100). First row: Potential cut as function of θ at φ=-44° and -46° , resp. Second row: Potential cut as function of φ at θ=134° and 100° (data from Parneix [21]).*

As mentioned in the introductory remarks, I am interested in the angular behaviour of CO molecule on the surface and in an effective local potential (including angle) seen by the central molecule. This local potential will change from low to high coverage and permit a simple analysis of the evolution of the system due to coverage. In this analysis all the molecular adsorbate but the chosen central one, are assumed to be frozen at those values defined by the most stable adsorbate geometry.

Figures 2.4- 2.7 display the potentials for the $(CO)_1$ (2.4, 2.5) and the central CO molecule in the $(CO)_7$ cluster (2.6, 2.7) adsorbed on Ar(100), showing their dependence on the molecular orientation angles θ and φ. The difference between the two sets of graphs is remarkable.

First, the potential for $(CO)_1$/Ar(100) varies about 700 cm^{-1}, while that for the $(CO)_7$/Ar(100) central molecule varies by about 3000 cm^{-1}. Consequently, by rising coverage the hindered rotation motion rigidifies and one can anticipate that the quantum mechanical energy spacing increases. Secondly, the position of the minimum changes. For the single CO adsorbed on Ar(100), the minimum is at θ=134 ° and φ=-44° , while for the central CO molecule in the adsorbed $(CO)_7$ cluster it is found at θ=100° and φ=-46° . Thirdly, the general shape of both effective potentials is very different. For a single adsorbed CO, the potential is smoothly rising for θ going to zero. In φ the potential is flat and nearly constant. This fact can also be seen in the left column graphs in Figure 2.8. There, two cuts of the two-dimensional

potential surface at the minimum are presented, the upper in θ with fixed φ and the lower in φ with fixed θ. It is remarkable, that for $(CO)_1$/Ar(100) the potential is only changing by about 80 cm^{-1} in φ, corresponding to a slightly hindered precession (φ–motion) about the surface normal. For the central CO molecule of $(CO)_7$/Ar(100), the effective potential is totally different. In the 3–dimensional graph (Fig.2.6 and contour plot Fig.2.7), the hindered rotation is governed by two high barriers situated at θ=84° , 94° and φ=44° , 226° , respectively. Consequently, the nearly free precession in $(CO)_1$/Ar(100) becomes rigidified in $(CO)_7$/Ar(100). This can also be clearly seen in the cut in φ direction (presented in the the lower right graph of Fig.2.8).

2.1.3 $(CO)_n$ /Ar(100): Dynamics

The rigidification due to rising of the coverage must be seen in the rotational motion of the adsorbed CO molecules. In the following I present the results of a classical dynamical study of this motion, published by Parneix *et al.* [21]. To analyse the dynamical result, probability functions $p(\lambda)$ and $p(\rho)$ are calculated in the dynamical study. These two parameters λ and ρ represent a 'mean' value of the angular variables θ and φ associated to each molecule and are defined as:

$$\lambda = \frac{1}{n}\sum_{i=1}^{n}\cos(\theta_i) \tag{2.3a}$$

$$\rho = \frac{1}{n}\sum_{i=1}^{n}\cos(\varphi_i) \tag{2.3b}$$

The functions $p(\lambda)$ and $p(\rho)$ are the probability to find the system in the state λ and ρ, respectively. They were calculated each 200 fs during long trajectories of 4 ns. The results at around a temperature of 10 K are plotted for $(CO)_1$, $(CO)_2$ and $(CO)_4$/Ar(100) in Figure 2.9.

When the number of adsorbates n increases, the peaks widths of two probability functions diminishes, indicating the rigidification around the 'mean' value. There is also a remarkable shift of the peak position. For a single CO molecule, the mean value for the tilt angle θ is found at $\lambda \approx 0.8$ ($\theta \approx 134°$) and the probability function of ρ is not strongly peaked. This is in agreement with a free precession around the surface normal and a librational motion around the potential minimum (see p.104). If the number of adsorbed molecules rises, the width of the peaks diminishes and the maximum is shifted to zero. This indicates, that for rising coverage the molecules tend to undergo strongly hindered rovibrational motions around θ=90° , i.e. around a position of the intra-molecular axis parallel to the surface (in–plane adsorption).

Instead of averaging, one can plot the probability function of the θ and φ angles for each CO molecule. Fig.2.10 displays such a plot for $(CO)_4$/Ar(100) at a temperature of 14.8 K.

Looking at the probability graph of the θ motion (Fig.2.10 a), one sees, that the peak is slightly broadened (FWHM 23°) as compared to the one of the averaged probability graph (Fig.2.9, FWHM 20°). No separated features corresponding to the angles of 130° and 90° , found for the stable configuration of the dimer, are seen. The position of the peak maximum at $\approx$ 90° stresses the preference of in–plane adsorption sites. For the azimuthal angle φ two peaks are observed (Fig 2.10 b)), with maxima at 40 and 130° corresponding almost to the crystal directions [011] and [0$\bar{1}$1]. From the point of view of a clear surface, these two directions are equivalent for a fcc crystal, but not for a CO covered argon surface, as CO molecules occupy a slightly displaced two–fold bridge adsorption sites. The two separated peaks highlight the hindrance of adsorbate precession by the surface.

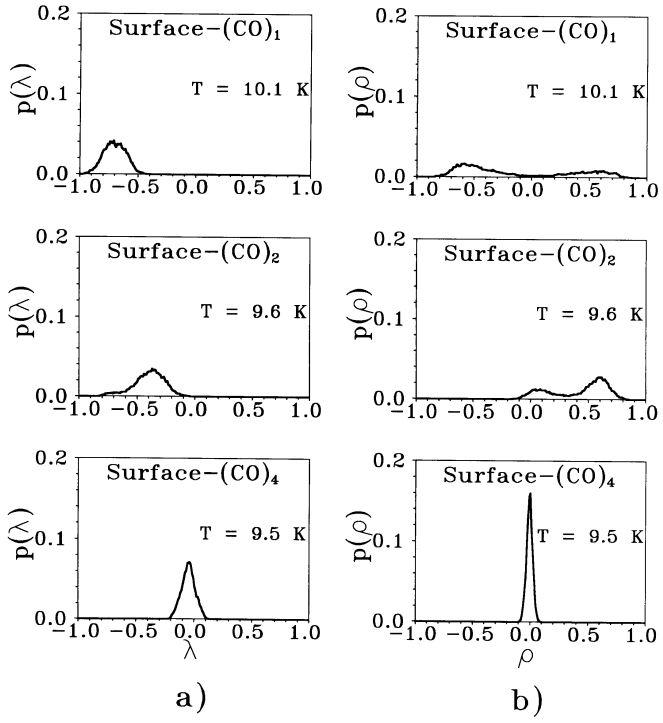

Figure 2.9: *Angular motion as function of adsorbed CO molecules: first row $(CO)_1$/Ar(100), second row $(CO)_2$/Ar(100) and third row $(CO)_4$/Ar(100) at the indicated temperatures. a) Probability function $p(\lambda)$, where $\lambda = \frac{1}{n}\sum_{i=1}^{n}\cos(\theta_i)$ is a 'mean' value of θ angle. b) Probability function $p(\rho)$ with $\rho = \frac{1}{n}\sum_{i=1}^{n}\cos(\varphi_i)$ as a 'mean' value of φ angle (from Parneix et al. [21]).*

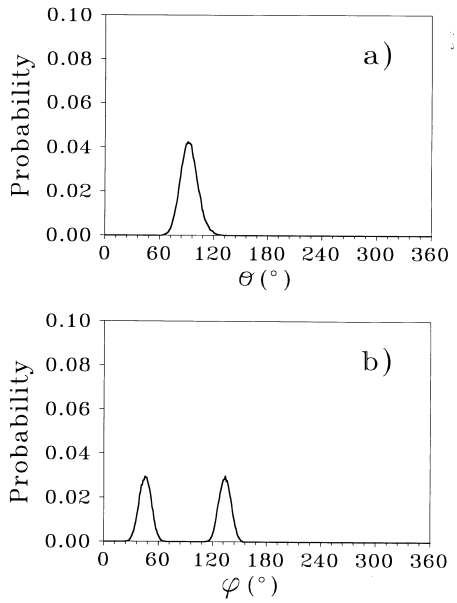

Figure 2.10: *$(CO)_4$/Ar(100) at T=14.8 K. Same dependency as on Fig.2.9, but no average is performed, i.e. the angles of all molecules are considered separately (from Parneix et al. [21].*

2.2 Quantum mechanical view for hindered rotation motion

In this section, I use the effective potential presented above in a quantum mechanical analysis of the coverage influence on the central molecule of $(CO)_n$/Ar(100) cluster. The analysis consists in the calculation of the energy levels and the corresponding wave function of the hindered rotation motion. Remember that from classical dynamics study, the precession around the surface normal becomes strongly hindered for high coverage. In the quantum mechanical model used for photoionization (part II, section 2.4.1), I assumed a surface potential of axial symmetry about the surface normal, i.e. corresponding to a free precession of the molecule with arbitrary angle φ. To introduce the presently obtained strong hindered precession, I present in the next section 2.2.1, a generalized model of hindered rotor moving in a non–axial symmetric surface potential. In section 2.2.2, the quantum mechanical energies wave functions of the hindered rotation are calculated numerically and are discussed in detail.

2.2.1 Theoretical model

As mentioned above, the potential is no longer axial symmetric with respect to arbitrary rotations about the surface normal. However the electron clouds of the adsorbate are assumed to keep their axial symmetry about the molecular axis of the adsorbate. This approximation may be important for the case of photoionization of some chemisorbed species, but can be considered as a good approximation for a manifold of adsorbate–surface systems, especially for physisorbed systems, where the interactions are of van–der–Waals type. The effective potential including coverage obtained in section 2.1.2 is now expanded in spherical harmonics $\mathrm{Y}^L_{M_L}$:

$$V(R_0, z_0, \varphi, \theta) = \sum_{L=0}^{\infty} \sum_{M_L=-L}^{L} V_{L,M_L}(R_0, z_0) \left(\mathrm{Y}_{M_L}^{L}(\theta, \varphi) \right)^* \tag{2.4}$$

Note, that for the molecular orientation the angles θ and φ are used instead of β and α, the notation used in part II, section 2.4.1 of this thesis. No other vibrational modes are taken into consideration, and consequently the coordinates R and z are frozen to the values R_0 and z_0, respectively. As in the model, detailed in part II, section 2.4.1, the hindered rotation wave function is expanded in Wigner function $\mathcal{D}_{M\Omega}^{(J)*}(\hat{R})$, the free rotor functions in active rotation convention (Zare [67], p.78):

$$\Theta_{\Omega}^{n}(\hat{R}) = \sum_{J \geq |\Omega|}^{\infty} \sum_{M=-J}^{J} c_{M,\Omega}^{J,n} \quad \mathcal{D}_{M\Omega}^{(J)*}(\hat{R}) \tag{2.5}$$

$\hbar\sqrt{J(J+1)}$ is the length of the total angular momentum $\vec{J}$, while $\hbar M$ and $\hbar\Omega$ are the projections of $\vec{J}$ onto the surface normal and the internuclear axis, respectively. In general, M is not a good quantum number, a summation over all possible projections M must be performed. The label n corresponds to the different energy levels of the hindered rotation with $n \geq |\Omega|$.

As in part II, section 2.4.1, the expansions (2.4) and (2.5) are inserted in the time independent Schrödinger equation (Eq.(2.19), part II, p.57) and a set of linear equations, similar to the one in Eq.(2.20) (part II, p.57), is obtained. Again, one has to solve numerically an eigenvalue problem.

2.2.2 Results: Energies and wave functions

In this subsection, I present the eigenenergies and wave functions of the hindered rotation dependent on the coverage. To simulate low and high coverage, I use the effective potentials, displayed in Figs. 2.4–2.7, for single CO and the central CO of the $(CO)_7$ cluster adsorbed on Ar(100) in their electronic ground states (CO: $^1\Sigma_0^+$). For the numerical calculation, the potential and wave function expansions are restricted to $L \leq 15$, $-5 \leq M_L \leq 5$ (Eq.2.4)) and $J \leq 40$, $-5 \leq M \leq 5$ (Eq.(2.5)), respectively. The expansion coefficients are tabulated in Appendix D (p.187).

In Tables 2.4 and 2.4, the rotational energies and the mean values for the tilt angle θ ($\bar{\theta}$) are tabulated. The difference between these values for the low and high coverage simulations is remarkable. First, the difference between the first two rotational energy level (n=0,1) for the low adsorbate coverage limit is about 20 cm^{-1}. In the high coverage limit, there is a group of four energy levels, which are nearly degenerated. Then, the fifth energy level (n=4) is about 36 cm^{-1}. The difference between low and high coverage energies and wave functions can be explained as follows.

For the low coverage, the effective potential has a shallow minimum at θ=135° and φ=316° (see p.104). Due to the shallow potential, the zero–energy is small, i.e. the rotational energy of the ground state is about 25 cm^{-1} above potential minimum. The neighbouring minima are higher in energy by $\geq$ 45 cm^{-1} (see Fig.2.5) and consequently no tunnelling between the absolute minimum and the higher lying

n	E_{rot} (cm^{-1})	$\bar{\theta}$
0	0.0	134.65°
1	19.9	131.01°
2	29.3	134.07°
3	37.8	127.38°
4	43.3	106.72°
5	45.8	122.99°
6	55.7	123.79°
7	56.8	122.15°
8	59.8	115.31°
9	60.8	124.99°
10	73.2	116.40°

Table 2.4: *Rotational energies and mean values of θ for CO/Ar(100) in the low adsorbate coverage simulation.*

n	E_{rot} (cm^{-1})	$\bar{\theta}$
0	0.0	66.47°
1	2.2	65.97°
2	2.6	156.50°
3	5.3	157.19°
4	35.9	66.57°
5	41.5	65.65°
6	80.5	68.31°
7	81.5	154.42°
8	88.7	155.03°
9	98.0	66.27°
10	135.0	70.72°

Table 2.5: *Same as in Table 2.4 for the high coverage simulation.*

ones takes place: The bottom graph of Figure 2.11 represents the density of the wave function for the rotational ground state n=0. One can see, that this density function has a Gaussian–like shape with its mean values near the potential minimum. The wave function density of n=1 has two maxima at φ=0 ° and 280° and conserves the same mean value of θ as n=0, the rotational energy is not sufficient to allow tunnelling. But, the next rotational state n=2 has an energy value (E_2-E_0=29.3 cm^{-1}), which is sufficient to allow tunnelling to other minima. As the potential is flat around these minima, the particle can be found in large angular variable space region.

As one can see in Fig.2.12, the situation is totally different for high coverage. The wave function densities are not located in the region around the absolute minimum at θ=100 ° . At first this situation seems to be strange or even incorrect.

To analyse this behaviour of the wave function densities one should first recall the effective potential for the central CO molecule of the CO_7/Ar(100) cluster. There are two points in my comparison between classical and quantum mechanics studies. First, one should look at the zero point energy of the hindered rotation motion. In the vicinity of the absolute minimum the potential is steep but then it becomes much smoother, i.e. it is highly anharmonic. Consequently the zero point energy is high (163 cm^{-1}), lifting the ground rotational state above all minima but then the levels are close to each other. In figure 2.13 I show a contour plot of the effective potential for a cut at zero point energy (-5347 cm^{-1}). In fact, a classical dynamic study for $(CO)_7$/Ar(100) on the angular behaviour [115] shows, that for a low temperature (10.5 K) the central molecule is moving around a mean position of $\theta \approx 97°$ and $\phi \approx 314°$, in agreement with the position of the potential minimum and it is inside in one of the two elipses drown in Figure 2.13. But, in a quantum mechanical picture tunnelling of the adsorbate from one potential well to another should easily take place. Secondly, from Figure 2.14 one can see, that tunnelling along $\theta \approx 100°$ direction is unfavoured due to the high potential barriers. A good compromise between potential barriers, minima and tunnelling seems to be the cut along θ fixed at 66° and 156° , visualised in Fig.2.14. The effective quantum mechanical mean angles for the first ten hindered rotational levels are presented in Table 2.5 and the first four wave function densities are displayed in Figure 2.12. One remarks that quantum mechanical

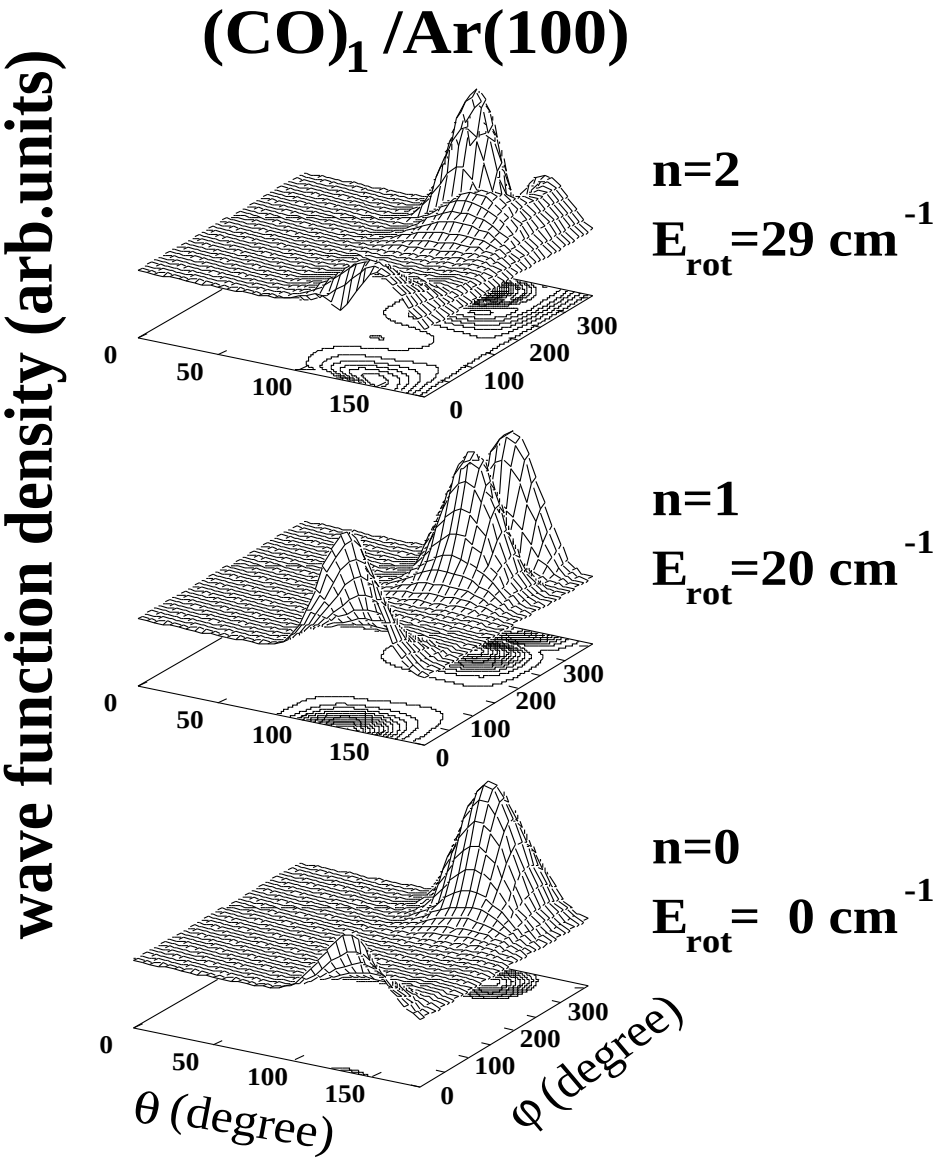

Figure 2.11: *Hindered rotation motion for $(CO)_1$/Ar(100). The density of the wave functions (square of the wave function multiplied by* $\sin\theta$*) for the first three rotational levels.* E_{rot} *is the corresponding rotational energy difference* E_n*-*E_0 *Note, that* φ*=0° and 360° are equivalent, i.e. for n=1 there are only two peaks with one starting near 360° and continuing at 0° . Remember that the CO molecule occupies a slightly displaced two–fold bridge adsorption site and consequently the density distribution is not symmetric in* φ*.*

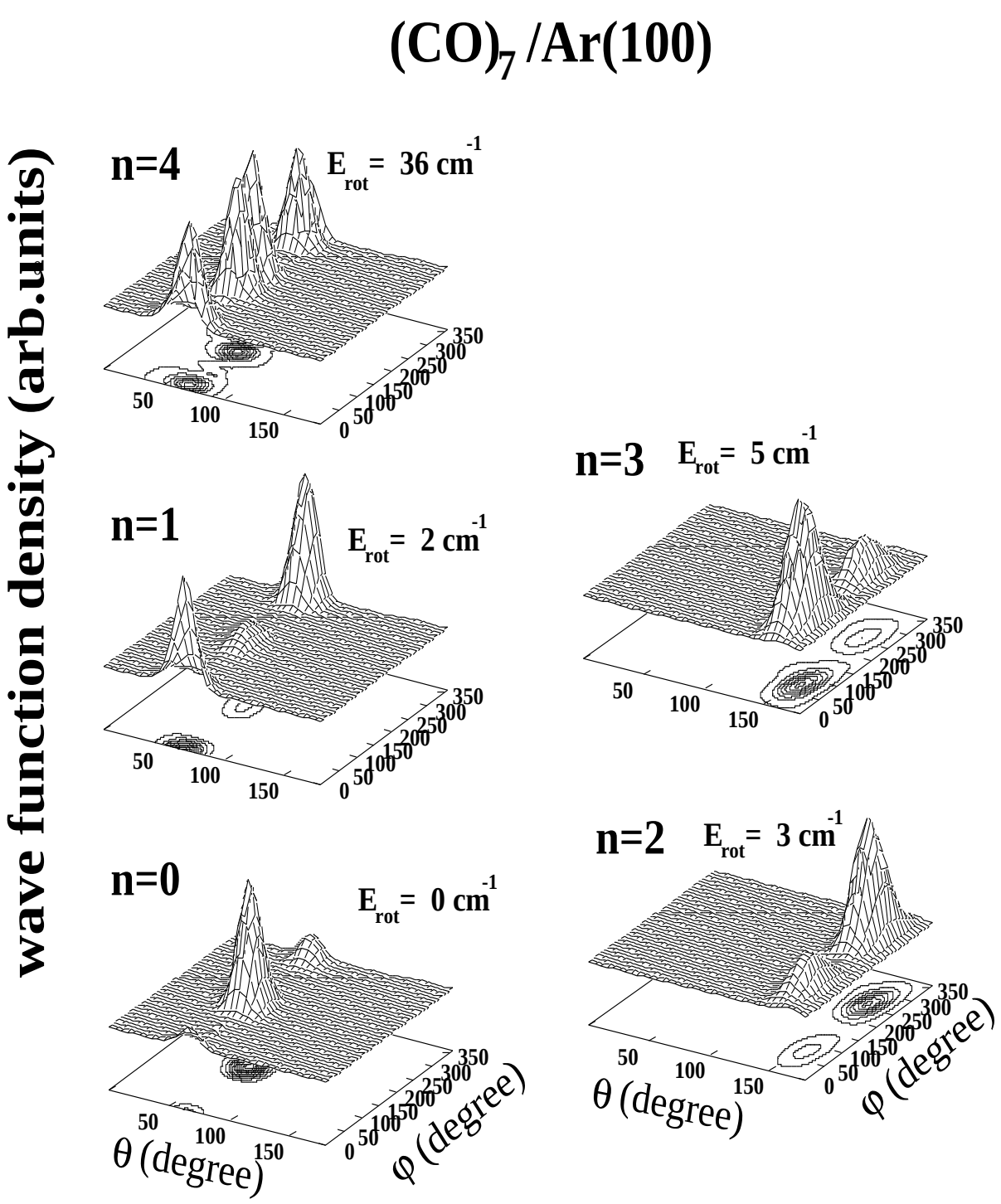

Figure 2.12: *Hindered rotation for $(CO)_7$/Ar(100). The density of the wave functions (square of the wave function multiplied by* $\sin\theta$*) for the first five rotational levels.* E_{rot} *is the corresponding rotational energy. Note, that as in Fig.2.11* φ*=0° and 360° are equivalent.*

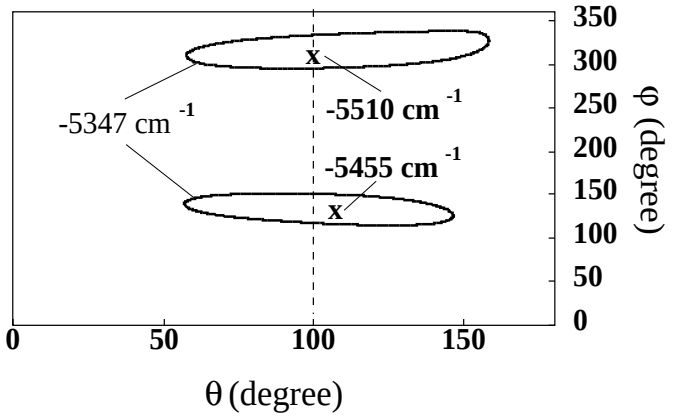

Figure 2.13: *High coverage: Surface potential contour plot at zero–point energy (-5347 cm^{-1}). 'x' marks the position of the two potential minima, while the dashed line marks the potential surface cut at the absolute minimum.*

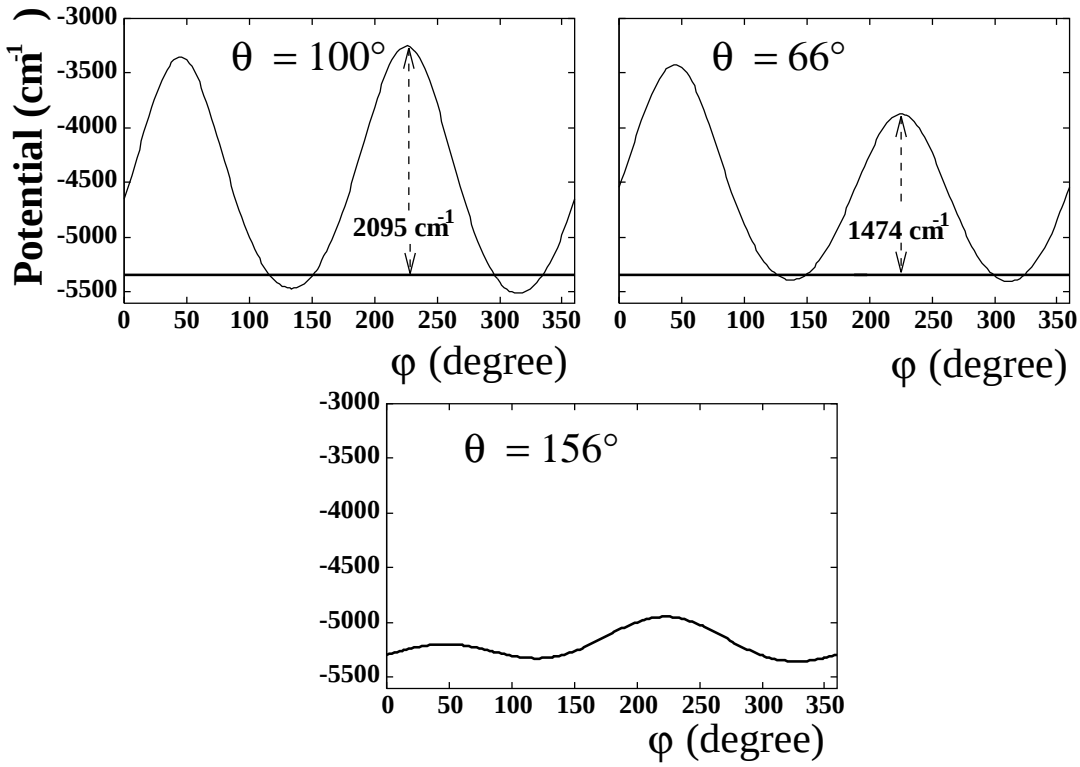

Figure 2.14: *High coverage: Potential cut at θ=100° , 66° and 156° . The straight line indicates the zero–point energy at -5347 cm^{-1}. In all three graphs two equivalent minima can be seen. Tunnelling effects between them take place, cause closely lying rotational energy levels and the molecular adsorbate is allowed to change easily angular orientation. The cut at θ=100° and 66° shows two different potential barriers heights, but in the minima the potential has comparable values. Consequently the latter value for $\bar{\theta}$ (66°) is prefered for the angular motion. The same argument holds for a comparision between the potential cuts at θ=156° and 100° , implying a preference for 156° .*

n	E_{rot} (cm^{-1})	(φ, θ)	(φ, θ)
0	0.0	(170° ,65°)	(340° , 65°)
1	2.2	(350° ,65.°)	(170° , 65°)
2	2.6	(260° ,155°)	(90° ,155°)
3	5.3	(80° ,155°)	(260° ,155°)

Table 2.6: *Preferential molecular orientation (φ, θ). The first pair corresponds to the highest maximum in the probability function, the second to the second one.*

mean values are different from the one obtained by a classical study. But, the energies or temperatures tested by classical and quantum mechanical studies are also different. The classical dynamic study was performed at 10.5 K, while for the quantum mechanics study the difference between the zero–point energy and the potential minimum (E_{rot}=163 cm^{-1}) implies a classical rotational temperature of T_{rot}=117 K. This temperature was obtained using the relation $E_{rot} = gkT_{rot}$, with g the number of degrees of freedom (g=2) and k the Boltzmann's constant. The conclusion of this discussion is that because of the particular form of the potential, its high anharmonicity and the presence of local minima, the results obtained by classical and quantum mechanical methods are very different. One should also mention that the quantum mechanical study was performed for fixed equilibrium z coordinate whereas in the classical study this coordinate was left unconstrained.

From the analysis of the wave function density one sees that the wave function can be symmetric and antisymmetric combination of local minimum wave functions. Consequently along each cut (θ=66 ° and 156°) the number of wave functions is doubled and their associated energies levels are nearly degenerated. In Table 2.6 I present for the first four rotational states the most probable set of molecular orientation angles (φ, θ) derived from the analysis of the wave function density distribution.

For next higher lying state (n=4), the steepness of the potential causes a rotational energy difference of 36 cm^{-1} from the ground state. This difference is higher than the corresponding energy difference for the low coverage limit (20 cm^{-1}) and stresses once again the rigidification due to coverage. The formation of nearly degenerate energy levels discussed above, becomes less strict for higher hindered rotational levels but is still present.

Summarising, the quantum mechanical model shows, that high coverage imposes a rigidification of angular motion. Contrary to the low coverage situation, quantum mechanical tunnelling effects produce four nearly degenerated rotational levels and cause the molecular adsorbate to undergo easily transitions between several molecular orientations. But, this presence of nearly degenerate energy levels does not allow the central molecule to undergo free rotational motion.

Chapter 3

Influence of coverage: Conclusion and Outlook

3.1 Conclusion

In this part of my thesis, I highlighted the influence of coverage on the adsorption geometry and the angular motion of molecular adsorbates. Taking the example of CO molecules physisorbed on an argon surface (Ar(100)), the coverage was modeled by CO clusters of variable size [21]. Classical trajectory techniques [107] determine the adsorption geometries and the motion of the adsorbate.

The CO molecules tend to form clusters to minimize the CO–CO interactions. In $(CO)_9$ all the neighboured adsorption sites are occupied. Consequently, a single CO and $(CO)_9$ adsorbed on Ar(100) can be used to model low and one monolayer (high) coverage, respectively. One spectacular result of the classical dynamical study is the rigidification in the azimuthal angle due to coverage.

A quantum mechanical analysis was performed for a single CO and the central CO of the $(CO)_7$/Ar(100) system, simulating low and high coverage. The central CO molecule in this cluster is not completely surrounded by the other adsorbates, i.e. a full monolayer is not modeled contrary to the $(CO)_9$/Ar(100) cluster, but the system is sufficiently dense to reflect a tendency. In fact, the calculational results for the $(CO)_7$/Ar(100) system verify the rigidification, found in the classical dynamical study. This rigidification manifests itself by an increase of hindered rotational energies and a sharpening of the associated wave function densities. The zero–point energy corresponds to a classical rotational temperature much higher than the energies introduced in the classical study. Consequently the angular variable region explored by the wave function is much larger. Quantum mechanical study predicts the existence of four geometrical configurations for the central molecular adsorbate that are nearly degenerated in energy. For some configurations the associated densities indicate tunnelling phenomena, which cause flips of molecular orientation about the surface. In fact, the associated wave function densities show that the angular motion of the molecular adsorbate is governed by a compromise between the minima of the angular potential and tunnelling phenomena through potential barriers giving rise to these configurations of molecular orientation. These quantum mechanical tunnelling phenomena and degeneracy do not mean that molecule is freely rotating, but that the classical picture should be supplemented by a quantum

mechanical approach. The results obtained by the two methods are very diffent and I explain them on the basis of the particular shape of the potential, zero–point energies and classical temperature difference.

3.2 Outlook

One interesting application of the present model is the effect of coverage on photoionization spectra. Remember, that experimental results in the photoionization experiment of 1s excitation of CO/Ni(100) [14] motivated the current study. One possible approach to introduce the coverage in a photoionization model is to use the effective potentials obtained in this part of the thesis instead of single molecule–surface potentials used in part II. But, the approximation of axial symmetry around the surface normal used in the photoionization model does not correspond to the high coverage situation having a large potential barrier in the azimuthal motion (φ). For this reason, I generalized the model, used in part II of this thesis. This generalized model can simultaneously include the hindered rotational motion in a generalized surface potential and the effect of photoelectron refraction by the surface (backscattering). The derived formulae are presented in Appendix C.2.

Based one these generalized formulae (Eq.(C.11), page 185), a computer program must be written. Then, the wave functions, derived in section 2.2.2 can be used to calculate photoionization cross sections dependent on coverage. The resulting program can be applied to other systems, like CO/Pt(111), which was used by Wesner *et al.* to study coverage influence [14]. Such a method can be used in the study of bridge sites as the one considered here. These sites often appear for high coverage and have a low local symmetry of C_{2v} (two–fold bridge) or C_{3v} (three–fold bridge). Consequently the corresponding surface potentials governing the hindered rotation, are definitely non–axially symmetric. The first classical and quantum mechanical calculations on the influence of adsorbate coverage are in progress [115].

Another interesting application is to model the photodesorption for dense coverage. The translational and rotational degrees of freedom will strongly be modified not only by the surface but also by interactions between neighboured adsorbates. Coverage influences on the desorption process probably appear through modification of the rotational, translational and vibrational distribution of the desorbed particles. Experimentally, these distribution are available [116, 117, 30, 22, 31–34]. As an example, one can study rotational alignment of the desorbed molecules, which is very sensitive to a rigidification of the azimuthal motion of the adsorbate. Work on photodesorption models is in progress and the first results for the weakly chemisorbed system CO/Cu(100) at low coverage will be presented in part IV of this thesis.

Part IV

Photodesorption of molecular adsorbates

Résumé

La troisième et dernière partie de cette thèse traite de la photodésorption en régime non thermique. La problématique des mécanismes d'évolution menant à la photodésorption s'apparente à celle qu'on peut trouver dans l'étape finale de la catalyse hétérogène. En effet dans les deux cas il s'agit de désorption mais dans le premier elle est non thermique tandis que dans le second thermique.

La désorption des adsorbats peut être engendrée par une excitation simultanée d'un nombre restreint de modes de vibration de l'adsorbat, de la surface ou du solide; des modes couplés qui, par un transfert d'énergie vers le mode de désorption, engendrent éventuellement la fragmentation. Expérimentalement, l'excitation peut être thermique (les phonons du solide) ou par impact photonique ou électronique. Dans ces deux derniers cas on excite un ou plusieurs modes de vibration de l'adsorbat, de la surface ou du solide ou même électroniquement le complexe qui dans une deuxième étape transfère l'énergie vers le mode de désorption. La distinction entre les excitations vibrationnelles et électroniques se fait en fonction de l'énergie apportée au complexe. Pour la désorption induite par excitation thermique le mécanisme est toujours non résonant tandis que pour l'impact photonique ou électronique le mécanisme peut, pour certaines énergies incidentes, devenir résonant.

Cette troisième partie de ma thèse présente un modèle qui traite la désorption non thermique incluant, après l'excitation, l'ensemble des voies importantes d'évolution du système. Les mouvements vibrationnels du solide et de la surface (phonons), influençant peu le mécanique en régime non thermique, sont négligés tandis que tous les modes vibrationnels de l'adsorbats sont explicitement pris en considération. Les quantités électroniques ne sont pas calculées et apparaissent dans la section efficace comme un facteur d'échelle global. Mais nous comptons les calculer dans un avenir proche. Le modèle implique deux étapes. Premièrement, le photon excite le système dans un état intermédiaire électroniquement excité ayant, à l'échelle électronique, mais pas vibrationnelle, un temps de vie long. Deuxièmement, par des interactions non–adiabatiques cet état est fortement couplé à l'état électronique final, permettant un transfert d'énergie électronique vers le mode nucléaire de désorption. Ce mécanique implique aussi une excitation des autres modes vibrationnels de l'adsorbat pouvant être une signature du mode de photodésorption.

Ce modèle a été utilisé pour l'étude d'un système faiblement chimisorbé: CO/Cu(111) sur un site linéaire à faible taux de couverture d'adsorbat. J'ai utilisé un potentiel modèle atome–atome publié dans la littérature, qui permet de prendre en considération la multidimensionalité du problème (par rapport à l'adsorbat). La fonction d'onde multidimensionnelle est développée sur une base de fonctions correspondant à chaque mouvement de l'adsorbat sauf le mode de désorption. Cette base consiste en un produit de fonctions rotationnelles de la phase gazeuse (rotation empêchée), de type Bloch (translation empêchée) et d'un oscillateur harmonique (vibration interne négligeant la dissociation). Pour la désorption, on utilise des fonctions numériques simples correspondant à une coupe dans le potentiel multidimensionnel et on résout un système d'équations couplées (incluant les autres degrés de liberté) par rapport à ce mode. Les distributions rotationnelles, translationnelles et vibrationnelles des molécules désorbées ont étés calculées. Comme il semble que le temps d'excitation est court par rapport aux temps caractéristiques de mouvements nucléaires, j'ai supposé que l'état déterminées par

un recouvrement de type Franck–Condon pour la rotation et la vibration interne et par une l'état initial et

J'ai trouvé, que la rotation empêchée est fortement couplée au mode désorption, mais que ces modes sont découplés de la vibration de la translation empêchée. Les distributions caractéristiques semblables aux distributions expérimentales. Si l'on suppose que la rotation empêchée est découplée des autres modes, la distribution rotationnelle trouvée littérature. Mais, empêchée fragments désorbés est trouvée en accord avec les résultats Mon modèle montre que l'origine de la distribution à un processus non thermique de désorption. Comme proposé par l'expérience ce modèle n'exclut pas qu'une des branches de la distribution soit d'origine thermique soit mixte. Finalement cette partie de la thèse a crée le cadre d'un modèle, qui est capable de traiter les divers dégrées de liberté nucléaires essentiels de thermique. La dans un continuum électronique et une estimation des interactions non–adiabatiques. Cette partie du modèle permettra de savoir si court de l'état excité est valable. La dynamique de désorption doit être prise en considération par une les degrés de liberté nucléaires. D'après la littérature, les effets multiphotoniques jouent un rôle essentiel dans la désorption non thermique de CO/Cu(111) et je les inclurai prochainement dans mon modèle.

Chapter 1

Photodesorption of adsorbates: experimental data and theoretical models

Photodesorption of adsorbates from metallic surfaces is a prototype phenomenon of great practical interest. It can be related to heterogeneous catalysis, corrosion of metallic materials and reactions on grains in atmosphere and interstellar space. This phenomenon is the easiest to control by the simple fundamental physics techniques and shows that the presence of the solid surface plays an essential role in orienting the adsorbate, changing its physical and possibly chemical properties, serving as a reservoir for the excess energy, or donating/backdonating electrons from adsorbate to the metal. In one word presence of the surface is opening a series of new reaction channels which are not present in gas phase reactions.

The difficulty in developing meaningful theoretical models for nonthermal photodesorption is that this variety of new deexcitation channels should be opposed to the need to concentrate specifically the energy in a single nuclear vibration mode (photodesorption mode). As mentioned above, experimentally this phenomenon is easy to monitor by the techniques of fundamental physics as the excitation energy and momentum is given by the photon, electron or heavy particle hitting the adsorbate-substrate system. The desorbed fragments which mass, internal and kinetic energies and escaping direction can be measured are a probe of the photodesorption mechanism. These measurements can be done by mass spectrometric and time of flight techniques or more recent techniques applied to photodesorption like Resonant Enhanced Multi Photon Ionization (REMPI) or Laser Induced Fluorence (LIF) techniques.

Nonthermal and thermal desorption can be produced by simultaneous excitation of a restricted number of vibrational modes. One can cite Temperature Programmed Desorption (TPD), the substrate is heated and the excited phonons of the solid transfer their energy to the desorption mode. One can further cite Electron Stimulated Desorption (ESD) or Photon Stimulated Desorption (PSD) to excite directly one vibrational mode, e.g. internal vibration of the molecular adsorbate. As the nuclear modes are coupled, the energy is then transfered to the molecule–surface mode and the particle desorbes. The same technique, but at higher photon energies, can be used to excite electronically the adsorbate, the energy is then transfer directly or via other nuclear modes to the desorption mode. There is a fundamental difference between TPD, PSD and ESD. In TPD the substrate is heated and a manifold of phonons is excited and desorption occurs in a non–resonant way. For the two other processes, one can vary the

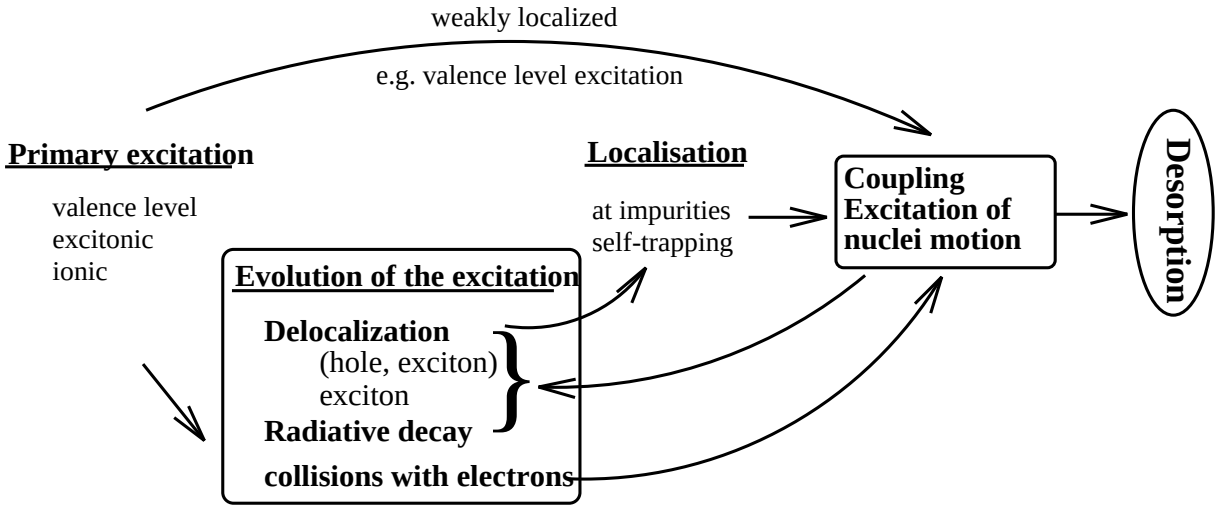

Figure 1.1: *Elementary processes in electronically stimulated desorption (adapted from P.Feulner and D.Menzel [118]).*

incident energy and at specific excitation energies a resonant transfer occurs directly to the desorption mode. This resonant transfer is called nonthermal photodesorption. In PSD, there are experimental proofs, that one can work in the nonthermal regime, i.e. the incident radiation only causes a negligible local heating of the surface, which can not explain a thermal desorption mechanism [32].

In reality the desorption process can be much more complicated and several competitive processes are present, that lower or enhance the desorption probability [118]. There are at least three relatively recent review papers discussing the photodesorption by Zhu *et al.* [119] P. Feulner and D. Menzel [118] and G.P. Brivio and T.B. Grimley [120]. For the description of Desorption Induced by Electronic Transition (DIET) process, I follow the review of P. Feulner and D. Menzel [118], emphasising these processes in the valence electrons excitation region (2–8 eV; see Figure 1.1.

In the valence region, electrons or photons lead to a primary excitation of the initial state (the ground state) to a final neutral or ionic state. The positive or negative ionic states of the adsorbate are created by transitions of electrons from the surface or bulk to the adsorbed molecule. These excited states can be energetically in resonance with other surface or bulk states. If the resonant coupling is important then the excitation energy will be rapidly transfered to the solid and propagated out of the adsorbate region (delocalisation): this state is only weakly localised and its electronic life time is short. But, if the valence state lies in a band gap of the solid, no resonant coupling is present: the state is localised and its life time is long. It is the competition between these lifetimes and the coupling strength, that determines the desorption yield.

Energy propagation out of the excitation region (low box; Figure 1.1), e.g. by excitons, does not mean a complete loss of this excitation energy for desorption. Impurities or crystal defects in the solid disturb locally the energy bands and the propagated energy can be localised there, leading to excitation of nuclear motion and finally to desorption. The same effect of localisation can be achieved by self–trapping of two excitons, which form a couple by their electronic interactions.

If the incident energy is higher than the substrate work function (Figure 1.1), electrons are emitted

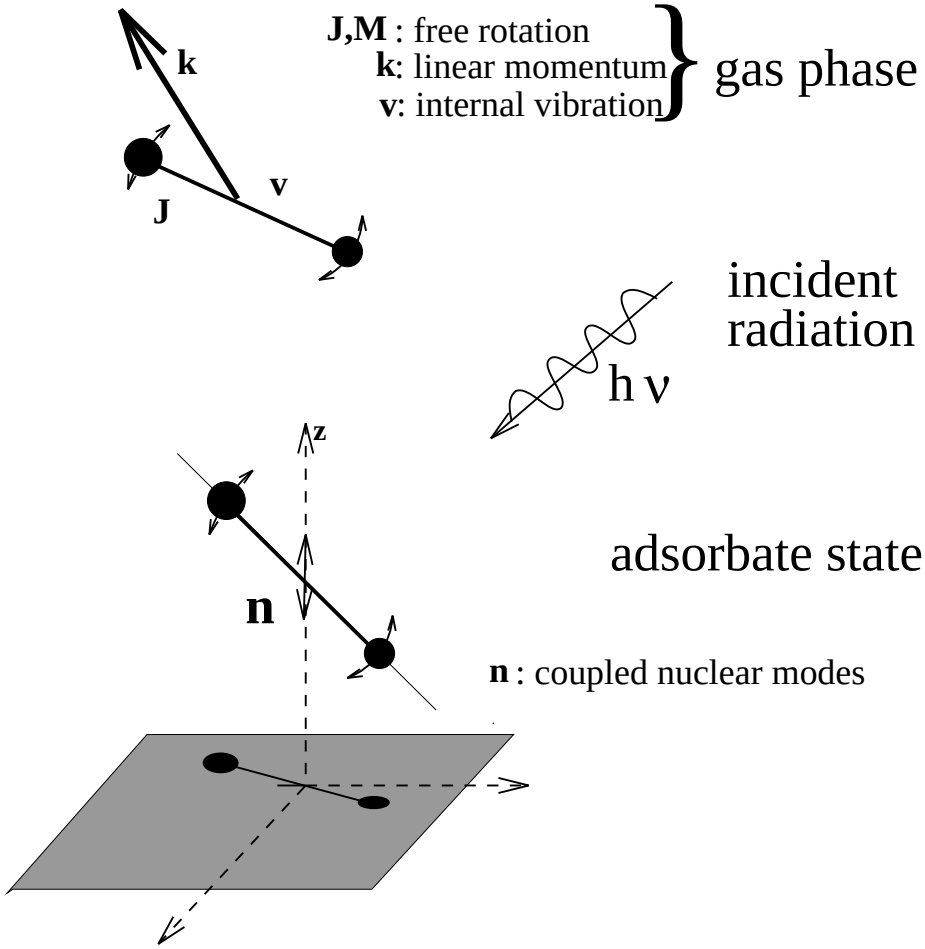

Figure 1.2: *Quantum numbers in photodesorption. For the adsorbate state, all nuclear motions of the molecular adsorbate, the hindered rotation, translation and internal vibration are coupled giving rise to nuclear motion state described by the quantum number n. A photon with an energy $h\nu$ excites the adsorbate and it desorbes. The hindered motions becomes free motions in gas phase with the quantum numbers (J, M) (rotation), v (internal vibration) and $\vec{k}$ describes the linear momentum connected to the spatial centre of mass motion.*

towards the vacuum. These electrons may undergo collisions with neighboured adsorbates, eventually exciting their nuclear motions and giving rise to desorption. Radiative decay of the excited system can lower the desorption yield, if the system is deexcited to a binding state, but it can rise it if this state is repulsive and consequently favours desorption. The latter process is only important for high incident energies, where different electronic states are available. Radiative decay has only to be considered, if electronic coupling of states is very small.

If a molecule is adsorbed on a surface, its nuclear motions are modified: the gas phase translational and rotational motions are hindered, the frequency of the internal vibration modified and a new bond is created between the molecule and the surface. Due to the presence of the surface all these nuclear

motions are in general coupled. If the adsorbate desorbes all these motions, but the internal vibration, become free and one can determine the distribution of kinetic energies and momenta together with the energies of the internal vibration and rotation. (see Fig.1.2). In gas phase the molecule is described by the quantum numbers J and M (rotation), v (internal vibration) and the linear momentum vector $\vec{k}$ (translation).

Experimentally, one measures the probability to find the desorbed molecule in a given state with a particular kinetic energy by means of REMPI, LIF or InfraRed Spectroscopy (IRS) techniques. In the case of diatomic adsorbates, the most studied systems are NO and CO on metallic [22–29] and oxide surfaces [30–36]. If one neglects the vacuum system and the experimental methods to characterize the surface and the adsorption process, a typical photodesorption set–up consists of a desorption laser, usually an excimer laser at 4.0 or 6.4 eV photon energy or a frequency doubled Nd–YAG laser at 532 nm, and a probe dye laser tunable in frequency to stimulate one LIF or REMPI transition. The former is usually oriented normal to the surface and the later parallel to it the distance from the surface being typically of few millimetres. Fixing this distance, but varying the delay time between both laser pulses, one obtains time–of–flight spectra for a given rotational and vibrational final state of the desorbed particle. To obtain a rotational distribution, one must fix the delay time and vary the frequency of the dye laser to obtain LIF transitions probing different rotational states of the molecule.

Figures 1.3 and 1.4 shows such spectra for CO desorbed from NiO. The VUV radiation was tuned to the $A^1\Pi(v' = 2, 3) \leftarrow X^1\Sigma^+(v" = 0)$ transition. Fig.1.3 displays two time–of–flight spectra for the rotational quantum numbers J=1 and 15 of the desorbed CO molecule. Their shapes can be fitted by a thermal velocity distribution at $T_{trans} = 1150 \pm 150$ K, which is in fact very different from the temperature of the sample of 70 K. In this experimental set–up the energy of the desorption laser can only provoke a local temperature change of about 12 K, which is not sufficient for a thermal desorption [32]. For other systems like NO/NiO [22] or NO/Pt [25] the corresponding velocity distribution is more complicated, one observes a slow and a fast component of desorbed molecules, associated to a thermal and a nonthermal desorption mechanism. In fact, the rotational population, shown in Fig.1.4, underlines the nonthermal character of the desorption mechanism, as this distribution can not be attributed to one single rotational temperature and even both derived temperatures of T_{rot}=200 and 634 K are hotter than the sample one.

Other systems like NH_3/Pt(111) [121] or H_2 and D_2 on Cu(111) [122] (see also the review papers by: X.-L. Zhu and J.M. White [119], P. Feulner and D. Menzel [118] and G.P. Brivio and T.B. Grimley [120]) have been studied and the desorbed molecules translational, vibrational and rotational distributions measured. Especially for oxidised surfaces the desorption yield is large and the distribution nonthermal. This proves that in many adsorbed systems there exist a nonthermal resonant desorption mechanism that shows its signature in these translational, vibrational and rotational distributions of the fragments. For example, only such mechanism can explain the fast photodesorption of CO/Cu(111) (<325 fs) found by Prybyla *et al.* [123] which completely excludes a relevant heating of the system before desorption. The desorption times measured by several authors can only be explained if a coupling between fast electronic and slow nuclear motions governs the mechanism. For high fluency femtosecond lasers, one interprets [123] the experimental data by considering a multiphotonic excitation.

Historically the first mechanism of nonthermal photodesorption considers a single nuclear coordinate (photodesorption) and two potential curves: a ground state attractive curve and an excited state repulsive one. The electronic excitation changes the adsorbate from the ground to the excited curve and the system

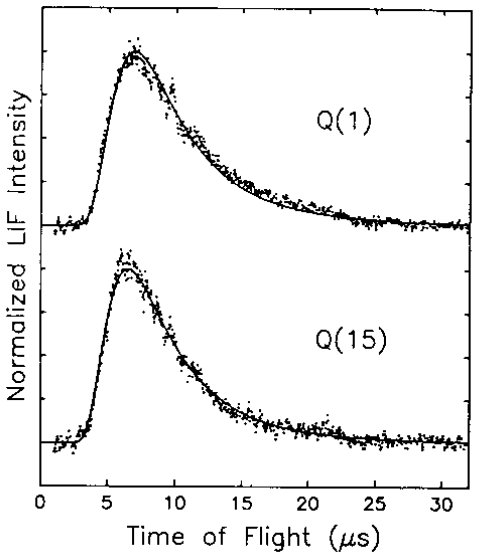

Figure 1.3: *Experimental time of flight spectra of CO desorbed from oxidised Ni(111). The LIF intensity signal of two transitions Q(1) and Q(15) (J=1, 15) are plotted against the delay time between the desorption laser ($h\nu$= 4.0 eV, 4.2mJ/cm^2 fluence/pulse) and the VUV pulses. Distance VUV–beam – surface 0.2 mm, sample temperature: 70 K. The drawn line corresponds to a fitted thermal velocity distribution with T_{trans} = 1150 ± 150 K (from M.Asscher et al. [32]).*

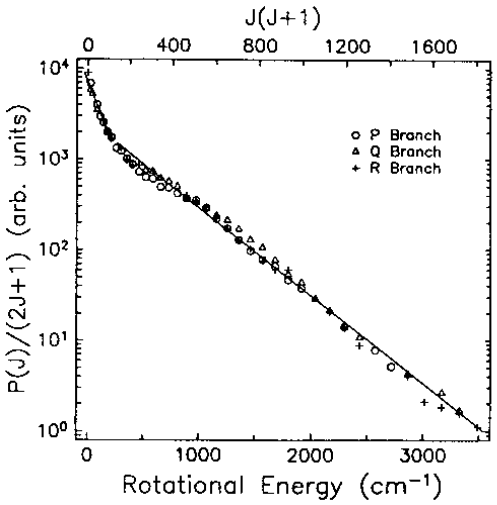

Figure 1.4: *Experimental rotational populations of CO desorbed from oxidised Ni(111), normalised to the degeneracy. 3.3 mJ/cm^2 fluence/pulse, same set–up as in Fig.1.3 The two straight lines correspond to rotational temperature population with T_{rot}=200 and 634 K, resp. (from M.Asscher et al. [32]).*

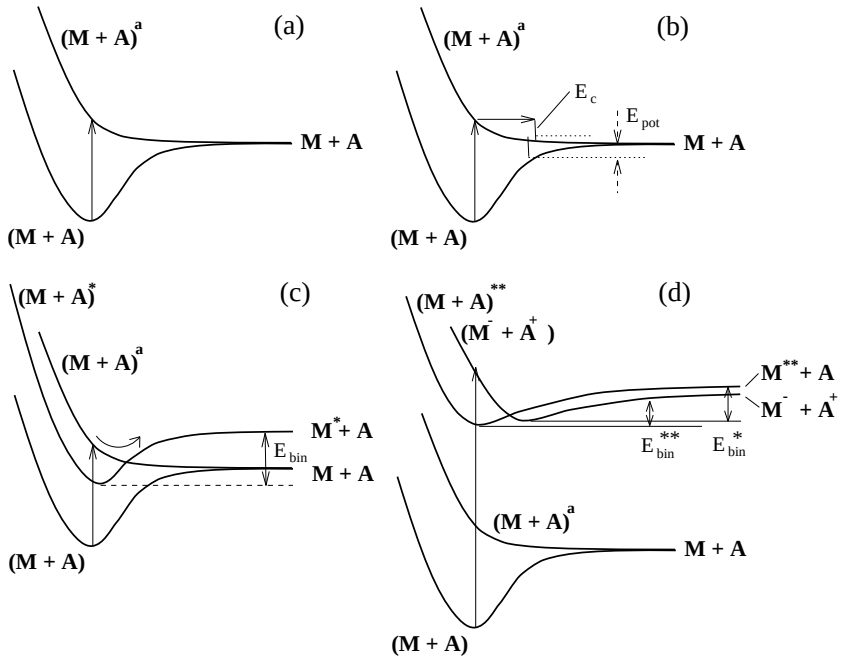

Figure 1.5: *Desorption mechanism in the Menzel–Gomer–Redhead model (from P.Feulner and D.Menzel [118]). Here A is the adsorbate and M is the metallic surface.*

desorbes from the repulsive curve in the gas phase. This is the well–known Menzel–Gomer–Redhead (MGR) model proposed in 1964. (D.Menzel and R.Gomer [124] for the electron stimulated desorption and P.A.Redhead [125] for the photon stimulated desorption).

Figure 1.5 displays different desorption scenarios which now contain more than two potential curves. In all the four figures potential curves of the fundamental and different types of electronic excited states are plotted in a adiabatic approximation with respect to the desorption coordinate z, the distance between the particle and the surface. The electronic excited states can be an antibonding state (Figure 1.5 (a)) with purely repulsive or a bonding state (Figure 1.5 (b)) with attractive–repulsive nature. In these figures the arrow represent the Franck–Condon (vertical) excitation from the fundamental state of the surface+adsorbate (M+A) system to an antibonding state $(M+A)^a$. If no relaxation into the ground state takes place (Figure 1.5 (a)), the particle moves on the repulsive potential curve and desorbes. If relaxation takes place (b), i.e. if electronic excited state decays after some time, the particle has gained some kinetic energy E_c while moving on the repulsive potential. If this energy is higher then the energy E_{pot}, the adsorbate can desorb. Other mechanisms (Figure 1.5 (c) and Figure 1.5 (d)) include potential curves corresponding to several excited states where curve crossing and excited desorbed fragments are considered. As show in Fig.1.5(c), the particle can be excited to the antibonding state potential $(M+A)^a$ curve but due to electrostatic interactions between the two diabatic states $(M+A)^a$ and $(M+A)^*$ it can be temporary trapped by the bonding excited state $(M+A)^*$ until the particle definitely desorbs leaving the surface either in its ground M or excited M^* states. This is the case, if the excitation energy is high and the particle accumulates sufficiently kinetic energy on the repulsive potential, before switching to the bonding state. The situation can be more complicated as show in Figure 1.5 (d)). The substrate and the adsorbate can exchange an electron, which can lead to a bonding state (M^-+A^+). As in Figure 1.5 (c)), the associated potential curve can cross with another excited diabatic state $(M+A)^{**}$ and the same

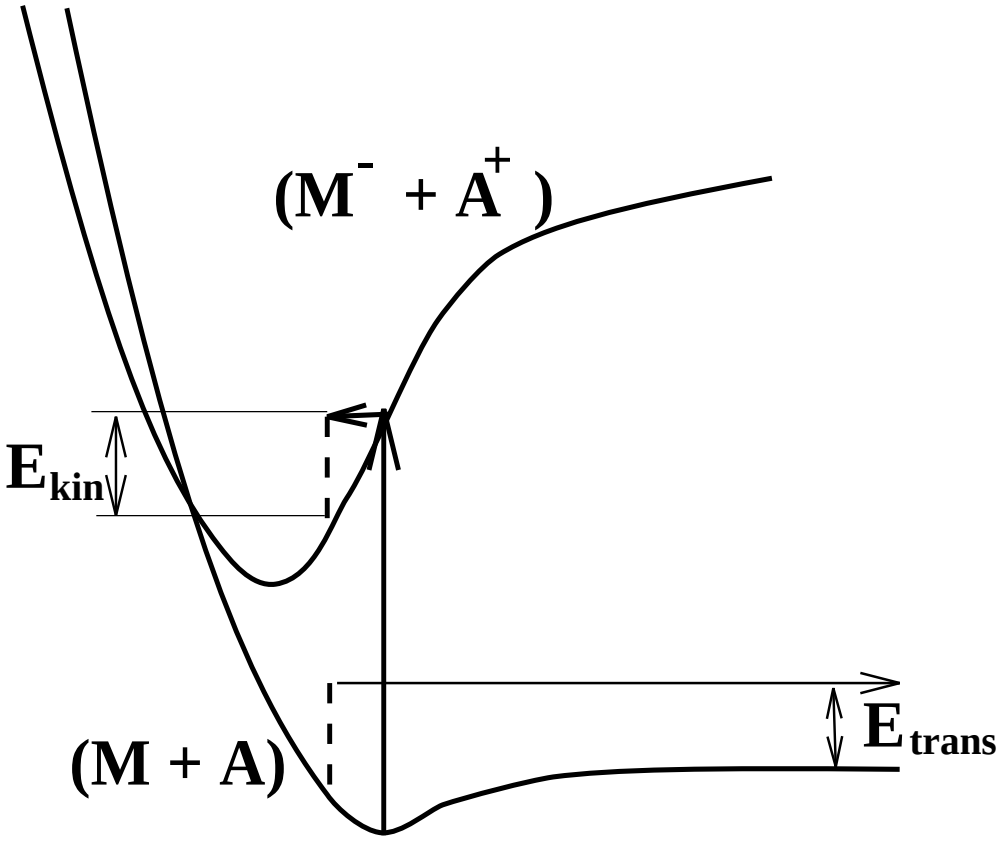

Figure 1.6: *Desorption mechanism in the Antoniewicz model [126]. Here A is the adsorbate and M is the metallic surface.*

phenomena described before can take place the desorption of an ionic or neutral fragment (A^+, A).

In all the examples of the MGR model presented in Figure 1.5, the desorption process is governed by the repulsive parts of excited states potentials. Because of the high energy involved in the process the relaxation from the repulsive part of the potential is fast.

P.R. Antoniewicz published a modified model for electronically stimulated desorption of physisorbed particles adsorbed on metallic surfaces [126]. As show in Figure 1.6, at excitation a temporary ionic adsorbate is formed. With respect to the desorption coordinate, the associated potential curve is displaced towards the surface due to the attractive Coulomb interaction between the charge of the ionic adsorbate and its image produced by the metallic surface. If a Franck–Condon excitation takes place, the particle finds itself on the attractive part of the excited potential curve (M^-+A^+) and accelerates towards the surface, accumulating kinetic energy E_{kin}. The time of relaxation into the ground state is short compared to the M–A vibrational period and the adsorbate returns to the ground state before reaching the repulsive branch of the potential. If this relaxation time is sufficient to allow accumulation of enough kinetic energy, then the desorption occurs and the particle leaves the surface with the translational energy E_{trans}.

A quantum mechanical extension of this model was proposed by W.Hübner and W.Brenig [127]. They used an optical potential of exponential form to couple the two states of the Antoniewicz model. The

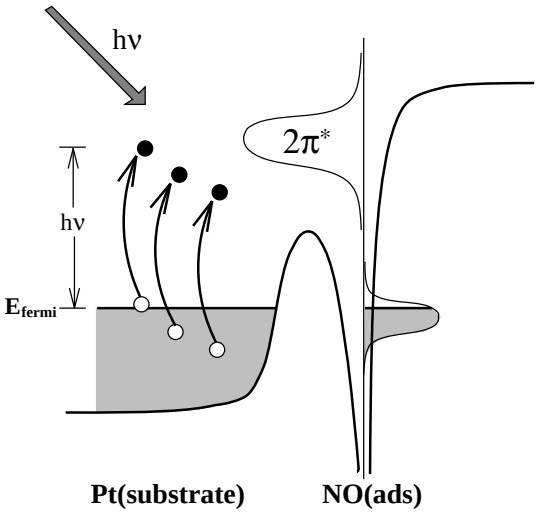

Figure 1.7: *Gadzuk–Model of photodesorption. Electrons from the solid are excited by the photon above the Fermi level. They form a negative ion state with the $(2\pi)^*$ molecular state of NO^-. This state decays, causing the molecular adsorbate to desorb (from Gadzuk et al. [130].*

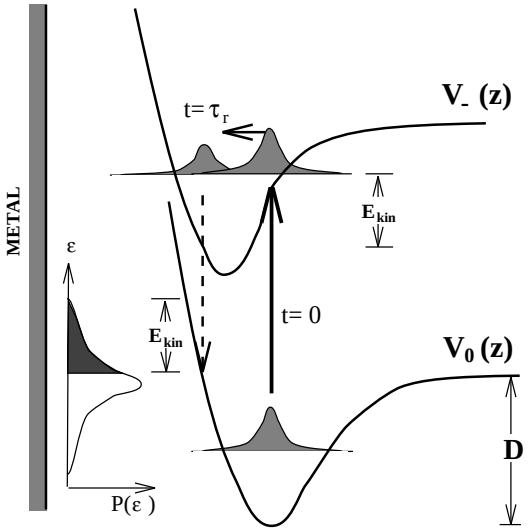

Figure 1.8: *Centre–of–mass translational motion of the adsorbate. The photon excites the ground state wave packet to the negative $2\pi^*$ resonance state with its associated potential curve ($V_-(z)$). The wave packet propagates in time on $V_-(z)$ during a characteristic decay time τ_r. Then it decays to the ground state and desorbs. (from Gadzuk et al. [130].*

parameters of the exponential are fitted to simulate the experimental electronic relaxation. The authors used WKB–method to apply their model to van–der–Waals bound adsorbates.

The Antoniewicz idea of displaced potential curves was improved by Gadzuk [128, 129]. Temporary adsorbate ion is formed by charge transfer/harpooning processes between the adsorbate and the surface electrons. Among other systems such a model was applied to nonthermal photodesorption of NO on Pt(111) [130]. As displayed in the pictural representation in the left part of Fig.1.7, the photon excites electrons from the solid, called 'hot electrons', which occupy the empty molecular orbital $(2\pi^*)$ of the adsorbed NO, lying above the Fermi level. At time t=0, the adsorbate is excited and a temporary negative ion is formed. During its characteristic decay time the wave packet moves on the negative ion potential curve $V_-(z)$ (Fig.1.8) until relaxation to the ground electronic state $V_0(z)$ takes place. The relaxation time τ_r determines the dispersion of the wave packet and the distribution of the desorbed fragments $P(\epsilon)$ with respect to their translational energy ϵ. It also determines the excitation of internal vibration due to the displacement of the corresponding potential curve of the excited state with respect to the ground state one.

In the MGR and Antoniewicz models there is no explicit introduction of the band structure of the solid. W. Brenig [131] and Z.W. Gortel [132, 133] introduced for the excited state this band structure of the solid. Like in Figure 1.5 (d)) there are curves crossing between excited adsorbate type state and solid–induced states but the number of these states is large and corresponds to a nearly continuum or band in the solid. First the adsorbate is excited by say a photon to the adsorbate like excited curve. Then it evolves on this curve and if it reaches the crossing region with the solid–induced states, reneutralization

occurs and the particle can desorb according to the Antoniewicz–scheme.

Gortel introduced also an interesting idea for a description of the translational motion [134, 135]. If the potentials of the ground and the excited state have the same minimum position but a different curvature (the excited state is much steeper then the ground state) the adsorbate adapts the characteristics of the excited state, i.e. it is trapped in a small cage and the squeezing of the coordinate takes place which, by quantum mechanics incertitude relations, results in a wide linear momentum distribution related. This is the case, if the relaxation time is longer than the particle–surface oscillation time, i.e. the wave function becomes 'stationary' in the excited state and it 'forgets' its origin. If now relaxation happens and the molecule desorbs, the translational distribution in the continuum reflects the linear momentum distribution of the excited state and consequently the translational distribution of the desorbed particle is 'hot'.

Harris *et al.* [136] explicitly treated the coupling of electronic motion with the desorption mode for NO/Pt during the formation of a negative ion. An effective model potential depending on two coordinates, that of the 'hot' electron, contributing to the negative ion NO, and that of the NO–surface distance is used to propagate in time the evolution of the wave packet until desorption. The model includes automatically the non-adiabatic corrections but the mass ratio between the electron and NO molecule is too large to justify the proposed model.

In the models discussed above only the desorption coordinate was explicitly introduced. If one wishes to calculate the yield for a desorbed particle in a particular vibrational and rotational state, a yield that can be measured experimentally (see above), then the associated models should include hindered rotation and translation and internal vibration degrees of freedom. In 1983 U. Landman [137] presented a model including hindered rotation in desorption. In this model the hindered rotation potential is defined as a cone of tilt angle β, where inside the cone the molecule can freely precess and librate and outside its motion is forbidden (see Fig.1.9). One can fix the origin of this cone at centre–of–mass of the molecule (a) or at one end (b). To obtain the rotational distribution of desorbed particles, one assumes that the bond between the molecule and the surface is suddenly broken and the molecule escapes rapidly from the surface. Due to the hindrance during adsorption, the free rotor states are mixed together and when projected on free rotor desorbed states give rise to an occupation of high rotational quantum numbers corresponding to high 'rotational temperature'.

This model of a hindered rotor was used by T. Mull *et al.* [33] to compare experimental results for NO photodesorbed from metallic oxides with results of trajectory calculations. The ground state is taken as a Landman hindered rotor whereas the excited state is represented as a free rotor. The photon excites the adsorbate to the upper state and the rotational Franck-Condon overlap gives the probability of rotational distribution on the excited state. This initial distribution is propagated on the excited curve using classical trajectories method. If the relaxation on this curve is long enough, then, in agreement with the experiment, a bimodal distribution is found.

A.R. Burns *et al.* [138, 139] studied desorption stimulated by electron impact, considering the competition of rotational and electronic motions for NO– and CO–metal systems. Self consistent ab–initio studies supply lifetimes of electronic transitions. With this information the authors performed quantum dynamical studies taking simultaneously into account the desorption mode and the rotation. For the rotational mode a hindered rotor for the ground and a nearly free rotor for the excited state are assumed. Following electron impact the adsorbate is excited to the upper potential curve where it feels nearly free

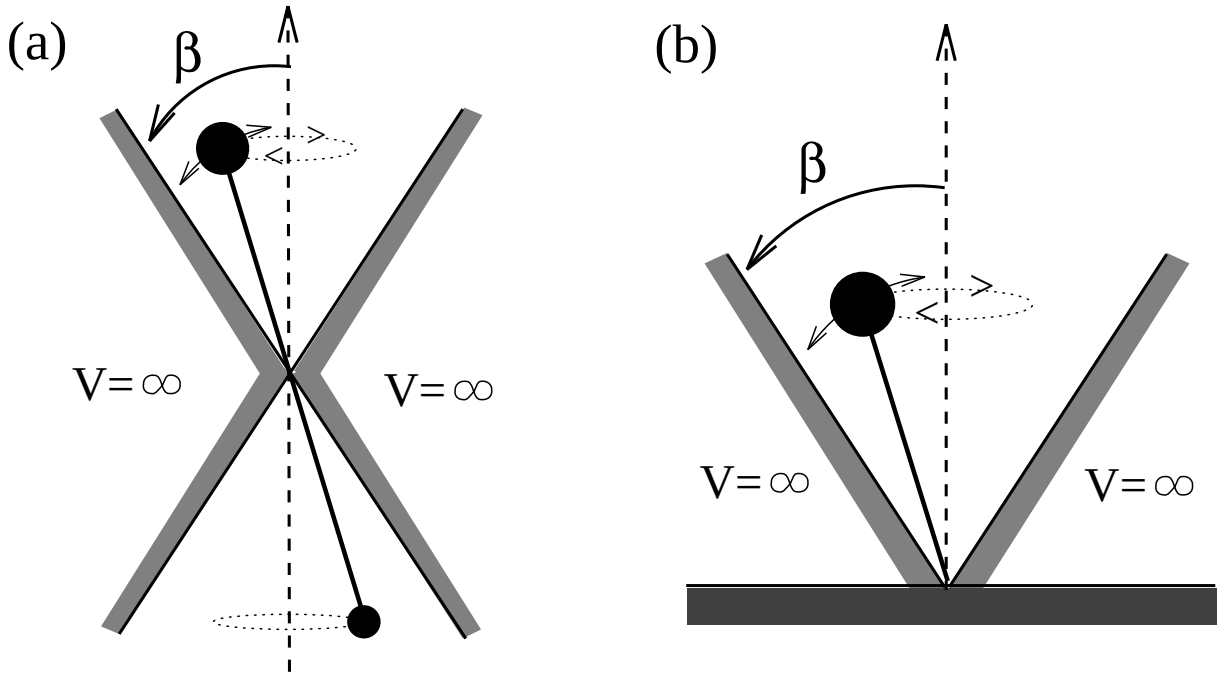

Figure 1.9: *Hindered rotor model of U.Landman [137].*

rotation potential. The lifetime of this excited state is short and when it deexcites to the ground state the instantaneous hindered rotation angle can correspond to the repulsive hindered rotor potential region. By this mechanism the adsorbed molecule acquires enough kinetic energy to desorb. For NO/Pt(111), one obtains a satisfactory agreement between the experimental data and the theoretical calculations.

The coupling of rotational motion with electronic states was also considered by E.Hasselbrink [140]. He studied theoretically laser–induced desorption with classical trajectory techniques by using a elaborated model for the hindered rotor. A simple dependence of the excited state potential on the rotational angles with fitted parameters was taken as well as a simple exponential decaying interaction between the electronic excited and ground states.

A model including the two spin-orbit ground electronic states of adsorbed NO molecules, the rotational motion and the photodesorption coordinate was developed by F. Zimmermann and W.Ho [141]. The interaction between these states is assumed to be proportional to the rotational energy with a fitted proportional constant. The total angular momentum is different in the two spin orbit components and therefore the excitation from one spin orbit component to the other gives rise to a sudden change in the rotational energy. After excitation, the adsorbate moves towards the vacuum, but no change of states is allowed, i.e. the bond breaking between the molecule and the surface is abrupt and the kinetic energy of the fragment high.

Finally J.C. Tully [142] developed a semiclassical molecular dynamics model that includes non-adiabatic interaction between the electronic and nuclear motion. The electronic motion is quantal whereas the nuclear motion is based on classical trajectories. The non-adiabatic probability of transition is based on a potential surface hoping mechanism and the decision to switch from one potential curve to another is based on probabilistic 'fewest switches' mechanism. This delocalise the hoping probability from a

localised crossing point to a region of interaction. This model, as few others described above (see e.g. Harris *et al.* [136]) introduces explicitly the non-adiabatic interaction which is probably responsible for the redistribution of the energy between the electrons and nuclei after photon excitation.

There are other theoretical publications, which do not consider electronic excitations, but studied phenomena like interchange of nuclear motion energies and rotational predesorption phenomena with sophisticated nuclear motion models. Among them, one can cite Shiang et al [143], who used time dependent perturbation theory and Fermi's Golden rule and applied it to desorption of HF/LiF stimulated by infrared photons. A.B. Ephraim et al [144] studied the system CO/NaCl taking a complex coordinate method to predict energies and lifetimes of predesorption resonances, related to coupled translational, rotational and vibration nuclear motions of the adsorbed CO. The hindered rotation, translation, internal vibration and the phonons have been introduced by F. Dzegilenko and E. Herbst in a classical dynamics study for nonthermal desorption [145].

The panorama of numerous models for nonthermal photodesorption described above, show that there are many physical ideas of how the energy is concentrated in the photodesorption mode allowing bond breaking. What is still missing in these models is the complete nuclear motion multidimensionality and the precise calculation of the interaction that is responsible for the energy redistribution between the excited electrons and the photodesorption mode. The nuclear motion multidimensionality implies introduction of the nuclear coupling between photodesorption and hindered rotation which are close in energy. These considerations are valid for the ground state. If the excited negative ion appears in the proposed mechanism then the comparison with the results of gas phase and physisorbed systems (CO/Ag(111): Homann *et al.* [146]) shows that the internal vibration should also be introduced. The adiabatic interaction responsible for the vibronic coupling is only seldomly calculated precisely (by 'ab–initio methods') in the models.

The model I shall develop in the next section is based on three electronic states with their associated potential curves: initial, excited intermediate and final states. Here, the excited intermediate state is the negative ion resonance. The excitation from the ground to the intermediate state is photonic whereas the deexcited of this state invokes non-adiabatic interaction. I show that the simplest formulation based on the perturbation theory has to take into account the second order perturbation term. In chapter 3 I reduce the model to its simplest overlap form with two variants: one calculating rotational overlap only and the other including the desorption coordinate also. The method is applied to the photodesorption of CO/Cu(111).

Chapter 2

Theoretical model

In this chapter, I present a model, which can simultaneously take into account electronic excitation and deexcitation in competition with all coupled nuclear modes of the adsorbate, leading to photodesorption with characteristic rotational, translational and vibration distribution of fragments. The aim of this part of the thesis was to develop a theoretical framework for photodesorption including all electronic and nuclear degrees of freedom. The first application concerns mainly the coupling of adsorbate nuclear modes, the electronic deexcitation appears through a characteristic decay time of an intermediate excited state.

First, I discuss energies and characteristic times of processes which are playing a role in photodesorption (section 2.1). General considerations about the involved processes mainly based on these time scales lead to their relative importance. The coordinate system is introduced to enable the inclusion of all nuclear motions and the electronic excitation. Secondly I explain the framework of this multidimensional photodesorption model. The calculational method for the coupled nuclear wave functions is presented for a vibrating, hindered rotor translating on a structured surface. Finally, I derive the formulae of photodesorption cross sections by using a time dependent quantum mechanical approach.

2.1 General considerations and framework of the multi dim. model

The energies and characteristic times for the relevant processes are shown in Table 2.1. This table is the equivalence for photodesorption to the one shown in photoionization part of this thesis (part II, section 2.1.1, p.37, 38) for CO photodesorbed from a disordered copper surface. I discuss first the nuclear motions.

The ratio of the CO and electron masses is about $5*10^4$ and consequently the electron is moving much faster than the nuclei. Due to this velocity difference, the initial wave function can be written as a Born–Oppenheimer product of a the electronic and nuclear function. If a molecule is adsorbed on a surface, it can perform various nuclear motions. For the weakly chemisorbed CO on disordered copper surfaces, one finds the internal vibration, the CO–surface stretch, hindered rotation and translation in the order of decreasing energy. Crudely speaking, the hindered rotation motion is twofold, one can distinguish

	energy (cm^{-1}	characteristic time
internal vibration C–O	2102 cm^{-1}	32 fs
CO–surface stretch	355 cm^{-1}	100 fs
hindered rotation	282 cm^{-1}	
(precession)		175 fs
(libration)		166 fs
hindered translation	24 cm^{-1}	1400 fs
surface phonons	113 cm^{-1}	595 fs
negative ion shape res. FWHM	1.25 eV	0.5 fs
electronic relaxation inside the solid		0.1 fs
Desorbed CO kinetic energy (box of 4 Åwidth)		
potential (depth 0.4 eV)	3430 cm^{-1}	234 fs
(vacuum)	200 cm^{-1}	968 fs
overall time of desorption process (experimental)		< 325 fs

Table 2.1: *Typical energies and times for the nuclear motions of CO/Cu, the photodesorption and competitive processes, as reneutralization via a negative ion shape resonance, the energy CO photodesorbed from Cu(111) and electronic relaxation time inside the solid. The nuclear motions energies are taken from [49], the mean kinetic energy of CO taken to be that of CO/Pt [34]. The classical oscillation times of the internal vibration, the CO–surface stretch and hindered rotation were calculated by assuming a harmonic oscillator, where that of the hindered rotation was obtained by using the models, explained in Appendix B for* $\overline{\beta}$*=10° (precession). The limit of time of desorption process was measured by femtosecond laser techniques by Prybyla et al [123].*

between precession and libration, i.e. the molecular adsorbate is spinning around the surface normal or it librates in a plane perpendicular to the surface. As the inclination angle is small for chemisorbed systems, the associated time for precession is comparable to that of librational motion. The surface phonons have an energy in between the hindered rotation and translation. Note, that the values of the energies of the CO–surface stretch and hindered rotation are comparable. Using perturbation theory arguments, this is one condition, that both motions are strongly coupled. This is remarkable, as it is the CO–surface stretch motion coordinate, which is responsible for desorption. From the nuclear motion point of view, the other energies are different and can be supposed to be uncoupled from rotation and desorption modes. Due to the nonthermal character of the desorption process and regarding to the time scales, I neglect interaction with phonon. But, this is not necessarily the case for other systems, especially for physisorbed species like CO/Ar, where the energies of the hindered translation and rotation and molecule–surface stretch are much closer [61].

Consider, that a photon of 2–6.74 eV energy hits the absorbate–surface system. In this energy region only the excitation of an electron from the solid to the negative ion resonance $(2\pi)^*$ is possible, i.e. the excitation of an valence electron for CO is energetically not possible. The solid electrons in the band can have at least σ and π symmetry. These facts favour the assumption that the associated transition operator is neither dependent on the centre–of–mass position $\vec{X}$ nor on the orientation and intranuclear distance $\vec{R}$ of the adsorbate. For several experimental set–up's [22, 31], the laser fluence seems not to be sufficient to provoke multiphoton excitation, but for desorption stimulated by a femtolaser (4.5 10^{10} W/cm^2) multiphoton processes take place [123].

Following literature [130, 36] the photodesorption mechanism for molecules like CO absorbed on metals or their oxides involves a photon excitation of electrons from the solid into the empty $(2\pi)^*$ orbital of the adsorbed CO. This state is long living as in the considered energy region, a negative ion shape resonance is formed. By means of two photoemission, T. Hertel *et al.* [147] found, that this state is located at 3.35 ± 0.1 eV above the Fermi level, but below the work function of Cu(111) (4.85 eV, [147]). The deexcitation time $\Delta\tau$ can be calculated by the knowledge of the width. An ab–initio calculation for the negative ion CO^- in gas phase gives 1.25 eV [148], which is in reasonable agreement with the experimental values of 1.9 eV for low coverage CO/Cu(110), obtained by J. Rogozik [149] with inverse photoemission techniques. T.Hertel *et al.* [147] uses two photon photoemission techniques for this system and obtains $\approx$ 300 meV for this width. In fact, the used techniques are not the same and the widths do not necessarily coincide. Using the ab–initio value given above, one obtains a characteristic decay time of about $\Delta\tau$=0.5 fs. Then, after this time, the system decays due to electronic reneutralization. The kinetic energy of the adsorbate in the molecule–surface stretch necessary for desorption can be accumulated by classical motion on the repulsive part of the excited state potential, according to the Antoniewicz model. Or, there is a transfer of electronic to nuclear energies caused by diabatic interactions, especially to the internal vibration and desorption mode. Note, that for very rapid deexcitation (reneutralization) only the latter mechanism can explain an energy accumulation, that leads to desorption.

The excited electron escapes in the band structure. It can carry an energy, that lies in a wide–range (0 – hν) limited by the characteristics of the band structure. It is the energy dependent transition moment, that determines favourable energies. In fact, electronic dispersion to be taken into account. As the transition time is short against those for phonon or hindered translation the parallel wave vector $k_{||}^{\vec{elec}}$ is conserved during the photonic excitation and the electronic deexcitation. During the time, the adsorbate–surface system is in the excited state, this $k_{||}^{\vec{elec}}$ is changing due to dispersion of the wave packet in this state. One

can even say, that the lifetime is longer than electronical motion times in the solid (see Table 2.1) and, the wave packet distribution in $k_{||}^{\vec{elec}}$ is only governed by the properties of the excited state, the system forgets its origin.

The molecule desorbs now. The neutral molecule can have a slow speed of $\approx$ 200 cm^{-1} (see Table 2.1) or $\approx$ 1000 cm^{-1} for metallic or oxidised metal surfaces, respectively. The escape time is long enough (968 fs) compared to the internal vibration and rotation ones to allow surface potential induced interactions, which change the vibrational and the rotational distribution.

It is a fundamental question, if a time–dependent or a time–independent approach should be used for model calculations. Prybyla *et al.* gave an upper limit of 325 fs for the desorption time of CO/Cu(111). If one takes this limit and the characteristic times of nuclear motion and compares them to the lifetime of the excited state, the times are short and a time–dependent approach for the nuclear motion seems to be appropriate. But, the electronic motion is must faster, as one can easily see in Table 2.1 or derive by the mass ratio of 5*10^4 between CO and an electron. Therefore, one can choose a time–independent approach for the electronic motion.

Summarising, the following aspects have to taken into account by a theoretical model:

- coupling of all absorbate nuclear motions due to a realistic surface potential
- Born–Oppenheimer approximation for the initial and final wave functions (reasonable from time scales and mass ratio).
- Coupling of the intermediate (excited) state to the final one by non-adiabatic corrections, allowing an energy transfer from electronic to nuclear motion and in particular to the desorption mode.
- Time–independent ab–initio model for the electronic states. It must take correctly into account the continuum–like band structure of the solid, in particular for the $(2\pi)^*$ negative ion shape resonance
- eventual strong photon intensities, multiphoton effects
- Transition moment for photon excitations is independent on the nuclear coordinates of the adsorbed molecule.
- vertical transitions in $k_{||}^{\vec{electr}}$ space
- Time–dependent approach for the nuclear motion
- phonons are neglected

In the following, I introduce the coordinate system in order to respect all adsorbate nuclear motions on a structured surface. As displayed in Figure 2.1, the coordinate system is attached to the surface with the z–axis perpendicular to the surface and the others in preferential directions on the surface. The vector $\vec{X}$ gives the position of the centre–of–mass of the molecule about a chosen origin on the surface. The orientation of the molecular axis is described by the three Euler angles α, γ (not shown in the fig.) and β, the inclination angle between the intramolecular axis and the surface axis. α is the azimuthal angle between the projection of the intramolecular axis on the surface and the x axis, while γ is defined in a more complicated way (see R.Zare, p.78 [67]). The intranuclear distance of the diatomic molecule is defined by R. In this thesis I use the abbreviations $\vec{R} = (\hat{R}, R) = (\alpha, \beta, \gamma, R)$, $\vec{X} = (x, y, z)$. For circular polarized light stimulating desorption (m$_{ph}$=$\pm$1), the photon incident direction $\vec{q} = (\vartheta, \varphi)$ is

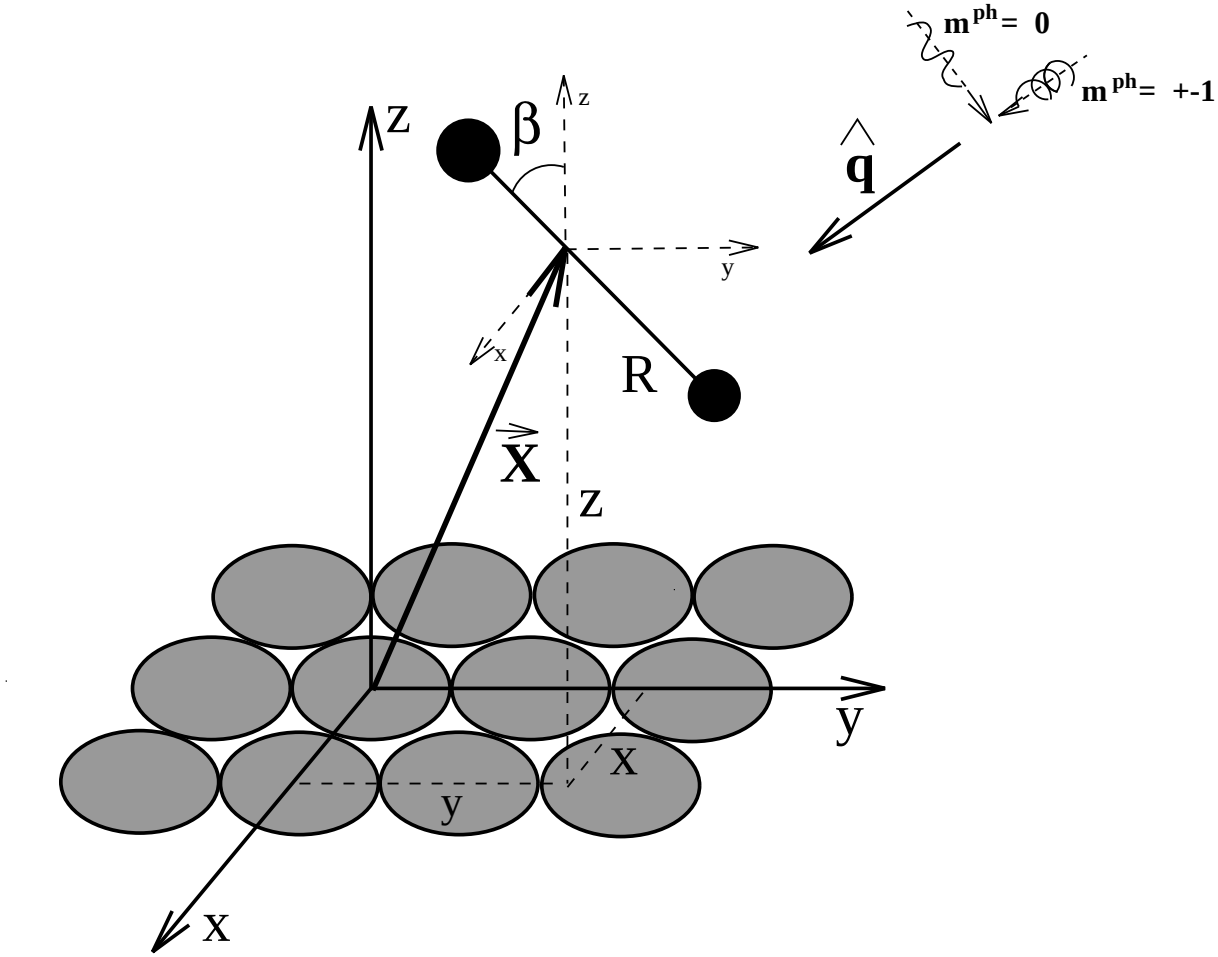

Figure 2.1: *Coordinate system for structured surface allowing hindered translation and rotation.* $\vec{X} = (x\,,y\,,z\,)$ *is the position of the centre of mass of the molecular adsorbate,* β *is the tilt angle of the molecular axis and defines together with* α *and* γ *(not shown here) the molecular orientation. R is the intranuclear distance of the the adsorbate.*

defined by the photon momentum and its quantisation axis, while for linear polarized light (m $_{ph}$=0) the polarization vector defines $\vec{q}$.

2.1.1 Photodesorption including rotation, translation and vibration

The differential cross section for photodesorption based on a time dependent approach can be written as:

$$\sigma^{J,M,v,\vec{k}_{\parallel}^{nuc,f}\,\Omega_f}_{n,\vec{k}_{\parallel}^{nuc,i}}\left(\hat{q},\vec{k}^{nuc},E_{ph}\right)=\frac{4\pi^2 E_{ph}}{\hbar c}\lim_{t\to\infty}\int d^2k_{\parallel}^{elec,f}\int d^2k_{\parallel}^{elec,i} \tag{2.1}$$

$$\left|\left\langle \Psi^{tot}_{\Omega_f,n,\vec{k}_{\parallel}^{elec,f},\vec{k}_{\parallel}^{nuc,f}}\left|\exp(-i\mathcal{H}t/\hbar)\right|\Psi^{tot}_{\Omega_i,n,\vec{k}_{\parallel}^{elec,i},\vec{k}_{\parallel}^{nuc,i}}\right\rangle_{\{\vec{r}\}_N,\vec{R},\vec{X}}\right|^2$$

In Eq.(2.1) E_{ph} is the photon energy, $\hat{q}$ are the angles of the incident photon direction, $\hbar$ Planck's constant and c the speed of the light. $\Psi^{tot}_{\Omega,n,k_{\parallel}^{\vec{elec}},k_{\parallel}^{\vec{nuc}}}$ is the total wave function of the initial (index i) and final (f) state. It is a function of the nuclear variables $\vec{R}$ and $\vec{X}$, defined in the Figure 2.1 and of the spatial coordinates of all the electrons $\{\vec{r}\}_N=(\vec{r_1},\vec{r_2},...,\vec{r_N})$. The quantum number n labels either the eigenfunctions of the total initial or final states. For the initial state all the nuclear modes are coupled. For the final state n now stands for a collection of gas phase quantum numbers (J,M,v,k_z), with the vector $\vec{k}=(k_{\parallel}^{\vec{nuc},f},k_z)$ being the linear momentum vector of the desorbing particle. $k_{\parallel}^{\vec{elec}}$ and $k_{\parallel}^{\vec{nuc}}$ are the two dimensional wave vectors in the reciprocal space necessary for a description by means of Bloch wave functions of the electron and nuclear hindered translation motion parallel to the surface. As the reciprocal vectors for the electronical motions are not determined experimentally, one has to integrate over them. The operator $\exp(-i\mathcal{H}t/\hbar)$ is the time evolution operator from a time $t_0=0$ to $t'=t$. As one is interested in the asymptotic behaviour of the system, the limit $t\to\infty$ has to be taken. I neglected all quantum numbers related to the production of excitons in order to simplify the equations. This is not a general restriction, they can be easily reintroduced in the formalism.

The above equation is quite complicated due to the high number of degrees of freedoms. If numerical propagation techniques is used, calculations become very complicated and time consuming. Instead, I will work with a set of basis wave functions for the electronic and nuclear motions. This wave functions are chosen to prediagonalize the total Hamiltonian.

The total wave function is written as a Born–Oppenheimer product of electronic and nuclear wave functions. There are three states involved in the mechanism: initial, intermediate and final (see Figure 2.2). All non-adiabatic interactions between electronic and nuclear motions are considered in the Hamiltonian, which I will precise later. The Born–Oppenheimer product of the wave function reads:

$$\Psi^{tot}_{\xi,\Omega,n,\vec{k}_{\parallel}^{elec},\vec{k}_{\parallel}^{nuc}}\left(\{\vec{r}\}_N,\vec{R},\vec{X}\right)=\quad\psi_{\xi,\Omega,\vec{k}_{\parallel}^{elec}}(\{\vec{r}\}_N;\vec{R},\vec{X})\quad\Theta^n_{\Omega\vec{k}_{\parallel}^{nuc}}(\hat{R},\vec{X}) \tag{2.2}$$

In Eq.2.2 $\psi_{\xi,\Omega,\vec{k}_{\parallel}^{elec}}(\{\vec{r}\}_N;\vec{R},\vec{X})$ is the electronic wave function, which depends parametrically on the nuclear coordinates $\vec{R},\vec{X}$. ξ stands for all other electronic quantum numbers. The nuclear wave function is $\Theta^n_{\Omega\vec{k}_{\parallel}^{nuc}}(\hat{R},\vec{X})$ labelled by n, defined above. In this context, Ω is the quantum number associated to the projection of the total angular momentum of the adsorbed molecule onto the intramolecular axis. Due to

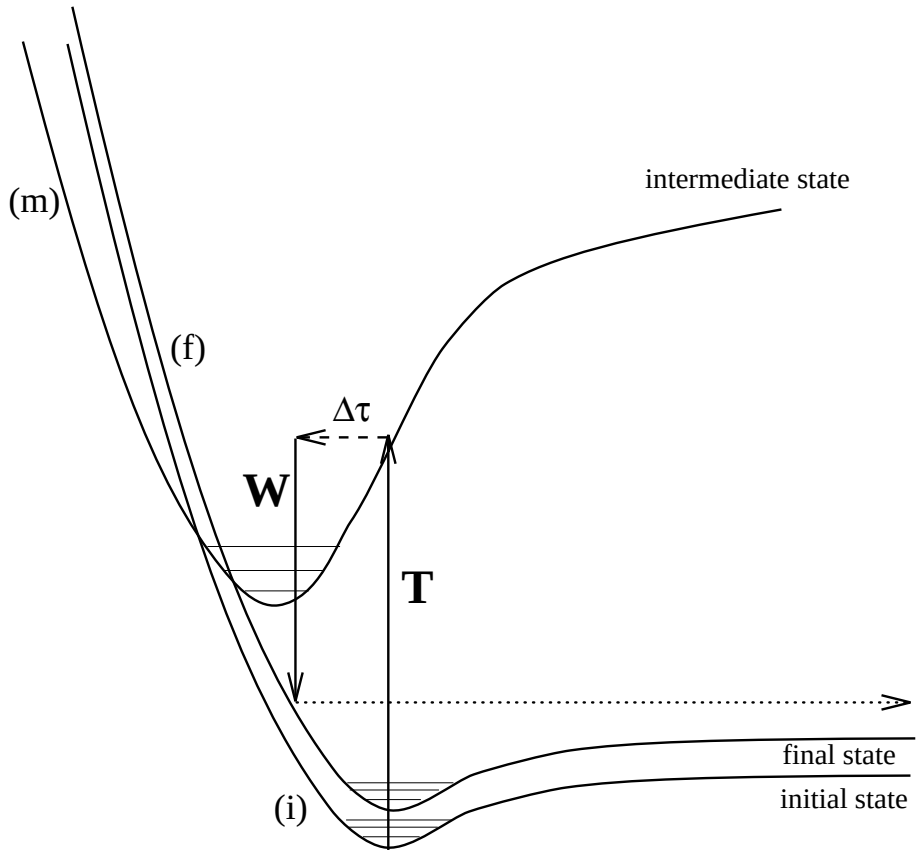

Figure 2.2: *Present two step model. The photon excites the molecule–surface system from the initial (i) to the upper state (m) (photon operator T). The excited state is coupled by non-adiabatic interactions W to the final state (f). These interactions determines a decay time* $\Delta\tau$.

the molecule–surface interactions in general $\mathbf{\Omega}$ is not a good quantum number for the total system. But, in the present model the corresponding corrections are neglected.

The Hamiltonian $\mathcal{H}^{tot}$ contains all kinetic energy operators and the molecule–surface potential:

$$\mathcal{H}^{tot} = \mathcal{H}^{elec}_{kin}(\{\vec{r}_N\}) + \mathcal{H}^{nuc}_{kin}(\vec{R},\vec{X}) + V^{molecule}(\{\vec{r}_N\},\vec{R}) + V^{mol-surf}(\{\vec{r}_N\},\vec{R},\vec{X}) + {}^{m^{ph}}T^{photon}(\{\vec{r}_N\},\hat{q},t) \tag{2.3}$$

Here, $\mathcal{H}^{elec}_{kin}$ is the kinetic energy operator of all electrons, and $\mathcal{H}^{nuc}_{kin}$ the one of the nuclear motions. $V^{molecule}(\{\vec{r}_N\},\vec{R})$ and $V^{mol-surf}(\{\vec{r}_N\},\vec{R},\vec{X})$ are the internal molecule and the molecule–surface interaction potentials respectively. ${}^{m^{ph}}T^{photon}(\{\vec{r}_N\},\hat{q},t)$ is the operator associated to the photon, that gives rise to electronic excitations. If a femtosecond laser is used, i.e. if the duration of the laser pulse is short compared to the duration of the photodesorption, ${}^{m^{ph}}T^{photon}$ and the total Hamiltonian is explicitly depending on time and the equation (2.1) should be used. For nanosecond pulses, this time dependence can be neglected and the corresponding equation simplified. The electronic wave function in the Born–Oppenheimer product solves the electronic Schrödinger equation, taking $V^{molecule}$ and $V^{mol-surf}$ for parametrically fixed $\vec{R}$ and $\vec{X}$.

Before detailing the nuclear wave function I want to discuss in greater detail the involved electronic states (see Figure 2.2). Initially, the system is in the fundamental state $\xi, \mathbf{\Omega}_i, \vec{k}^{elec,i}_{||}$. The photon induces a transition into the excited state, labelled by an index m. This excited state is coupled by non-adiabatic electronic interaction to the final state (index f). The final state quantum number $\mathbf{\Omega}^f$, that describes the main contributing electronic state of CO to the total electronical wave function, is identical to the one of the initial state: $\mathbf{\Omega}^i = \mathbf{\Omega}^f$, i.e. no electronic excitation of the desorbing molecule takes place. This is the case of photodesorbed neutral CO, but in general not for NO, which has a spin–orbit splitted fundamental state. Note, that during the excitation and deexcitation processes, $\delta\vec{k}^{elec}_{||}$ is not changing, but the initial and final state $\vec{k}^{elec}_{||}$ may not be identical due to the considerable evolution time (from the electronic motion point of view) of the system on the excited state (m). Note also, that the initial and final states are assumed to be well described by a simple Born–Oppenheimer product. This is the case as the interactions are not resonant in the considered variables space, e.g. no curve crossing occurs in the neighbourhood. This is not the case for the intermediate state, it is in general strongly coupled to the final one.

The nuclear wave functions in the Born–Oppenheimer product (2.2) are obtained by neglecting all interactions that couple electronic states and solving the Schrödinger equation using the corresponding nuclear and the electronic wave functions. One can now construct a complete basis set of wave functions in the adiabatic Born–Oppenheimer approximation.

Neglecting dissociation, the basis set of nuclear wave function includes discrete states for internal vibration and hindered rotation and discrete and continuum states for translational and desorption motions. During the propagation on the excited potential curve, the nuclear motion can in general populate all discrete and continuum states. But from the point of view of initial state the molecule–surface motion is discrete and the electronic lifetime is too short to allow a population of the associated continuum states. Therefore in the intermediate state only the sum over all discrete states for the molecule–surface motion has to be taken. However, the free/hindered translation must be described by Bloch functions and the integration over the two-dimensional wave vector $\vec{k}^{nuc,m}_{||}$ in reciprocal space is conserved in the

formulation.

In the following, I only give the final desorption cross formula. The complete derivation and a generalized formula are given in Appendix E.2. Briefly, I treat all non-adiabatic interactions and the photonic transition as weak perturbations and obtain the final expression given below in the framework of the second order time dependent perturbation theory. The resulting photodesorption cross section reads:

$$\sigma^{J,M,v,\vec{k}_{\parallel}^{nuc,f}\Omega}_{n,\vec{k}_{\parallel}^{nuc,i}}(\hat{q},E_{ph}) = \frac{4\pi^2 E_{ph}}{\hbar c}\int d^2k_{||}^{elec}\lim_{\varepsilon\to 0} \tag{2.4a}$$

$$\left|\sum_{n_m}\int d^2k_{||}^{nuc,m}\left\langle \Theta^{n_f}_{\Omega,\vec{k}_{\parallel}^{nuc,f}}\middle| W^{\Omega_m}_{\Omega,\vec{k}_{\parallel}^{elec}}(\vec{R},\vec{X})\middle|\Theta^{n_m}_{\Omega\vec{k}_{\parallel}^{nuc,m}}\right\rangle_{\vec{R},\vec{X}}\right.$$

$$\left.\frac{1}{E^{n_i,\vec{k}_{\parallel}^{nuc,i}}_{\Omega,\vec{k}_{\parallel}^{elec}} + h\nu - E^{n_m,\vec{k}_{\parallel}^{nuc,m}}_{\Omega,\vec{k}_{\parallel}^{elec}} + i\varepsilon}\left\langle \Theta^{n'}_{\Omega,\vec{k}_{\parallel}^{nuc,l}}\middle|\ ^{m^{ph}}T^{\Omega_m}_{\Omega,\vec{k}_{\parallel}^{elec}}\middle|\Theta^{n_i}_{\Omega\vec{k}_{\parallel}^{nuc,i}}\right\rangle_{\vec{R},\vec{X}}\right|^2$$

where

$$W^{\Omega_m}_{\Omega,\vec{k}_{\parallel}^{elec}}(\vec{R},\vec{X}) = \int d^{3N}r\left(\psi_{\xi_f,\Omega,\vec{k}_{\parallel}^{elec}}(\{\vec{r}\}_N;\vec{R},\vec{X})\right)^* \mathcal{H}^{tot}\psi_{\xi_m,\Omega_m,\vec{k}_{\parallel}^{elec}}(\{\vec{r}\}_N;\vec{R},\vec{X}) \tag{2.4b}$$

Actually, Equation 2.4 represents a two step process visualised in Figure 2.2. First, the photon excites the adsorbate–surface system to the electronically excited state (m) having different excited nuclear states. Secondly, the system can decay from the state (m) into the final state (f). These steps are presented in second order perturbation theory Equation 2.4, supposing that the photon and non-adiabatic interactions are weak. The interactions will allow the adsorbate–substrate system to deexcite and the molecule–surface degree of freedom will finally allow desorption of the adsorbate. The interaction function is determining the distribution of the other nuclear modes of the desorbing molecule, like internal vibration and rotation, by an explicit dependence of the function W, that couples these modes of the intermediate and final state. One can visualise two extreme examples. The initial and intermediate state potential curves are different and consequently the associated energies and wave functions of the nuclear adsorbate modes do not correspond to each other. The transit time on the excited state (m) is long and its characteristics are imposed on the fragment distribution: the system forgets its origin. Then the intermediate state will impose its characteristics on the final state distribution. The other extreme corresponds to an intermediate state that does not really contribute, i.e. the particle passes only a very short time on the excited state (m) and the initial state imposes its characteristics on the fragment distribution.

Generally, the approximation of weak non-adiabatic interactions is a crude approximation particularly because the Born–Oppenheimer basis is inappropriate. In addition, in the derivation from Equation (2.1) to Equation (2.4) one assumes that the kinetic energy perturbation terms responsible for nondiabatic

corrections and the zero order Hamiltonian commute, which again may be a crude approximation. Appendix E.2 shows a generalized version of the photodesorption cross section, that goes beyond these approximations.

2.1.2 Potential and wave functions of the coupled hindered nuclear motions

As discussed above in relation to the Equation 2.2 for the electronic wave functions Ω is assumed to be a good quantum number. Consequently the electronic clouds of the molecular adsorbate are assumed to keep their axial symmetry around arbitrary rotations around the intramolecular axis. For nuclear motions, the adsorbate is allowed to undergo rotation (α, β), C–O and CO–surface vibrations (R, z)and translation ($\vec{X_{||}} \equiv (x, y)$) on a periodic structured surface. The potential dependence on the associated variables can be expanded in spherical harmonics (hindered rotation), Taylor (internal vibration) and Fourier series (hindered translation). However, the expansion coefficients remain a function of the CO–surface distance z:

$$V(\vec{X}, \vec{R}) = \sum_{L=0}^{\infty} \sum_{M_L=-L}^{L} \sum_{i=0,1,2} \sum_{all \vec{q_{||}}} V_{LM_L}(z, R_0) \times \tag{2.5}$$

$$\times \left(\mathrm{Y}^L_{M_L}(\beta, \alpha) \right)^* \quad \times (R - R_0)^i \quad \times \exp\left(-i \left[\frac{2\pi}{a_x^0} q_x x + \frac{2\pi}{a_y^0} \vec{q_x} x \right] \right)$$

In (2.5) q_x and q_y are integer values related to the expansion of the periodic potential in Fourier series with the periodicity constant a_x^0 and a_y^0 along the x and y directions, respectively. As no photodissociation is considered here and the distance R remains close to its mean value R_0, the Taylor expansion around R_0 can be restricted to a few tems.

Analogically, the wave function of the coupled nuclear motions can be expanded in a base of functions for the different degrees of freedom:

$$\Theta_{\Omega}^{n,\vec{k_{||}}}(\vec{R}, \vec{X}; R_0) = \tag{2.6}$$

$$\sum_{M=-J,\ldots,J}^{J} \sum_{v,v_z=0}^{\infty} \sum_{all \ \vec{g_{||}}} c^{n,\Omega}_{JM,v,v_z,\vec{g_{||}}} \times$$

$$\times \mathcal{D}^{(J)*}_{M\Omega}(\hat{R}) \times \exp\left[-i \left(k_x - \frac{2\pi}{a_x^0} g_x x + k_y - \frac{2\pi}{a_y^0} g_y y \right) \right] \times \mathcal{H}_v(R - R_0; \nu_{int.vib}) \times \mathcal{F}(z; x_0, y_0, \alpha_0, \beta_0)$$

For the rotation the basis set are the Wigner functions of free rotation $\mathcal{D}^{(J)*}_{M\Omega}(\hat{R})$ in active rotation notation ([67], p.78). The quantum numbers M and Ω are the projections of the total angular momentum $\vec{J}$

onto the surface normal and the intramolecular axis, while $\hbar J(J+1)$ is its length. Due to the structured surface, M is in general not a good quantum number, i.e. one has to sum over it, and has to be replaced for example by a quantum number associated to the irreducible representation of the local symmetry group. The internal vibration is normally only slightly modified by the surface. Therefore it is expanded in the wave functions of a harmonic oscillator $\mathcal{H}_v(R-R_0;\nu_{int.vib})$, where the mean value R_0 and the oscillation frequency $\nu_{int.vib}$) are adjusted by an iterative procedure to fit the eigenvalues of the potential given above. The latter approximation is justified if no photodissociation takes place and if in the final state only the first states of the internal vibration can be excited. This approximation is not justified for the photodesorption coordinate z. Consequently, for this degree of freedom I do not assume a basis of analytical functions. The functions $\mathcal{F}(z;x_0,y_0,\alpha_0,\beta_0)$ can have any dependence on z with fixed variables x_0,y_0,α_0,β_0. Due to the periodicy, the hindered transition motion can be described by Block functions $\left[\exp\left(-i\left(k_x-\frac{2\pi}{a_x^0}g_x x+k_y-\frac{2\pi}{a_y^0}g_y y\right)\right)\right]$ with g_x,g_y integer. The Schrödinger equation for the nuclear motion reads:

$$\mathcal{H}^{nuc}\Theta_{M\Omega}^{n,\vec{k_\parallel}}\left(\vec{R},\vec{X};R_0\right)=E_n\Theta_{\Omega}^{n,\vec{k_\parallel}}\left(\vec{R},\vec{X};R_0\right) \quad (2.7a)$$

$$\mathcal{H}^{nuc}=\left[B\vec{R}^2-\frac{\hbar^2}{2m_{CO}}\left\{\left(\frac{\partial}{\partial x}\right)^2+\left(\frac{\partial}{\partial y}\right)^2+\left(\frac{\partial}{\partial z}\right)^2\right\}-\frac{\hbar^2}{2\mu_{CO}}\left(\frac{\partial}{\partial R}\right)^2+V(\vec{R},\vec{X})\right] \quad (2.7b)$$

In (2.7) $B\vec{R}^2$ is the kinetic energy operator for a rotor [81], where B is the rotational constant in gas phase (B_{CO}=1.93 cm^{-1}). $\frac{\hbar}{2m_{CO}}\left\{\left(\frac{\partial}{\partial x}\right)^2+\left(\frac{\partial}{\partial y}\right)^2+\left(\frac{\partial}{\partial z}\right)^2\right\}$ and $\frac{\hbar}{2\mu_{CO}}\left(\frac{\partial}{\partial R}\right)^2$ is the kinetic energy of the hindered translation parallel to the surface (x,y), the CO–stretch (z) and of C–O internal vibration (R) with the associated total mass m_{CO}=28 a.m.u. and the reduced mass μ_{CO}=6.856 a.m.u. $V(\vec{R},\vec{X})$ is the surface potential with a periodicity in x and y.

One can now insert (2.5) and (2.6) in the Schrödinger equation (2.7), left multiplies (2.7)) by one multidimensional basis set wave function $\sqrt{\frac{2J+1}{8\pi^2}}\mathcal{D}_{M\Omega}^{(J)*}(\hat{R})\mathcal{H}_v(R-R_0;\nu_{int.vib})\mathcal{F}(z;x_0,y_0,\alpha_0,\beta_0)$. After integration over all variables $\vec{R},\vec{X}$ one finally obtains a set of linear equations similar to those of part II, section 2.4.1 (Eq.(2.20), 57). The problem is now a standard eigenvalue and eigenvector problem. Library routines are used to calculate the coefficients of the expansion and the nuclear motion energies, parametrically dependent on the twodimensional vector $\vec{k_\parallel}$.

Chapter 3

Photodesorption of CO from Cu(111) surface

As a first application of the model described in the preceding chapter, I chose the weak chemisorbed system CO/Cu(111). The choice was dictated by experimental observation of photodesorbed CO by Prybyla *et al.* [123] and the existence of a model potential for the ground state of CO on Cu(111) in literature, published by Q. Ge *et al.* [150]. The experiment of Prybyla et al [123] was very reach because it was performed with a femtosecond laser, therefore ruling out completely the thermal regime. Moreover the mechanism advocated by Prybyla is multiphotonic (with 3-4 photons) and considers the formation of an intermediate negative ion resonance on the adsorbate. Although I do not present electronic calculations of the CO/Cu(111) system in this thesis, a supplementary reason for this choice was the relative small number of electrons for CO–Cu model cluster which will be used in the future for the electronic ab–initio calculations.

This chapter is divided in two sections. First, I present the potential and the wave functions for the different nuclear modes of the adsorbed system. Secondly, I discuss the rotational, translational and vibrational distributions for the simplified model based on overlap scheme including the nuclear desorption mode.

3.1 Potential and wave functions for the nuclear motion

To represent the nuclear motions of the molecular adsorbate, i.e. the hindered rotation, translation, internal vibration and the CO–surface stretch for CO adsorbed on Cu, I used the model potential cited above [150]. Briefly, this potential valid for the ground state is based on atom–atom pair potential scheme. The experimentally known adsorption energies and the energies of the CO–surface stretch together with an assumed mean distance z_0 for both on–top and two–fold bridge adsorption sites are used to fit the model potential.

To model the fcc copper crystal with a surface cut in the (111) plan, I considered 99 Cu atoms in three surface layers (Figure 3.1). The first layer contains 45, the second 30 and the last 24 atoms. The

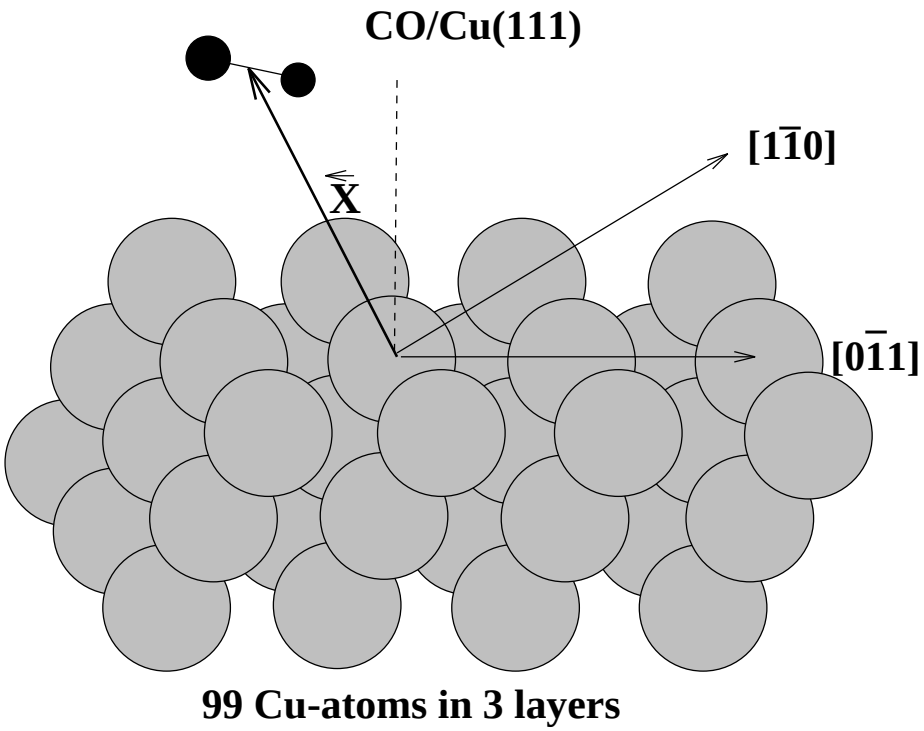

Figure 3.1: *CO adsorbed on the (111) surface of a fcc copper crystal. The crystal is modelled by 99 Cu atoms in three layers. The crystal structure is fcc with a lattice constant of 3.61 Å.*

authors [150] proved, that this assembly is sufficient to model the potential with respect to all adsorbate coordinates.

In the publication of Q. Ge *et al* [150], the mass of carbon was used for the effective mass for the CO–surface stretch motion instead of the total mass of CO. The C–O bond is strong and the energy for internal vibration is high compared to that of the CO–surface stretch. Therefore the coupling between these vibrational motions is small. Considering the CO–surface motion both the carbon and the oxygen are simultaneously moved and the total reduced mass should be taken for this motion. To bypass this error, I used the wrong mass (m_C=12 a.m.u) to calculate the CO–surface stretch frequency. For the calculation of energies associated to the other motions, but not for potential plots and desorption thresholds, I scaled the potential by an arbitrary constant. For a value of 0.245, the adjusted potential reproduces crudely the experimental energies for the internal vibration, hindered rotation and translation.

Now I discuss the characteristics of this potential with respect to different vibrational modes. First, for on–top adsorption sites, calculations show, that the potential is nearly axial symmetric about the surface normal [111].

Secondly one would like to know for CO/Cu(111) what is the strength of the coupling between the hindered rotation and the CO–surface stretch. Figure 3.2 displays the surface potential dependent of the tilt angle β and the CO–surface distance z for fixed on–top adsorption site and fixed intranuclear distance R_0=1.167 Å. The upper part of the Figure 3.2, shows the behaviour of the potential as function of z and β. For small tilt angles (β<40°) the potential has a minimum around z_0=2.4 Å. For higher β the potential

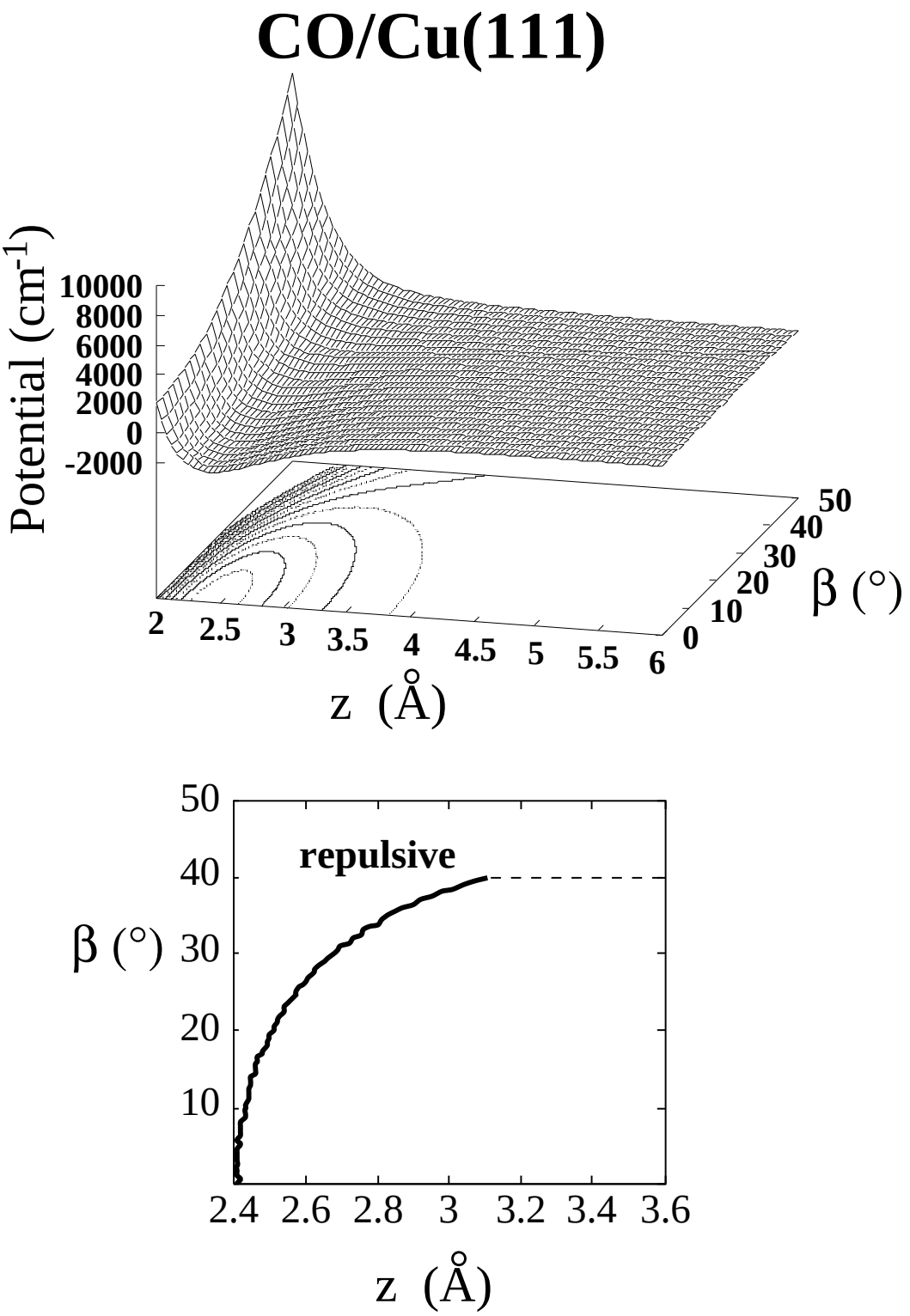

Figure 3.2: *CO/Cu(111): potential for hindered rotation and CO–surface stretch in cm^{-1}. Upper figure: Potential with respect to the tilt angle β and the CO–centre–of–mass surface distance z. The molecule is adsorbed on–top site with the intramolecular distance fixed at R=1.167 Å. Lower figure: position of potential minimum. Note, that for β>40° , the potential in z is purely repulsive.*

hindered rotation		
$n^{"}$	M	$E^{(initial)}(cm^{-1})$
0	0	0.0
1	$\pm$ 1	197.0
1	0	388.0
2	$\pm$ 1	583.5
2	0	775.3

CO–surface stretch	
$n^{"}$	$E^{(initial)}(cm^{-1})$
0	0.0
1	368.9
2	726.6
3	1072.9

Table 3.1: *Energies of the hindered rotation and CO–surface stretch motion with the intramolecular distance fixed at 1.167 Åat on–top site. Left table: energies due to hindered rotation, CO–surface stretch frozen (z_0=2.41 Å). Right table: CO–surface stretch only, hindered rotation frozen (upright position).*

coupled motion		
$n^{"}$	M	$E^{(initial)}(cm^{-1})$
0	0	0.0
1	-1	50.9
2	0	78.1
3	1	83.0
4	-1	129.1
5	1	161.1
6	0	180.9
7	0	258.9
8	0	261.7
9	-1	284.9
10	-1	312.6
11	1	344.6
12	-1	363.9

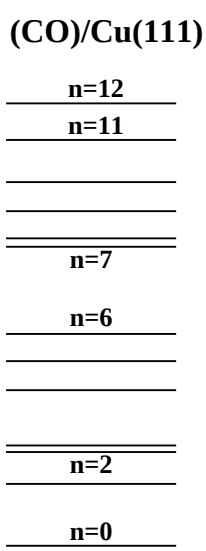

Table 3.2: *Energies for the coupled hindered rotation — z–stretch motion.*

becomes purely repulsive. The lower part of the figure shows in greater detail the change of position of the local minimum. Its position varies from 0° for z=2.4 Å to 15° for 3.4 Å. The behaviour presented in Figure 3.2 shows, that a coupling between the hindered rotation motion and the CO–surface stretch is significant. It further shows, that for large β angles, desorption is favoured due to the repulsive part of the potential. In fact, these large tilt angles can be generated if one populates highly excited rotational states. For example directly by thermal heating (Boltzmann population), by rotational excitation (photons in the infrared region) or indirectly by an excitation of electronic motion or internal vibration of the adsorbate together with an efficient transfer of the energy to the hindered rotation and desorption modes.

Table 3.1 displays the energies of the uncoupled molecule–surface (z–stretch) and the hindered rotation motion for on–top adsorption site, freezing all other motions. Note, that due to the quasi–axial symmetry for this adsorbed species, M is a good quantum number. The experimental values of 282 cm^{-1} and 355 cm^{-1} for the z–stretch and hindered rotation of CO on disordered copper surface [49] agrees fairly with our calculated energies.

If one allows the more realistic coupling of hindered rotation and z–stretch motion the picture completely

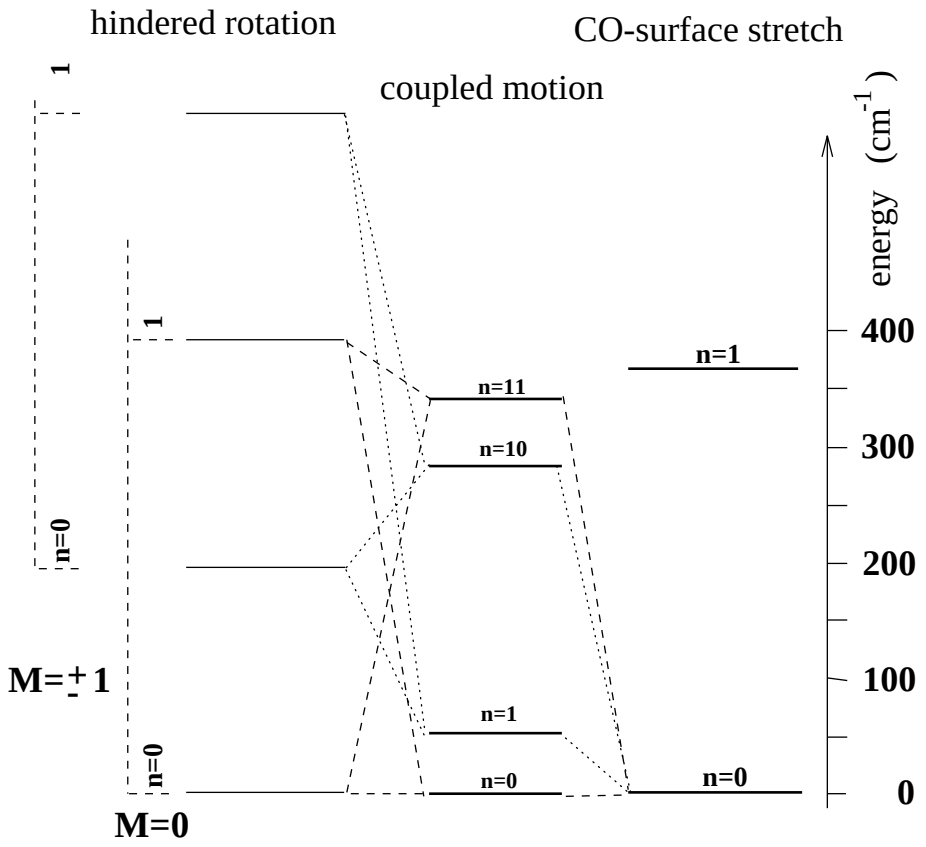

Figure 3.3: *Coupling of hindered rotation and z–stretch motion. The first two wave functions of the basis set forming wave function of the coupled wave function are shown. Note, that all fundamental energy levels of the unperturbed motion are lowered down.*

changes. The Table 3.2 and Figure 3.2 show the energies of the coupled motions. One observes several near lying levels with energy differences about 5 – 80 cm^{-1}. Obviously a strong coupling takes place for the chosen CO/Cu(111) potential. The way uncoupled states are correlated to the coupled ones is visualised in Fig.3.3.

The energy levels of the unperturbed motion couple giving rise to low lying and high lying perturbed states. Taking the example of the $M = 0, n = 0$ (hindered rotation) and $n = 0$ (z–stretch) levels in uncoupled notation, they couple and form two states, one becomes the fundamental state $n = 0$, the other is lying higher in energy at 344.6 cm^{-1} ($n = 11$). In general more than two states are involved in the coupling.

The nature of state splitting due to coupling can also be found in the shape of the wave function. In Figure 3.4 the density of the wave function is plotted as function of the tilt angle β and the molecule–surface distance z. One sees that the two wave functions densities originating from the ground levels of the unperturbed system are associated to the $n = 0$ and $n = 11$ levels. They show a symmetric and antisymmetric behaviour in terms of symmetric and antisymmetric combinations of the two main contributions of the uncoupled wave functions. One can further analyse directly the coupling. Taking $n = 2$, one sees, that there is a node in z, but not in β direction. Therefore this states originates

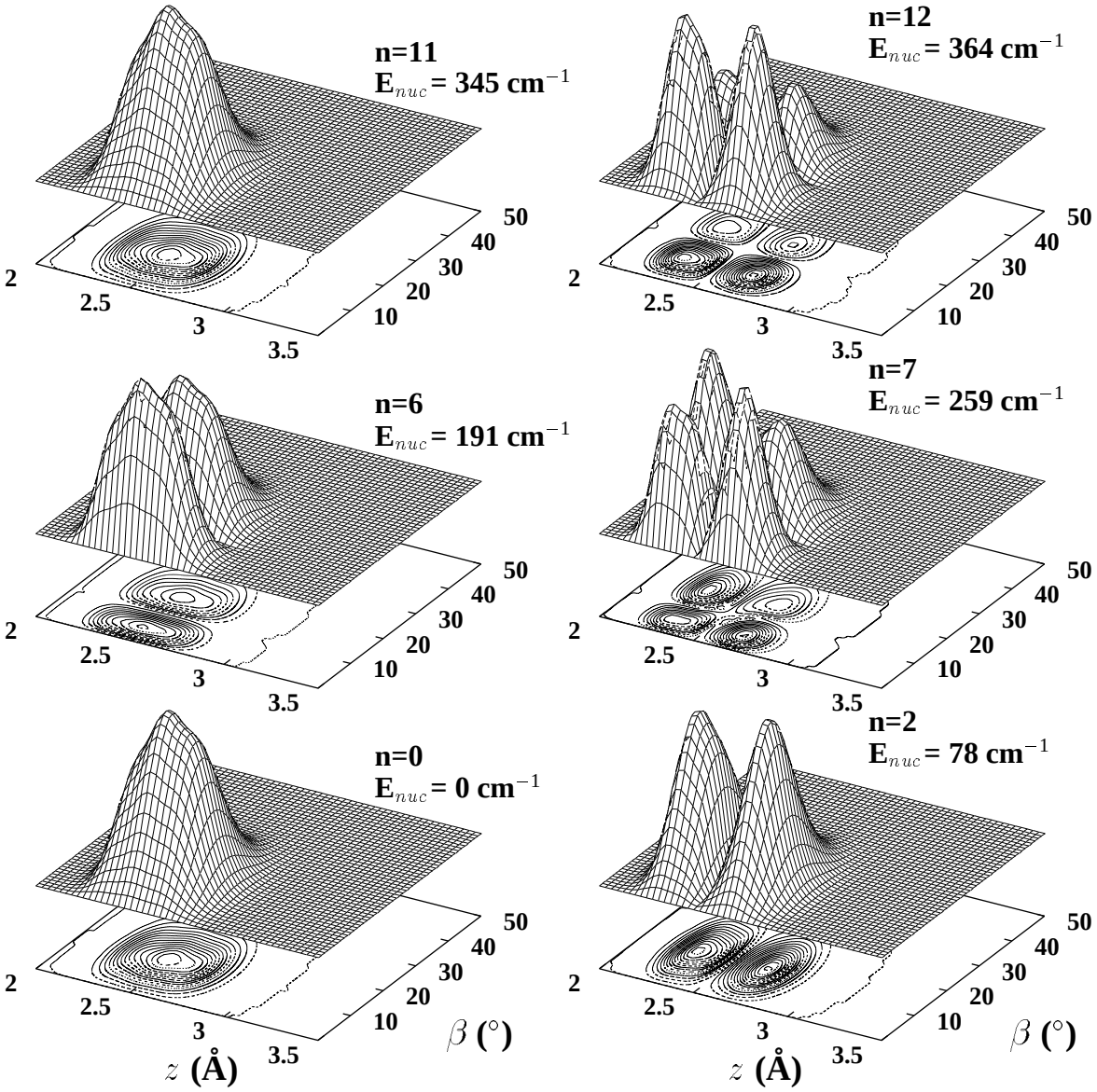

Figure 3.4: *Wave function density for the coupled hindered rotation — z–stretch motion. (square of the wave function multiplied by* $\sin\beta$*).*

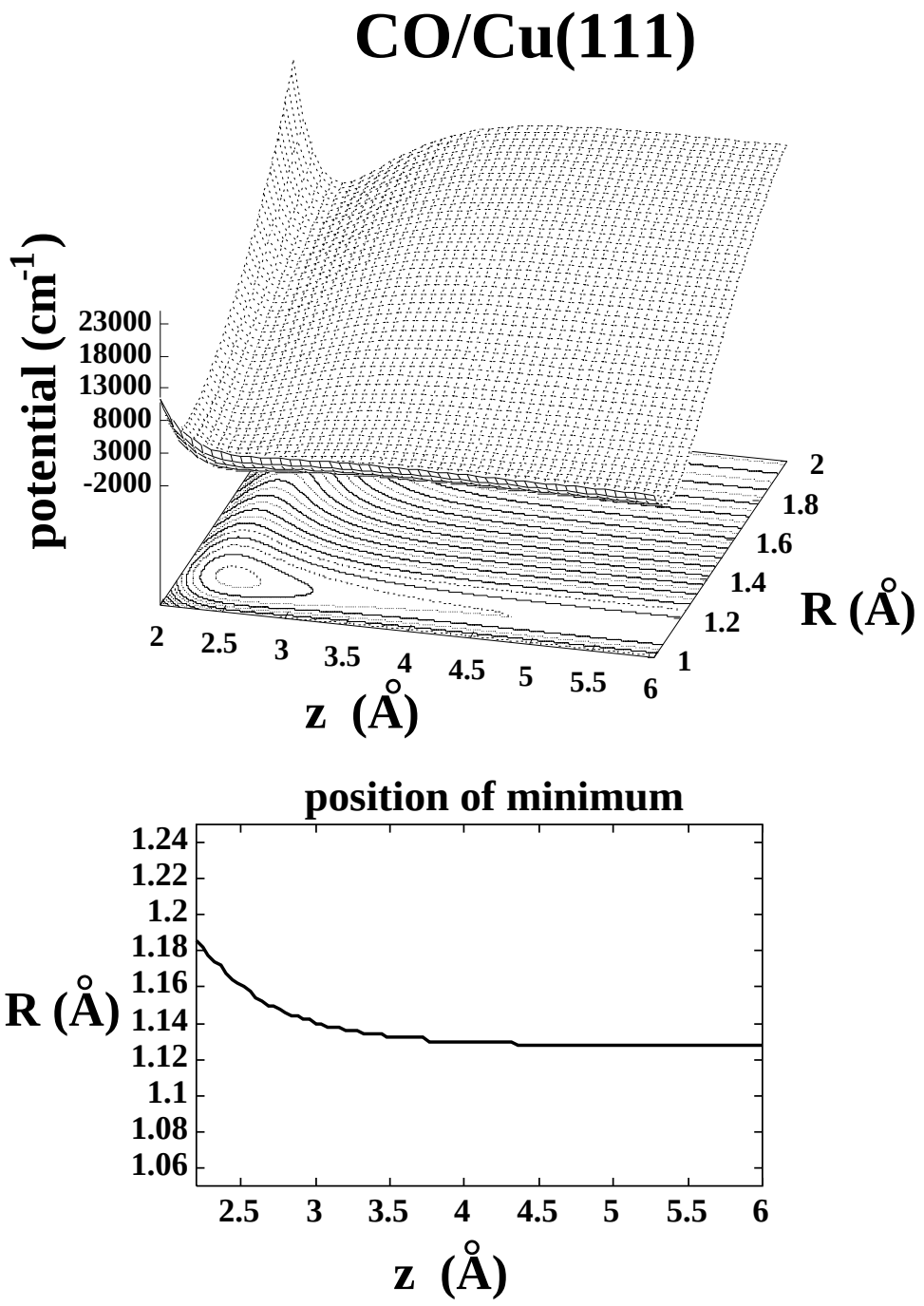

Figure 3.5: *CO/Cu(111): potential for CO–surface and internal vibration in cm^{-1}. The adsorbate is kept in upright position (α, β=0°) with R=1.167 Å. Upper figure: Potential respect to the intranuclear distance R and the CO–centre–of–mass surface distance z. Lower figure: position of potential minimum. The position of the minimum is only slightly varying in R.*

essentially from the $n = 1$ (z–motion) and $n = 0, M = 0$ (hindered rotation). A still more complicated nodal structure can be observed for $n = 12$: a 2×2 node structure appears in z and hindered rotation coordinates.

The analysis made above is valid for rigid CO. As I show in the following, the internal vibration is not coupled to the z–motion. In Figure3.6 I plotted the CO/Cu(111) potential as function of intranuclear distance R and and desorption coordinate z, keeping the molecular adsorbate at on–top site in upright orientation. In the lower part of the Figure3.6, one can see that the position of the minimum varies only slightly with R and consequently the coupling between these two modes can be neglected. The analysis of the coupling coefficients of the uncoupled wave functions confirms the above statement. In fact, the internal vibration and hindered rotation quanta are too different to give rise to accidental degeneracy which will generate coupling between these motions.

As the last point of the analysis of absorbate nuclear motions, I want to discuss briefly the hindered translation. The corresponding energies are low (see Table 2.1). Figures 3.6 and 3.7 show the potential in $[01\overline{1}]$ and $[1\overline{1}1]$ directions on the surface. The potential is relatively deep with a minimum at about 500 cm^{-1}.

In general, the molecular adsorbate can hop from site to site. In order to analyse the motion, one can plot the band structure for hindered translation. If the energy varies strongly with the $\vec{k}_{||}$ vector in reciprocal space, then molecule can easily hop between the adsorbate sites. In fact, for CO/Cu(111) this is not the case. Fig.3.8 displays the dependency of the hindered translation energy with respect to the 2–dimensional vector in reciprocal space. For $n = 31$ ($E_{trans} \approx 205$ cm^{-1}, the variation is only about 5 cm^{-1} and for all lower lying levels, it is neglectably small. If the sample temperature is low, only the first translational levels are Boltzmann populated and hopping can be excluded. If the temperature rises, higher levels are populated and the relative potential barrier is lower and its width smaller. Hopping may take place, but with the used model potential it appears unlikely. This conclusion is particular for the studied system. For example, the physisorbed systems can have high hoping probability even if the sample temperature is low.

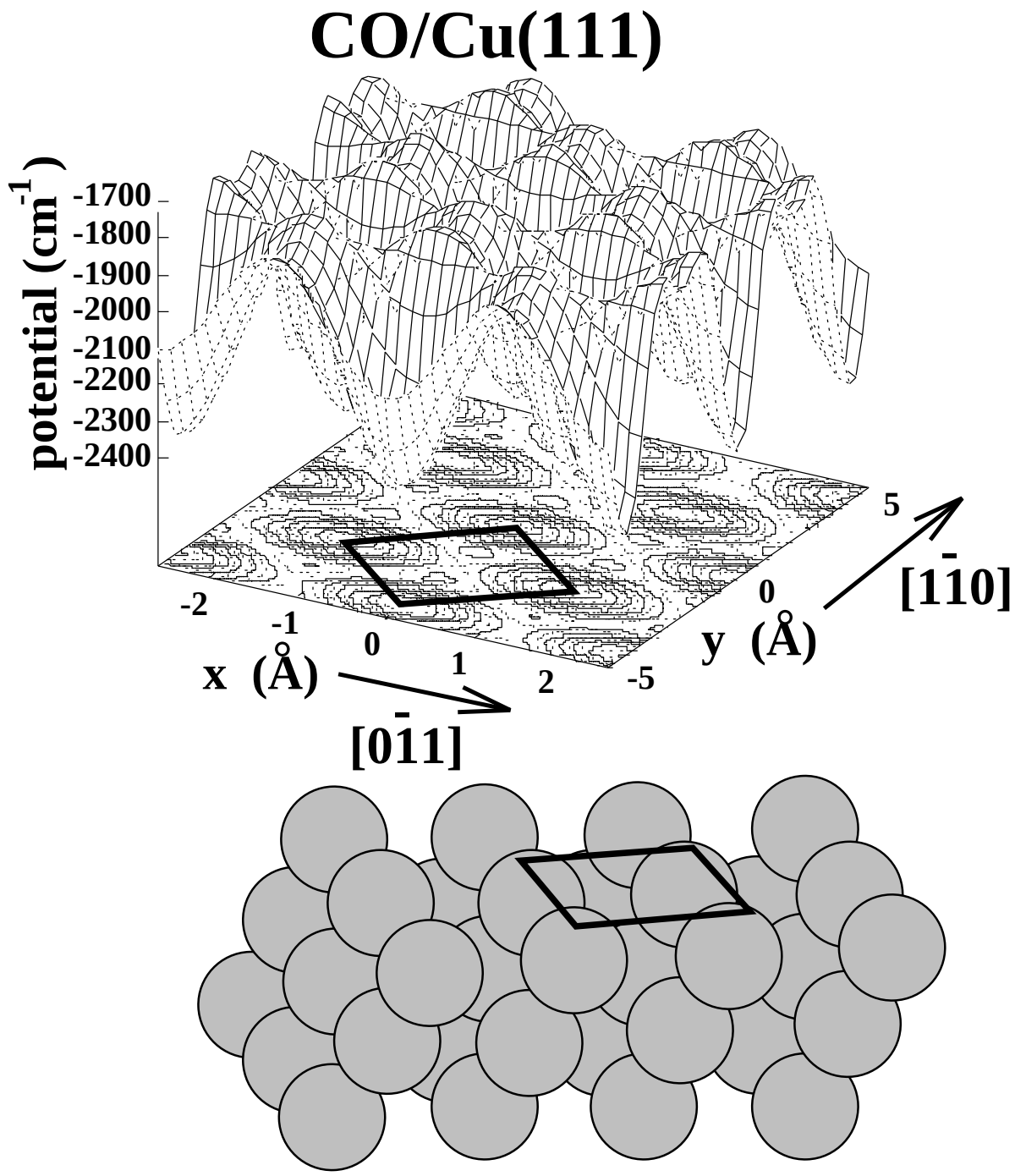

Figure 3.6: *Potential for hindered translation motion of the CO adsorbate parallel to the (111) surface of the fcc copper crystal in cm^{-1}. The molecule is kept in upright position to the surface with R=1.167 Å. The x axis is defined by [01$\bar{1}$] direction one the surface and the y axis by [1$\bar{1}$1]. The potential in xy is varies by about 500 cm^{-1}.*

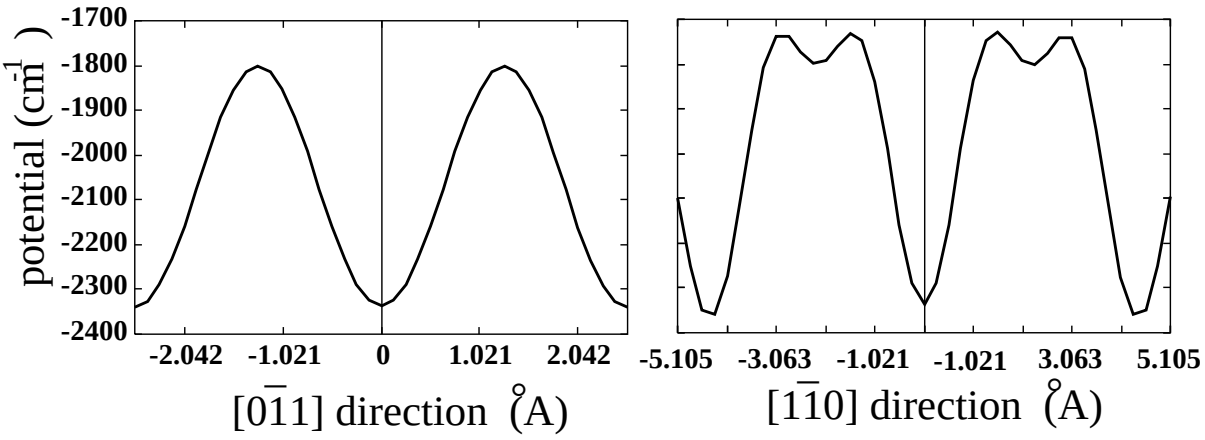

Figure 3.7: *Cuts for the hindered translation potential in x and y direction.*

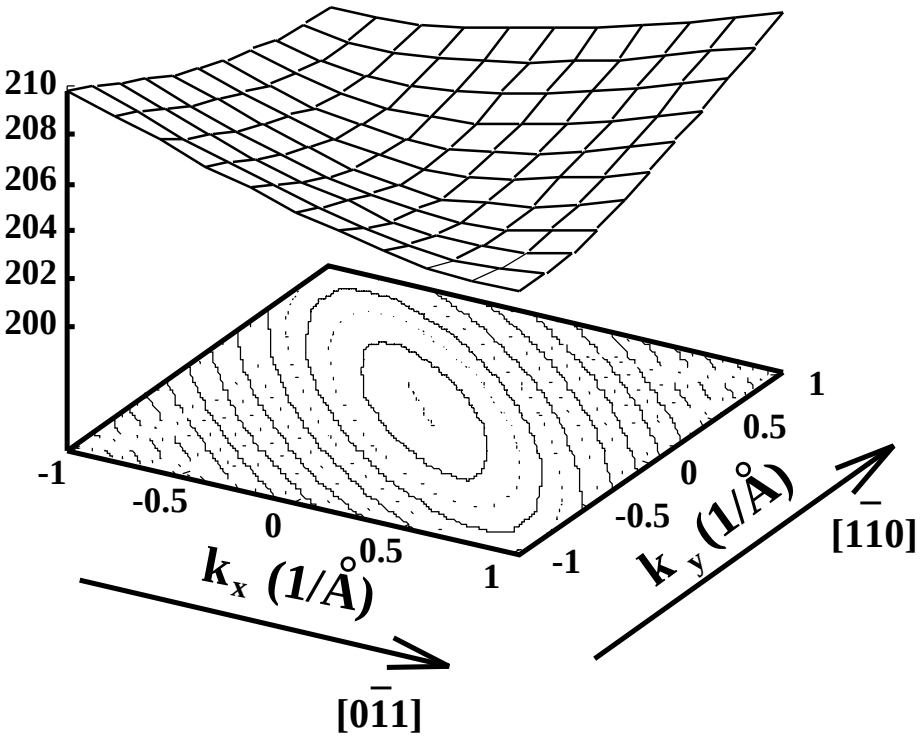

Figure 3.8: *Band structure for hindered translation of rigid CO moving in perpendicular position for n=31 in cm^{-1}. The dispersion of the adsorbate motion is small ($\approx$ 5 cm^{-1}).*

3.2 CO rotational, translational and vibrational distributions

In this section, I present the first results for the translational, vibrational and rotational distributions of neutral CO photodesorbed from Cu(111) surface. I used the general formula (Eq.2.4) for photodesorption with three approximations. First no photon transition moment is calculated. It appears only as a global factor and to a good approximation it does not modify the hindered rotation and the z–stretch motion and associated desorption probabilities. Secondly, the lifetime of the excited electronic state is assumed to be short as compared to the characteristic time of hindered rotation, vibration and z–stretch and the non adiabatic corrections do not influence these motions. In other words, the excited intermediate state does not modify these motions and it plays a role only in the redistribution of the energy between the electronic and nuclear motion. Thirdly, after deexcitation the nuclear motion distributions are not changed during the escape trajectory of the desorbed molecule. With these assumptions, the rotational, vibrational and translational distribution is proportional to the Franck–Condon overlap between initial state and final state nuclear wave functions. The initial state wave functions describe the coupled nuclear motions of the adsorbed molecule, while the final state wave functions are composed by those of gas phase: free rotation, internal vibration and free translation in space.

Figure 3.9 shows the rotational distribution of the desorbed hindered rotor, freezing all motions, but rotation. This kind of plot was already calculated by J.W. Gadzuk *et al.* [151] using the simple model for hindered rotation, restricting the motion inside a cone (see section 1). Here the molecule–surface interaction corresponds to a realistic fitted potential described in the preceding section and the hindered rotation wave function is obtained by solving the Schrödinger equation for hindered rotor.

If during adsorption, the molecule is in its fundamental state $n^{"}$=0,$M^{"}$=0 (Figure 3.9 (a)), the rotational distribution is governed by one maximum at E_{rot}=11.9 cm^{-1}, that corresponds to a rotational quantum number of $J^{"}$=5. For the degenerate rotational levels $n^{"}$=1,$M^{"}$=$\pm$1 (Figure 3.9 (b)) the shape is likely the same, but the maximum is shifted to E_{rot}=139.0 cm^{-1} ($J^{"}$=8). For CO photodesorbed from the $n^{"}$=1,$M^{"}$=0 and the $n^{"}$=2,$M^{"}$=$\pm$1 hindered rotational levels (Figure 3.9 (c) and (d)), two maxima appear in the rotational distributions, again shifted with respect to each other. Experimentally, one should see a mixture of these distributions due to the thermal Boltzmann population of the initial states. The rotational energy levels in gas phase are degenerated with respect to M, but if the desorption analysis is made using REMPI techniques then orientation and alignment of the photodesorbed fragment due to the surface can be measured experimentally and is already available theoretically.

A similar plot of the vibrational and translational (z direction) distributions of the fragments can also be calculated. In this case all the other nuclear motions are frozen. For upright oriented CO at on–top site, one obtains the graphs, plotted in Figure3.10.

In this figure the real velocity v_{speed} of the fragment is obtained as a sum of velocities v_0 and Δv. v_0 is related to the energy difference between the incoming photon and the sum of electron energy taken by the electron when returning in the solid and the nuclear energy needed to overcome the desorption threshold. This difference must fulfil the energy conservation. The contribution to Δv comes from the momentum of the particle in the initial state. More precisely the translational motion is determined by Fourier transformation of the initial state, which is the overlap between initial and final wave function of exponential type.

If one compares the different translational distribution depending on the internal vibrational quantum

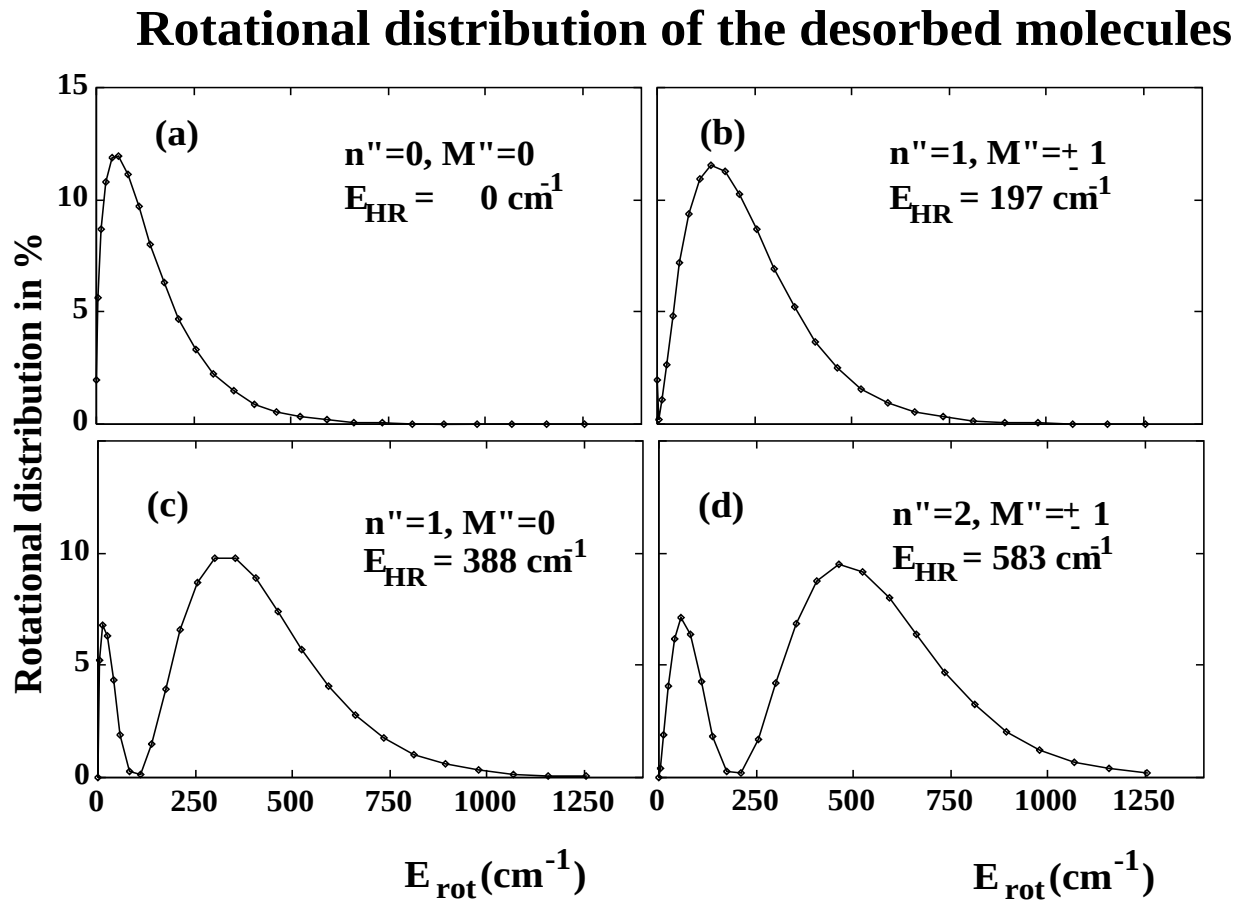

Figure 3.9: *Rotational distribution of CO desorbed from Cu(111) by calculation of the Franck–Condon overlap between the hindered rotation and free rotation wave functions. CO adsorbed on–top at $z = 2.41$ and $R = 1.167$ Å.*

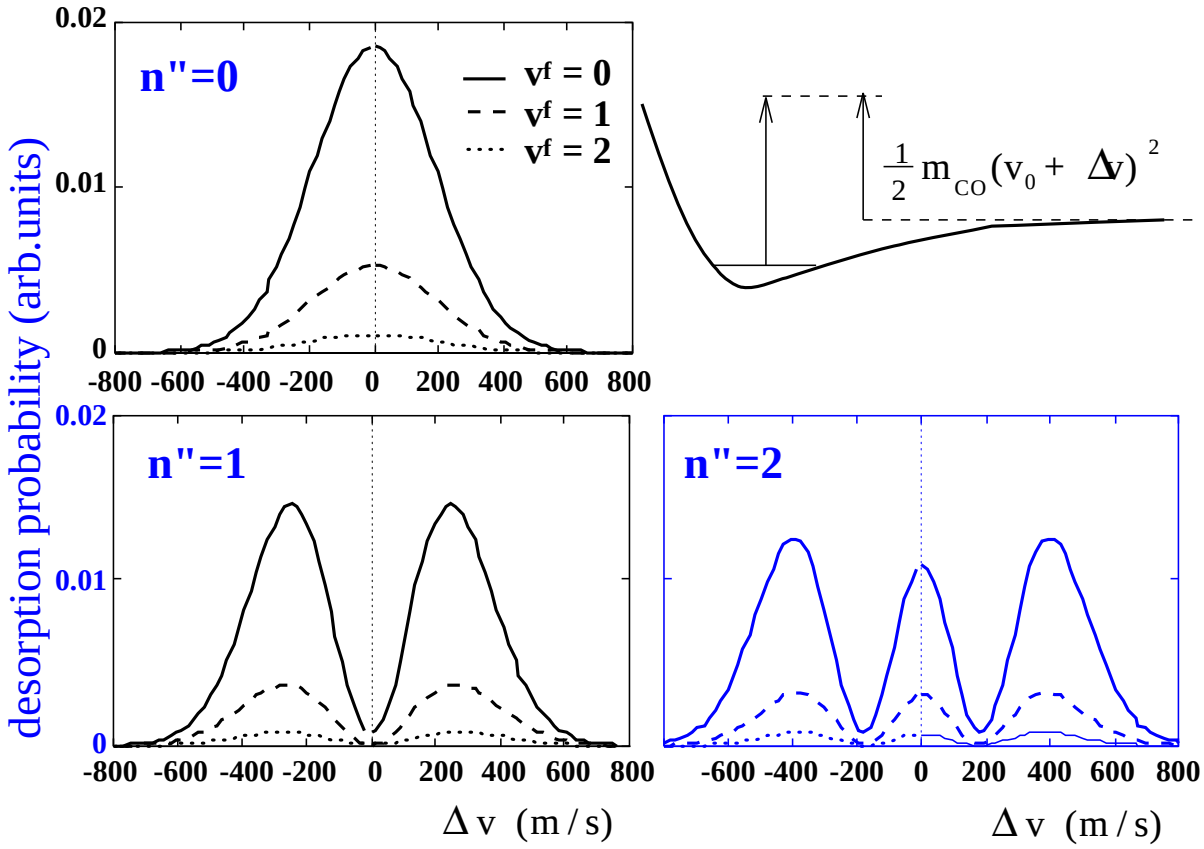

Figure 3.10: *Translational velocity distributions of CO desorbed from Cu(111) perpendicular to the surface. The molecule is considered to be upright at on top position. The initial adsorbed states are n=0,1,2 and the final vibrational states of the desorbed molecule are* v^f *=0,1,2. The particles have a velocity* $v_{speed} = v_0 + \Delta v$ *in* z *direction.* v_0 *is a velocity dependent on the energy of the incoming radiation, vibrational and rotational energies of CO and the electron energy losses due to the surface.*

number of the final state v_f for a given initial state n=0 (Figure3.10), one observes that the preferential vibration channel is v_f=0. But the other channels weakly contribute also. One finds that the desorption probability is around 78% for v_f=0, 21% for v_f=1 and 1% for v_f=2. This significant population in the first excited vibrational level is mainly due to the difference in potential curves of adsorbed and gas phase CO molecule. It can easily be visualised by the difference in the corresponding equilibrium distance: for adsorbed CO R is about 1.167 Å, whereas in gas phase this distance is 1.128 Å. The distributions from other initial states show all characteristics of excited initial levels with one (n=1) and two (n=2) nodes. Again one observes a nonzero vibrational excitation in the final states. Experimentally one has a thermal population of initial levels and one observes a superposition of the distributions shown in Figure3.10 weighted by Boltzmann factors.

Assuming a velocity of v_0=434 m/s and a spread similar to the one given in Figure 3.10 the time of flight spectrum for the initial state n=0 using a probe laser parallel to the surface located at 1.5 mm is displayed in Figure 3.11. This behaviour is common for many systems and can be found experimentally for example in the case of CO/NiO system [32] (see Figure 1.3). This distribution is related to the uncertainty principle.

A further step consist in considering simultaneously the coupled hindered rotation and molecule–surface stretch motions and study the resulting rotational and translational fragments distributions. They are displayed in Figure 3.12 for the initial states $n = 0, M = 0$, $n = 0, M = -1$ and $n = 1, M = 0$ in a representation similar to one dimensional Figure 3.10. For the transition M=0 $\leftarrow$ n=0,M= 0 one observes a peak with a maximum at v_0=0 m/s and E_{rot}= 11.6 cm^{-1} (J=3). For a transition from the next higher initial state (n=1,M=1) to the (J,M=-1) continuum the distribution becomes broader and the maximum is shifted to E_{rot}= 81.1 cm^{-1} (J=6). The last plot of the M=0 $\leftarrow$ n=1,M= 0 transition reflects the characteristics of the initial state level, i.e. two peaks appear at v_0=$\pm$ 160.3 m/s and E_{rot}= 23.2 cm^{-1}. As already mentioned, the initial nuclear motion levels are thermally populated and one has to respect this for theoretical distribution explaining theoretical results.

The plots of the Figure 3.12 can be compared with the Landman–Gadzuk type plots displayed on Figure 3.9. One realizes that the most probable rotational quantum number is different by at least two quantum numbers. Moreover in the case of the transition M=0 $\leftarrow$ n=1,M= 0 depending of the fragment velocity, one can have neglectable probability for all the rotational levels, a situation which is impossible in the case of the Landman Gadzuk model.

The last plot shows an interesting aspect for a cut corresponding to a given rotational energy (similar to Figure 3.10). After a Boltzmann weighted superposition of the contributing transitions, this M=0 $\leftarrow$ n=1,M= 0 transition will modulate the final results. Assuming some realistic v_0, one can plot a corresponding time–of–flight spectra, like the one in Fig.3.11. Experimentally, a bimodal velocity distribution has been observed for NO/Pt by Burgess *et al.*. The question is now, if this distribution comes from a fast resonant superposed by a slow thermal (phonon) desorption channel as the authors claim or does it comes from the Boltzmann distribution of the initial states ? The answer to this question can not be given in this thesis: it imposes a knowledge of v_0 and consequently a detailed knowledge of the electronic and nuclear processes leading to desorption.

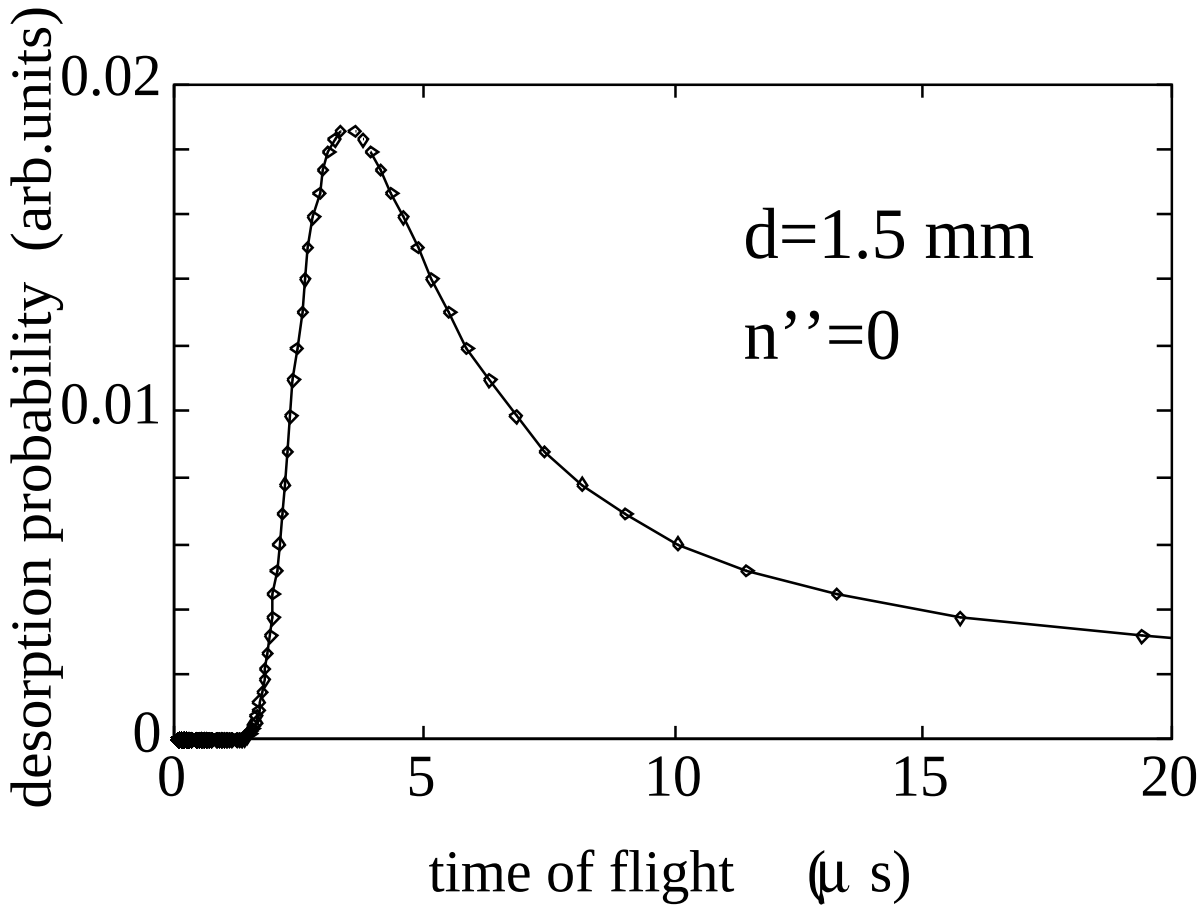

Figure 3.11: *Time of flight spectrum of CO desorbed from Cu(111) in μs. The distance surface–probe laser is d=1.5 mm. Before desorption The CO molecules are assumed to be adsorbed in their ground vibrational state (n''=0). The hindered rotation and translation, but not the CO–surface and internal vibration are frozen (upright on–top adsorption site). $E_{kin}^{max} = \frac{1}{2m_{CO}} \left(E_{kin}^{max}\right)^2$= 220 cm^{-1}.*

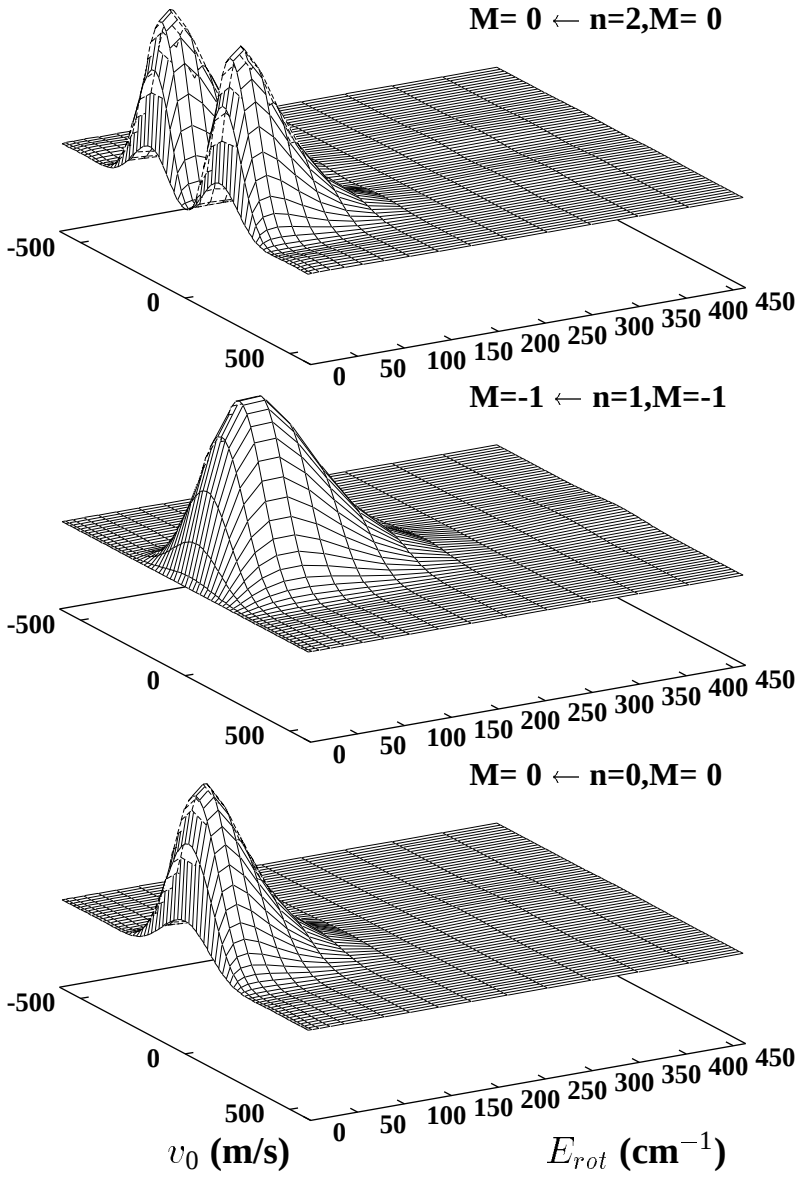

Figure 3.12: *Rotational and translation distribution of CO desorbed from Cu(111) in arb.units. The particles have a velocity* $v_{speed} = v_0 + \Delta v$ *in* z *direction. Their rotational energy is* $E_{rot} = B_{CO} * J(J+1)$ *with* B_{CO}*=1.93 cm*$^{-1}$.

Chapter 4

Photodesorption: Conclusions and outlook

In this part of the thesis I presented a model for the non-thermal desorption of molecular adsorbates. The previous chapter involved a detailed discussion of coupling between the nuclear motions of the adsorbate–substrate system neglecting the surface and bulk nuclear degrees of freedom. This last approximation is not essential for the non-thermal desorption. I have postponed the explicit calculation of the electronic quantities and consider them as global constant factor. The present non-thermal photodesorption model includes two steps. First the photon excites by one or multi-photon process the adsorbate–surface system to an upper electronic state. The photon energy corresponds to a state of the negative ion resonance of the molecular adsorbate (CO or NO). Secondly, this state decays due to non-adiabatic interactions into a final state corresponding to an excited state of the solid and the ground state of the desorbed molecule (see Figure 2.2). The non-adiabatic interaction allows an energy flow between the electronic and nuclear motions and gives enough energy to the nuclear desorption mode to allow desorption. One observes a rotational, translational and vibrational excitation of the desorbed fragments.

The model, can include coupled motion of all nuclear degrees of freedom of the adsorbate like hindered rotation, translation and internal vibration and the molecule–surface stretch. Using a model potential for weakly chemisorbed system CO/Cu(111), published in the literature, I studied the desorption of CO molecules from on–top adsorption sites. Briefly, the present model is based on a basis functions expansion of the nuclear potential. The nuclear basis set of the wave functions is formed from gas phase rotational wave functions for hindered rotation, Bloch functions for hindered translation, harmonic oscillator functions for internal vibration (dissociated neglected) and discrete and numerical functions for one–dimensional molecule–surface stretch mode. Using the Schrödinger equation, the resulting set of linear equations for the desorption mode is solved numerically. For CO/Cu(111) the hindered rotation and desorption mode (molecule–surface stretch) are strongly coupled, but are not coupled to the C–O vibration and the hindered translation. In the present first application of the model, the translational, vibrational and rotational distributions of the photodesorbed CO molecules were calculated by using simple approximations. First, the excited state is assumed not to change with nuclear desorption mode, i.e. the nuclear desorption coordinate is not explicitly introduced. This approximation seems to be justified if the electronic lifetime of this state is very short compared to characteristic time of the nuclear motions. Secondly, after electronic deexcitation (neutralisation) the molecule desorbs and one map the sudden release of the bond on the free translational function of the desorbed system.

In the future, part of these approximations will be lifted. First we will perform ab–initio calculation to determine the excited negative ion electronic molecule–surface state, the electronic transition moments (taken constant here) and non-adiabatic interactions to allow the coupling between electronic and nuclear motions and the energy flow between the electrons and the nuclear desorption mode. Then the explicit propagation of the time dependent Schrödinger equation for the nuclear desorption mode will be considered allowing the real evolution of the system from repulsive wall to the asymptote.

There are other interesting aspects. Multi-photon effects seems to play an essential role for photodesorption by a femtosecond of CO/Cu(111) system. For the metallic substrates excitons play an important role and they should be included in a future model.

It is also considered to apply the photodesorption model to other systems. CO on metallic oxides like NiO are widely studied in literature and their desorption cross section is two orders of magnitude higher than for metallic surfaces. The NO molecule has a spin–orbit splitted ground state and, although slightly difficult to be treated by ab–initio methods, can probe in a complementary way the molecule–surface interaction. These two molecules are well studied in literature, as they are important for heterogeneous catalysis reactions. But, for a fundamental understanding of photodesorption mechanisms, one has also to consider physisorbed systems. A possible candidate can be CO/Ar which have already been discussed in the present thesis in a different context. Another interesting type of surface of high practical interest are the zeolithes. They have a very high surface–volume ratio and the modelling of photodesorption from such complicated systems is a challenge to theoreticians.

Part V

General conclusion on photofragmentation

General conclusion on photofragmentation

In this work, I presented selected aspects on photofragmention of molecules adsorbed on surfaces and tried to answer the questions risen in the introduction on page 19. First, specific phenomena related to photoionization, mainly hindered rotation and backscattering of photoelectrons were discussed. Hindered rotation is the most important nuclear mode, as it changes the orientation of the intranuclear axis and therefore the photoelectron angular distribution. Secondly, I discussed the influence of coverage (including angular behaviour of the adsorbate) on preferable adsorption sites, adsorbate geometries and dynamics of vibrational modes of the adsorbate. The third and last aspect of this work discusses photodesorption in the non-thermal regime, i.e. in an energy region where resonant energy transfer from electronic and/or nuclear to the desorption modes takes place.

Concerning the photoionization part of this thesis, I presented a theoretical model and new formulae for the photoionization cross section including hindered rotation. The model is based on the dipole transition, Born-Oppenheimer and Franck Condon approximations. In the hindered rotation model I introduced a realistic coordinate system that is defined by the surface normal and not by the molecule internuclear axis as in 'oriented–in–space' model. Therefore four preferential directions are defined including the surface normal, the direction of the adsorbate nuclear axis, the incident angles of the radiation and of the escaping photoelectron. This model was applied to two adsorbate systems, representing one chemisorbed and one physisorbed system: CO/Ni(100) and CO/Ar.

Hindered rotation is a quantum mechanical phenomena and is always present due to its zero–point energy. The associated mean tilt angle can be small for strong chemisorbed and large for physisorbed species, but is always non zero: a strict upright orientation is theoretically excluded. For the chemisorbed system CO/Ni(100) adsorbed at on–top sites in the low coverage limit the influence of the hindered rotation on the cross section is small, but measurable. I showed, that the adsorbate is tilted with respect to the surface normal and precess about it. In literature, a theoretical model developed by Dill and Dehmer [38] and Davenport [37] was used to interpret the experimental spectra. This model is based on the assumption, that the surface only orients the molecules in space. Within this model, 'allowed' and 'forbidden' experimental arrangements can be distinguished, arrangements that imposes a maximum ('allowed') and a vanishing ('forbidden') photoelectron current for excitations from electronic orbitals having a particular symmetry. For the $(4\sigma)^{-1}$ ionization of CO/Ni(100) ($^1\Sigma_0^+$) state in an 'allowed' geometry set–up, I showed that 'oriented–in- space' model can explain the experimental data. But, a temperature dependent broadening was observed by Wesner *et al* [14] in the photoelectron angular distribution of core level excitation of CO/Ni(100). I showed here, that this broadening comes from additional transitions from thermally occupied hindered rotational levels in the ground state of CO.

For the 'forbidden' experimental set–up, the breaking of 'oriented–in–space' selection rules due to hindered rotation plays an important role. In literature, these selection rules were used in the interpretation of the experiment to derive a tilted angle of the adsorbate about the surface normal. But the surface normal is not defined or do not exist in the oriented–in–space' model. Using the present hindered rotation model, I gave a recipe to derive a mean tilt angle of the adsorbate. The corresponding calculation is not much more complicated that the one using the 'oriented–in–space' model and should be used in the interpretation of the experiment.

I also applied the model including hindered rotation for the 4σ shape resonance (hν=36 eV) of the physisorbed system CO/Ar at one–top sites in the low coverage limit. In this case the hindered rotation

changes significantly the photoionization spectrum. I compared my elaborate model to simple models, like one corresponding to the gas phase, a model allowing the precession ('helicopter' motion') but not the libration (the tilt angle is frozen at 90°) and an 'oriented–in–space' model. The difference between the photoelectron angular distribution predicted by the four models is very large and none can replace the model including fully the hindered rotation for CO/Ar surface system.

I discussed the influence of backscattering on photoemission spectra using a model step potential developed in our group by Pavel Budău [13]. This potential causes a partial reflection and consequently destructive and constructive interference effects in the photoelectron angular distributions. For a first application, we chose the 'allowed' experimental arrangement and supposed that the molecule is normal to the surface neglecting hindered rotation. Shape resonances are dominating the cross section of 4σ and (5σ) excitation. For $4\sigma^{-1}$ ionization, the photoelectron emission towards the surface is small and the effect of backscattering is negligible. For the $(5\sigma)^{-1}$ ionization the emission towards the surface is considerable and the backscattering changes significantly the angular photoelectron distribution. I have extended this backscattering model for molecular adsorbates in an inclined orientation about the surface normal. In this case backscattering breaks 'oriented–in space' symmetry selection rules in the comparable way to the hindered rotation.

The second part of this thesis investigates the influence of the coverage on adsorbate–surface system. In the first and third part of the thesis, my models assumed low coverage limit, i.e. one molecule on the surface, situation which is unrealistic for normal experimental conditions where partial pressure of the adsorbate in the chamber is risen to allow adsorption. A theoretical model for the study of high coverage (one full mono-layer) of the adsorbates should include large number of degrees of freedom, rising dramatically with the number of adsorbates. This situation can be handled in the framework of classical trajectories methods. The essential novelty of the present application of classical mechanics trajectories methods is the inclusion of an angular term in the lateral interaction potential between adsorbates and the systematic study of the coverage influence. Specifically, using an algorithm developed by Francois Amar and Pascal Parneix, the influence of coverage for the physisorbed system CO/Ar(100) have been studied [21]. This simulation was performed using CO clusters adsorbed on argon and varying the cluster size from $(CO)_1$ (simulating low coverage) to $(CO)_9$ (simulating one mono-layer high coverage) and determining the adsorption geometries and the classical motion of the adsorbates. To minimise the CO–CO interaction, the CO molecules tend to cluster and the angular motion corresponding to precession is strongly hindered. One speaks about rigidification of the monolayer due to increasing coverage which essentially takes place for precession of the adsorbate about the surface normal. The libration is only slightly influenced by the coverage.

I also presented a quantum mechanical study for a single $(CO)_1$/Ar(100) and a central CO molecule in the $(CO)_7$/Ar(100) cluster. The results of this model verify the rigidification obtained by the classical dynamical study. It manifests itself by an increase of rotational energies and a sharpening of the associated wave functions. But in addition, the quantum mechanical approach shows aspects that can not be obtained by classical dynamical studies. The high zero–point energy implies a high classical rotational energy of 117 K, allowing the classical accessibility of other potential minima then the adsolute one. In fact, four configurations of the central CO in the $(CO)_7$/Ar cluster are predicted, that are nearly degenerated in energy. For some configurations tunnelling phenomena take place, which cause a flip from one molecular orientation to another. The analysis of the wave function density shows that the angular motion is governed by a compromise between the potential minima and tunnelling through potential barriers. These tunnelling phenomena and the presence of nearly degenerated energy levels are not

indicating a free rotation, but nearly equivalent orientations of the molecule on the surface. Moreover the flip from one structure to another is governed by an energy barrier. Consequently, the classical picture should be supplemented by a quantum mechanical approach.

The last part of this thesis discusses aspects of photodesorption in non-thermal regime. Non-thermal photodesorption means, that desorption is induced by a resonant energy transfer from electronic or nuclear motions to the desorption mode (i.e. molecule–surface stretch motion) and not by a simple thermal heating of the surface. If the kinetic energy in the desorption mode is sufficient, the molecule desorbs. For photons of less than 7 eV considered here the electronic excitation can take place followed by its partial transfer to the nuclear degrees of freedom. Several nuclear degrees of freedom can be simultaneously excited including the photodesorption mode. The signature of non thermal regime is usually seen in the high translational and rotational temperature of the desorbed fragments showing that the transfer to all the nuclear modes takes effectively place.

The model I have developed in this thesis takes into consideration several nuclear degrees of freedom of the adsorbate–surface system. It freezes the surface and bulk nuclear degrees of freedom but this approximation is not essential for non thermal desorption. In the photodesorption model, I have postponed the explicit calculation of the needed electronic quantities and considered them as a global constant factor. The present multidimensional (for vibration) non-thermal photodesorption model includes two steps. First, by one or multi-photon process, the adsorbate–surface system is excited to an upper electronic state. The photon energy corresponds to a state of a negative ion resonance of the molecular adsorbate (CO or NO). Secondly, this state decays due to non-adiabatic interactions into a final state corresponding to an excited state of the solid and the ground electronic state of the desorbed molecule. The nonadiabatic interaction allows an energy flow between the electronic and nuclear motions that in some cases gives enough energy to the nuclear desorption mode (molecule–surface stretch) to generate fragmentation. It allows also a simultaneous excitation of other nuclear modes and can explain the observed rotational and vibrational excitations of the desorbed fragments and their high kinetic energy.

This model was applied to the photodesorption of weakly chemisorbed system CO/Cu(111). Using a multidimensional potential for this system based on a model atom–atom potential published in the literature [150], I studied the desorption of CO molecules from on–top adsorption sites. Briefly, the different nuclear degrees of freedom are introduced through basis function expansion and numerical solution of the Schödinger equation. For hindered rotation the basis set is formed from gas phase rotational wave functions, Bloch functions are used for hindered translation and harmonic oscillator functions are introduce for internal vibration (dissociated neglected). One integrates over all the nuclear degrees of freedom except nuclear photodesorption mode. Then one obtains a system of close coupled equations that are solved numerically for the molecule–surface stretch mode. For CO/Cu(111) the hindered rotation and desorption mode (molecule surface stretch) are strongly coupled, but are not coupled to the C–O vibration and the hindered translation. In the first application of the model presented here, the translational, rotational and vibrational distributions of the photodesorbed CO molecules were calculated using simple approximations. First, the excited state is assumed not to change with nuclear desorption mode, i.e. the nuclear desorption coordinate is not explicitly introduced. This approximation seems to be justified if the electronic lifetime of this state is very short compared to characteristic time of the nuclear motions. Secondly, after electronic deexcitation (neutralisation) the molecule desorbs and one map the sudden release of the bond on the free translational function of the desorbed system.

The results of this model confirm that the hindered rotation and the desorption modes (molecule–

surface stretch) are strongly coupled whereas the C–O internal vibration and hindered translation are weakly coupled. The resulting rotational, internal vibrational and translational distributions of desorbed molecules show all the characteristics of the experimental results. For a model where the vibrations are uncoupled, the non-thermal distribution of the fragments is obtained from Franck-Condon overlaps for rotational and Fourier transform overlap for the translational motions. Although I used exact hindered rotor wave functions, the obtained distributions are in agreement with those of the Landman–Gadzuk [151] model. For a more realistic model including coupling between the rotation and translation, I obtained a bimodal distribution of fragment velocities assuming non-thermal photodesorption. This bimodal distribution was seen experimentally and interpreted as corresponding to thermal and non-thermal contributions to the photodesorption yield. With the present model, unfortunately one can not calculate the distribution corresponding to thermal mechanism. Therefore the origin of the bimodal distribution can be due to two non-thermal components, one thermal and one non-thermal component or to a mixed origin.

Outlook

The present thesis has much of an exploratory research. I have touched several problems related to photofragmentation of molecular adsorbates and considered photoionization and photodesorption in an effort to have a complete panorama of the fragmentation phenomena related to the photon. I have answered the questions risen in the introduction on page 19 but there are many points that were left to future developments. Below I will mention few of them.

For photoionization the hindered rotation and backscattering must be included at an equal footing in a generalized model. This is straightforward, and in the near future generalize our method and apply it to the weakly chemisorbed system CO/Cu(111). This method will also allow the study of adsorbates in experimental arrangements, where both hindered rotation and backscattering are important thus testing the validity of our generalized model. In the applications presented in this thesis, I used the electronic transition moments of CO in gas phase, a reasonable approximation for ionization of physisorbed CO and for $(4\sigma)^1$ ionization of chemisorbed CO, but not for the $(5\sigma)^1$ ionization of chemisorbed CO. Recently, the photoemission of linear Ni–CO and Cu– CO clusters was calculated in our group [46, 99]. Our generalized hindered rotational model including backscattering can be applied for these linear clusters that are closer to the actual chemisorbed species.

The influence of coverage must be studied for the photoionization. Taking the effective adsorbate–surface potential for the central CO obtained from the coverage studies performed in the second part of this thesis, the coverage dependent photoionization cross section can be calculated. Unfortunately, for physisorbed CO/Ar system this potential is not axial symmetric and, as shown in our studies including coverage, the molecule does not undergo free precession around the surface normal. Our expression for the photoionization cross section supposed axial symmetry with free precession. Before performing these studies the photoionization cross section should be generalized.

In this work molecules adsorbed on on-top sites have been considered. For example for bridge sites the local symmetry is of low order (e.g.twofold) and, as in the case of the preceding paragraph, the hindered rotation wave function and cross section expressions have to be generalized for the corresponding symmetry. One should also consider a modified model for the electronic motion, that corresponds to the twofold local symmetry. Work for a generalisation of the electronic wave functions including any site

symmetries is in progress in our group and will be soon published [152,153]. Then a manifold of systems and sites can be studied. The first applications are the study of the photoemission of CO/Cu(111) and CO/Ni(100), including low and high coverages.

The coverage dependent studies started in this thesis open a whole new area of possible extensions and applications. I have mentioned above its relation with photoionization. For photodesorption, the CO/Ar system can immediately be studied but it does not have practical interest and present experimental difficulties. The CO/Cu(111) system is a good candidate as the corresponding classical trajectories including coverage will be a complement of the quantum mechanical studies I have performed in this thesis. Work in this direction is in progress.

Photodesorption model I presented in this thesis should be completed and extended. For one photon excitation, the most urgent task is the explicit calculation of electronic quantities as transition moments and non–adiabatic interactions. These non-adiabatic interactions play an essential role in the redistribution of the available energy between the electronic and nuclear degrees of freedom. Then one should consider the evolution of the system in the excited and ground states by a time–dependent approach. It is only at this price that the present multidimensional model with respect to the nuclear coordinates will become realistic for CO/Cu(111) photodesorption and meaningful comparison with the experiment would be possible. For multi-photon excitation, mentioned as a possible mechanism for CO/Cu(111) photodesorption [123], one should introduce simultaneously strong field couplings corresponding to absorption of several photons and non-adiabatic interactions. Work in this direction is in progress in our group and we will apply the resulting model to the multiphoton photodesorption of CO/Cu(111).

The photodesorption model discussed above, can be applied to other systems and, because of high photodesorption rate, the most interesting are adsorbates on metallic oxides [30–36]. In the near future, we will try to extend our model to these more complicated systems. The major difficulty is the availability of reasonably good potential energy surfaces.

Among the different experimental methods, I want to cite the techniques of electron–adsorbate collision and Electron Stimulated Desorption (ESD). For the associated processes the problematic is the same, but the time scales and selection rules are different. My studies about the nuclear motions and backscattering together with the influence of adsorbates coverage can be adapted to study these processes. With these techniques the physical reality can be highlighted in a different and complementary way.

The study of photodesorption of moleuclar adsorbates on surfaces is fascinating but difficult. The adsorbate and the surface have their own properties and the adsorbate–surface system is not just a sum of them. As the number of degrees of freedom is high and the evolution path of the system can be very different from system to system, developing models to interpret the experiments is hard but exciting. This explains why the field is a challenge and the collaboration between experimentalists and theoreticians essential.

Conclusion générale sur la photofragmentation

Dans ce travail, j'ai présenté des aspects de la photofragmentation des molécules adsorbées sur des surfaces solides en essayant de répondre aux questions posées dans l'introduction (page 19). D'abord, j'ai discuté des phénomènes spécifiques associés à la photoionisation, essentiellement la rotation empêchée et la rétrodiffusion des électrons. La rotation empêchée est le mouvement nucléaire le plus important parcequ'il change l'orientation de l'axe intranucléaire et par conséquent la distribution angulaire des électrons éjectés. Ensuite, j'ai discuté l'influence de la couverture (y compris le mouvement angulaire de l'adsorbat moléculaire) sur les sites d'adsorption, sur la géométrie et la dynamique des mouvements de vibration de l'adsorbat. Finalement, la dernière partie de ce travail discute la photodésorption en régime non–thermique, c'est–à–dire dans une région d'énergie où un transfert résonant entre les modes électroniques et/ou nucléaires vers le mode de désorption se produit.

Pour la photoionisation, j'ai développé une nouvelle formulation de la section efficace de collision incluant la rotation empêchée. Le modèle associé est basé sur les approximations de transition dipolaire, Born–Oppenheimer et Franck–Condon. Dans le modèle de la rotation empêchée, j'ai introduit un système de cordonnées du laboratoire réaliste défini par la normale à la surface et non plus par l'axe internucléaire comme dans le modèle de la molécule orientée ('oriented- in–space'). Par conséquent quatre directions préférentielles au lieu de trois sont définies: la normale à la surface, l'axe nucléaire de la molécule adsorbée, des directions de la radiation électromagnétique incidente et de l'éjection de l'électron. Ce modèle a été utilisé pour l'étude de deux systèmes CO/Ni(100) et CO/Ar représentant deux cas limites, le premier celui de la chimisorption le second celui de la physisorption.

La rotation empêchée est un phénomène quantique qui, dû à l'énergie du point nul, est toujours présent. L'angle moyen d'inclinaison est habituellement faible pour les systèmes chimisorbés et grand pour les systèmes physisorbés. Mais, parce que l'orientation strictement normale à la surface est théoriquement exclue, cet angle ne peut jamais être zéro. Pour CO adsorbé sur un site linéaire d'une surface de Ni(100) dans la limite d'une faible couverture, l'influence de la rotation empêchée est faible mais mesurable. J'ai montré que l'adsorbat est incliné et subit une précession autour de la normale à la surface. Un modèle théorique développé dans la littérature par Dill et Dehmer [38] et Davenport [37] a été utilisé pour interpréter les résultats expérimentaux de photoionisation. Ce modèle est basé sur l'hypothèse qu'une surface qui ne fait qu'orienter la molécule dans l'espace lui interdisant de subir des rotations. Dans le cadre de ce modèle, on distingue entre des configurations expérimentales 'permises' et 'interdites' correspondant à un courant de photoélectrons maximal ou évanescent pour des excitations d'électrons provenant des orbitales d'une symétrie particulière. Pour l'ionisation d'un électron $(4\sigma)^{-1}$ de l'état $(^1\Sigma_0^+)$ du système CO/Ni(100) dans un arrangement expérimental permis', j'ai montré que le modèle de la molécule orientée peut expliquer les résultats expérimentaux. Mais un élargissement des structures dû à la température a été observé par Wesner et collaborateurs [14] dans la distribution angulaire des photoélectrons pour l'excitation d'une couche interne de CO/Ni(100). Dans la première partie de ma thèse, j'ai montré que cet élargissement provient des états rotationnels peuplés dans l'état électronique fondamental de la molécule CO.

Dans un arrangement expérimental 'interdit', la rotation empêchée brise les règles de sélection du modèle de la molécule orientée. Ces règles de sélection ont été utilisées dans la littérature pour dériver l'angle d'inclinaison de l'adsorbat par rapport à la normale à la surface, qui dans ce cadre n'est pas définie ou plus exactement n'existe pas. Utilisant le modèle de la rotation empêchée développé dans cette thèse, j'ai obtenu une règle simple qui donne l'angle moyen d'orientation de l'adsorbat par rapport à la normale à

la surface. Le calcul correspondant n'est pas plus complexe que celui du modèle de la molécule orientée et peut être utilisé pour l'interprétation des expériences.

Le calcul du spectre de photoionisation de la résonance de forme 4σ ($h\nu$=36 eV) de CO adsorbé sur les sites linéaires d'une surface d'argon à la limite d'une faible couverture montre une influence significative de la rotation empêchée. J'ai comparé le modèle de la rotation empêchée à d'autres plus simples par exemple celui de la phase gazeuse, celui permettant la précession mais pas la libration (modèle du 'mouvement hélicoptère', l'angle d'inclinaison est figé à 90°) et celui de la molécule orientée dans l'espace. Les différences entre ces modèles sont très significatives et aucun ne peut valablement remplacer le modèle introduisant d'une manière complète la rotation empêchée.

Dans ce travail, j'ai aussi discuté l'influence de la rétrodiffusion dans les spectres de photoémission. Pour la rétrodiffusion, j'ai utilisé un modèle basé sur un potentiel marche développé dans notre groupe par Pavel Budău [13]. L'électron est partiellement refléchi par ce potentiel engendrant des effets d'interférence constructive et destructive dans la distribution angulaire des photoélectrons. La première application du modèle concerne l'arrangement expérimental 'permis' et suppose que la molécule normale à la surface ne subit pas de rotation empêchée. Dans le domaine d'énergie étudié les résonances de forme 4σ and (5σ) dominent le spectre de photoionisation. Pour l'ionisation $4\sigma^{-1}$, l'émission du photoélectron vers la surface est faible et la rétrodiffusion négligeable. Pour l'ionisation $(5\sigma)^{-1}$ l'émission vers la surface est considérable et la rétrodiffusion change d'une manière significative la distribution angulaire de photoélectrons. J'ai étendu ce modèle pour le cas des molécules ayant une position inclinée sur la surface où les règles de sélection de la molécule orientée ne sont plus valables. C'est une situation analogue à la rotation empêchée évoquée plus haut.

Dans la seconde partie de ma thèse, j'ai étudié l'influence de la couverture sur le système adsorbat–surface. Notons que dans les autres parties de ma thèse les modèles développés sont valables à la limite d'une couverture faible, c'est–à–dire pour une molécule unique sur la surface, qui est une situation irréaliste dans les conditions normales de l'expérience ou le taux de couverture est contrôlé par la pression dans l'enceinte expérimentale. L'introduction de la couverture dans un modèle de photoionisation implique la prise en considération d'un très grand nombre de dégrés de liberté, nombre qui augmente considérablement pour une monocouche complète (couverture dense). Pour relever ce défi, nous avons utilisé les méthodes de la dynamique classique bien adaptées pour prendre en considération un nombre important de degrés de liberté. L'originalité du modèle réside dans l'introduction d'un terme d'interaction angulaire CO–CO et l'étude systématique de l'influence de la couverture. L'influence de la couverture pour le système physisorbé CO/Ar(100) a été étudiée [21] utilisant un algorithme développé par Francois Amar et Pacal Parneix. Les agrégats adsorbés sur une surface d'argon composée de trois couches d'atomes avaient de dimensions variant de $(CO)_1$ (simulant la couverture faible) à $(CO)_9$ (simulant une monocouche complète-couverture dense). Nous avons étudié les mouvements des noyaux et déterminé les géometries d'équilibre et constaté que, pour minimiser l'interaction CO–CO, les molécules de CO forment des agrégats. De plus le mouvement de précession autour de la normale à la surface est fortement empêché et on parle d'une rigidification de la monocouche due à la couverture. La libration est faiblement influencée par la couverture.

J'ai aussi effectué une étude basée sur la mécanique quantique pour une seule molécule de $(CO)_1$/Ar(100) et une molécule de CO centrale dans un agrégat $(CO)_7$/Ar(100). Ce modèle confirme la rigidification obtenue par l'étude classique. Cette rigidification qui se manifeste par une augmentation des énergies rotationnelles et une localisation de la fonction d'onde associée. L'approche quantique montre des

aspects qui ne peuvent pas être obtenus par des modèles de dynamique classique. Si l'on analyse l'énergie de point–zéro en termes de température rotationnelle classique, on obtient 117 K bien au dessus de la température de l'étude classique de 10.5 K. Ce fait permet au système traité quantiquement une accessibilité à d'autres minima que le minimum absolu. Cette accessibilité fait qu'on obtient quatre configurations géométriques qui sont presque dégénérés en énergie. Pour certaines configurations géométriques des phénomènes tunnel peuvent se produire faisant basculer la molécule centrale d'une configuration à une autre. L'analyse de la densité de la fonction d'onde montre que le mouvement angulaire est dominé par un compromis entre les minima du potentiel et les effets tunnel à travers les barrières de potentiel. Les phénomènes tunnel et la présence des niveaux presque dégénérés en énergie ne correspondent pas à une rotation libre mais à des orientations équivalentes des molécules sur la surface. Pour une description et compréhension des problèmes de couverture, le traitement classique doit être combiné avec un traitement quantique.

La dernière partie de ma thèse discute des aspects de la photodésorption en régime non thermique, induite non par la simple agitation thermique mais par un transfert résonant d'énergie des mouvements électroniques et nucléaires vers le mode de désorption (le mouvement de vibration molécule–surface). La molécule désorbe si, par transfert résonant, l'énergie accumulée dans le mode de désorption est suffisante. J'ai considéré des photons de moins de 7 eV et le mécanisme passe par une excitation électronique suivie d'un transfert partiel d'énergie dans le mode de photodésorption. Mais, avec ce mode, d'autres modes vibrationnels sont excités et peuvent même servir d'intermédiaire au transfert d'énergie vers la photodésorption. Le régime nonthermique est habituellement identifié par des énergies élevées de translation et rotation des fragments désorbés montrant que le transfert d'énergie se fait vers tous les modes de vibration nucléaires.

Le modèle que j'ai développé dans cette thèse prend en considération plusieurs degrés de liberté du système adsorbat–surface. Il fige les mouvements vibrationnels de la surface et du solide (phonons), mais cette approximation n'est pas essentielle pour la photodésorption en régime non–thermique. Dans le modèle de photodésorption, j'ai simplifié le calcul des quantités électroniques les considérant comme un facteur global constant. Le modèle multidimensionnel par rapport à la vibration de la photodésorption en régime non–thermique implique deux étapes. D'abord, par un mécanisme à un ou plusieurs photons, le système adsorbat–surface est porté dans un état électronique excité. L'énergie du photon correspond à un état de résonance de l'ion négatif de l'adsorbat moléculaire (CO ou NO). Ensuite cet état se désexcite par interaction non–adiabatique vers l'état final correspondant à un état excité du solide et l'état électronique fondamental de la molécule désorbée. L'interaction non–adiabatique permet le flux d'énergie entre les mouvements électroniques et nucléaires qui dans certains cas transfère suffisamment d'énergie au mode de désorption (vibration molécule–surface) pour engendrer la fragmentation. Il permet aussi l'excitation simultanée des autres modes nucléaires qui peut expliquer l'excitation de la rotation et vibration des fragments désorbés ainsi que leur énergie cinétique élevée.

Le modèle a été utilisé dans l'étude de la photodésorption du système faiblement chimisorbé CO/Cu(111). J'ai utilisé un potentiel multidimensionnel basé sur un potentiel modèle atome–atome publié dans la littérature [150] en considérant une molécule CO adsorbée sur des sites linéaires. Brièvement, les différents dégrés de liberté nucléaires sont introduits à partir d'un développement sur des fonctions de base appropriées suivi de la résolution numérique de l'équation de Schrödinger. Pour la rotation empêchée, j'utilise une base de fonctions de rotations de la phase gazeuse, pour la translation empêchée des fonctions de Bloch et pour la vibration interne des fonctions de l'oscillateur harmonique (dissociation négligée). D'abord, on intègre sur tous les dégrés de liberté sauf le mode de désorption. Ensuite on obtient

un système d'équations couplées qui sont résolues numériquement pour le mode de photodésorption. Dans le cas de CO/Cu(111) la rotation empêchée et le mode de photodésorption sont fortement couplées mais découplées de la vibration interne C-O et la translation empêchée. Dans la première utilisation de ce modèle présenté dans ce travail, les distributions transitionnelles, rotationnelles et vibrationelles des molécules CO photodésorbées ont été calculées utilisant des approximations simples. D'abord, l'état excité est supposé ne pas changer avec le mode de photodésorption, c'est–à–dire que la coordonnée de photodésorption n'est pas explicitement introduite. Cette approximation semble justifiée si le temps de vie de l'état électroniquement excité est très court par rapport aux temps caractéristiques de mouvements nucléaires. Ensuite, après la désexcitation électronique par le départ d'un électron dans le solide, la molécule désorbe et on calcule la distribution des fragments due au relâchement soudain de la liaison adsorbat–surface par le calcul du recouvrement entre la fonction de la molécule adsorbée et sa fonction d'onde de translation libre en phase gazeuse.

Les résultats de ce modèle confirment que la rotation empêchée et la désorption (vibration adsorbat–surface) sont fortement couplées entre elles tandis que la vibration interne C–O et la translation empêchée sont faiblement couplées. Les distributions de rotation, vibration interne et translation des fragments desorbés montrent des caractéristiques semblables aux résultats expérimentaux. Pour un modèle où les vibrations sont découplées, les distributions non–thermiques des fragments sont obtenues par un recouvrement de type Franck-Condon pour la rotation et par transformée de Fourier pour le mouvement de translation. Pour la rotation empêchée, même si j'utilise des fonctions de rotation exactes, mes résultats sont proches du modèle de Landmann–Gadzuk [151]. Dans le cas d'un modèle de désorption non–thermique plus réaliste introduisant le couplage entre la rotation empêchée et la translation, j'obtiens une distribution bimodale des vitesses des fragments désorbés. Cette distribution est expérimentalement observée mais elle est attribuée à des contributions thermique et non–thermiques du mécanisme de désorption. Le modèle actuel ne permet pas le calcul de la distribution des fragments dans le cadre d'un mécanisme thermique. Par conséquent l'origine de la distribution bimodale peut être due soit à deux composantes non–thermiques, une composante thermique et une non–thermique, ou encore à une origine mixte.

Perspectives

Cette thèse doit être considérée comme une recherche exploratoire. J'ai abordé plusieurs sujets en relation avec la photofragmentation des adsorbats moléculaires et étudié la photoionisation et la photodésorption pour aborder une grande partie des phénomènes de fragmentation en relation avec l'excitation photonique. J'ai répondu à plusieurs des questions posées dans l'introduction à la page mais il y a beaucoup de points qui feront l'objet d'extensions et d'études futures. Dans ces perspectives, je vais mentionner une partie de ces développements possibles.

Pour la photoionisation la rotation empêchée et la rétrodiffusion doivent être inclues simultanément dans un modèle généralisé. Dans un futur proche le modèle sera étendu testé dans l'étude des adsorbats pour des arrangements expérimentaux où la rotation empêchée et la rétrodiffusion devraient jouer un rôle important. Dans les exemples considères dans cette thèse, j'ai utilisé les moments de transition électroniques de la molécule CO de la phase gazeuse, une approximation raisonnable pour l'ionisation $(4\sigma)^1$ du CO physisorbé mais pas pour l'ionisation et pour $(5\sigma)^1$ du CO chimisorbé. Récemment, la photoémission des agrégats linéaires modèles tels Ni–CO ou Cu–CO a été calculée dans notre groupe [46, 99]. Le modèle généralisé discuté ici peut être utilisé pour l'étude de ces agrégats linéaires représentant

mieux les espèces chimisorbées.

L'influence de la couverture sur les spectres de photoionisation doit aussi être étudiée. Les résultats de la seconde partie de ma thèse obtenus pour des agrégats de CO sur l'argon de taille différente, permettent d'obtenir un potentiel effectif adsorbat–surface pour le CO central de cet agrégat. Ce potentiel effectif sera utilisé pour le calcul de la section efficace de photoionisation en fonction de la couverture. Malheureusement, pour le système physisorbé CO/Ar, le potentiel effectif mentionné ci-dessus n'a pas une symétrie axiale et, comme nous l'avons démontré dans les travaux tenant compte de la couverture, la molécule n'effectue pas une précession libre autour de la normale à la surface. Notre expression de la section efficace de photoionisation implique une symétrie axiale avec précession libre. Avant d'effectuer ces études notre section efficace doit être généralisée.

Dans cette thèse, j'ai présenté des études sur des molécules adsorbées sur des sites linéaires. Pour les sites pontés par exemple, la symétrie locale est inférieure (e.g. d'ordre deux) et, comme dans le cas du paragraphe précédent, les méthodes calculant les fonctions de rotation et les expressions de la section efficace doivent être généralisées pour prendre en considération la symétrie correspondante. Dans le modèle calculant le mouvement électronique la même généralisation vers la symétrie d'ordre inférieur doit être effectuée. Cette généralisation est en cours dans notre groupe et sera publié prochainement [152, 153]. Avec ces méthodes généralisées, des systèmes adsorbés comme CO/Cu(111), CO/Cu(100) et CO/Ni(100) introduisant aussi l'influence de la couverture pourront être étudié.

Les études en fonction de la couverture commencées dans cette thèse, ouvrent un domaine nouveau d'extensions et d'applications. J'ai mentionné ci–dessus sa relation avec la photoionisation. Pour la photodésorption, le système CO/Ar peut être étudié dès à présent mais n'a pas un grand intérêt pratique et présente des difficultés expérimentales. Le système CO/Cu(111) est un bon candidat parce que les études par trajectoires classiques introduisant la couverture seront un complément indispensable aux calculs de mécanique quantique que j'ai effectué dans cette thèse. Des travaux sont en cours dans cette direction.

Le modèle de photodésorption présenté dans cette thèse doit être complété et amélioré. Pour l'excitation à un photon, il faut calculer explicitement les quantités électroniques comme les moments de transition et les interactions non–adiabatiques. Ces interactions non–adiabatiques jouent un rôle essentiel dans la redistribution d'énergie disponible entre les dégrées de liberté électroniques et nucléaires. Ensuite, il faut considérer l'évolution du système dans les états excité et fondamental utilisant par exemple une méthode dépendante de temps. Ce n'est qu'à ce prix que le modèle multidimensionnel actuel (par rapport aux coordonnées nucléaires) deviendra réaliste pour la photodésorption de CO/Cu(111) et des comparaisons valables avec l'expérience seront possibles. Pour l'excitation multiphotonique, mentionnée comme mécanisme possible pour la photodésorption de CO/Cu(111) [123], il faut introduire simultanément les couplages dûs au champ intense permettant l'absorption de plusieurs photons simultanément et les interactions non–adiabatiques. Des travaux dans cette direction sont en cours dans notre groupe et nous appliquerons le modèle résultant à la photodésorption multiphotonique de CO/Cu(111).

Le modèle de photodésorption discuté ci–dessus peut être utilisé dans l'étude d'autres systèmes comme par exemple des molécules adsorbées sur des oxydes métalliques pour lesquels les taux de photodésorption sont élevés [30–36]. Dans l'avenir, nous allons essayer d'étendre notre modèle à ces systèmes plus complexes. La difficulté majeure est la disponibilité des surfaces d'énergie potentielle d'une qualité satisfaisante.

Parmi les diverses méthodes, je veux citer les collisions d'électron–adsorbats et la désorption induite par impact d'électron sont des méthodes ou la problématique est la même que pour l'impact par le photon mais les échelles de temps et les règles de sélection sont différentes. Mes études des mouvements nucléaires et la rétrodiffusion y compris l'étude sur l'influence de la couverture d'adsorbats peuvent être utilisées dans cette autre technique expérimentale. La réalité physique est éclaircie d'une façon differente et complémentaire.

L'étude de la photofragmentation des adsorbats moléculaires est un domaine fascinant mais difficile. L'adsorbat et la surface ont leur propriétés propres et le système adsorbat–surface n'est pas une simple addition de ces propriétés. Vu le très grand nombre de degrés de liberté, le chemin d'évolution du système peut être diffèrent d'un système adsorbé à un autre. Par conséquent le développement des modèles pour interpréter les expériences est difficile mais excitant. Ceci explique pourquoi ce domaine est un défi et la collaboration entre expérimentateurs et théoriciens est essentielle.

Appendix A

Hindered rotation: analytical expressions for strongly bound molecules

If a molecule is strongly chemisorbed on a surface, the potential for the hindered rotation motion is steep and the inclination angle of the intramolecular axis is small. For this limiting case, one can derive analytical wave functions and energies for the hindered rotor assuming a frozen molecule in a given adsorption site with the distance between the centre–of–mass and the surface equal to z_0. In the vicinity of $\beta = 0°$ the surface potential is taken as independent of the azimuthal angle α (axial–symmetry approximation) and as harmonic in the tilt angle β:

$$V(\beta) = \frac{1}{2}\omega\beta^2 + C \tag{A.1}$$

In Eq.A.1 ω is the harmonicity constant and C a constant term, which is set to zero in the following to simplify the derivation. In order to obtain the energies and wave functions, one inserts this surface potential into the Schrödinger equation for the nuclear motion:

$$\mathcal{H}\Theta^{n,rot}_{M,\Omega}(\hat{R}) = E^{n,rot}_{M,\Omega}\Theta^{n,rot}_{M,\Omega}(\hat{R}) \tag{A.2a}$$

where

$$\mathcal{H} = B_{rot}\left[\frac{\partial^2}{\partial\beta^2} + \cot\beta\frac{\partial}{\partial\beta} + \frac{1}{\sin^2\beta}\left(\frac{\partial^2}{\partial\alpha^2} + \frac{\partial^2}{\partial\gamma^2} - 2\cos\beta\frac{\partial^2}{\partial\alpha\partial\gamma}\right)\right] + \frac{1}{2}\omega\beta^2 - B_{rot}\Omega^2 \tag{A.2b}$$

In Eq.A.2 $\hat{R} = (\alpha, \beta, \gamma)$ are the Euler angles, defining the absorbate orientation about the surface normal. The kinetic operator (bracket [...] in (A.2)) for the rotational motion is taken from Varshalovich (p. 74, [97]), with B_{rot} the rotational constant of gas phase. n is the rotational quantum number and M and Ω are projections of the total angular vector onto the surface normal and intramolecular axis. The wave function is written in the similar way to the Wigner rotational function as a product of three

functions :

$$\Theta^{n}_{M\Omega}(\hat{R}) = \frac{1}{\sqrt{4\pi}} \quad e^{iM\alpha} \quad \frac{\varphi^{n}_{M\Omega}(\beta)}{\sin\beta} \quad e^{i\Omega\gamma} \tag{A.3}$$

and inserting (A.3) in (A.2) on obtains [154]:

$$\left\{ \frac{\partial^2}{\partial\beta^2} \frac{M^2+\Omega^2}{\sin^2\beta} \frac{M\Omega}{\sin^2\beta} \cos\beta + \frac{1}{4}\cot^2\beta - V(\beta)/B_{rot} + E^{n,rot}_{M,\Omega}/B_{rot} + \Omega^2 \right\} \varphi^{n,rot}_{M,\Omega} = 0 \tag{A.4}$$

For small β the angular functions in Eq.(A.4) can be expanded in Taylor series around β =0° up to the second order. Rewriting the resulting expression in compact form, Eq.(A.4) becomes:

$$\left\{ \tfrac{\partial^2}{\partial\beta^2} - \tfrac{1}{4\beta^2}\left(1 - 4(M-\Omega)^2\right)\beta^2 \left(\tfrac{4(M+\Omega)^2 - M\Omega}{60} + \tfrac{\omega}{2B_{rot}} \right) - \tilde{E}^{n,rot}_{M,\Omega} \right\} \varphi^{n,rot}_{M,\Omega} = 0 \tag{A.5}$$

with

$$\tilde{E}^{n,rot}_{M,\Omega} = E^{n,rot}_{M,\Omega}/B_{rot} - \tfrac{1}{3}(M+\Omega)^2 - \tfrac{1}{6} - \tfrac{1}{3}M\Omega \tag{A.6}$$

The solutions of this differential equation of second order are essentially Laguerre polynomials. More precisely, the wave functions and energies, that solves the Schrödinger equation (A.5), read following M. Abramowitz and I. A. Stegun [155], page 781):

$$\Theta^{n}_{M\Omega}(\hat{R}) = \tfrac{1}{\sqrt{4\pi}} \quad e^{iM\alpha} \quad e^{i\Omega\gamma} \quad \tfrac{1}{\sqrt{\beta}} \exp\left(\tfrac{-a^2\beta^2}{2}\right) (a\beta)^{|M-\Omega|+1/2} \quad \mathrm{L}^{|M-\Omega|}_{n}(a^2\beta^2) \tag{A.7}$$

with $n \geq 0$ integer and

$$a = \sqrt[4]{\tfrac{\omega}{2B_{rot}} + \tfrac{4(M+\Omega)^2 - M\Omega - 1}{60}} \tag{A.8}$$

and the rotational energies

$$E^{n,rot}_{M,\Omega} = 2B_{rot}a^2\left[2n + \tfrac{M-\Omega}{2} + 1\right] + 2B_{rot}\left\{-\Omega^2 + \tfrac{1}{2}\right\} + \tfrac{1}{3}B_{rot}\left\{(M+\Omega)^2 + M\Omega + \tfrac{1}{2}\right\} \tag{A.9}$$

Here, $\mathrm{L}^{k}_{n}(a^2\beta^2)$ are second order Laguerre's polynomials. One can see, that, as for a harmonic oscillator, the spacing between the hindered rotational levels are equidistant. There is a zero–point energy (n=0) depending on the quantum numbers M and Ω. But, the wave functions are not of Hermite type, as it is the case for an ordinary harmonic oscillator. Note, that for β=0° the wave function density $\left|\Theta^{n}_{M\Omega}(\hat{R})\right|^2 \sin\beta$ is zero, the molecule can never be found in an upright position. This fact has already been explained in part II, section 2.4 (page 55) by a 'rotation' with vanishing inertia moment, that is quantum mechanically excluded.

Appendix B

About hindered rotor times scales

In this section, two characteristic times for hindered rotational motion of a chemisorbed molecule are calculated, i.e. the characteristic time for the precession and that for the libration motions. More precisely, the influence of the surface is considered to cause an inclination of the adsorbate about the surface normal. For precession the classical time of one rotation about the surface normal, for a fixed angle $\bar{\beta}$ (i.e. excluding libration), will be taken as the characteristic time T_{prec}. For the libration the characteristic time T_{lib} is calculated supposing that the molecule is moving in a plane including the surface normal (as a physical pendulum). It is allowed to undergo a free spinning rotation (precession) about the surface normal.

B.1 Characteristic time for precession (Fig.B.1b))

For the precession motion the tilt angle $\bar{\beta}$ is taken as the quantum mechanical mean value for a given rotational state. It is normally about 8° –12° for chemisorbed molecules in the low coverage limit. In order to calculate the classical time, one first express the inertia moment I in terms of the rotational constant B_{rot}:

$$\begin{aligned} I &= \left(m_1 r_1^2 + m_2 r_2^2\right) \sin^2 \bar{\beta} \\ &= \hbar^2 / \left(2B_{rot}\right) \sin^2 \bar{\beta} \end{aligned} \tag{B.1}$$

Here, m_i and r_i are the masses of the two nuclei and their distances from the centre of mass and again B_{rot} is the gas phase rotational constant. Note, that in (B.1) a factor of $\sin^2 \bar{\beta}$ appears due to the inclination of molecular adsorbate. With the relation $E_{rot} = \frac{1}{2} I \left(\frac{2\pi}{T_{prec}}\right)^2$, one derive the characteristic time T_{prec}:

$$T_{prec} = \pi \sqrt{\frac{\hbar^2}{B_{rot} E_{rot}}} \sin \bar{\beta} \tag{B.2}$$

One can take the quantum mechanical zero–point energy, known from the experimental frequencies, as reference energy E_{rot}.

B.2 Characteristic time for the pendulum motion (Fig.B.1b))

The starting point is the calculation of the classical force acting on the molecule. For small β and using the form of the potential (Eq.A.1), the force is equal to $\omega\beta$, where ω is the harmonic constant. The classical oscillation time T_{lib} is now given by:

$$T_{lib} = 2\pi\sqrt{\frac{I}{\omega}} = 2\pi\sqrt{\frac{\hbar^2}{4B_{rot}\omega}} \tag{B.3}$$

In Eq.(B.3), I is the inertia moment, equal to $I = \hbar^2/(2B_{rot})$. Note, that the rotational axis is perpendicular to the intramolecular axis (β=90°), contrary to the precession case. The harmonic constant ω can be derived by inserting the experimentally known rotational energies in the analytical expression for these energies in Eq.(A.7).

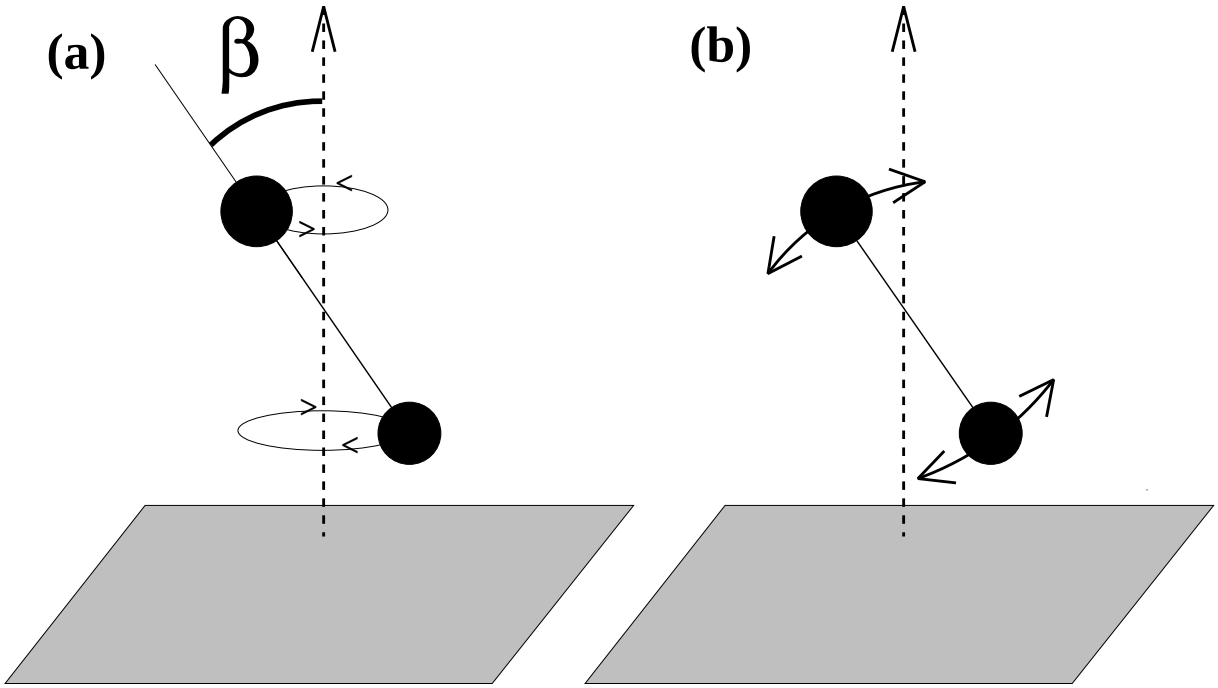

Figure B.1: *Characteristic times: (a) The adsorbed molecule is spinning around the surface normal, enclosing a constant angle β. (b) The pendulum motion.*

Appendix C

Photoionization cross section

This appendix contains two parts. First, I present the organisation of the computer program, which calculates the photoionization cross section of adsorbed molecules including hindered rotation in an axial symmetric surface potential. Secondly I give the generalized expression of the cross section for non-axially symmetric surface potential.

C.1 Structure of the computer program

There were two main difficulties related to the program calculating the photoionization cross section of adsorbed molecules including hindered rotation in an axial symmetric surface potential. First, one must structure the given problem in a way to gain a balanced economization of computer time and memory. Secondly, the complexity of the analytical formulae imposed a careful independent study of all intermediate step of the calculation to ensure the correctness of the results. The flowchart of the program is shown in Fig.C.1.

The starting point is the read in of the parameters as the initial and final electronic states, the associated the rotational constants $B^{''}$ and B^{+} and the rotational temperature T_{rot} giving the Boltzmann distribution of the initial rotational states (subroutine 'RGLOBAL'). In the subroutines 'READIN' and 'CONVERTING' the electronic transition moments are read in and stored, while 'HIN_READ' reads all parameters related to the hindered rotor of the initial and final electronic states. They are composed by the rotational energies and the expansion coefficients of Eq.(2.18) on page 57. To supplement informations about the hindered rotation motion in the initial neutral and final ionic state, the mean values of the tilt angle ($\overline{\beta}$) of the molecular adsorbate about the surface normal are calculated in subroutine 'MEANBETA'.

The next step concerns the calculation of the geometrical coefficients of the differential cross section containing mainly $3j$ coefficients. They do not dependent on the photon energy but on the initial and final quantum numbers. Due to the high number of possible final states, the program is structured in two subroutines 'GEOMETRICAL' and 'GEOM_NMFDEP', the first concerned mainly with the initial states and the last with the final states. Then, the photon energy is varied and in 'DYNAM' subroutine the differential cross section is derived by summation containing the geometrical parts and the electronic

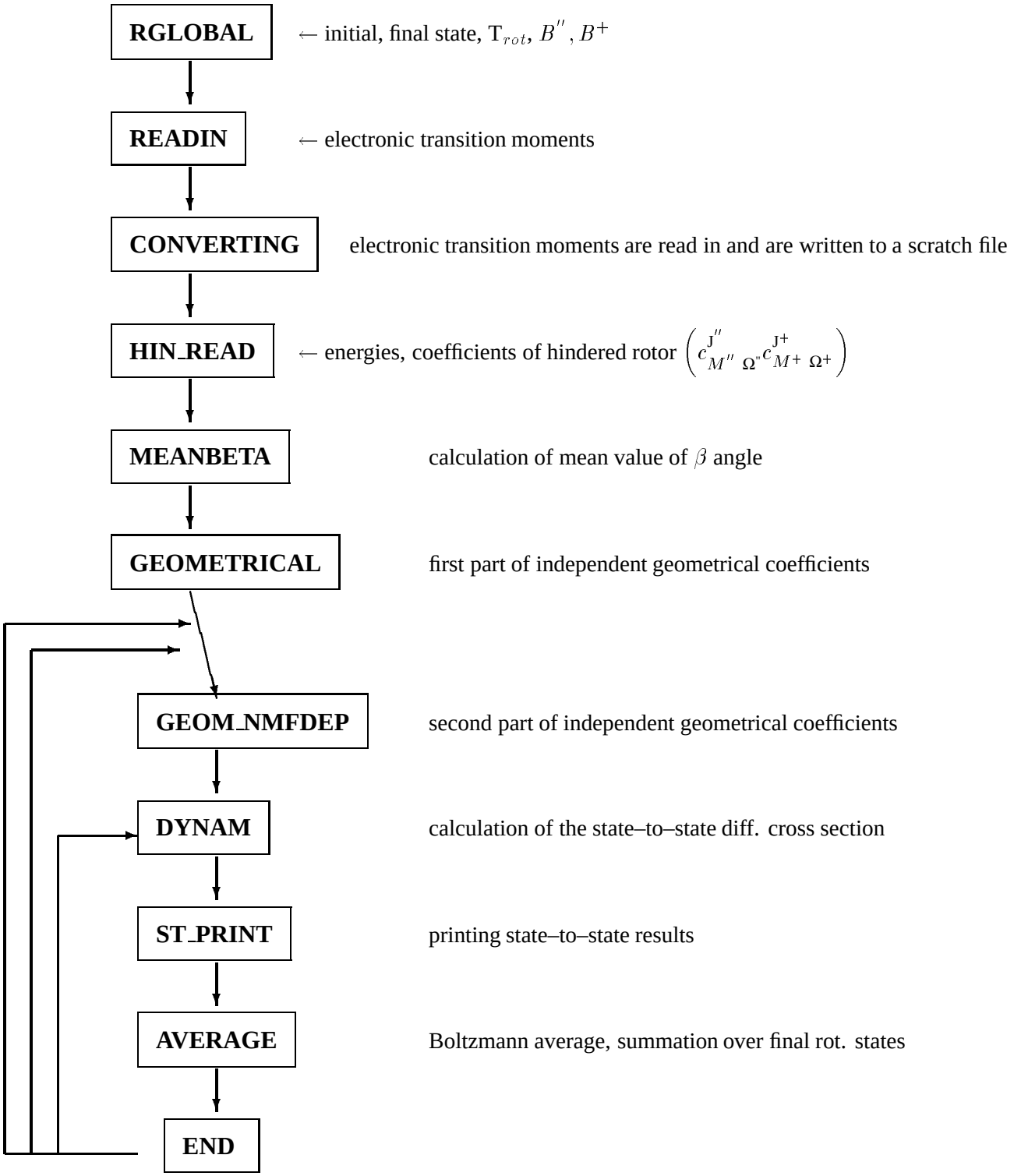

Figure C.1: Flowchart of the program, calculating the photoionization cross section for molecular adsorbates, including hindered rotation.

transition moments.

These state–to–state results depending on the photon energy, i.e. the differential cross section from a initial rotational level ($n^{"}$, $M^{"}$, $\Omega^{"}$) to a final one (n^{+}, M^{+}, Ω^{+}) is printed in files ('ST_STATE'). Finally, a Boltzmann average over the initial state and a sum over all final rotational states ('AVERAGE') are performed to obtain a differential cross section comparable to existing experimental results, which do not resolve rotational structures in their photoionization spectra of molecular adsorbates.

I give now the detailed partition scheme of the general formula for the state–to–state differential cross section (Eq.2.23 on page 59). I rewrite this equation taking explicitly the names of the arrays used in the program. Remember that $\vec{k} = (k, \vartheta_k, \varphi_k)$ and $\hat{q}$=(ϑ_q, φ_q) stand for the linear momentum (k) of the escaping photoelectron, while the four angles represent the directions of the photoelectron (index 'k') and the incident photon (index 'q'), respectively.

$$ {}^{m^{ph}}\mathrm{I}\,{}^{\Omega^{+}\ M^{+}\ n^{+}}_{\Omega^{"}\ M^{"}\ n^{"}}(\vec{k},\hat{q}) = \tag{C.1a} $$

$$ N_E \sum_{\substack{K=0 \\ M_K=-K}}^{K=\infty} \sum_{\substack{L=0 \\ M_L=-L}}^{L=\infty} \sum_{\substack{l_1=0 \\ m_1=-l_1}}^{l_1=\infty} \sum_{\substack{l_2=0 \\ m_2=-l_2}}^{l_2=\infty} \sum_{\substack{m_1^{\gamma}=-1,\cdots,1 \\ m_2^{\gamma}=-1,\cdots,1}} (-1)^{m_1 - \ m_1^{\gamma} + \ m^{ph}} $$

$$ \mathbf{glmp}(m_1^{\gamma}, m_2^{\gamma}, \vartheta_q) \quad \mathbf{glm}(l_1, l_2, m_1, m_2, \vartheta_k) \quad B^{l_1 m_1\ m_1^{\gamma}}_{l_2 m_2\ m_2^{\gamma}} $$

$$ B^{l_1 m_1\ m_1^{\gamma}}_{l_2 m_2\ m_2^{\gamma}} = \tag{C.1b} $$

$$ \sum_{\substack{J_1'', J_2'' \geq |M'',\ \Omega"| \\ J_1^{+}, J_2^{+} \geq |M^{+},\ \Omega^{+}|}} \sum_{\substack{J_1 M_1 \Omega_1 \\ J_2 M_2 \Omega_2}} \sum_{\substack{\lambda_1^{\gamma}=-1,\cdots,1 \\ \lambda_2^{\gamma}=-1,\cdots,1}} \sum_{1 m_1^{j} \omega_1} \sum_{2 m_2^{j} \omega_2} \sum_{\sigma_1 \sigma_2} {}^{\lambda_1^{\gamma}}\mathrm{t}^{\Omega^{+}\ell_1\lambda_1\sigma_1}_{\Omega^{"}}(k,R) \left({}^{\lambda_2^{\gamma}}\mathrm{t}^{\Omega^{+}\ell_2\lambda_2\sigma_2}_{\Omega^{"}}(k,R) \right) $$

$$ \mathbf{helprfi}\left(\left\{ \begin{array}{ccc} 1 & : & \Omega^{+} \\ 0 & : & -\Omega^{+} \end{array} \right\}, \lambda_1, \mu, m_1^{\gamma} \right) \mathbf{helprfi}\left(\left\{ \begin{array}{ccc} 1 & : & \Omega^{+} \\ 0 & : & -\Omega^{+} \end{array} \right\}, \lambda_2, \mu, m_2^{\gamma} \right) $$

$$ \mathbf{potini}(\ M^{"},\ n^{"}, m_1^{\gamma}, J) \mathbf{potini}(\ M^{"},\ n^{"}, m_2^{\gamma}, J) $$

$$ \tilde{T}^{\Omega^{+} l\lambda m\sigma j m^{j}}_{\Omega^{"}\ \lambda^{\gamma}}(\vec{k}) = \mathbf{tra}(j,l,m,\lambda,\mu,\sigma)\ {}^{\lambda^{\gamma}}\mathrm{t}^{\Omega^{+}\ell\lambda\sigma}_{\Omega^{"}}(k,R) $$

(C.1c)

Subroutine 'GEOMETRICAL'

- **transition moment part**

$$\mathbf{tra}(j,l,m,\lambda,\mu,\sigma) = [j](-1)^{m+\mu-\lambda-\sigma} \begin{pmatrix} \mathrm{J}_l'' & 1/2 & j \\ m & \mu & -m-\mu \end{pmatrix} \begin{pmatrix} \mathrm{J}_l'' & 1/2 & j \\ \lambda & \sigma & -\lambda-\sigma \end{pmatrix} \tag{C.2}$$

- **geometrical part of the electron**

$$\mathbf{glm}(l_1,l_2,m_1,m_2,\vartheta_k) = \sqrt{(2l_1+1)(2l_2+1)}(-1)^{m_1} \begin{cases} 1 & : \quad m_1-m_2 \geq 0 \\ (-1)^{m_2-m_1} & : \quad m_1-m_2 < 0 \end{cases} \tag{C.3}$$

$$\sum_L \sqrt{(2L+1)}\mathrm{ylm}(L,|m_1-m_2|,\vartheta_k) \begin{pmatrix} l_1 & l_2 & L \\ 0 & 0 & 0 \end{pmatrix} \begin{pmatrix} l_1 & l_2 & L \\ -m_1 & m_2 & m_1-m_2 \end{pmatrix} \tag{C.4}$$

- **geometrical part of the photon**

$$\mathbf{glmp}(m_1^\gamma,m_2^\gamma,\vartheta_q) = \begin{cases} 1 & : \quad m_1^\gamma - m_2^\gamma \geq 0 \\ (-1)^{m_2^\gamma - m_1^\gamma} & : \quad m_1^\gamma - m_2^\gamma < 0 \end{cases} \tag{C.5}$$

$$\sum_K \sqrt{(2K+1)}\mathrm{ylm}(K,|m_1^\gamma - m_2|,\vartheta_k) \begin{pmatrix} 1 & 1 & K \\ 0 & 0 & 0 \end{pmatrix} \begin{pmatrix} 1 & 1 & K \\ -m_1^\gamma & m_2^\gamma & m_1^\gamma - m_2^\gamma \end{pmatrix} \tag{C.6}$$

- **potential part related to quantum numbers of the initial state**

$$\mathbf{potini}(\,\mathrm{M}",\ n",m_1^\gamma,J) = \tag{C.7}$$

$$\sqrt{2\mathrm{J}_+''1}(2J+1) \left\{ \begin{array}{rcl} 1 & : & \Omega" \geq 0 \\ -(-1)^{\mathrm{J}''+J+1} & : & \Omega" < 0 \end{array} \right\} \left\{ \begin{array}{rcl} 1 & : & \mathrm{M}" \geq 0 \\ -(-1)^{\mathrm{J}''+J+1} & : & \mathrm{M}" < 0 \end{array} \right\}$$

$$\begin{pmatrix} \mathrm{J}'' & 1 & J \\ |\,\Omega"| & \lambda^\gamma & -|\,\Omega"| - \lambda^\gamma \end{pmatrix} \begin{pmatrix} \mathrm{J}'' & 1 & J \\ \mathrm{M}" & m^\gamma & -\mathrm{M}" - m^\gamma \end{pmatrix} c^{\mathrm{J}''\ n"}_{\mathrm{M}"\ \Omega"} \tag{C.8}$$

Subroutine 'GEOM_NMFDEP'

- **part of the potential related to quantum numbers of the final state**

$$\mathbf{helprfi}\left(\left\{ \begin{array}{rcl} 1 & : & \Omega^+ \\ 0 & : & -\Omega^+ \end{array} \right\}, \lambda,\mu,m^\gamma \right) = \sqrt{2J^+ + 1}\mathbf{tra}(j,l,m,\lambda,\mu,\sigma) \tag{C.9}$$

$$\begin{pmatrix} \mathrm{J}^+ & j & J \\ \pm\,\Omega^+ & \omega_j & \mp\,\Omega^+ - \omega_j \end{pmatrix} \begin{pmatrix} \mathrm{J}^+ & j & J \\ \mathrm{M}^+ & m_j & -m_j - \mathrm{M}^+ \end{pmatrix} c^{\mathrm{J}^+\ n^+}_{\pm M^+\ \Omega^+} \tag{C.10}$$

Note, that for $-\,\Omega^+ - \mathrm{M}^+$ has to be taken for the wave function expansion coefficients $c^{\mathrm{J}^+\ n^+}_{M^+\ \Omega^+}$ as they are calculated only for one Ω^+ but due to the degeneracy the coefficients for the set $(\,\Omega^+, M^+)$ are identical to those for $(-\,\Omega^+, -M^+)$.

Using these arrays, the final summation part is done, which calculate the total and differential cross section.

C.2 Formulae for photoionization cross sections including hindered rotation in non–axial symmetric potentials and photoelectron backscattering

In this section, I derive formulae for the differential photoionization cross sections including now the hindered rotation motion for non–axial symmetric surface potentials and photoelectron backscattering. The latter effect was discussed in section 2.3.3 using a published model [13].

The derivation is similar to the one, presented in part II, and I restrict the discussion to a brief presentation of the formulae for differential photoionization cross section. Again, Born–Oppenheimer and Franck–Condon approximations are used to separate the electronic and nuclear motion. For the electronic transition moments, an ab–initio method, summarised in section 2.3.1 (part II) or its generalized version can be used. The hindered rotation wave functions are calculated by the model, detailed in this part of the thesis, section 2.2.1. The derived wave functions take into account any non–axial symmetric potential. The backscattering was introduced in the surface frame using a model, discussed in section 2.3.3, part II.

Performing the frame transformation and some analytical derivations, one obtain the following equations for differential photoionization cross sections, describing dipole excitations from a given initial rotational level to a final one (state-to–state cross section):

$$ {}^{m^{ph}}\mathrm{I}^{\ \Omega^{+}\ n^{+}}_{\Omega^{"}\ n^{"}}(\vec{k},\hat{q}) = \tag{C.11a} $$

$$ N_E \sum_{\substack{K=0 \\ M_K=-K}}^{\infty} \sum_{\substack{L=0 \\ M_L=-L}}^{\infty} [L,K]^{1/2} \quad \mathrm{Y}_{KM_K}(\hat{q}) \quad \mathrm{Y}_{LM_L}(\hat{k}) $$

$$ \sum_{\substack{\ell_1=0 \\ m_1=-\ell_1}}^{\infty} \sum_{\substack{\ell_2=0 \\ m_2=-\ell_2}}^{\infty} \sum_{\substack{m_1^{\gamma}=-1,\cdots,1 \\ m_2^{\gamma}=-1,\cdots,1}} [\ell_1,\ell_2]^{1/2}(-1)^{m_1-\ m_1^{\gamma}+\ m^{ph}} $$

$$ \begin{pmatrix} \ell_1 & \ell_2 & L \\ -m_1 & m_2 & M \end{pmatrix} \begin{pmatrix} \ell_1 & \ell_2 & L \\ 0 & 0 & 0 \end{pmatrix} \begin{pmatrix} 1 & 1 & K \\ -\ m_1^{\gamma} & m_2^{\gamma} & M_K \end{pmatrix} \begin{pmatrix} 1 & 1 & K \\ -\ m^{ph} & m^{ph} & 0 \end{pmatrix} \tilde{B}^{\ell_1 m_1\ m_1^{\gamma}}_{\ell_2 m_2\ m_2^{\gamma}} $$

(C.11b)

$$ \tilde{T}^{\ \Omega^{+}\ell\lambda m\sigma j m^{j}}_{\Omega^{"}\ \lambda^{\gamma}}(\vec{k}) = (-1)^{\omega-m_j}[j] \begin{pmatrix} l & 1/2 & j \\ m & \mu & -m_j \end{pmatrix} \begin{pmatrix} \ell & 1/2 & j \\ \lambda & \sigma & -\omega \end{pmatrix} \ {}^{\lambda^{\gamma}}\mathrm{t}^{\ \Omega^{+}\ell\lambda\sigma}_{\Omega^{"}}(k,R) $$

$$ \tilde{B}^{\ell_1 m_1\ m_1^{\gamma}}_{\ell_2 m_2\ m_2^{\gamma}} = \left[1+(-1)^{l_1+m_1}R^{*}(k,\vartheta_k\right]\left[1+(-1)^{l_2+m_2}R^{*}(k,\vartheta_k\right] \tag{C.11c} $$

$$\sum_{\substack{J_1'',J_2''\geq|\,\Omega"|\\ J_1^+,J_2^+\geq|\,\Omega^+|}} \sum_{\substack{M_1''=-J_1''\\ M_2''=-J_2''}}^{J_1'',J_2''} \sum_{\substack{M_1^+=-J_1^+\\ M_2^+=-J_2^+}}^{J_1^+,J_2^+} [J_1'',J_2'',J_1^+,J_2^+]^{1/2} \quad c^{J_1''}_{M" \,\Omega"} c^{J_2''}_{M" \,\Omega"} c^{J_1^+}_{M^+ \,\Omega^+} c^{J_2^+}_{M^+ \,\Omega^+}$$

$$\sum_{\substack{J_1M_1\Omega_1\\ J_2M_2\Omega_2}} \sum_{\substack{\lambda_1^\gamma=-1,\cdots,1\\ \lambda_2^\gamma=-1,\cdots,1}} \sum_{\substack{j_1m_1^j\omega_1\\ j_2m_2^j\omega_2}} [J_1,J_2] \sum_{\sigma_1\sigma_2} \tilde{T}^{\,\Omega^+ l_1\lambda_1 m_1\sigma_1 j_1 m_1^j}_{\Omega" \,\lambda_1^\gamma}(\vec{k}) \quad \left(\tilde{T}^{\,\Omega^+ l_2\lambda_2 m_2\sigma_2 j_2 m_2^j}_{\Omega" \,\lambda_2^\gamma}(\vec{k})\right)^*$$

$$\begin{pmatrix} J_1'' & 1 & J_1 \\ M_1'' & m_1^\gamma & -M_1 \end{pmatrix} \begin{pmatrix} J_1'' & 1 & J_1 \\ \Omega" & \lambda_1^\gamma & -\Omega_1 \end{pmatrix} \begin{pmatrix} J_1^+ & j_1 & J_1 \\ M_1^+ & m_1^j & -M_1 \end{pmatrix} \begin{pmatrix} J_1^+ & j_1 & J_1 \\ \Omega^+ & \omega_1 & -\Omega_1 \end{pmatrix}$$

$$\begin{pmatrix} J_2'' & 1 & J_2 \\ M_2'' & m_2^\gamma & -M_2 \end{pmatrix} \begin{pmatrix} J_2'' & 2 & J_2 \\ \Omega" & \lambda_2^\gamma & -\Omega_2 \end{pmatrix} \begin{pmatrix} J_2^+ & j_2 & J_2 \\ M_2^+ & m_2^j & -M_2 \end{pmatrix} \begin{pmatrix} J_2^+ & j_2 & J_2 \\ \Omega^+ & \omega_2 & -\Omega_2 \end{pmatrix}$$

The Eq.(C.11) looks similar to the corresponding equation (2.23) on page 59 of section 2.4.2, part II. Consequently only the differences between Eq.(C.11) and (2.23) are discussed here. The reader is referred to section 2.4.2, part II (p.58ff) for general discussion and definitions.

The main difference between formulas concerns that the projection of the total angular momentum $\vec{J}$ onto the surface normal that is no longer a good quantum number. Consequently, four additional sums over its projections on different directions appear for the initial and final state.

Backscattering appears as a factor $\left[1+(-1)^{l_1+m_1}R^*(k,\vartheta_k\right]$, where R is defined in Eq.(2.12) (p.50) as the complex backscattering factor, reducing the photoelectron flux and shifting the phase of the electron wave.

Appendix D

Coefficients of the hindered rotation potentials for low and high coverage

L=	M_L= 0	M_L=1	M_L=2	M_L=3	M_L=4	M_L=5
0	-1272.39					
1	519.14	81.98 - 72.49 i				
2	191.20	116.27 - 102.43 i	2.97 + 17.93 i			
3	-43.66	28.35 - 24.91 i	1.41 + 8.52 i	15.26 + 13.73i		
4	-53.72	7.91 - 6.85 i	1.01 + 5.12 i	15.96 + 14.36i	16.70 + .01i	
5	-11.59	-.28 + .28 i	.22 + .91 i	4.81 + 4.32i	8.19 + .01i	-.08 + .08i
6	-1.66	-.72 + .64 i	.05 + .13 i	1.68 + 1.50i	4.04 + .00i	-.01 + .03i
4	.26	-.19 + .17 i	.00 - .02 i	.23 + .21i	.88 + .00i	.01 + .00i
8	.17	-.04 + .03 i	.00 - .01 i	.01 + .01i	.18 + .00i	.01 - .01i
9	.04	.00 + .00 i	.00 + .00 i	-.01 - .01i	.01 + .00i	.00 + .00i
10	.00	.00 + .00 i	.00 + .00 i	.00 .00i	.00 + .00i	.00 + .00i
11	.01	.00 + .00 i	.00 + .00 i	.00 .00i	.00 + .00i	.00 + .00i
12	-.01	.00 + .00 i	.00 + .00 i	.00 .00i	.00 + .00i	.00 + .00i
13	.01	.00 + .00 i	.00 + .00 i	.00 .00i	.00 + .00i	.00 + .00i
14	-.01	.00 + .00 i	.00 + .00 i	.00 .00i	.00 + .00i	.00 + .00i
15	.01	.00 + .00 i	.00 + .00 i	.00 .00i	.00 + .00i	.00 + .00i

Table D.1: *Single CO adsorbed on Ar(100) (low coverage): complex expansion coefficients of the hindered rotation potential in cm^{-1} at z_0= 2.59 Åand R_0= 1.1283 Å(see part Eq.(2.4) on page 109). As the surface potential is real, the coefficients for negative M_L are connected to those of positive M_L in the following way: identical values for odd and complex conjugated for even M_L.*

L=	M_L= 0	M_L=1	M_L=2	M_L=3	M_L=4	M_L=5
0	-17288.37					
1	14.00	-7.57 + .37 i				
2	20.32	.39 + 7.88 i	260.90 + 319.25 i			
3	1147.36	12.47 + 22.86 i	-388.86 - 505.15 i	6.14 - 3.19 i		
4	23.00	-3.31 - .94 i	-287.38 - 69.86 i	-3.06 - 12.15 i	-5.88 + 56.36 i	
5	-463.25	-1.09 - 6.97 i	38.16 - 7.28 i	-2.14 + 14.57 i	43.31 - 45.19 i	1.92 - .03i
6	55.24	20.76 + 1.92 i	-145.82 - 362.29 i	8.14 - 4.79 i	-38.86 - 9.41 i	1.45 - 6.40i
4	-128.75	1.81 - 11.39 i	-315.78 - 54.41 i	-2.16 - 14.16 i	-10.52 + 40.33 i	-2.47 + 5.83i
8	-84.24	-.71 - 3.52 i	-70.04 + 33.88 i	-3.33 + .38 i	5.64 - 18.88 i	.50 - 1.11i
9	-50.25	3.76 - 4.62 i	-115.73 - 51.35 i	-.64 - 4.49 i	-46.16 + 22.43 i	-.93 - 4.18i
10	-8.56	.44 - 1.98 i	-86.16 + 27.42 i	-4.93 - 3.40 i	5.21 + 39.74 i	-3.15 + 1.24i
11	-35.55	-1.34 - 3.32 i	-57.19 + 8.95 i	-2.18 + .04 i	-2.99 + 9.63 i	.12 - .02i
12	.59	.37 + .06 i	-40.03 + 21.88 i	-3.02 - 1.07 i	-4.28 + 23.57 i	-1.56 - 1.09i
13	-14.61	.31 - 1.99 i	-38.72 - .08 i	-2.79 + .31 i	2.86 + 21.52 i	-1.06 + .98i
14	-.81	-.24 - .03 i	-29.02 + 21.83 i	-2.24 + .49 i	11.19 + 14.38 i	-.47 + .61i
15	-10.49	.12 - 1.37 i	-23.47 - 1.86 i	-1.33 + .92 i	2.88 + 8.20 i	-.31 + .58i

Table D.2: *Central CO of $(CO)_7$ on Ar(100) (high coverage): complex expansion coefficients of the hindered rotation potential in cm^{-1} at z_0=2.67 Å and R_0= 1.1283 Å*

Appendix E

Photodesorption

E.1 Structure of the computer program

Figure E.1 displays the flowchart of the program, that calculates the energies and wave functions of the coupled nuclear adsorbate modes, hindered rotation, translation, internal vibration and molecule–surface stretch and their projections onto the gas phase wave functions, i.e. the Franck–Condon and Fourier integral overlaps.

The starting point is the read in of all parameters, as the type of surface–adsorbate system, expansion parameter *etc.* Then the potential is determined in subroutine 'POT_EXPAN'. Either from numerical data, i.e. the potential was calculated by other methods or it is calculated for each point of a multidimensional grid, containing the orientation, centre–of–mass position and intra-nuclear distance of the molecular adsorbate. The potential is now expanded in Fourier series (centre–of–mass position parallel to the surface) and spherical harmonics (orientation). In the next step the dependence of the intra-nuclear distance is expanded in Taylor series up to the second order ('POTPARAB'). Up to this point of the program no expansion about the centre–of–mass distance z to the surface is performed, i.e. the expansion coefficients still depend on z.

In order to have a feeling about the motions, in subroutine 'UNIDIM' the decoupled motions are analysed, the energies and wave functions are calculated by expanding the wave functions and solving the Schrödinger type of linear set of equations numerically. The basis set consists of Bloch functions (hindered translation), gas phase Wigner functions (hindered rotation) and harmonic oscillator functions (internal vibration). The only exception is the molecule–surface stretch. For this motion, the energies and wave functions are calculated by renormalised Numerov propagation techniques. I obtained the guess energies but fitting either the potential to a Morse or to a harmonic potential.

In the subroutine 'HINROTTRAN' all nuclear adsorbate motions, but the molecule–surface stretch one are coupled, fixing z at a given value z_0, and the linear set of equations corresponds to an eigenvalue, -vector problem. With the obtained expansion coefficients the mean values are calculated in 'MEAN'.

In 'ELEMENTS' I derive potential matrix elements. The basis set of wave functions is that of all coupled nuclear modes, but the molecule–surface stretch motion, and consequently the potential matrix elements

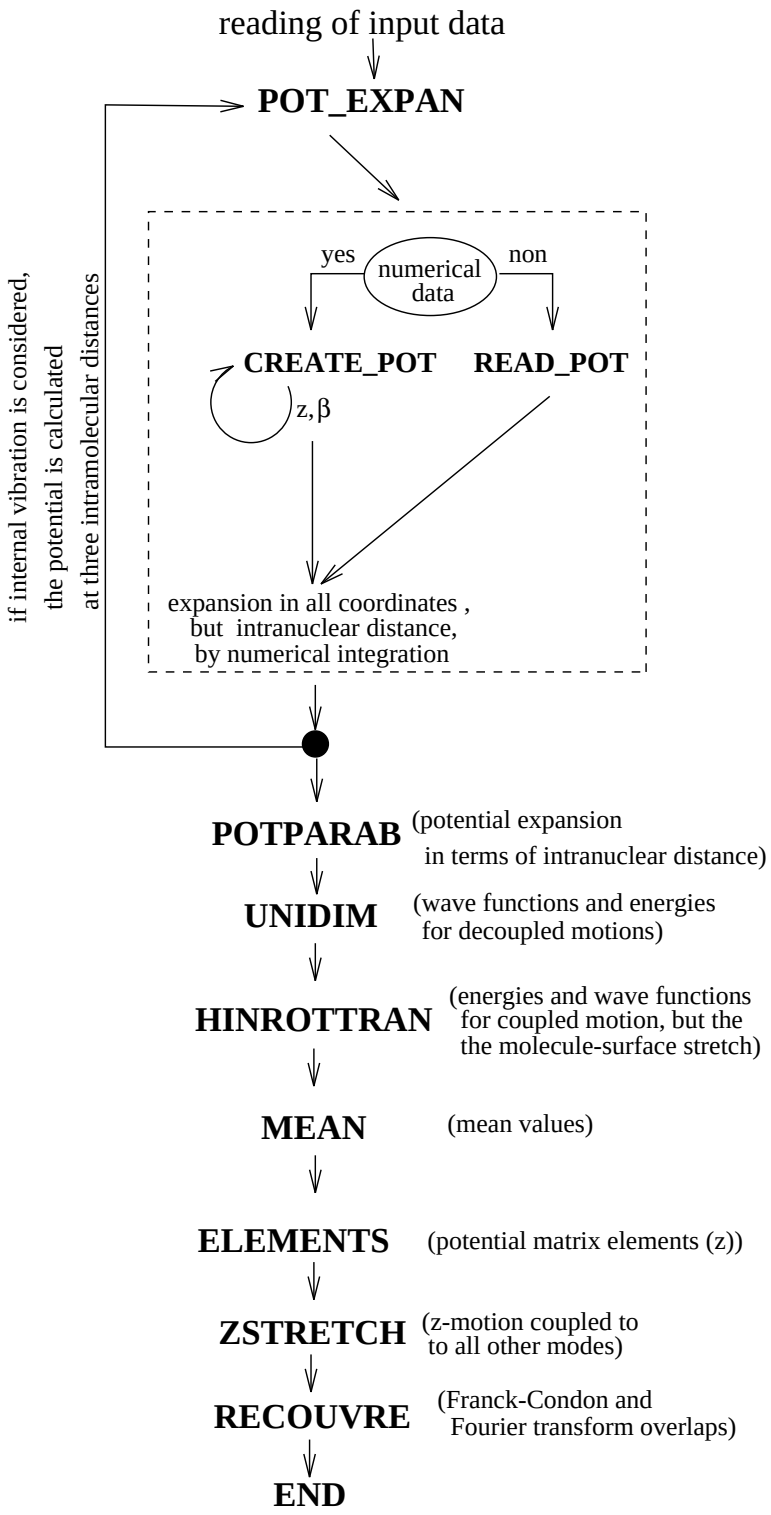

Figure E.1: Flowchart of the program, calculating the Franck–Condon and Fourier transform overlap between the coupled hindered rotation, translation, internal vibration, molecule–surface stretch of the adsorbed molecule and those of the gas phase. rotation.

are functions of the molecule–surface distance z. Note, that at z_0 the matrix is diagonal, as at this point the wave functions of the basis set are eigenfunctions of the system. These elements are not used in this thesis, but the subroutine was programmed for future use.

The next step is the coupling of the z–stretch motion to other other modes. This is done is 'ZSTRETCH', using the basis set wave functions derived in 'UNIDIM' (one-dimensional z–stretch motion) and 'HIN-ROTTRAN' (all other nuclear modes). Finally the Franck–Condon and Fourier integral overlap are calculated in subroutine 'RECOUVRE' by means of Simpson integration and standard Fast–Fourier transform subroutines.

E.2 Formulae for photodesorption cross section

The starting point is the formula for the photodesorption differential cross section based on a time dependent approach, which was already given in part III, Eq.2.1, p.139.

$$\sigma^{J,M,v,\vec{k}_{\parallel}^{trans,f}\Omega_f}_{n,\vec{k}_{\parallel}^{trans,i}}\left(\hat{q},\vec{k}^{nuc},E_{ph}\right) = \int d^2k_{||}^{elec,f}\int d^2k_{||}^{elec,i} \tag{E.1}$$

$$\frac{4\pi^2 E_{ph}}{\hbar c}\lim_{t\to\infty}\left|\left\langle \Psi^{tot}_{\Omega_f,n,\vec{k}_{\parallel}^{elec,f},\vec{k}_{\parallel}^{trans,f}}\right|\exp(-i\mathcal{H}t/\hbar)\left|\Psi^{tot}_{\Omega_i,n,\vec{k}_{\parallel}^{elec,i},\vec{k}_{\parallel}^{trans,i}}\right\rangle\right|^2_{\{\vec{r}\}_N,\vec{R},\vec{X}}$$

Summarising the definitions:

- E_{ph}: photon energy with incident angles $\hat{q}$=(ϑ_q, φ_q)
- $\hbar$ Planck's constant, c the speed of the light
- $\Psi^{tot}_{\Omega,n,k_{\parallel}^{\vec{elec}},k_{\parallel}^{\vec{trans}}}$ of the initial (index i) and final (f) states.
- $\{\vec{r}\}_N = (\vec{r_1}, \vec{r_2}, ..., \vec{r_N})$: electronic, $\vec{R}$ and $\vec{X}$: nuclear coordinates
- n for initial state: quantum number of the coupled nuclear modes
  n for final state: gas phase quantum numbers $n = (J, M, v, k_z)$
- $\vec{k} = (\vec{k}_{||}^{nuc,f}, k_z)$ is the linear momentum vector of the desorbing particle
- $\vec{k}_{||}^{nuc,f}$: two–dimensional vector in reciproke space parallel to the surface.
- $\exp(-i\mathcal{H}t/\hbar)$ is the time evolution operator for $t' = 0$ to $t' = t$.

Concerning the electronic wave function, I use as basis set function Born– Oppenheimer wave functions (see part III, Eq.(2.2, page 139)) for three states. All non-adiabatic interactions coupling electronical and nuclear motion states are considered in the Hamiltonian, already given in part III, Eq.(2.3), page 141:

$$\mathcal{H} = \mathcal{H}^{elec}_{kin}(\{\vec{r}_N\}) + \mathcal{H}^{nuc}_{kin}(\vec{R},\vec{X}) + V^{molecule}(\{\vec{r}_N\},\vec{R}) + V^{surface}(\{\vec{r}_N\},\vec{R},\vec{X}) + {}^{m^{ph}}T^{photon}(\{\vec{r}_N\},\hat{q},t) \tag{E.2}$$

Before the desorption, the system is in the fundamental state $\xi_i, \mathbf{\Omega}_i, \vec{k}^{elec,i}_{\parallel}$. The photon causes a transition into the excited state (m), noted as $\xi_i, \mathbf{\Omega}^m$, $\vec{k}^{elec,m}_{\parallel}$. This excited state is coupled by non-adiabatic interaction to the final state $\xi_f, \mathbf{\Omega}^f$, $\vec{k}^{elec,f}_{\parallel}$. For molecular adsorbates like CO, the final state quantum number $\mathbf{\Omega}^f$ is identical to the one of the initial state: $\mathbf{\Omega}^i = \mathbf{\Omega}^f$, i.e. no electronic excitation of the desorbing molecule takes place. Note, that during the excitation and deexcitation processes, $\Delta\vec{k}^{elec}_{\parallel}$ is not changing, but the initial and final state $\vec{k}^{elec}_{\parallel}$ are not identical due to the considerable time of the system being in the excited state (m).

Therefore, there are three wave functions with respect to ξ, $\mathbf{\Omega}$ and $\vec{k}^{elec}_{\parallel}$ forming the complete basis set for the electronical motion:

$$\psi^{E}_{\xi_i,\mathbf{\Omega},\vec{k}^{elec}_{\parallel}} := \psi^{E}_{\xi_i,\mathbf{\Omega},\vec{k}^{elec}_{\parallel}}(\{\vec{r}\}_N;\vec{R},\vec{X}) \tag{E.3}$$

$$\psi^{E_m}_{\xi_m,\mathbf{\Omega}_m,\vec{k}^{elec,m}_{\parallel}} := \psi^{E_m}_{\xi_m,\mathbf{\Omega}_m,\vec{k}^{elec,m}_{\parallel}}(\{\vec{r}\}_N;\vec{R},\vec{X}) \tag{E.4}$$

$$\psi^{E_f}_{\xi_f,\mathbf{\Omega},\vec{k}^{elec,f}_{\parallel}} := \psi^{E_f}_{\xi_f,\mathbf{\Omega},\vec{k}^{elec,f}_{\parallel}}(\{\vec{r}\}_N;\vec{R},\vec{X}) \tag{E.5}$$

In Eq.2.2 $\psi_{\mathbf{\Omega},\vec{k}^{elec}_{\parallel}}(\{\vec{r}\}_N;\vec{R},\vec{X})$ is the electronical wave function, which depends parametrically on the nuclear coordinates $\vec{R},\vec{X}$. The wave function is $\Theta^{n}_{\mathbf{\Omega}\vec{k}^{nuc}_{\parallel}}(\hat{R},\vec{X})$.

The integration over electronic coordinates give rise to 3×3 matrix $\tilde{\mathcal{H}}$:

$$\tilde{\mathcal{H}} = \begin{pmatrix} \left\langle \psi^{E}_{\mathbf{\Omega},\vec{k}^{elec,i}_{\parallel}} \right| \mathcal{H} \left| \psi^{E}_{\mathbf{\Omega},\vec{k}^{elec,i}_{\parallel}} \right\rangle & \left\langle \psi^{E}_{\mathbf{\Omega},\vec{k}^{elec,i}_{\parallel}} \right| \mathcal{H} \left| \psi^{E_m}_{\mathbf{\Omega}_m,\vec{k}^{elec,m}_{\parallel}} \right\rangle & \left\langle \psi^{E}_{\mathbf{\Omega},\vec{k}^{elec,i}_{\parallel}} \right| \mathcal{H} \left| \psi^{E_f}_{\mathbf{\Omega},\vec{k}^{elec,f}_{\parallel}} \right\rangle \\ \left\langle \psi^{E_i}_{\mathbf{\Omega}_m,\vec{k}^{elec,m}_{\parallel}} \right| \mathcal{H} \left| \psi^{E}_{\mathbf{\Omega},\vec{k}^{elec}_{\parallel}} \right\rangle & \left\langle \psi^{E_m}_{\mathbf{\Omega}_m,\vec{k}^{elec,m}_{\parallel}} \right| \mathcal{H} \left| \psi^{E_m}_{\mathbf{\Omega}_m,\vec{k}^{elec,m}_{\parallel}} \right\rangle & \left\langle \psi^{E_m}_{\mathbf{\Omega}_m,\vec{k}^{elec,m}_{\parallel}} \right| \mathcal{H} \left| \psi^{E_f}_{\mathbf{\Omega},\vec{k}^{elec,f}_{\parallel}} \right\rangle \\ \left\langle \psi^{E_i}_{\mathbf{\Omega},\vec{k}^{elec,i}_{\parallel}} \right| \mathcal{H} \left| \psi^{E}_{\mathbf{\Omega},\vec{k}^{elec}_{\parallel}} \right\rangle & \left\langle \psi^{E_m}_{\mathbf{\Omega},\vec{k}^{elec,f}_{\parallel}} \right| \mathcal{H} \left| \psi^{E_m}_{\mathbf{\Omega}_m,\vec{k}^{elec,m}_{\parallel}} \right\rangle & \left\langle \psi^{E_m}_{\mathbf{\Omega},\vec{k}^{elec,f}_{\parallel}} \right| \mathcal{H} \left| \psi^{E_f}_{\mathbf{\Omega},\vec{k}^{elec,f}_{\parallel}} \right\rangle \end{pmatrix} \tag{E.6}$$

In (E.6) $\mathcal{H}$ is the Hamiltonian operator (E.2) and $\psi^{E}_{\mathbf{\Omega},\vec{k}^{elec}_{\parallel}}$ are the functions (E.3). The electronic wave functions (E.3) have been calculate neglecting the non-adiabatic and photon field interactions. Therefore, only these terms contribute to the non-diagonal terms. Using some assumptions the matrix (E.6) can be simplified. For the elements between the initial (i) and the intermediate (m) state, mainly the transition

operator contribute. In other words, the photonic resonant transition dominates over the non-adiabatic contribution. For the non-diagonal matrix elements between the intermediate (m) and the final (f) state, the contrary happens. The non-adiabatic term is essential for the description of the desexcitation process and is usually relatively large. The electronic transition between excited and final states is dominated by stimulated emission and is consequently related to the laser fluence. It has to be taken into account for strong laser fields. The last non-diagonal matrix element is that between the final (f) and initial (i) states where none is resonant and the non-diagonal term can be neglected. Rembering, that only vertical transitions in $\vec{k}_{||}^{elec}$ are considered ($\vec{k}_{||}^{elec,i} = \vec{k}_{||}^{elec,m} = \vec{k}_{||}^{elec,f} \equiv \vec{k}_{||}^{elec}$) Eq.(E.6) can now be rewritten as:

$$\tilde{\mathcal{H}}_{\vec{k}_{||}^{elec}}(\vec{R},\vec{X}) = \begin{pmatrix} \mathcal{H}_{kin}^{nuc} + V^{(nuc)}_{\Omega,\vec{k}_{||}^{elec}}(\vec{R},\vec{X}) & {}^{m^{ph}}T^{\Omega_m}_{\Omega,\vec{k}_{||}^{elec}}(\vec{R},\vec{X}) & 0 \\ {}^{m^{ph}}T^{\Omega_m}_{\Omega,\vec{k}_{||}^{elec}}(\vec{R},\vec{X}) & \mathcal{H}_{kin}^{nuc} + V^{(nuc)}_{\Omega_m,\vec{k}_{||}^{elec}}(\vec{R},\vec{X}) & W^{\Omega_m,\vec{k}_{||}^{elec,m}}_{\Omega,\vec{k}_{||}^{elec,f}}(\vec{R},\vec{X}) \\ 0 & W^{\Omega_m,\vec{k}_{||}^{elec,m}}_{\Omega,\vec{k}_{||}^{elec,f}}(\vec{R},\vec{X}) & \mathcal{H}_{kin}^{nuc} + V^{(nuc)}_{\Omega,\vec{k}_{||}^{elec}}(\vec{R},\vec{X}) \end{pmatrix} \tag{E.7}$$

In Eq.(E.7) the diagonal elements consist of the nuclear kinetic operator $\mathcal{H}_{kin}^{nuc}$ and the potential $V^{(nuc)}$ for the nuclear motion. The non diagonal terms are related to the photonic transition ${}^{m^{ph}}T^{\Omega_m}_{\Omega,\vec{k}_{||}^{elec,i}}$ and to the non-adiabatic interaction terms $W^{\Omega_m,\vec{k}_{||}^{elec,m}}_{\Omega,\vec{k}_{||}^{elec,f}}$.

The nuclear wave functions in the Born–Oppenheimer product (2.2) are obtained by solving the Schrödinger equation neglecting all non diagonal elements in the matrix of Eq.E.7. With these nuclear and the electronic wave functions one can construct a complete basis set of wave functions in the Born–Oppenheimer approximation.

Photodesorption cross section in second order perturbation theory

To simplify the photodesorption cross section, I apply second order perturbation theory, considering the non-diagonal part of the Hamiltonian (E.7) as a weak perturbation. This is not the case here, as the non-adiabatic interactions are strong and lead to a rapid electronic decay of the excited state. In addition, the resulting formulae are valid for commuting zero–order Hamiltonian (diagonal part of (E.7)) and the perturbation (non-diagonal part). This approximation may not be valid for non-adiabatic interactions, as they contain derivatives.

The idea of the following part is to develop the Hamiltonian in a Born–expansion and to take the second order term, that consists of $V \times G \times V$, where V is the perturbation and G the Green's operator. Note, that the Green's operator is diagonal in the chosen basis set.

Neglecting dissociation, the basis set of nuclear wave function include discrete state and in the hindered translation and molecule–surface coordinates also continuum states. During the propagation on the excited potential curve, the nuclear motion can in general populate all discrete and continuum states. But the initial state concerning the molecule–surface motion is discrete and the electronic lifetime is too short to allow a population of the associated continuum states. Therefore the identity operator in nuclear

coordinate space includes only discrete states for this motion. This operator is a diagonal 3×3 matrix with the elements depending on the electronic state $\Omega' = \Omega, \Omega_m$ and Ω for the initial, intermediate and final state, respectively.

$$\mathcal{I} = \left(\sum_{n'} \int d^2k_{\parallel}^{trans,l} \left| \Theta^{n'}_{\Omega,\vec{k}_{\parallel}^{nuc,l}} \right\rangle \left\langle \Theta^{n'}_{\Omega,\vec{k}_{\parallel}^{nuc,l}} \right| \right) \tag{E.8}$$

Inserting the identity twice between the perturbation and the Green's operator, one finds the formula for the photodesorption cross section, given in part III, Eq.2.4):

$$\sigma^{J,M,v,\vec{k}_{\parallel}^{nuc,f}\Omega}_{n,\vec{k}_{\parallel}^{nuc,i}}(\hat{q}, E_{ph}) = \frac{4\pi^2 E_{ph}}{\hbar c} \int d^2k_{\parallel}^{elec} \lim_{\varepsilon\to 0} \tag{E.9a}$$

$$\left| \sum_{n_m} \int d^2k_{\parallel}^{nuc,m} \left\langle \Theta^{n_f}_{\Omega,\vec{k}_{\parallel}^{nuc,f}} \right| W^{\Omega_m}_{\Omega,\vec{k}_{\parallel}^{elec}}(\vec{R},\vec{X}) \left| \Theta^{n_m}_{\Omega\vec{k}_{\parallel}^{nuc,m}} \right\rangle_{\vec{R},\vec{X}} \right.$$

$$\left. \frac{1}{E^{n_i,\vec{k}_{\parallel}^{nuc,i}}_{\Omega,\vec{k}_{\parallel}^{elec}} + h\nu - E^{n_m,\vec{k}_{\parallel}^{nuc,m}}_{\Omega,\vec{k}_{\parallel}^{elec}} + i\varepsilon} \left\langle \Theta^{n'}_{\Omega,\vec{k}_{\parallel}^{nuc,l}} \right| {}^{m^{ph}} T^{\Omega_m}_{\Omega,\vec{k}_{\parallel}^{elec}} \left| \Theta^{n_i}_{\Omega\vec{k}_{\parallel}^{nuc,i}} \right\rangle_{\vec{R},\vec{X}} \right|^2$$

where

$$W^{\Omega_m}_{\Omega,\vec{k}_{\parallel}^{elec}}(\vec{R},\vec{X}) = \int d^{3N}r \left(\psi_{\xi_f,\Omega,\vec{k}_{\parallel}^{elec}}(\{\vec{r}\}_N;\vec{R},\vec{X}) \right)^* \mathcal{H}^{tot} \psi_{\xi_m,\Omega_m,\vec{k}_{\parallel}^{elec}}(\{\vec{r}\}_N;\vec{R},\vec{X})$$

(E.9b)

Beyond the second–order perturbation approximation

.

Above, I have discussed the validity of the second–order perturbation theory that breaks–down when the non–adiabatic interaction is strong. To solve this problem, one can still use perturbation theory and split the total Hamiltonian differently. One idea is to consider only the weak photon transition as perturbation and put the strong non–adiabatic interactions in the unpertubated Hamiltonian. The resulting electronic functions are difficult to obtain because they contain a non-adiabatic contribution.

If the photon interaction correspond to strong multi-photon fields, the perturbation theory does not applies anymore and the two step process explained for the second order perturbation formula Eq.(E.9) is no more valid. A more complicated cycle, allowing several excitation–deexcitation cycles of the intermediate state should be introduced. First, the photon excites the adsorbate–surface system. Then, electronically the system is in the excited state (m), with different excited nuclear states. Secondly, the

system can decay into the final state. Looking at the molecule– surface degree of freedom, it can be deexcited into the continuum and desorb. Contrary to the second order perturbation formula it can also pass deexcitation – excitation cycles until after some time being deexcitated into the continuum and desorb. The repetition rate and duration of this cycle strongly depends on the non-adiabatic interaction and laser fluency. The resulting distribution of the nuclear modes of the desorbing molecule, like internal vibration and rotation, will be different from the second perturbation approximation and weak field regime case. The photon and non-adiabatic coupling will now be dependent of the fluency and the time spent by the adsorbate in the excited state will be much higher than in the one photon case.

Bibliography

[1] H. i.A. des Exekutivkomitees der Internationalen Arbeitsgemeinschaft Sozialistischer Jugen-Organisationen, Unser Lied, Juni 1922.

[2] J. R.J.Smith and G.J.Lapeyre, Phys.Rev.Lett. **37**, 1081 (1976).

[3] G.Apai *et al.*, Phys.Rev.Lett. **37**, 1497 (1976).

[4] C.L.Allyn, T.Gustafsson, and E.W.Plummer, Chem.Phys.Lett. **47**, 127 (1977).

[5] R. M.Trenary, S.L.Tang and F.R.McFreely, Surf.Sci **127**, 555 (1983).

[6] D.Rieger, R.D.Schnell, and W.Steinmann, Surf. Sci. **143**, 157 (1984).

[7] R.Miranda, K.Wandelt, D.Rieger, and R.D.Schnell, Surf.Sci **139**, 430 (1984).

[8] D. Heskett *et al.*, Surf.Sci. **164**, 490 (1985).

[9] S.Krause, C.Mariani, K.C.Prince, and K.Horn, Surf.Sci **138**, 305 (1984).

[10] A.Puschmann *et al.*, Surf. Sci. **251/252**, 356 (1991).

[11] M.Büchner and G.Raşeev, Phys.Rev.B **49**, 2768 (1994).

[12] S.Nagano *et al.*, J.Chem.Phys. **85**, 6153 (1986).

[13] P.Budău, M.Büchner, and G.Raşeev, Surf.Sci. **292**, 67 (1993).

[14] F. D.A.Wesner and H.P.Bonzel, Surf.Sci **199**, 419 (1988).

[15] K.Horn, A.M.Bradshaw, and K.Jacobi, Surf.Sci. **72**, 719 (1978).

[16] E.S.Jensen and T.N.Rhodin, Phys.Rev.B **27**, 3338 (1983).

[17] M.Scheffler, Surf.Sci **81**, 562 (1979).

[18] Yu.A.Tsyganenko, A.A.Tsyganenko, and K.S.Smirnov, Vibrational Spectroscopy **6**, 15 (1993).

[19] M.D.Alvey, M.J.Dresser, and J. Jr., Surf.Sci. **165**, 447 (1986).

[20] W.Riedl and D.Menzel, Surf.Sci. **163**, 39 (1985).

[21] P.Parneix, M.Büchner, G.Raşeev, and N.Halberstadt, Chem.Phys.Lett. **233**, 431 (1995).

[22] D.Burgess, R.R.Cavanagh, and D.S.King, J.Chem.Phys. **88**, 6556 (1988).

[23] R. D.C Jacobs, K.M.Kolasinski and R.N.Zare, J.Chem.Phys. **87**, 5038 (1987).

[24] D.Weide, P.Andresen, and H.-J. Freund, Chem.Phys.Letters **136**, 106 (1987).

[25] S.A.Buntin, L.J.Richter, D.S.King, and R.R.Cavanagh, J.Chem.Phys. **91**, 6429 (1989).

[26] J.A.Prybyla *et al.*, Phys.Rev.Letters **64**, 1537 (1990).

[27] J.A.Prybyla, T.F.Heinz, J.A.Misewich, and M.M.T.Loy, Surf. Sci. Letters **230**, L173 (1990).

[28] K.Mase, S.Mizuno, Y.Achiba, and Y.Murata, Surf.Sci **242**, 444 (1991).

[29] J.Yoshinobu *et al.*, Surf.Sci **255**, 295 (1991).

[30] F.Budde *et al.*, Phy.Rev.Lett. **60**, 1518 (1988).

[31] P.M.Ferm *et al.*, Surf.Sci. **218**, 467 (1989).

[32] M.Asscher *et al.*, J.Chem.Phys. **96**, 4808 (1992).

[33] Th.Mull *et al.*, J.Chem.Phys. **96**, 7108 (1992).

[34] A.Peremans, K.Fukutani, K.Mase, and Y.Murata, Surf.Sci. **283**, 189 (1993).

[35] M.Menges *et al.*, in *Desorption Induced by Electronic Transitions (DIET V)*, edited by A.R.Burns, E.B.Stechel, and D.R.Jennison (Springer Series in Surface Science, Heidelberg, 1993).

[36] K.Al-Shamery, I.Beauport, H.-J. Freund, and H. Zacharias, Chem.Phys.Lett. **222**, 107 (1994).

[37] J.W.Davenport, Phys.Rev.Lett. **36**, 945 (1976).

[38] D.Dill, J.Chem.Phys. **65**, 1130 (1976).

[39] G.L.Nyberg and N.V.Richardson, Surf.Sci **85**, 335 (1979).

[40] C.M.Friend, Scientific American 42 (1993).

[41] H.-J. Freund and M.Neumann, Appl.Phy.A **47**, 3 (1988).

[42] G.Blyholder, J.Phys.Chem. **68**, 2772 (1964).

[43] G.Doyen and G.Ertl, Surf.Sci. **43**, 197 (1974).

[44] G.Brodén *et al.*, Surf.Sci. **59**, 593 (1976).

[45] Dill and Dehmer, J.Chem.Phys. **61**, 692 (1974).

[46] P.Budău and G.Raşeev, Phys.Rev.B submitted (1995).

[47] N.V.Richardson and A.M.Bradshaw, Surf.Sci. **88**, 255 (1979).

[48] C.J.Hirschmugl, G.P.Williams, F.M.Hoffmann, and Y.J.Chabal, J. El.Spec. Rel.Phenom. **54/55**, 109 (1990).

[49] W.Akemann and A.Otto, J.of Raman Spec. **22**, 797 (1991).

[50] H.Steininger, S.Lehwald, and H.Ibach, Surf. Sci. **123**, 264 (1982).

[51] A.M.Lahee, J.P.Toennies, and Ch.Wöll, Surf.Sci **177**, 371 (1986).

[52] J.W.Gadzuk, S.Holloway, C.Mariani, and K.Horn, Phys.Rev.Lett. **48**, 1288 (1982).

[53] G. Herzberg, *Molecular Spectra and Molecular Structures: I Spectra of Diatomic Molecules*, 2nd ed. (van Nostrand Reinhold Company, New York, 1950).

[54] H.Antonsson, A.Nilsson, and N.Martensson, J. El.Spec. Rel.Phenom. **54/55**, 601 (1990).

[55] K.A.Thompson and C.S.Fadley, J. El.Spec. Rel.Phenom. **33**, 29 (1984).

[56] D.Rieger, Ph.D. thesis, Ludwig–Maximilian Universität, (1984).

[57] C.L.Allyn, T.Gustafsson, and E.W.Plummer, Solid State Comm. **28**, 85 (1978).

[58] O.Björneholm, Ph.D. thesis, University of Uppsala, (1992).

[59] B.Leyh, Ph.D. thesis, Universit de Li ge, (1987).

[60] W.Eberhardt, E.W.Plummer, C.T.Chen, and W.K.Ford, Aust.J.Phys. **39**, 853 (1986).

[61] P.Parneix, private communication (1994).

[62] P. M.Bertolo, W.Hansen and K.Jacobi, Surf.Sci. **251/252**, 359 (1991).

[63] R.Berndt, J.P.Toennies, and Ch.Wöll, J. El.Spec. Rel.Phenom. **44**, 183 (1987).

[64] Gupta and Gupta, Can.J.Phys **47**, 617 (1969).

[65] A.Messiah, *Quantum Mechanics* (North Holland Publishing Company, Amsterdam, 1961).

[66] G.Raşeev, Comp.Phys.Commun. **20**, 267 (1980).

[67] R. N. Zare, *Angular Momentum* (John Wiley & Sons, Inc., New York, 1988).

[68] G.Raşeev, in *Half Collision Resonance Phenomena in Molecules*, edited by M. Garciá-Sucre, G.Raşeev, and S.C.Ross (American Institute of Physics, New York, 1990).

[69] O.Atabek, J.A.Beswick, and G.Delgado-Barrio, Chem.Phys.Lett. **82**, 2954 (1985).

[70] N.A.Cherepkov, Chem.Phys.Lett. **87**, 344 (1982).

[71] N.A.Cherepkov and V.V.Kuznetsov, Z.Phys.D **7**, 271 (1987).

[72] B.H.Bransden and C.J.Joachain, *Physics of Atoms and Molecules* (Longman, Harlow, Essex, 1988).

[73] G.Raşeev, Surf.Sci. **269/270**, 247 (1992).

[74] G.Raşeev and L.E.Machado, in *Half Collision Resonance Phenomena in Molecules*, edited by M. Garciá-Sucre, G.Raşeev, and S.C.Ross (American Institute of Physics, New York, 1990).

[75] R. Parr, *The Quantum Theory of Molecular Electronic Structure* (W.A. Benjamin, Inc., New York, 1963).

[76] P.J.Jennings, R.O.Jones, and M.Weinert, Phys.Rev.B **37**, 6113 (1988).

[77] J.B.Pendry, *Low Energy Electron Diffraction* (Academic, London, 1974).

[78] Sébilleau *et al.*, J.Phys. France **49**, 227 (1988).

[79] C.Westphal, A.P.Kaduwela, C.S.Fadley, and M. Hove, Phys.Rev.B **50**, 6203 (1994).

[80] C.W.Seabury *et al.*, Surf.Sci **97**, 363, (1980).

[81] J.T.Hougen, Monograph 115, National Bureau of Standarts (U.S.) (unpublished).

[82] *Engineering and Scientific Subroutine Library, version 2*, second edition (january 1994) ed., IBM Corporation, 1994.

[83] S.Andersson and J.B.Pendry, Phys.Rev.Lett. **43**, 363 (1979).

[84] M.Passler *et al.*, Phys.Rev.Lett. **43**, 360 (1979).

[85] G. Herzberg and K.P.Huber, *Molecular Spectra and Molecular Structures VI: Constants of diatomic molecules* (van Nostrand Reinhold Company, New York, 1979).

[86] K.Mirsky, Chem.Phy. **46**, 445 (1980).

[87] G.Parlant, P.Archirel, and E. Gislason, J.Chem.Phys. **92**, 1211 (1990).

[88] K. von Meyenn, Z.Physik **231**, 154 (1970).

[89] D.E.Eastman and J.K.Cashion, Phys.Rev.Letters **27**, 1520 (1971).

[90] C.L.Allyn *et al.*, Phys.Rev..Letters **37**, 1497 (1976).

[91] N.Martensson and A.Nilsson, J.Elect.Spec. Rel.Phenon. **52**, 1 (1990).

[92] O.Björneholm *et al.*, Phys.Rev.B **46**, 10353 (1992).

[93] Z. Huang, Z.Hussain, W.T.Huff, and E.J.Moler, Phys.Rev.B **48**, 1696 (1993).

[94] N.Pangher and J.Haase, Surf.Sci. **293**, L908 (1993).

[95] C.M.Kao and R.P.Messmer, Phys.Rev.B **31**, 4835 (1985).

[96] J.A.R.Sampson, J. of the Opt. Soc. of America **59**, 356 (1969).

[97] D.A.Varshalovich, A.N.Moskalev, and V.K.Khersonskii, *Quantum Theory of Angular Momentum* (Word Scientific, Singapore, 1988).

[98] J.E.Houston, Surf.Sci. **255**, 303 (1991).

[99] D.Bejan, private communication (1995).

[100] D.Teillet-Billy and J.P.Gauyacq, Nucl.Instr. and Meth.in Phy.Res.B **58**, 393 (1991).

[101] K.Jacobi, *13th General Conference of the Condensed Matter Division, European Physical Society in conj. with Arbeitskreis Festkörperphysik, Deutsche Physikalische Gesellschaft* (European Physical Society and Deutsche Physikalische Gesellschaft, Regensburg, 1993).

[102] K.Jacobi, private communication (1993).

[103] I.P.Batra, K.Hermann, A.M.Bradshaw, and K.Horn, Phys.Rev.B **20**, 801 (1979).

[104] B.N.J.Persson, M.Tushans, and A.M.Bradshaw, J.Chem.Phys. **92**, 5034 (1990).

[105] H.Evens, D.J.Tildesley, and T.J.Sluckin, J.Phys.C **17**, 4907 (1984).

[106] R. Lynden-Bell, J. Talbot, D. Tildesley, and W. Steele, Mol. Phys. **54**, 183 (1985).

[107] P.Parneix, Ph.D. thesis, Universit de Paris–Sud, (1993).

[108] S.Picaud, P.N.M.Hoang, and C.Girardet, Surf.Sci. **294**, 149 (1993).

[109] J.C.Tully, J.Chem.Phys **73**, 6333 (1980).

[110] C.W.Mulhausen, L.R.Williams, and J.C.Tully, J.Chem.Phys. **83**, 2594 (1985).

[111] N.Moiseyev and T.Maniv, Mol. Phys **55**, 1369 (1985).

[112] M.P.Allen and D.J.Tildesley, *Computer Simulation of Liquids* (Oxford Press, Oxford, 1987).

[113] P.Henrici, *Elements of Numerical Analysis* (John Wiley and Sons, Inc., New York, 1964).

[114] W.H.Press, B.P.Flannery, S.A.Teukolsky, and W.T.Vettering, in *Numerical Recipes: The Art of Scientific Computering* (Cambridge University Press, Cambridge, 1986).

[115] P.Parneix, private communication (1995).

[116] H.Zacharias, Appl.Phys.A **47**, 37 (1988).

[117] W.C.Natzle, D.Padowitz, and S.J.Sibener, J.Chem.Phys. **88**, 7975 (1988).

[118] P.Feulner and D.Menzel, in *Laser spectroscopy and photochemistry on metal surfaces*, edited by Hai-Lung and W. Ho (Word Scientific Publishing Company, Singapore, 1995).

[119] X.-L.Zhu and J.M.White, Surf.Sci.Rep. **13**, 73 (1991).

[120] G.P.Brivio and T.B.Grimley, Surf.Sci.Rep. **17**, 1 (1993).

[121] A.R.Burns, E.B.Stechel, D.R.Jennison, and Y.S.Li, J. Chem. Phys. **101**, 6318 (1994).

[122] D.J.Auerbach, C.T.Rettner, and H.A.Michelsen, Surf. Sci. **283**, 1 (1993).

[123] J.A.Prybyla, H.W.Tom, and G.D.Aumiller, Phys.Rev.Lett. **68**, 503 (1992).

[124] D.Menzel and R.Gomer, J.Chem.Phys. **41**, 3311 (1964).

[125] P.A.Redhead, Can.J. of Phys. **42**, 886 (1964).

[126] P.Antoniewicz, Phys.Rev. B **21**, 3811 (1981).

[127] W.Hübner and W.Brenig, Z.Phys.B **74**, 361 (1989).

[128] J.W.Gadzuk, J.Chem.Phys. **79**, 6341 (1983).

[129] J.W.Gadzuk, Comments At. Mol. Phys. **16**, 219 (1985).

[130] J.W.Gadzuk *et al.*, Surf.Sci. **235**, 317 (1990).

[131] W.Brenig, Z.Phys.B **23**, 361 (1975).

[132] Z.W.Gortel, R.Teshima, and H.J.Kreuzer, Phys.Rev.B **37**, 3183 (1988).

[133] Z.W.Gortel, Surf.Sci. **231**, 193 (1990).

[134] Z.W.Gortel and A.Wierzbicki, Phys.Rev.B **43**, 7487 (1991).

[135] Z.W.Gortel, R.Teshima, and H.J.Kreuzer, Phys.Rev.B **47**, 9825 (1993).

[136] S.M.Harris and S.Holloway, in *Desorption Induced by Electronic Transitions (DIET)* (Springer Press, in press, 1995).

[137] U. Landman, Isr.J.of Chem. **22**, 339 (1982).

[138] A.R.Burns, E.B.Stechel, and D.R.Jennison, Phys.Rev.Lett. **58**, 250 (1987).

[139] A.R.Burns, E.B.Stechel, and D.R.Jennison, J.Vac.Sci.Technol A **6**, 865 (1988).

[140] E.Hasselbrink, Chem.Phys.Lett. **170**, 329 (1990).

[141] F.M.Zimmermann and W.Ho, Phy.Rev.Lett. **72**, 1295 (1994).

[142] J.C.Tully, J.Chem.Phys **93**, 1061 (1990).

[143] K.-D.Shiang, Surf.Sci. **292**, 145 (1993).

[144] A.B.Ephraim, M.Folman, J.Heidberg, and N.Moiseyev, J.Chem.Phys. **89**, 3840 (1988).

[145] F.Dzegilenko and E.Herbst, J.Chem.Phys. **100**, 9205 (1994).

[146] K.Homann, R.M.Jäger, and H.Kuhlenbeck, J.of Electr.Spec.and Rel.Pheno **62**, 273 (1993).

[147] T.Hertel, E.Knoesel, M.Wolf, and G.Ertl, in *Desorption Induced by Electronic Transitions (DIET)* (Springer Press, in press, 1995).

[148] G.Raşeev, private communication (1995).

[149] J.Rogozik *et al.*, Surf.Sci. **145**, L481 (1984).

[150] Q.Ge, L.Wang, and G.D.Billing, Surf.Sci. **277**, 237 (1992).

[151] J.W.Gadzuk *et al.*, J. Elec.Spec. Rel.Phenom. **30**, 103 (1983).

[152] H.LeRouzo and G.Raşeev, in redaction (1995).

[153] N. V.V.Kuznetsov and G.Raşeev, in redaction (1995).

[154] A.Keller, Ph.D. thesis, Universit de Paris–Sud, (1991).

[155] M.Abramowitz and I.A.Stegun, *Handbook of Mathematical Functions* (Dover Publications, Inc., New York, 1972).

List of Tables

List of Figures

Photodesorption of molecular adsorbates **119**

Annexes **176**

Curriculum Vitae

Matthias Büchner,
de nationalité allemande
né le 20 mai 1966 à Gadderbaum (actuellement Stadt Bielefeld) en Allemagne

Baccalauréat	15/5/1985	Abitur au Widukind–Gymnasium Enger
Etudes Supérieures:	1/10/1985	Etudes de Physique à l'Université de Bielefeld
	20/1/1992	Diplôme en Physique (Diplom in Physik) Titre de la Thèse de diplôme : "Theoretische und experimentelle Untersuchungen der winkelaufgelösten Photoionisation: Rotationsaufgelöste Ergebnisse am HI–Molekül im Bereich der Spin–Bahn–Autoionisation" chez Prof. Dr. U. Heinzmann
	19 april 1995	soutenance de thèse de doctorat à l'Université de Paris–Sud, Orsay
Activités:	1/11/91–31/10/93	boursier de la CEE au Laboratoire de Photophysique Moléculaire du CNRS, Université de Paris–Sud, Orsay, chez Dr. G. Raşeev et Dr. O. Atabek pour obtenir le titre de docteur
	depuis 1/12/1994	Attaché témporaire d'Enseignement et de Recherche à l'Université de Paris–Sud, Orsay

Photofragmentation des adsorbats moléculaires: étude théorique de la photoionisation, de la photodésorption et des processus connexes.

Cette thèse porte sur l'étude de la photofragmentation des molécules adsorbées sur des surfaces solides: la photoionisation, la photodésorption et l'influence du taux de couverture d'adsorbat.

Dans la première partie, la rotation empêchée de l'adsorbat et la rétrodiffusion des photoélectrons sont présentées. Elles modifient les spectres de photoionisation, car la rotation empêchée change l'orientation de l'axe moléculaire et la rétrodiffusion donne naissance à des effets d'interférence entre les ondes directe et réfléchie par la surface. Ces deux phénomènes vont au–delà du modèle de la molécule orientée dans l'espace connu dans la littérature.

Les distributions angulaires des électrons excités d'une orbitale 4 sigma de CO pour les systèmes physisorbé (CO/Ar) et chimisorbé (CO/Ni(100)) sont calculées incluant la rotation empêchée. Pour CO/Ar, les résultats sont fortement influencés par la rotation empêchée. Pour CO/Ni(100) elle joue un rôle mineur apparaissant surtout comme élargissement des structures de la distribution angulaire des électrons éjectés. Une recette permettant d'estimer l'angle d'inclinaison de l'adsorbat par rapport à la normale à la surface incluant la rotation empêchée est discutée. La rétrodiffusion, calculée pour le système CO/Ni, est importante pour l'ionisation d'un électron 5 sigma de CO, mais négligeable pour 4 sigma.

Dans la seconde partie, l'influence du taux de couverture pour le système CO/Ar(100) étudiée par des méthodes de dynamique classique et quantique, apparaît comme rigidification du mouvement angulaire de précession. Pour une couverture dense, les premiers états rotationels sont dominés par quatre géométries de l'adsorbat presque dégénérés en énergie ce qui n'implique pas une précession libre mais des directions équivalentes sur la surface.

La troisième partie traite de la photodésorption en régime nonthermique des adsorbats moléculaires. Pour une énergie photonique de 2 à 7 eV, l'adsorbat est d'abord excité électroniquement. La désexcitation transfère une partie de l'énergie électronique dans les modes nucléaires et particulièrement dans le mode associé à la désorption. Un modèle multidimensionnel de désorption qui couple les mouvements nucléaires et appliqué à CO adsorbé sur des sites linéaire d'une surface de Cu(111) est analysé. La rotation empêchée est fortement couplée au mode de désorption, mais découplée de la vibration interne de CO et de la translation empêchée. Dans l'interpretation de l'expérience, la distribution translationnelle bimodale a été attribuée à la présence des désorptions thermique et nonthermique. Les résultats du modèle présent montrent que cette distribution peut aussi être uniquement de nature nonthermique.